ABSTRACT

PARKHIDEH, BABAK. Control Methods and Architectures for Voltage-Sourced Converter Based Systems for Utility Applications. (Under the direction of Dr. Subhashish Bhattacharya).

The voltage-Sourced Converter (VSC) is the preferred building block for Flexible AC Transmission Systems (FACTS) and utility-scale power electronics applications including HVDC transmission. Despite recent advances in the semiconductor technology, there are still many issues to address. This dissertation investigates the potentials and challenges that have been introduced for VSC-based transmission technologies. The technology is characterized in terms of switching frequency operation and switching patterns as either vector- or angle-controlled-based converters. Through the detail study of the VSC technology, this dissertation also offers unique applications of the VSC for utility applications which can be extended to high power mobile mining equipment.

This dissertation addresses the DC link voltage control issues for vector-controlled VSC-based transmission systems under power system disturbances. Having analyzed the state-of-the-art methods to mitigate the DC link voltage fluctuations under grid faults, a control structure in commonly used dq-synchronous frame is proposed. The proposed structure obviates the need for sequence extraction block or resonant notch compensator. Therefore, there is no diminishing bandwidth factor making it suitable for transmission applications for which the switching frequency is limited.

This dissertation introduces the possibility of automatic control of active and reactive power for voltage-sourced converters through angle control structure. A new control

framework which uses the properties of Single Input Two Output (SITO) feedback system is developed for voltage-sourced converters. Clearly, one actuator, in this case angle cannot be used to regulate two outputs (active and reactive power) to arbitrary setpoint values. Nevertheless, this dissertation shows that a one-dimensional class of setpoint values is feasible for the VSC technology. This work is an enhancement in the operational region of existing shunt family of FACTS devices that can also be extended for transmission level VSC based HVDC systems.

Currently, transmission level power electronics use custom designed converter structures to meet power system requirements including efficiency and harmonic spectrum. This fact for the VSC technology typically requires extensive engineering effort which makes the power electronic solution costly and therefore precludes broad deployment of the technology like FACTS controllers. Therefore, this research work focuses on development the concept of Modular Transformer Converter (MTC) which is a standard drive converter system. Through development of MTC, this dissertation identifies and introduces several applications and architectures based on VSC technology. These applications include *Recovery Transformer*, *Transformer Life Extender*, *Re-locatable Transmission Controller,* and *Seasonal Renewable Transmission Controller*. In fact, MTC enables a versatile transmission controller which is called Convertible Static Transmission Controller (CSTC). This research introduces Dual Series Static Controller (DSSC) which is available in the CSTC concept as a new FACTS controller. The DSSC provides significantly superior performance in terms of operational characteristics compared to conventional power flow controllers such as UPFC or IPFC. It is believed that 10 to 100 MVA MTC based CSTC which can be retrofitted into existing

transmission substations and transformers have a strong potential for the reliability, controllability and efficiency of the grid.

Energy storage systems are expected to play key roles in future energy management. Current state-of-the-art mobile mining equipment such as shovels and draglines are grid-connected high power multi-machine systems up to 24 MW. This dissertation proposes the integration of supplementary energy storage to capture and reuse the regenerative power which is currently burnt into the DC choppers. In particular, it will be shown that ultracapacitor is the technology of the choice in terms of energy price, temperature characteristics and engineering efforts for mining equipment. However, this dissertation identifies that advanced VSC technology is the enabling technology for this integration. Consequently, the so-called “Hybrid Configuration” is introduced which enjoys greatly from efficiency, density, and reliability compared to current state-of-the-art technologies.

Control Methods and Architectures for Voltage-Sourced Converter Based Systems for Utility Applications

by
Babak Parkhideh

A dissertation submitted to the Graduate Faculty of
North Carolina State University
in partial fulfillment of the
requirements for the degree of
Doctor of Philosophy

Electrical Engineering

Raleigh, North Carolina

2012

APPROVED BY:

_____	_____
Dr. Subhashish Bhattacharya Committee Chair	Dr. Mesut Baran
_____	_____
Dr. Srdjan Lukić	Dr. Aranya Chakrabortty
_____	
Dr. Xiangwu Zhang	

DEDICATION

To My Parents

DR. VILA SHOKOUHIAN AND DR. SHAPOUR PARKHIDEH

BIOGRAPHY

The author, Babak Parkhideh was born in Tehran, Iran. He received the B.Sc degree with honors in Electrical Engineering from University of Tehran, Tehran, Iran and the M.Sc in Electrical Power Engineering from the Institute of Power Electronics and Electrical Drives of RWTH-Aachen University, Aachen, Germany. In 2007, he started to pursue his PhD in Electrical Engineering in North Carolina State University. In the summer of 2008, he was a Co-op at Siemens Industry, Alpharetta, GA working on supplementary energy storage for high power mobile mining equipment. From September 2009- July 2010, He was visiting ABB corporate research center, Raleigh, NC where he was working on the utility applications of power electronics and energy storage. His research interests are high power electronics control and topologies and energy storage systems.

ACKNOWLEDGMENTS

First and foremost, I would like to express my sincere appreciation to my advisor, Dr. Subhashish Bhattacharya for his constant support and encouragement. Dr. Bhattacharya's deep knowledge and great enthusiasm have been very inspirational to my research and development at North Carolina State University. Dr. Bhattacharya taught me how to conduct research independently and think out of the box. I hope to be privileged to benefit from his mentorship and collaboration throughout my future career.

I am grateful to my committee members, Professor Mesut Baran, Dr. Srdjan Lukic, Dr. Aranya Chakrabortty, and Dr. Xiangwu Zhang for their valuable suggestions and helps. I would also like to thank Professor Alex Huang, whom I had the opportunity to work with during my early years of graduate studies.

It has been a great pleasure to work at the Semiconductor Power Electronics Center (SPEC) as well as the National Science Foundation funded Future Renewable Electric Energy Delivery and Management (FREEDM) Systems Center. Working in these premier research centers provided me with a special opportunity to collaborate with the brightest minds in power electronics. I would like to thank my colleagues Dr. Jinseok Park, Dr. Zhigang Liang, Dr. Xiahu Zhou, Dr. Tiefu Zhao, Mrs. Zhengping Xi, Mr. Daniel Fregosi, Mr. Sumit Dutta, Mr. Arun Kadavelugu, Mr. Gangyao Wang, Mr. Edward van Brunt, Ms. Misha Kumar, Mr. Behzad Nabavi, Mrs. Ghazal Fallahi, Mr. Vahraz Zamani and Mr Maziar Vanouni. I would like to especially thank my friends that I was pleased to work with, Mr. Hesam Mirzaee, Mr. Nima Yousefpoor, Mr. Seunghun Baek, and Mr. Saman Babaei.

During my graduate studies, I had an opportunity to work with the New York Power Authority, US ABB Corporate Research Center, and Siemens Mining Industries. I would like to thank my mentors for their support, Dr. Bruce Fardanesh, Dr. Waqas Arshad, Dr. Hongrae Kim, Dr. Sandeep Bala, and Dr. Joy Mazumdar.

I appreciate the assistance from the staff members of the SPEC, FREEDM Systems Center and the ECE department, including Mr. Rogelio Sullivan, Ms. Karen Autry, Ms. Colleen Reid, Mr. Hulgize Kassa and Mrs. Elaine Hardin.

Outside work, many friends made my days in beautiful Raleigh. I would like to thank all of them specially Mr. Behzad Aghdashi, Mr. Koroush Sasan, Dr. Arash Sahbaee, Mr. Amirhosein Norouzi, Dr. Reza Yaesoubi, Dr. Mahmoud Moradi, Dr. Nariman Moezzi, Mr. Morteza Ashouri, Dr. Maryam Mazloumpour, Mrs. Azadeh Nakhostin, Dr. Hamed Mojarrad, Mr. Ali Marjani, Mr. Mohammad Etemadrezaei, Mr. Mohsen Dehghan, Mr. Ramin Safavizadeh, Dr. Salman Mohagheghi, Dr. Mahyar Zarghami, and Mr. Farbod Jahanbakhsh.

My deepest appreciation goes toward my parents and family, Dr. Vila Shokouhian, Dr. Shapour Parkhideh, Dr. Sayeh Parkhideh, Dr. Sahar Parkhideh, Dr. Roya Parkhideh, and Dr. Hamed Ghodsi who have always encouraged me to pursue my goals.

Last but not least, I would like to thank my all-time partner, friend, and love, for her endless support and love. Sometimes, we were thousands of miles away from each other, but she stood strong and helped me to be strong. Thank you my love, *Nooshin Kiarashi*!

TABLE OF CONTENTS

LIST OF FIGURES ix
LIST OF TABLES xvii
Chapter 1. Introduction 1

1.1 Dissertation Scope 2

1.2 Dissertation Structure 2
Chapter 2. Vector-Controlled Voltage-Sourced Converter 5

2.1 Introduction 5

2.2 Background on Controlling the Voltage-Sourced Converter under Unbalanced Conditions 7
2.2.1 Single VSC Control under Unbalanced Conditions 7
2.2.2 BTB VSC Control under Unbalanced Conditions 11

2.3 Modeling of Voltage-Sourced Converter 13

2.4 Model Validation 16
2.4.1 BTB VSC Closed-Loop Functions 16
2.4.2 System Configuration 20
2.4.3 Simulation Results to Verify the Modeling and Control Functions 21

2.5 VSC-Based BTB System Operation under Power Line Faults with Existing Controllers 25

2.6 Resilient Operation of Vector-Controlled VSC-Based BTB HVDC Systems 29
2.6.1 Method I: Integrator Factor Control (IFC) 30
2.6.2 Method II: BackStepping Control (BSC) 33
2.6.3 Performance Comparison with the Proposed Control Structures 36

2.7 Generalized Controller for Back-to-Back Voltage-Sourced Converter under Power System Disturbance 42
2.7.1 Modified Back-Stepping Control (BSC) for BTB VSC Systems 42

2.8 Dynamic Performance Evaluation of BTB VSC Systems with the Proposed Generalized Control Architecture in RTDS 47
2.8.1 BTB VSC System for HVDC Applications 50
2.8.2 BTB VSC System for Drive (Wind) Applications 60
2.8.3 BTB VSC System for Transmission Transformer (Partial) Bypass 64

2.9 Summary 66

Chapter 3. Angle-Controlled Voltage-Sourced Converter 69

3.1 Introduction 69

3.2 Feasibility Study 75

3.3 Single Input Two Output (SITO) Feedback Systems 79
3.3.1 Introduction 79
3.3.2 Preliminaries 80
3.3.3 Plant and Controller Directions 82
3.3.4 Plant/Controller Alignment 83
3.3.5 Plant Direction vs. Frequency 84
3.3.6 Perfect Plant/Controller Alignment 86
3.3.7 Disturbance Rejection 87

3.4 Feedback System Design for VSC as a SITO Closed-Loop System 89

3.5 Verification of the Proposed SITO Control Structure for VSC 97
3.5.1 Unified Power Flow Controller 97
3.5.2 Point-to-Point BTB HVDC Applications 101
3.5.3 Discussion of Component Design in Angle-Controlled Converters 103

3.6 Summary 108
Chapter 4. Modular Transformer Converter 110

4.1 Background 110
4.1.1 Transformer Outages 115
4.1.2 Effect of New Intermittent Distributed Generation on Existing Assets 121

4.2 Towards Smart Transmission Substations 124
4.2.1 Controllable Transformers 125
4.2.2 Recovery Power Transformer 126
4.2.3 Phase Shifting Transformer (PST) 127
4.2.4 Unified Power Flow Controller (UPFC) 130
4.2.5 Power Flow Control at Transmission Substations 131

4.3 Substation Power Flow Controller Connecting Configurations 136
4.3.1 Shunt-Shunt Connecting Configuration - Substation Voltage/Phase Angle Controller 136
4.3.2 Series-Shunt Connecting Configuration – Substation Power Flow Controller 144
4.3.3 Series-Series Connecting Configuration – Dual Series Static Compensator 149
4.3.4 Comparison of the Proposed CSTC- and Conventional FACTS-Based Power Flow Controllers 151

4.4 Modular Transformer Converter (MTC) System 154

4.5 Dynamic Performance of MTC-Based CSTC 165
4.5.1 Shunt-Shunt Connecting Configuration – Substation Voltage/Phase Angle Regulator 165
4.5.2 Series-Shunt Connecting Configuration – Substation Power Flow Controller 169
4.5.3 Series-Series Connecting Configuration – Substation Power Flow Controller 170

4.6 Summary 186
Chapter 5. Supplementary Energy Storage and Advanced architectures for Grid-Connected High Power AC Multi-Motor Applications 189

5.1 Introduction 189

5.2 All-AC Drive System for High power Mobile Mining Applications 190

5.3 Front-End Converters for Mobile Mining Equipment 192

5.4 The Current State-of-the-Art Active Front End Performance for Mobile Mining Equipment 194

5.5 Supplementary Energy Storage System for Mobile Mining Equipment 200
5.5.1 Energy Storage Technology Selection 200
5.5.2 Energy Storage System Factors 203
5.5.3 Annuity Method to Select Energy Storage Technology 205
5.5.4 Energy Storage Properties and Assumptions 207
5.5.5 Energy Storage Comparison for High Power Mining Equipment 210

5.6 Ultracapacitor Integration into Existing Mobile Mining Converters 215

5.7 Hybrid Front End Configurations for High Power Multi-Motor Applications 219
5.7.1 Unidirectional Front End Converters 219
5.7.2 Hybrid Front End Converters 223

5.8 Summary 227
Chapter 6. Conclusions and Future Work 229

6.1 Conclusion of Present Work 229

6.2 Contributions 233

6.3 Future Work 235
Bibliography 239

LIST OF FIGURES

Figure 1-1. Example of VSC-based transmission. 1
Figure 1-2. Example of CSC-based transmission. 2
Figure 2-1. Simplified schematic of existing closed loop BTB VSC systems. 5
Figure 2-2. Bus voltage variations under normal and single-line-to ground fault in three phase abc-stationary and two phase dq-synchronous reference frames. 8
Figure 2-3. An Example of current state-of-the-art VSC controller under unbalanced conditions, 18. 10
Figure 2-4. Schematic of a voltage-sourced converter. 13
Figure 2-5. Conventional (Existing) BTB VSC-based HVDC system controller implementation. 17
Figure 2-6. Proposed BTB VSC-based HVDC system controller implementation. 17
Figure 2-7. BTB VSC system standby operation performance with a change in the reference DC link voltage from 250V to 220V. 22
Figure 2-8. BtB VSC system performance with a change in the reference reactive power command from -12 KVAr to +12 KVAr for the rectifier side and from +12 KVAr to -12 KVAr for the inverter side. 24
Figure 2-9. BtB HVDC system performance with a change in the reference active power command from zero to 10.8 KW while the rectifier and inverter sides provide -8.1 KVAr and +8.1 KVAr reactive power respectively. 25
Figure 2-10. Performance of the conventional VSC-based BTB system when a SLG fault occurs in the rectifier side. 27
Figure 2-11. Performance of the conventional VSC-based BTB system when a SLG fault occurs in the inverter side. 28
Figure 2-12. Proposed Integral Factor Control (IFC) structure for the DC link controller in VSC-based HVDC applications. 32
Figure 2-13. Proposed Back-Stepping Control (BSC) structure for the DC link controller in VSC-based HVDC applications. 35
Figure 2-14. DC link voltage performance comparison with the proposed controllers under a single line to ground fault. 37
Figure 2-15. Effect of the proposed controllers on the d-component of the current under a single line to ground fault. 38
Figure 2-16. DC link voltage performance comparison with the proposed controllers under phase reversal. 39
Figure 2-17. Effect of the proposed controllers on the d-component of the current under phase reversal. 40
Figure 2-18. Phase compensation effect of the proposed controllers under phase reversal. .. 41
Figure 2-19. Proposed backstepping control structure for the DC link voltage controller converter in a BTB VSC system. 46
Figure 2-20. Implemented proposed control structure in the synchronous frame to generate the reference vectors for the DC link voltage controller converter. 47
Figure 2-21. Real Time Digital Simulator (RTDS) facility at FREEDM Systems Center. 49

Figure 2-22. BTB VSC system for HVDC applications 51
Figure 2-23 Start-up dynamic performance of the BTB VSC system as in HVDC applications and unity power factor operation of 1 PU power under balanced conditions-RTDS results. 52
Figure 2-24. Dynamic performance of the BTB VSC system as in HVDC applications, changing power flow direction, with no change in reactive power reference under balanced conditions- RTDS results. 53
Figure 2-25. Performance comparison of the BTB VSC system with the proposed controller and commonly used control schemes for HVDC applications under an unbalanced condition of 50% single-line voltage sag in the power flow controller side (average model). 54
Figure 2-26. Dynamic performance of the BTB VSC system as in HVDC applications under an unbalanced condition of 50% single-line voltage sag in the power flow controller side- RTDS results. 55
Figure 2-27. Performance comparison of the BTB VSC system with the proposed controller and commonly used control schemes for HVDC applications under an unbalanced condition of 50% single-line voltage sag in the DC link voltage controller side (average model). 56
Figure 2-28. Dynamic performance of the BTB VSC system as in HVDC applications under an unbalanced condition of 50% single-line voltage sag in the DC link voltage controller side- RTDS results. 56
Figure 2-29. Performance comparison of the BTB VSC system with the proposed controller and commonly used control schemes for HVDC applications under an unbalanced condition of 50% single-line voltage sag in the DC link voltage controller side operated as an inverter (average model). 58
Figure 2-30. Dynamic performance of the BTB VSC system in HVDC applications under an unbalanced condition of 50% single-line voltage sag in the DC link voltage controller side operated as an inverter- RTDS results. 58
Figure 2-31. Performance comparison of the BTB VSC system with the proposed controller and commonly used control schemes for HVDC applications under an unbalanced condition of 50% in phase B and 90% in phase C voltage sag in the power flow controller side operated as the rectifier (average model). 59
Figure 2-32. Dynamic performance of the BTB VSC system in HVDC applications under unbalanced condition of 50% in phase B and 90% in phase C voltage sag in the power flow controller side operated as the rectifier- RTDS results. 59
Figure 2-33. Simplified BTB VSC system in drive (wind) applications. 61
Figure 2-34. Performance comparison of the BTB VSC system with the proposed controller and commonly used control schemes under an unbalanced condition of 50% single line voltage sag in the DC link voltage controller for the drive application operated at 30 Hz (average model). 61
Figure 2-35. Dynamic performance of the BTB VSC system in drive (wind) applications under an unbalanced condition of 50% single-line voltage sag in the DC link voltage controller side and drive side operates at 30Hz- RTDS results. 62

Figure 2-36. Performance comparison of the BTB VSC system with the proposed controller and commonly used control schemes under an unbalanced condition of 50% in phase B and 30% in phase C voltage sag in the DC link voltage controller for a drive application operated at 30 Hz (average model). 63
Figure 2-37. Dynamic performance of the BTB VSC system in drive (wind) applications under an unbalanced condition of 50% in phase B and 30% in phase C voltage sag in the DC link voltage controller side (grid) and drive side operating at 30 Hz- RTDS results. 63
Figure 2-38. BTB VSC system in hybrid power system as transmission transformer (partial) back-up for life extension of the transmission transformer or contingencies. 64
Figure 2-39. Performance comparison of the BTB VSC system with the proposed controller and commonly used control schemes under unbalanced condition of 90% voltage sage in phase A for hybrid power system applications (average model). 65
Figure 2-40. Dynamic performance of the BTB VSC system as in hybrid systems for transmission transformer (partial) back-up under unbalanced condition of 90% voltage sag in phase A- RTDS results. 66
Figure 3-1. General schematic of voltage-sourced converter. 70
Figure 3-2. A 24 pulse angle-controlled VSC. 71
Figure 3-3. Operating characteristics of angle-controlled VSC as STATCOM. 71
Figure 3-4. Output voltage vector construction in pulse-VSCs. 73
Figure 3-5. Reactive power transfer capability of the power system with constant active power. 75
Figure 3-6. DC link voltage steady state operating points vs. output voltage angle. 78
Figure 3-7. d-component of the current(representing the active power) steady state operating points vs. output voltage angle. 78
Figure 3-8. q-component of the current (representing the reactive power) steady state operating points vs. output voltage angle. 79
Figure 3-9. General Single Input Two Output (SITO) automatic feedback system. 80
Figure 3-10. Low bound on $\frac{\|T_o\|_\infty}{|T_I(0)|}$ 91
Figure 3-11. Plant (converter system) direction vs. frequency. 91
Figure 3-12. Alignment angles variations vs frequency. 93
Figure 3-13. Gain/phase plot of the input complementary sensitivity function. 94
Figure 3-14. Converter performance when it is controlled with just the output voltage angle. 95
Figure 3-15. Transient response of the angle-controlled VSC for a change in active power in rectifier mode. 96
Figure 3-16. Transient response of the angle-controlled VSC for a change in active power in inverter mode. 96
Figure 3-17. Transient response of the angle-controlled VSC for a change in reactive power. 97
Figure 3-18. Hybrid-controlled BTB VSC for power flow control. 98
Figure 3-19. 24-pulse shunt converter output voltage with angle control. 99

Figure 3-20. Substation transformer power flow dynamics with hybrid-controlled BTB VSC. 99
Figure 3-21. Operational performance (voltages) of the BTB VSC system as the power flow controller. 100
Figure 3-22. Angle-controlled BTB VSCs for HVDC applications. 102
Figure 3-23. Active power dynamic performance of the angle-controlled BTB VSC system. 102
Figure 3-24. Reactive power dynamic performance of the angle-controlled BTB VSC system. 103
Figure 3-25. DC link voltage dynamic performance of the angle-controlled BTB VSC system. 103
Figure 3-26. Theoretical load rejection capability of an angle-controlled VSC vs. interfacing inductance value for an active power reference of 1.5PU. 106
Figure 3-27. Dynamic performance analysis of the angle-controlled BTB VSC system to show the converter system disturbance rejection capability with interfacing inductance of 15% PU. 107
Figure 3-28. Dynamic performance analysis of the angle-controlled BTB VSC system to show the converter system disturbance rejection capability with an interfacing inductance of 50% PU. 108
Figure 4-1. Power interruption effects on power loss and number of affected customers. .. 111
Figure 4-2. Cost of power interruptions for U.S. customers in 2002..... 112
Figure 4-3. Wind and solar generation availability for selected countries. 114
Figure 4-4. US Midwest region wind generation capacity profile..... 114
Figure 4-5. Installation of power transformers base GVA per year additions in US..... 116
Figure 4-6. Transformer "Element-Initiated Only" sustained automatic outage data based on different transmission voltage levels. 118
Figure 4-7. Transformer other than "Element-Initiated Only" sustained automatic outage data based on different transmission voltage levels. 118
Figure 4-8. Transformer sustained automatic outage attributes-Outage Mode code. 119
Figure 4-9. Transformer sustained automatic outage attributes-Event Type. 120
Figure 4-10. US Transmission transformer (>200 kV) availability in 2010. 121
Figure 4-11. New generation effects on existing assets - wind generation, State level. 123
Figure 4-12. Alternative solution to reroute the power flow for new wind generator output (expensive solution, yet ineffective). 124
Figure 4-13. Recent advances in active transformers (simplified schematics) - not commercialized yet. 125
Figure 4-14. An example of an ABB polytransformer installation in Spain, 2005, 64. 127
Figure 4-15. Simplified circuit diagram of phase shifting transformer, 82. 129
Figure 4-16. Two phase-shifting transformers, 525kV, 650 MVA throughput power, angle variations =+/-24º, Siemens. 129
Figure 4-17. 2x100 MVA NYPA CSC at Marcy on 345kV Transmission lines. 131
Figure 4-18. IEEE 30 bus test system; it is less complex to install in substations rather than lines, 83. 132

Figure 4-19. Schematic of introduced power flow controller at substation. 134
Figure 4-20. Possible connecting configurations of the proposed power flow controller. ... 135
Figure 4-21. Flexible transmission controller frame with Modular Transformer Converter (MTC). 135
Figure 4-22. Representative schematic of MTC-based Convertible Static Transmission Controller (CSTC). 136
Figure 4-23. Two hardware-based asset management approaches for life time extension of a transformer under forced reduced operation and distorted power throughput. 138
Figure 4-24. Distributed CSTC application in normal forced reduced operation of transformers and distributed and aggregated CSTCs under contingencies on IEEE 30 bus mesh AC system. 138
Figure 4-25. Test system to analyze the CSTC in a shunt-shunt connecting configuration. 140
Figure 4-26. Vector analysis of the CSTC for shunt-shunt configuration operated as voltage/phase-angle regulator for transformer back-up as shown in Figure 4-25. 140
Figure 4-27. Shunt-shunt connecting configuration for supporting only reactive power injection to increase the transmittable power. 141
Figure 4-28. Range of active power through the transformer relative to the initial power, shunt-shunt configuration. 143
Figure 4-29. Relative PQ effective operating region of a shunt-shunt controller. 143
Figure 4-30. Vector analysis of the transformer power flow controller for a series-shunt configuration. 145
Figure 4-31. Example of a series-shunt option vector analysis for zero reactive power transfer. 146
Figure 4-32. MTC based CSTC test system values in series-shunt mode of operation in IEEE 30 bus. 146
Figure 4-33. Power flow model for the series-shunt connecting configurations. 147
Figure 4-34. MTC-based CSTC as the substation power controller in the IEEE 30-bus system. 147
Figure 4-35. Range of active power through the transformer relative to the initial power, series-shunt configuration. 148
Figure 4-36. Relative PQ effective operating region of the series-shunt controller. 148
Figure 4-37. Single phase equivalent circuit of MTC in series-series mode. 149
Figure 4-38. Vector analysis of transformer power flow controller for series-series configuration. 150
Figure 4-39. Test system to compare different modes of the CSTC and common FACTS. 152
Figure 4-40. P-Q operating characteristics with DSSC, UPFC, IPFC, and SSSC (*Natural Power Flow: P_0=0.9174 (pu), Q_0=0.0401(pu)*). 153
Figure 4-41. P-Q operating characteristics with DSSC, UPFC, IPFC, and SSSC (*Natural Power Flow: P_0=0.9248 (pu), Q_0=1.0351(pu)*). 153
Figure 4-42. P-Q operating characteristics with DSSC, UPFC, IPFC, and SSSC (*Natural Power Flow: P_0=0.9195 (pu), Q_0=-1.0099(pu)*). 154
Figure 4-43. 10~15 MVA IGCT based back-to-back three phase module. 157

Figure 4-44. An example of MTC based on three-level NPC MV drive converters- Medium Risk. 158
Figure 4-45. Single phase approaches for some transformerless integrations, more applicable for large transformers- High Risk. 159
Figure 4-46. Efficiency comparison of an MTC shown in Figure 4-44 with different semiconductor devices and controls (no passive filters). 161
Figure 4-47. Advanced angle-control structure for a VSC. 161
Figure 4-48, A 24-pulse angle-controlled VSC. 162
Figure 4-49. Generalized vector-control structure for VSC 162
Figure 4-50. Representative Modular Transformer Converter (MTC)-based systems (red lines indicate parallel integration and blue ones show series integration). 163
Figure 4-51. Representative voltage construction and scale-up in two series MTCs. 164
Figure 4-52. Control structure of the CSTC in the shunt-shunt mode of operation with an approximately constant substation power line. 167
Figure 4-53. Proposed control structure of the CSTC in the shunt-shunt mode of operation as a substation voltage/phase angle regulator. 168
Figure 4-54. PSCAD simulation results in per unit for the shunt-shunt mode of operation for transformer partial bypass or power flow control without changing the power system power flow shown in Figure 4-39. 169
Figure 4-55. PSCAD simulation results in per unit for the CSTC series-shunt mode of operation in the test system shown in Figure 4-39. 170
Figure 4-56.Active and reactive power Bode plot representation of the DSSC with operating points of P=1.0024, Q=0.02, and Id0=1.0026 PU (High current, high active power, and low reactive power case). 175
Figure 4-57. DC link voltage (V_{dc}^2) Bode plot representation of the DSSC with operating points of P=1.0024, Q=0.02, and Id0=1.0026 PU (High current, high active power, and low reactive power case). 176
Figure 4-58.Active and reactive power Bode plot representation of the DSSC with operating points of P=-0.0912, Q=-0.1986, Id0=0.2186 PU (Low current, low active power, and low reactive power case). 177
Figure 4-59. DC link voltage (V_{dc}^2) Bode plot representation of the DSSC with operating points of P=-0.0912, Q=-0.1986, Id0=0.2186 PU (Low current, low active power, and low reactive power case). 178
Figure 4-60.Active and reactive power Bode plot representation of the DSSC with operating points of P=1.0925, Q=1.8177, Id0=2.1208 PU (High current, high active power, and high reactive power case). 179
Figure 4-61. DC link voltage (V_{dc}^2) Bode plot representation of the DSSC with operating points of P=1.0925, Q=1.8177, Id0=2.1208 PU (High current, high active power, and high reactive power case). 180
Figure 4-62. Power flow controller inverter control structure of DSSC. 181
Figure 4-63. DC link controller inverter control structure of DSSC. 182

Figure 4-64. Dynamics of active power flow control in a DSSC under low reactive power loading..... 183
Figure 4-65. Dynamics of reactive power change in a DSSC under low reactive power loading..... 184
Figure 4-66. Dynamics of active power control in DSSC under high reactive power loading. 185
Figure 4-67. Dynamics of reactive power control in a DSSC under high reactive power loading..... 186
Figure 5-1. 24MW AC-drive dragline in an open-pit mine, 89. 190
Figure 5-2. An example of a 24MW AC-drive dragline deck plan, 87. 191
Figure 5-3. State-of-the-art high power AC drive system. 193
Figure 5-4. Example of a typical mining load profile. 193
Figure 5-5. Simplified synchronous frame-based controller implementation for staggered Active Front Ends (AFE). 196
Figure 5-6. Simulated 1.5MW shovel currents with two staggered AFEs. 197
Figure 5-7. Simulated 3MW shovel currents with four staggered AFEs. 198
Figure 5-8. Simulated PCC currents in the 24MW dragline with 32 staggered (11.25° degree) AFEs and 8 split DC link voltages. 200
Figure 5-9. Capital cost comparison of selected energy storage technologies, 94. 201
Figure 5-10. Energy density comparison of selected energy storage technologies, 94. 202
Figure 5-11. Efficiency comparison of selected energy storage technologies, 94..... 202
Figure 5-12. The factor influencing battery technology comparison. 204
Figure 5-13. An example of a cash flow diagram. 206
Figure 5-14. Cash flow model with multiple replacements. 206
Figure 5-15. Comparison of commercially available energy storage technology for a dragline. 211
Figure 5-16. Comparison of energy prices for selected energy storage technologies for a dragline. 211
Figure 5-17. Comparison of energy prices of selected energy storage technologies for shovels..... 213
Figure 5-18. Comparison of selected energy storage technologies for shovel. 214
Figure 5-19. Replacement of selected energy storage technologies for shovel. 215
Figure 5-20. Simulated dynamic performance of the 1.5MW shovel integrated with an ultracapacitor directly at the DC link. 217
Figure 5-21. Schematic of a multi-motor AC drive system integrated with an ultracapacitor with a separate DC/DC converter. 217
Figure 5-22. Example of an ultracapacitor module and a DC/DC converter suitable for mining applications. 218
Figure 5-23. Proposed control structure of the shovel converter system when the integrated DC/DC converter as shown in Figure 5-21 contributes to the drive DC link voltage control. 218
Figure 5-24. Simulated dynamic performance of the 1.5MW shovel integrated with ultracapacitors with a separate DC/DC converter as shown in Figure 5-21. 219

Figure 5-25. Unidirectional front end assisted with fractionally rated hybrid active filter integrated with ultracapacitor. 221
Figure 5-26. Simulated 1.5MW unidirectional front end assisted with hybrid active filter as shown in Figure 5-25. 222
Figure 5-27. Results of active filter controller hardware verification for a six-pulse diode bridge front-end. 222
Figure 5-28. Hybrid configuration for large multi-motor applications..... 223
Figure 5-29. Proposed control structure of hybrid front end architecture for large multi-machine systems including mining equipment. 224
Figure 5-30. Hybrid front end's PCC current as shown in Figure 5-28. 225
Figure 5-31. Frequency spectrum of load and PCC currents for the proposed hybrid configuration. 226
Figure 5-32. DC link dynamics of hybrid configuration- an example..... 226
Figure 5-33. Nominal PCC current (ph A) of the hybrid configuration with a two-thyristor bridge and one AFE as shown in Figure 5-28..... 226

LIST OF TABLES

Table I. Prototype BTB VSC System Parameters to Verify the Modeling 20
Table II. VSC BTB System Parameters with the Generalized Control Structure 50
TABLE III. Angle-Controlled System Parameters in P.U. 76
Table IV. High Power Mobile Mining System Parameters 196
Table V. Project Requirements for Integrating Energy Storage Systems 208
Table VI. Energy Storage Technology Properties-I 209
Table VII. Energy Storage Technology Properties-II 209
Table VIII. Energy Storage Technology Properties-III 209

Chapter 1. INTRODUCTION

The Voltage-Sourced Converter (VSC) is the preferred building block for Flexible AC Transmission Systems (FACTS) and utility-scale power electronics applications including High Voltage DC (HVDC) Transmission, Figure 1-1. Despite of advances in semiconductor technology, there are still many issues to address, including efficiency, reliability, availability, quality, and effectiveness of the utility power electronics. This PhD dissertation is organized to address these issues focusing on utility applications of power electronics using VSC technology. Currently, the most prominent application and outlook for VSC technology is (multi-terminal) HVDC transmission where traditionally Current-Sourced Converter (CSC) technology with line-commutated semiconductor devices is deployed, Figure 1-2.

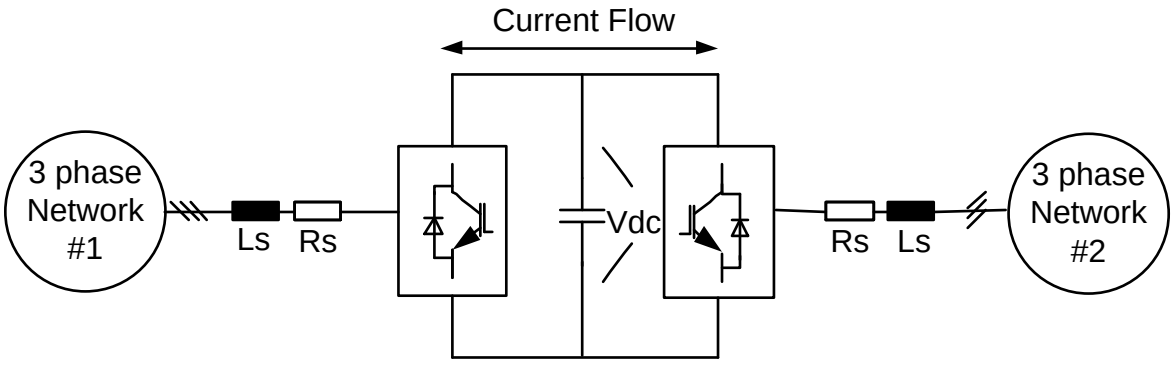

Figure 1-1. Example of VSC-based transmission.

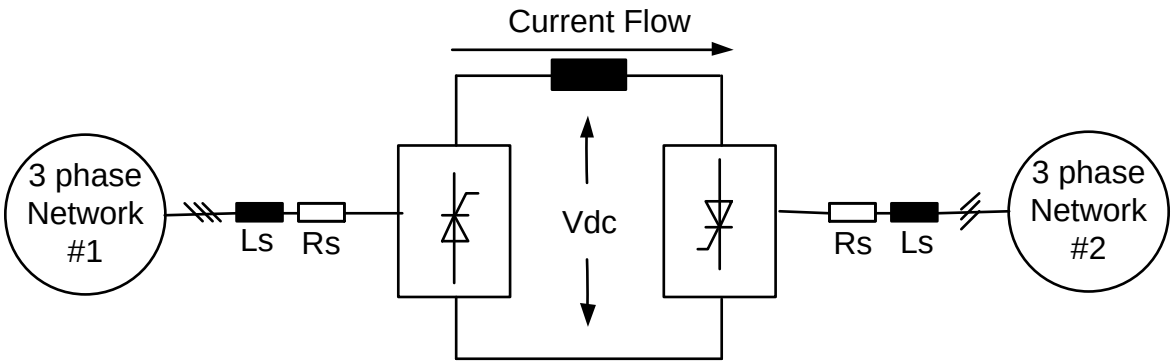

Figure 1-2. Example of CSC-based transmission.

1.1 **Dissertation Scope**

This dissertation is divided into two main parts. The first part deals with the problem of efficiency, reliability, availability, and quality of the converter (VSC) operation when they are installed in the grid. The proposed solutions are based on comprehensive modeling and analyzing the results which will be covered in Chapter 2 and Chapter 3. The second part, Chapter 4 and Chapter 5 of this dissertation offers some unique applications and architectures for which VSC is deployed. With the help of the knowledge gained in the first part, the proposed system benefits from high efficiency, high availability, and potentially low cost.

1.2 **Dissertation Structure**

Chapter 2- examines the vector-controlled or PWM-(Pulse Width Modulation) based VSC for transmission applications and presents detailed modeling of this type of converter.

In particular, resilient operation of the converters under power system disturbances is proposed, considering the rating and low switching frequency operation of the converters.

Chapter 3 introduces the active power transfer capability of VSC through the angle control structure. This chapter provides a design framework that enables the high power high voltage VSC to operate at line frequency with a superior harmonic spectrum.

Chapter 4 introduces the Modular Transformer Converter (MTC) which is the building block for a versatile and transportable transmission controller. Several MTCs can be arranged to form a Convertible Static Transmission Controller (CSTC). The proposed transmission controller can perform several functions including power flow control for renewable resources transmission and transformer back-up for disaster management or life extension purposes. This structure has several advantages in comparison with conventional FACTS controllers, one of which is modularity for manufacturers and utilities using standard high power electronic systems. In addition, different connecting configuration options with different functions can be obtained in the transmission controller with MTC structures. These features allow them to be deployed dispersed or aggregated to meet power, voltage, VAR and configuration requirements.

Chapter 5 proposes the utilization of supplementary energy storage in high power mining equipment for which the building block is the vector-controlled VSC system. This dissertation shows that despite the economical values of a particular energy storage technology, each technology suffers greatly from other factors such as large volume. For instance, the ultracapacitor is significantly heavier and bulkier than lithium-ion batteries for mining applications. On the other hand, the ultracapacitor exceeds other technologies in

terms of the required number of replacement units over the life time of the mining equipment. Consequently, this dissertation proposes that the enabling technology for energy storage integration for mobile mining equipment will be front end converters with higher power density than the current state-of-the-art technologies.

Chapter 6 presents the conclusions of the present work and offers future work and research paths that can be taken from the opportunities that this dissertation has identified.

Chapter 2. VECTOR-CONTROLLED VOLTAGE-SOURCED CONVERTER

2.1 Introduction

It is desirable to have high power high-voltage electronics based systems available during power system faults when they may be needed the most. If the protection measures trip the converter system it can take several fractions of an hour, depending on the size of the converter, to discharge the DC link and check the healthiness of the whole system. Hence, several practical methods have been proposed and implemented to keep a system running under power system faults and disturbances, 1-2.

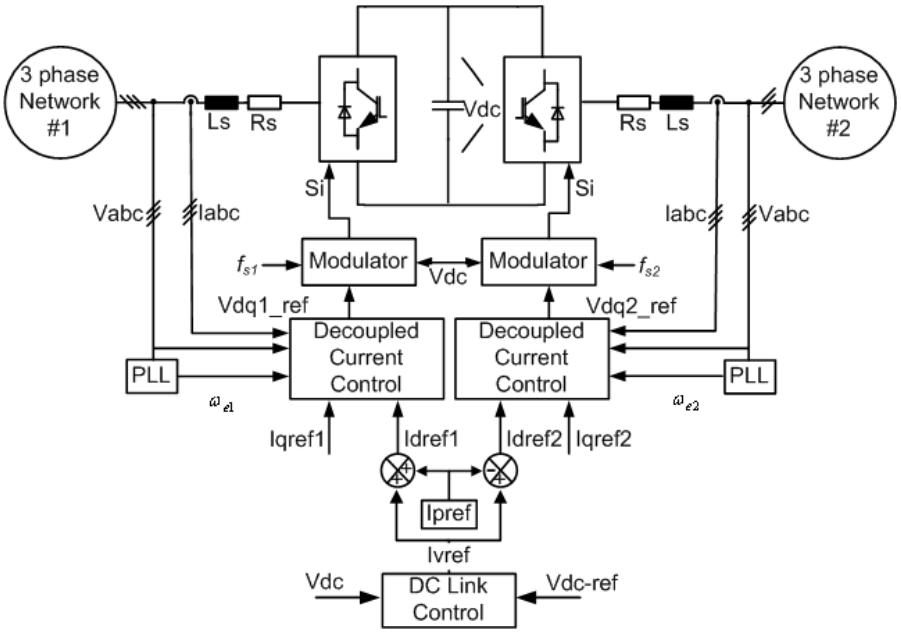

Figure 2-1. Simplified schematic of existing closed loop BTB VSC systems.

Today, the most promising market for HVDC technology is interconnection of the networks where the centers of the loads are located far from the points of connection. The problem of AC systems arises as the phase angle drifts and varies over a wide range of angles with daily load changes, 3. This phenomenon especially in a weak network along with the power line faults endangers the operation of HVDC systems. A voltage-sourced converter is the main building block for FACTS devices and as of today, HVDC technology up to about 1 GW. The increasing emergence of VSC-based transmission is the result of development in semiconductor devices, power electronic circuits, control, and executive engineering, 4-6. Previously, the lack of these developments had prohibited this technology from being the first choice. While each development is moving forward individually, the result of each one influences the design criteria and application requirements of the system. However, generally, the less dependence on power semiconductor characteristics amounts to having more supplier possibilities for VSC-based transmission. The most important limiting factor of power semiconductors is their switching properties since they are usually optimized for the conduction intervals. Hence, high power electronic converters are desired to operate with relatively low switching frequencies (max 9~15 times the line frequency, and even lower for multilevel converters). Low switching frequency operation of the VSC systems imposes control limitations in case of power system faults and disturbances when they may be needed the most. To the best of the author's knowledge, in the practiced FACTS and HVDC projects, the ride-through capability is obtained either by proper passive elements design, 7-8 or a change in the control mode, 1. On the other hand, with emerging high power applications such as 10MW wind generation turbines, 9 or transportable recovery

transformers, 10 the dynamic operation of the VSC under power system disturbances must be revisited. This dissertation proposes an alternative control framework to obtain robust DC link voltage with specific attention to designing the DC link controller VSC in a Back-To-Back (BTB) configuration which is different from existing control structures as shown in Figure 2-1. The proposed controller is implemented in the commonly used dq-synchronous frame without sequence extraction.

2.2 Background on Controlling the Voltage-Sourced Converter under Unbalanced Conditions

2.2.1 Single VSC Control under Unbalanced Conditions

The voltage-sourced converter is the main building block for FACTS devices and, as of today HVDC technology up to about 1 GW. Therefore, the study on the methods to improve the converter performance as a single system under network unbalanced conditions is unavoidable. The theory of instantaneous active and reactive power for three phase switching converters control was proposed by Akagi *et al.*, 11. It has been shown that the power quality in terms of current harmonics and reactive power can be improved using the instantaneous reactive power definition. The work of 12 and 13 showed that network voltage imbalances cause input current distortions which can transfer to the DC side due to the negative sequence component of the voltage. An example of negative sequence appearance in the positive sequence dq-synchronous frame is shown in Figure 2-2.

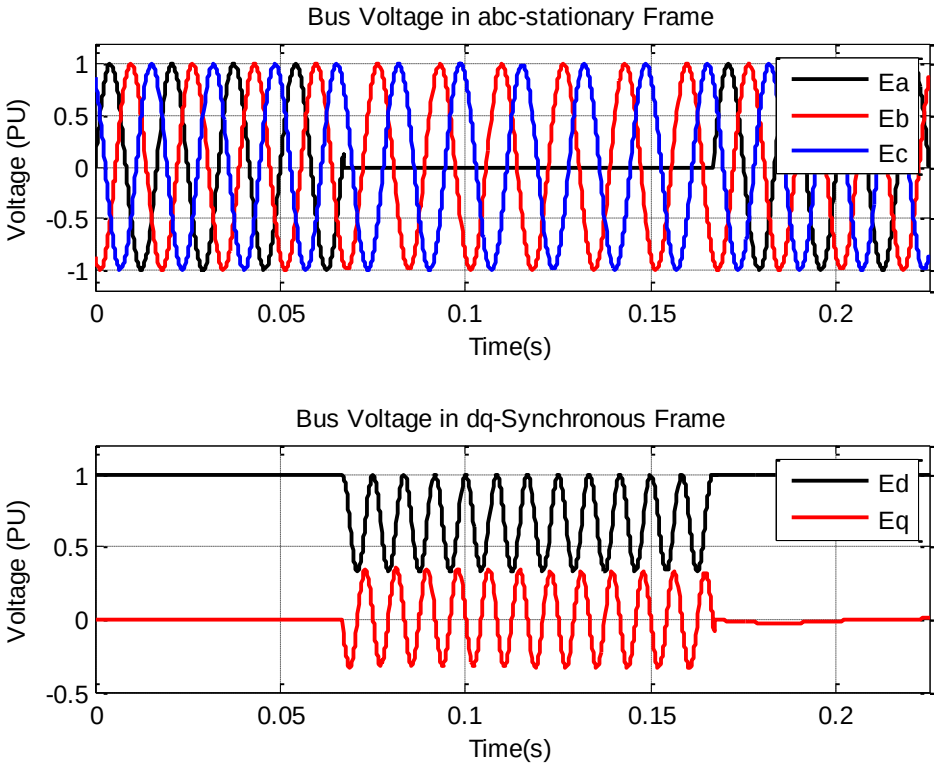

Figure 2-2. Bus voltage variations under normal and single-line-to ground fault in three phase abc-stationary and two phase dq-synchronous reference frames.

Rioual *et al.* in 14 probably proposed the very first control scheme for the VSC that regulates the instantaneous power generated under network voltage dips. Their work of 14 is mainly generated current references in both positive and negative synchronous references to regulate the power at the PCC. Since then researchers have been developing "enhanced" control schemes mostly to minimize input harmonics which is coupled to DC link voltage ripples. For instance, Stankovic *et al*, 15 presented a model that can eliminate the harmonics for generalized unbalanced conditions. However, this method needs a great deal of computations steps for DSP-based control. In 16 and 17, authors consider the instantaneous

power at the converter poles not the PCC and consequently obtain better harmonic responses. Although these methods are more effective than the work of 14 and relatively simpler than that of 15, the proposed methods suffer from solving nonlinear equations in real time and low bandwidth of the current regulator due to the extraction of the current sequence components. Suh *et al.* continued their work 18 which resulted in a hybrid synchronous stationary frame with oscillating reference currents, as presented in Figure 2-3. Consequently, the bandwidth-diminishing functions are avoided. They also proposed a simplified current reference generator that can be implemented more easily than that of 16 and 17. It is of interest that in 16-18 the instantaneous reactive power definition is different from "classical" notion of outer products of vectors presented in 11. Instead, these authors mainly employed the work of 19 in which the authors developed the so-called "extension PQ theory" to resolve the singularity issues existing in the work of 11 for the generalized unbalanced conditions. Accordingly, the instantaneous reactive power is re-defined on the basis of a set of voltages that lag the pole voltages by 90° and is not the imaginary part of the complex power. Despite satisfactory operation of a three phase rectifier under unbalanced conditions, the proposed scheme in 18 requires several feedback and feedforward compensators. A simplified controller is proposed in 20 which uses a stationary current controller (resonant compensator) that considers both positive and negative sequences simultaneously. Notch filters tuned at 120°, 21 are nonetheless used to extract the bus voltage sequences for current reference generation. In 22, authors also consider notch filters but to separate the positive and negative sequence current controllers. One potential constraint of these methods is emerging of 3^{rd} harmonics in the input current that is proportional with the voltage dip. The very recent work

as of today is reported in 23 which has implemented the whole control frame in the stationary frame resulting in a new current reference generator. Fast dynamic performance with small DC link voltage ripple in a 20 kVA/10 kHz PWM prototype converter under 30% supply voltage dip is reported. A nice feature of the scheme is that no PLL strategies are needed but constant line frequency is assumed and sinusoidal compensators as 18 are deployed due to the control logic of the oscillating references.

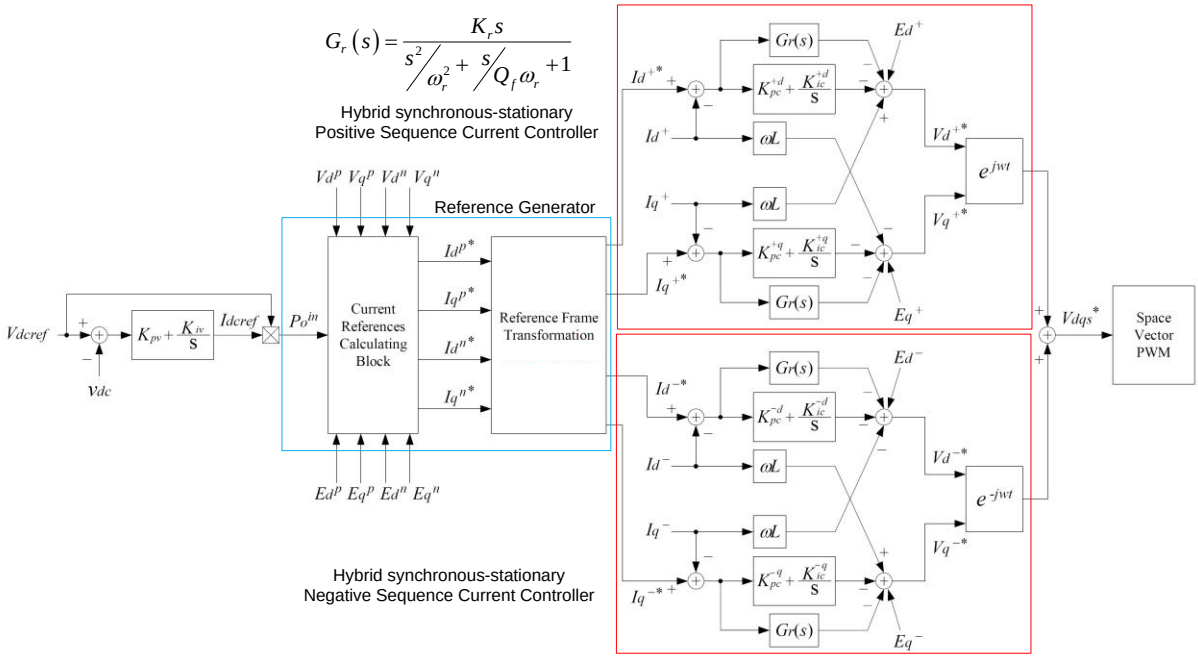

Figure 2-3. An Example of current state-of-the-art VSC controller under unbalanced conditions, 18.

2.2.2 **BTB VSC Control under Unbalanced Conditions**

The transmission level multi-VSC option requires a careful consideration of system interactions while switching frequency is kept relatively low (9~15 times the line frequency). An example of this theme is investigated for a Unified Power Flow Controller (UPFC) in 24 where additional compensating terms are added to reduce or remove the interactions of rectifier and inverter. The interaction has been highlighted as one of the potential issues of BTB VSC system operation with conventional controllers applied to single VSCs, 25. This fact is more critical under power system faults since the controllers introduced before should take these interactions into account. Therefore, simply separating sequence controllers may not achieve the desired performance due to the system coupling, filtering delays, etc. To solve these problems 25 introduced a framework which mainly used the results of 14 and 26. Xu et al. in 25 propose to nullify the oscillating power as in 14 by generating a current reference. In addition, 25 considers the improved "cross coupling control" mentioned for UPFC in 26. This control scheme was first proposed for UPFC applications in 27 where authors showed that the crossing-gain of a transmission line is much larger than its direct-gain. The cross-coupling controller uses the q-axis voltage vector, to control the d-axis current and the d-axis voltage vector to control the q-axis current. Numerical results in 25 illustrate the satisfactory performance under a single-line-to-ground fault but with more than double the rated current. The latter one is important in VSC HVDC transient dynamics. It has been pointed out in 28 that increase of the current limit significantly improves the power quality of the system. Yazdani *et al.* mention in 29 that it is possible to suppress the DC link

voltage oscillations by using the notch filter approach; therefore, the same issues exist as for a single VSC. For a specific voltage-sourced converter BTB HVDC system, Hagiwara *et al.*, 30 proposes a unique DC link control structure that has the load feedforward term. With the proposed structure a robust DC link voltage is achieved if the fault occurs in the inverter side. It has been shown that load estimation can improve the converter performance. In fact, 31 had shown that adding the load estimation into the main controller better attunes the DC link voltage to load power change attuned more. Parkhideh *et al.* 32 also showed how it is possible to remove the varying load effect from a closed loop large mining converter control system (1.5-24 MW) which is basically a BTB VSC system.

On the other hand, there are emerging interests to have medium voltage interfaces for renewable integration such as wind generation, currently up to 10 MVA with direct drive technologies (BTB VSC), 9. Authors of 33 have presented a unique controller in the stationary frame for direct drive wind generation systems that is based on reactive power compensation. Applying the proposed method insures balanced grid currents even under power system faults. Nonetheless, due to possible low speed operation of wind turbines, DC link dynamics have been addressed as one of the key factors which affect the operation of the turbine, 34. Therefore, more investigations are essential to determine the proper control strategy; balanced currents or a stiff DC link voltage.

This dissertation proposes control structures specifically for the DC link controller converter in the BTB VSC system which is implemented in a single synchronous frame without any sequence extraction or resonant compensator. It will be shown that DC link dynamics are coupled to the interaction imposed by the inverter performance. On the other

hand, there is no direct control input that can remove this interaction or disturbance with conventional frequency oriented controller design. This work introduces a commonly used dq-synchronous-based framework to design a more robust controller for relatively low switching frequency (9~15 times) PWM or vector-controlled BTB VSC systems.

2.3 **Modeling of Voltage-Sourced Converter**

The modeling of voltage-sourced converter, the building block of the BTB system is coming mainly from Middlebrook's work stated in many literatures such as 35. This modeling is based on the principal circuit analysis writing voltage and current equations for storage elements known as state equations. The general schematic of a three phase voltage-sourced converter circuit is shown in Figure 2-4 and the state equations of a VSC in the three phase stationary coordinates are as follows:

$$\frac{dI_{abc}}{dt} = -\frac{R_s}{L_s} I_{abc} + \frac{E_{abc}}{L_s} - \frac{V_{abc}}{L_s} \tag{2.1}$$

$$\frac{dV_{DC}}{dt} = \frac{I_{DC}}{C_{DC}} - \frac{V_{DC}}{R_p C_{DC}} - \frac{P_{load}}{C_{DC} V_{DC}} \tag{2.2}$$

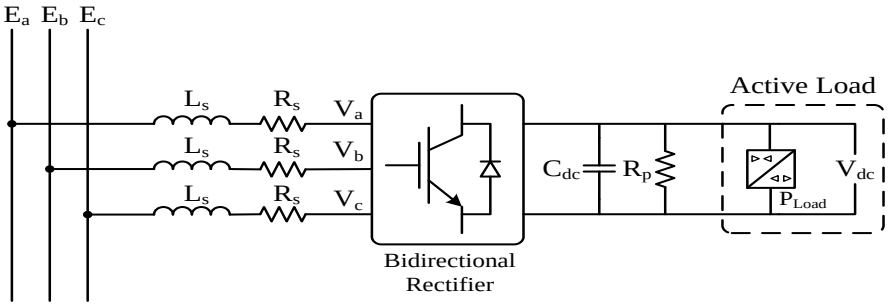

Figure 2-4. Schematic of a voltage-sourced converter.

In order to benefit all decoupling and constant properties of a two phase system instead of a three phase one, dq- transformation is considered to convert all quantities in the abc-stationary coordinate frame to the synchronous reference frame.

$$\frac{dI_d}{dt} = -\frac{R_s}{L_s} I_d + \omega I_q + \frac{E_d}{L_s} - \frac{V_d}{L_s} \tag{2.3}$$

$$\frac{dI_q}{dt} = -\frac{R_s}{L_s} I_q - \omega I_d + \frac{E_q}{L_s} - \frac{V_q}{L_s} \tag{2.4}$$

In (2.3) and (2.4), V_d and V_q are the converter output voltages in the synchronous frame. The modulation index can be also written in this frame as (2.5), where k depends on the modulation technique. In this work, we use the vector control method denoted by Schauder *et al.* in 7.

$$m_d = \frac{V_d}{kV_{DC}} \qquad m_q = \frac{V_q}{kV_{DC}} \tag{2.5}$$

In many literature sources, especially for DC/DC converters, the modulation index is used as the control input; therefore, (2.3) and (2.4) present the non-linear system. DC link dynamics are also non-linear by introducing the definition for I_{DC} as (2.6). However, by considering V_d and V_q as the control inputs, those equations, (2.3) and (2.4), can be treated as linear ones. Also, power balance is used to derive the equation for the DC link voltage, neglecting the interface losses as in (2.7). E_a (the PCC phase-A voltage) is aligned with the *d*-axis in the synchronous frame. The result of DC link dynamics shown in (2.7) is linear as

long as E_d and E_q are constant. Consequently, no linearization around specific operating points is needed and the small-signal VSC model looks similar to the large-signal model. The state-space representation of the VSC can be obtained from (2.3), (2.4), and (2.7). From what has been mentioned, the matrix form of the state space equations can be represented as (2.8) and (2.9), where x(t) is the state variable vector, u(t) is the input vector and e(t) is considered as the disturbance vector, (2.10)[1].

$$I_{DC} = \frac{3}{2}\left(m_d I_d + m_q I_q\right) \tag{2.6}$$

$$\frac{dV_{DC}^2}{dt} = \frac{3E_d I_d}{C_{DC}} + \frac{3E_q I_q}{C_{DC}} - \frac{2V_{DC}^2}{R_p C_{DC}} - \frac{2P_{load}}{C_{DC}} \tag{2.7}$$

$$\dot{x}(t) = Ax(t) + Bu(t) + Ke(t) \tag{2.8}$$

$$y(t) = Cx(t) + \underline{0} \cdot u(t) \tag{2.9}$$

$$\mathrm{x}(t) = \begin{pmatrix} I_d \\ I_q \\ V_{DC}^2 \end{pmatrix},\ \mathrm{u}(t) = \begin{pmatrix} V_d \\ V_q \end{pmatrix},\ \mathrm{e}(t) = \begin{pmatrix} E_d \\ E_q \\ P_{load} \end{pmatrix} \tag{2.10}$$

Although there is a possibility of using the so-called Instantaneous PLL (IPLL) presented in 38 to discard the effect of the q-component of the voltage vector even under unbalanced conditions (at least in the model), this work considers common PLL structures in order to unify the problem.

[1] Notation remark: No linearization has been made for the state-space representation of the converter system under normal and unbalanced conditions. Hence, the time dependence notation of the variables in (8) has been eliminated for the sake of ease of presentation.

2.4 Model Validation

2.4.1 BTB VSC Closed-Loop Functions

Currently, in most of the literature the BTB VSC system is designed and seen as a single device, hence the two sides support the DC link. The detailed VSC-based BTB HVDC converter system is depicted in Figure 2-5. While the private power system model suggests that the consumer parties should bid and pay for only the portion they acquire, the available correct models usually ignore this practical fact. It should be noted that DC link variations are mainly due to converter losses and transient operation of the system. Therefore, in this work, the one-sided DC link voltage controller shown in Figure 2-6 is proposed. The summary of controller function is divided in two parts:

- The rectifier side which should supply or provide active power while it can support its side reactive power.
- The inverter side which absorbs or acquires active power from the supplier while it can support its side reactive power as well.

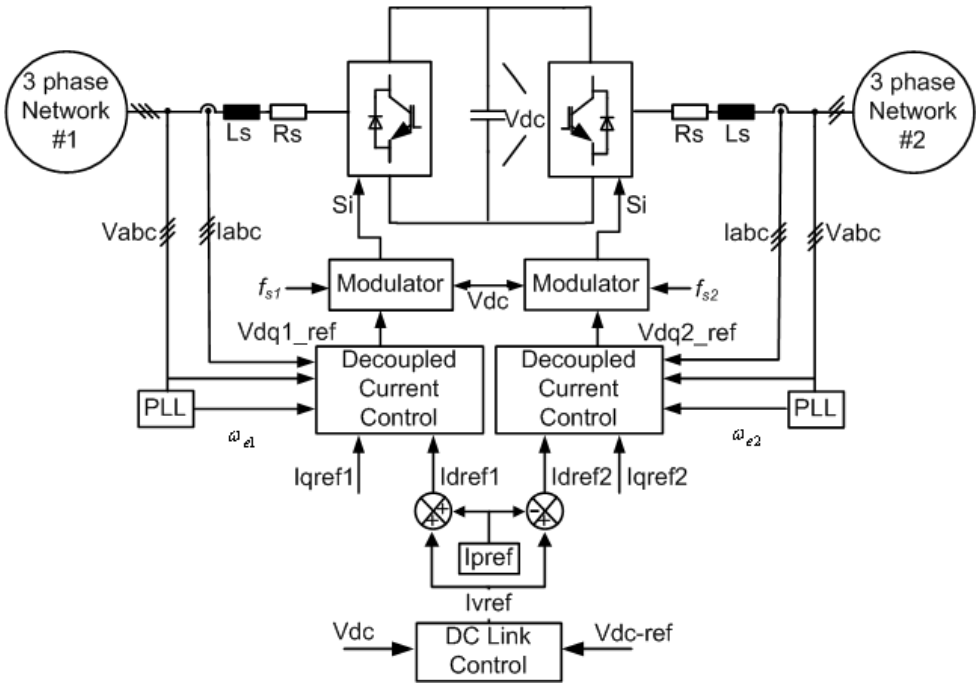

Figure 2-5. Conventional (Existing) BTB VSC-based HVDC system controller implementation.

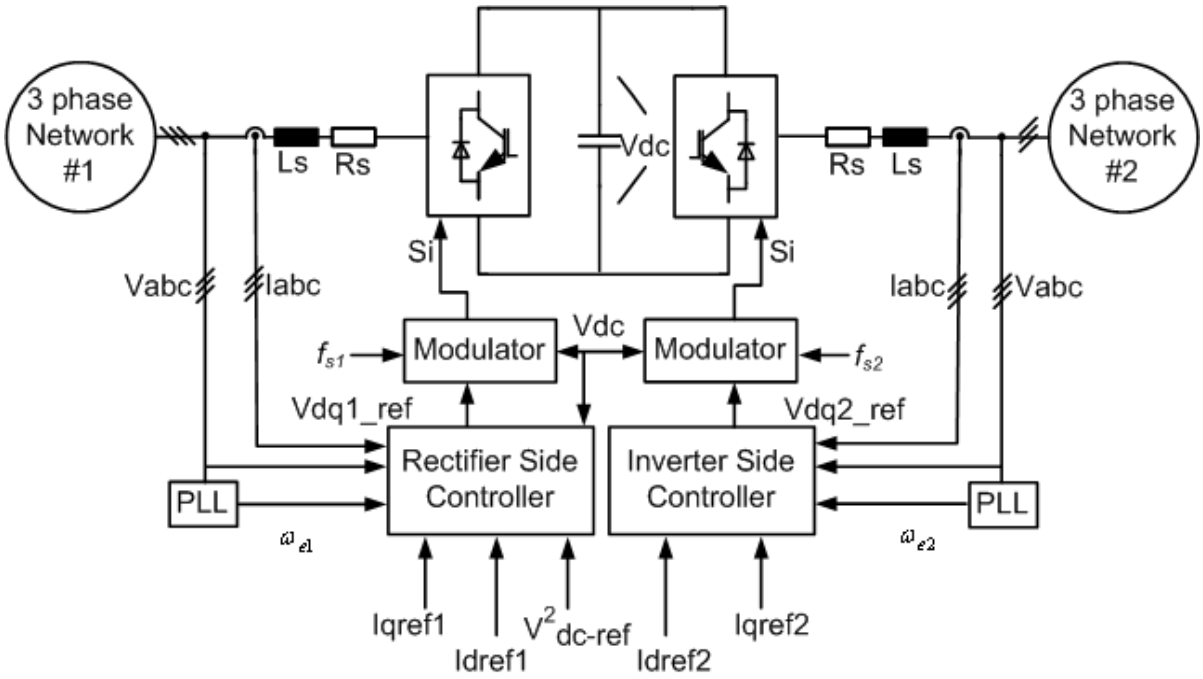

Figure 2-6. Proposed BTB VSC-based HVDC system controller implementation.

To design a closed loop system, the eigenstructure assignment or any linear feedback design method can be used to place the poles at the desired locations. Eigenstructure assignment is explained for STATCOM in 39 and this method is extended to BTB VSC systems to develop the general controller.

The control input can be determined based on the matrix network of (2.11). *F* is the state feedback matrix, which should be designed based on the response time according to the eigenstructure. Matrix *T* for external input access and Matrix *M* for disturbance rejection purposes are assumed.

$$u(t) = -Fx(t) + Ty_{ref}(t) + Me(t) \tag{2.11}$$

It is appreciable that the VSC-based converters are now designed based on decoupled current controllers. This happens with considering the small portion to be compensated with PI compensators or variable change algebraic manipulation mentioned in 41. The decoupled controller with state feedback, however, is a straightforward procedure. The closed loop output transfer function matrix is in the form of (2.12). Therefore, some of the elements of matrix *F* can be assigned such that the output matrix becomes diagonal or the selected states do not influence a particular output.

$$G_{cl}(s) = C\left(sI - A + BF\right)^{-1} B \tag{2.12}$$

To have a zero steady state error, unity feedback of the output is needed. This fact combined with having external output references leads to a design for matrix *T* as in (2.13). The same analogy can be applied to design the *M* matrix for disturbance rejection. In other

words, inclusion of Matrix *M* eliminates the effects on steady state quantities while the dynamic performance of the system is taken over by other elements as well. Therefore, matrix *M* is the solution of (2.14); in the case of no specific solution the generalized limit criteria can be used.

$$T = G_{cl}^{-1}(0) \tag{2.13}$$

$$G_d(0) = C\left(-A + BF\right)^{-1}\left(BM + K\right) = \underline{0} \tag{2.14}$$

The objective of the controller for the rectifier side is to keep the DC link voltage at the desired level to support the required active and reactive power commands. According to the system equations, the mode associated with the q-component of the current can be adjusted based on the AC side interface parameters and required response time. The V_{DC}^2 state consists of the modes associated with two eigenvalues. One of the system poles affects the charging and discharging of the capacitor, λ_c. This eigenvalue should be placed near the origin to avoid high charging or discharging currents. The other pole can be placed as for the reactive current component, λ_i. It should be noted that the poles associated with the current mode can be placed as far as the inherent delay of the converter modeling allows; current regulators often present a fast first order behavior. To achieve a non-oscillatory output response, it is sufficient to place the poles at the real axis. Consequently, the DC link voltage regulator can be designed based on the system specifications and requirements.

The inverter side of the proposed controller is assumed to be the active power consumer which is able to supply its side reactive power demand as well. Since the DC-link dynamics are taken over by the supplier side, there is no need to include them into the consumer side,

which is the inverter. This fact simplifies the state-space model of the VSC. The three dimensional input space of the previous section is reduced to two dimensions for the inverter side. In other words, the rectifier system theoretically should provide the required current demand to the consumer side no matter how the DC-link behaves. This fact makes the power transactions more robust and reliable under which the load demand is met.

2.4.2 **System Configuration**

To evaluate the proposed controller a prototype system has been designed whose parameters are tabulated in Table I. It is intended to operate the system at a low switching frequency (9~11 times of the line) to not only reduce the switching losses but also ensure the reliable operation of the semiconductor switches.

It should be also mentioned that system operation modes can be implemented easily in today's digital control apparatus. Therefore, every converter can be reconfigured to work as either a rectifier or an inverter in the order of the signal processor's delay.

Table I. Prototype BTB VSC System Parameters to Verify the Modeling

Line-to-line voltage	E	110 V
Line frequency	F	60 Hz
Leakage inductance	L_s	15%
DC link voltage	V_{DC}	250 V
DC link capacitance	C_{DC}	2 mF
Rated power	S	13.5 kVA
Switching frequency	f_s	540 Hz
Converter loss resistor	R_P	154 Ω (3%)
Current controller pole location	λ_i	-1000
Voltage controller pole location	λ_c	-250

2.4.3 **Simulation Results to Verify the Modeling and Control Functions**

Switching and average models are implemented in a Matlab/Simulink environment. These two different approaches are compared for each case study to evaluate the new linear modeling of the system and its proposed controller.

The standby mode operation performance of the BTB HVDC system is shown in Figure 2-7. The DC capacitor is pre-charged to 200V through the freewheeling diodes then the converter is turned on at t=0 s while the power reference commands are kept at zero. At t=0.025 s a step change in the DC link voltage is applied and the system response is observed. The Id change of the supplier side at the transient periods is unavoidable since it is needed to either charge or discharge the capacitor based on the demand; however, the controller should be able to limit the response within the converter rating. The initial conditions could be adjusted analytically to excite only the particular modes of the system, but the result is shown without considering this fact which may not be practical. It can be also seen that the DC link voltage has no oscillatory behavior due to the pole placement at the real axis. The system states response time in this simulation is shown intentionally equal to the system currently implemented with improved performance in terms of damped waveforms. The controller is capable of achieving faster response time.

The difference between the switching model and the average model is hardly observable, which proves that the methods functions in the standby mode under both transient and steady state conditions.

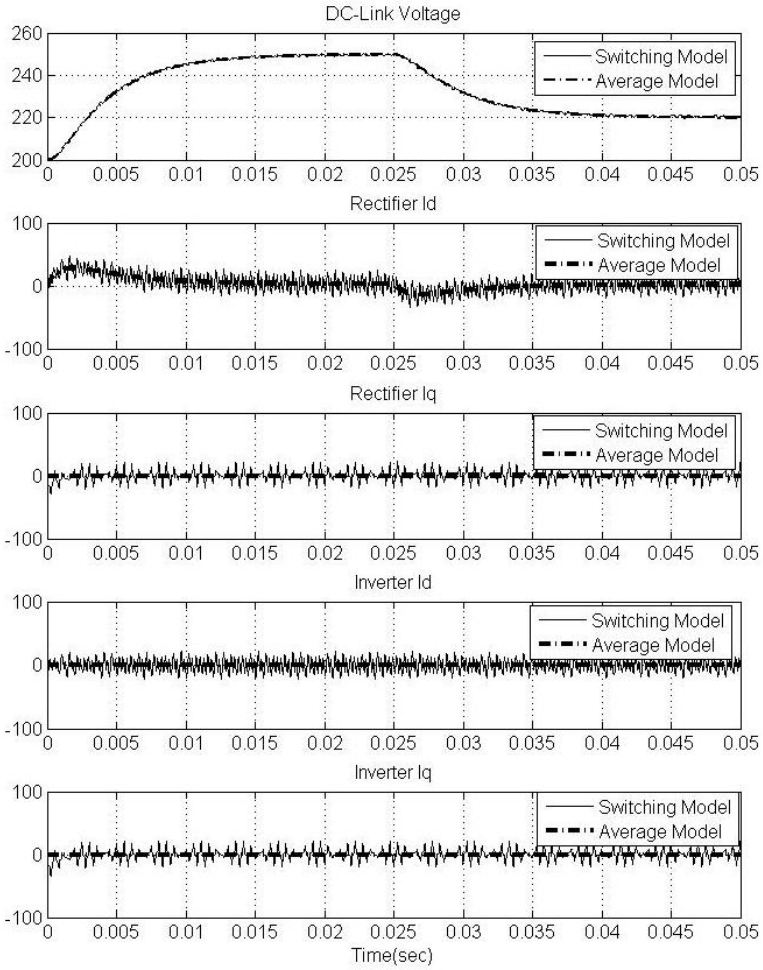

Figure 2-7. BTB VSC system standby operation performance with a change in the reference DC link voltage from 250V to 220V.

The operational performance of the system under a reactive power supply is presented in Figure 2-8. The performance is observed at the same initial conditions as before. Each converter now supplies its own system's reactive power demand for instance, to regulate the bus voltage at each respective power system. The rectifier side starts to provide 12 KVAr capacitive reactive power at I_q=-90 A whereas the inverter side provides 12 KVAr inductive reactive power at *Iq*=90 A. It can be seen that while the DC-link voltage ramps up to its

reference value, the demand current requirement is met much faster as designed. The operation is altered at t=0.025s as the reactive power transfer is reversed from 12 KVAr capacitive to 12 KVAr inductive for the rectifier side and vice versa for the inverter side.

The main validation of the model should be proved for the active power transfer. Figure 2-9 shows the operational performance of the BTB HVDC system where the 10.8 KW power (I_d=80 A) is transferred from the main to the consumer. In this simulation it is also shown that while the active power is transferred, each converter can provide either capacitive or inductive reactive power for its respective power system as long as it does not exceed the converter rating. The amount of reactive power is 8.1 capacitive KVAr (I_q=-60 A) for the rectifier side and 8.1 inductive KVAr (I_q=60 A) for the inverter side.

From the results shown in this section it can be seen how well the average model based on the mathematical approach corresponds to the switching model. This correspondence verifies and validates the HVDC system modeling and the proposed controller function.

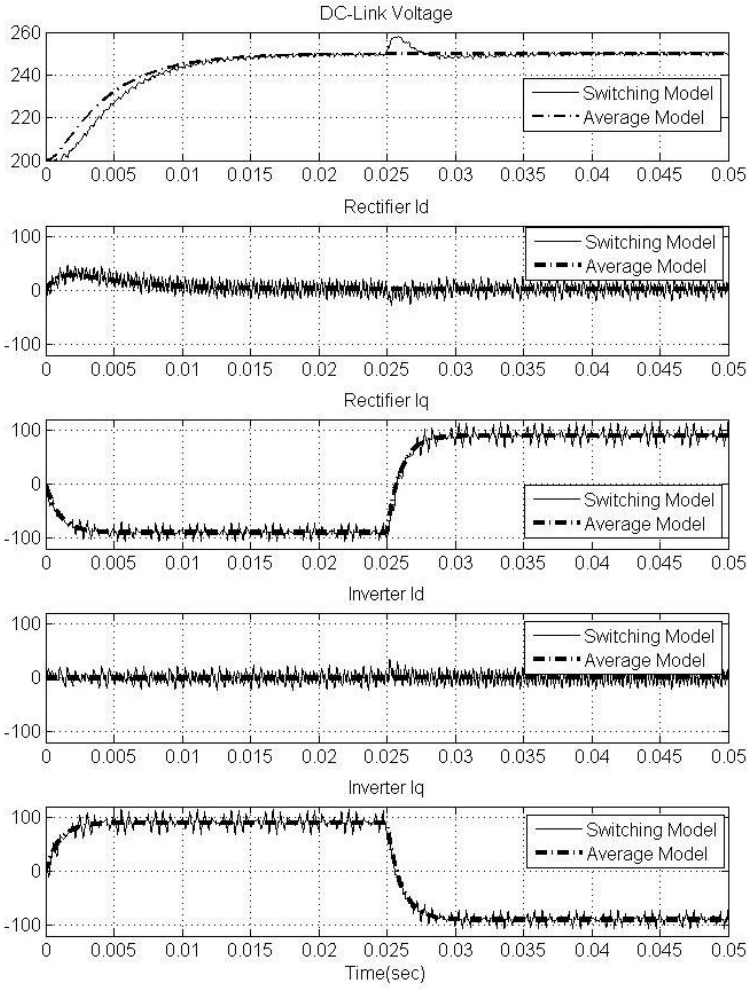

Figure 2-8. BtB VSC system performance with a change in the reference reactive power command from -12 KVAr to +12 KVAr for the rectifier side and from +12 KVAr to -12 KVAr for the inverter side.

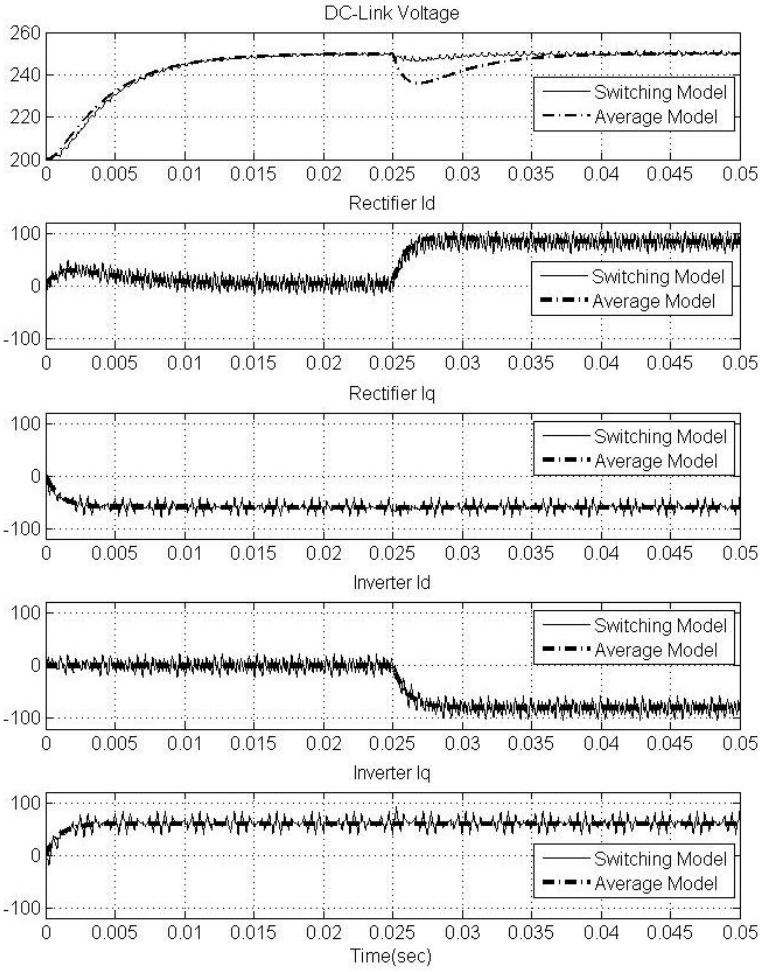

Figure 2-9. BtB HVDC system performance with a change in the reference active power command from zero to 10.8 KW while the rectifier and inverter sides provide -8.1 KVAr and +8.1 KVAr reactive power respectively.

2.5 VSC-Based BTB System Operation under Power Line Faults with Existing Controllers

One of the main desirable objectives of the controller is to have a decoupled performance while a fault occurs. The validity and precision of the proposed VSC based

BTB HVDC control system was examined in Section 2.4; now, the performance of the system under common power line faults is considered.

The single line to ground fault case is implemented by making the voltage of phase A go to zero at the main bus. This fault occurs at the supplier or rectifier side first. The system response to this fault is shown in Figure 2-10. The system starts to operate as the DC link reaches its steady state value of 250 V. At t=0.025 s, 10.8 KW active power begins to transfer to the load while two converters are operated in unity power factor mode (Q=0). The severe single line to fault occurs at t=0.07 s and remains for 100 ms and then the fault is cleared. As can be seen, the load side is supplied nearly independent of the occurring fault. The DC value error in the DC link voltage of the converter is due to the non-linearity of the PCC voltage in (2.7).

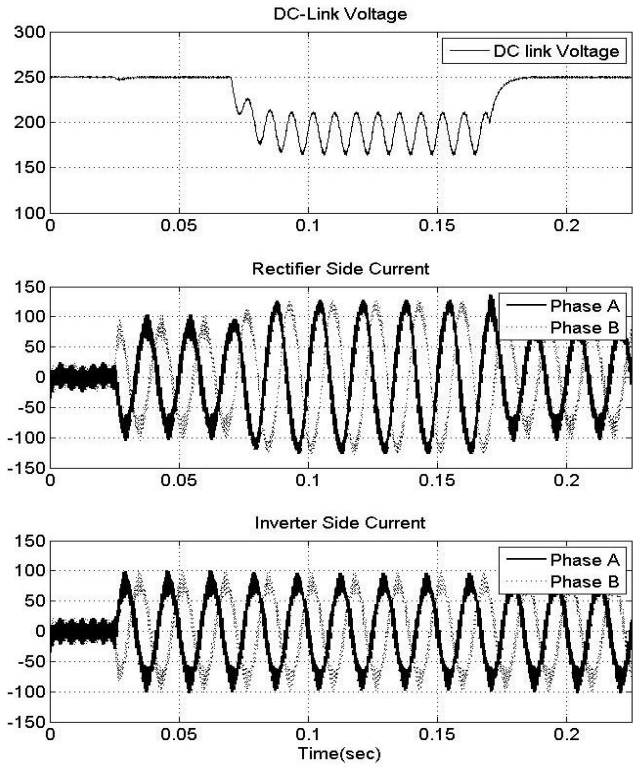

Figure 2-10. Performance of the conventional VSC-based BTB system when a SLG fault occurs in the rectifier side.

The operation performance of the system under single line to ground fault in the inverter side is presented in Figure 2-11. As can be seen the load current can be supplied and the current spectrum change is hardly distinguishable within and after the fault. Although the proposed method addresses a very powerful straightforward design procedure for this class of converter with a linear model, it is limited to operattion around steady state values without any frequency information in case of fault in the vicinity of the inverter side. Hence, for instance, the DC link voltage oscillates around the reference. Although this behavior is different and more convincing than what has been reported in the literature (due to the nature

of the disturbance rejection of the proposed controller), the oscillatory behavior of the DC link cannot be vanquished with the common controller structure.

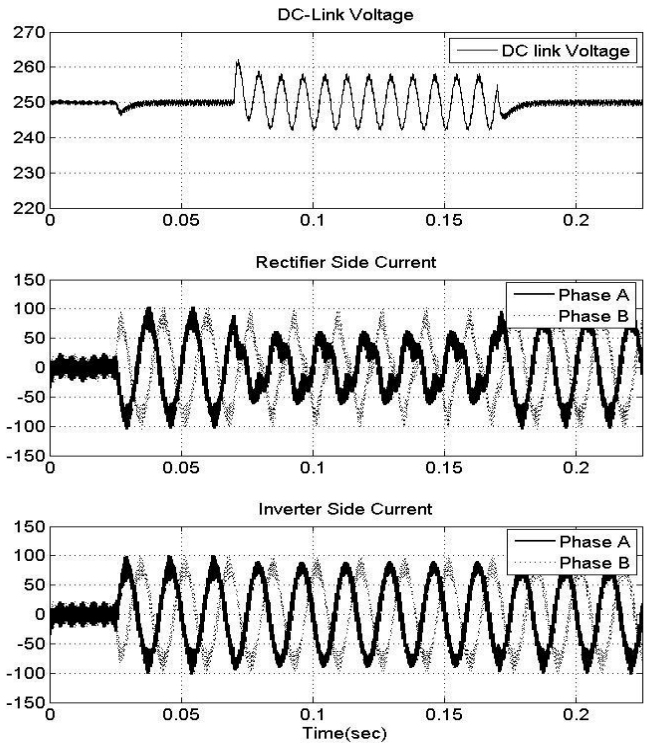

Figure 2-11. Performance of the conventional VSC-based BTB system when a SLG fault occurs in the inverter side.

In the following section, a fault in the inverter/load side is only considered due to the possible overvoltages occurring during the fault. It should be mentioned that a fault in the rectifier side may exceed the power switches' current rating. However, this current increase in the HVDC applications aiming for active power support is unavoidable unless some supplementary energy storage device is used in the DC link or the service mode is simply changed. The current practical solution would be a reduction in supply power or no gate

signalling to the rectifier within the fault. Although the main focus remains the power line faults in the inverter side the proposed methods can be applied to the faults in the rectifier side as well. The later will be covered later as the generalized control structure for BTB VSC systems.

2.6 Resilient Operation of Vector-Controlled VSC-Based BTB HVDC Systems

It has been shown in the previous section that conventional control methods are not able to regulate the DC bus voltage of VSC-based HVDC systems under power systems disturbances. This fact is mainly highlighted due to the low switching frequency operation of current semiconductor devices. Therefore, in this section two control structures are proposed that mitigate the DC bus voltage oscillations under power system faults for HVDC applications. These two structures, called "Integral Factor Control (IFC)" and "Backstepping Control (BSC)", are constructed based on local control of the states. The general idea of these two proposed methods is to create a virtual direct input to control the DC bus voltage dynamics in the time domain.

In the following, for the sake of simplicity (2.3), (2.4) and (2.7) are written with a_i coefficients. The states, inputs, outputs and disturbances are interpreted from (2.10) and presented in (2.15)-(2.17).

$$\dot{x}_1(t) = \frac{dI_d}{dt} = -\frac{R_s}{L_s} I_d + \omega I_q + \frac{E_d}{L_s} - \frac{V_d}{L_s} = a_1 x_1(t) + a_2 x_2(t) + a_3 e_1(t) + a_4 u_1(t) \tag{2.15}$$

$$\dot{x}_2(t) = \frac{dI_q}{dt} = -\frac{R_s}{L_s} I_q - \omega I_d + \frac{E_q}{L_s} - \frac{V_q}{L_s} = -a_2 x_1(t) + a_1 x_2(t) + a_3 e_2(t) + a_4 u_2(t) \tag{2.16}$$

$$\dot{x}_3(t) = \frac{dV_{DC}^2}{dt} = \frac{3E_d I_d}{C_{DC}} + \frac{3E_q I_q}{C_{DC}} - \frac{2V_{DC}^2}{R_p C_{DC}} - \frac{2P_{load}}{C_{DC}} = a_5 e_1(t) x_1(t) + a_6 x_3(t) + a_7 e_3(t) \tag{2.17}$$

It should be noted that the general control function does not change with the proposed methods in that the rectifier regulates the DC bus voltage and the fault is at the inverter side. Therefore, only the rectifier is considered in the following analysis. The inverter does not see the DC link dynamics in the controller design window.

2.6.1 **Method I: Integrator Factor Control (IFC)**

As mentioned before, the outputs for rectifier are reactive power and DC link voltage: I_q and V_{DC}^2. The idea is to select the inputs in order to get the desired response. This approach is first explained for $I_q(x_2)$ dynamics, which clarifies the overall controller design procedure.

The objective for the I_q controller is to have decoupled and disturbance rejection characteristics while it achieves the required response time. This criterion is obtained if its input u_2 has the form of (2.18). The first term in this equation is responsible for the response time of the state and the rest is for decoupling, disturbance rejection and command following in order regardless of the type of the functions. The result of the first order system is shown in (2.19).

$$u_2(t) = -f_2 x_2(t) + \frac{a_2}{a_4} x_1(t) - \frac{a_3}{a_4} e_2(t) + t_2 x_{2ref} \tag{2.18}$$

$$\dot{x}_2(t) = (a_1 - a_4 f_2)x_2 + a_4 t_2 x_{2ref} \tag{2.19}$$

The same analogy can be applied to get the input for x_1; however, this state should be controlled so as to maintain the required dynamics for x_3, which does not have access to a direct input. Hence, the input for x_1 should have the form of (2.20). The corresponding x_1 dynamics are shown in (2.21).

$$u_1(t) = \omega_1(t) - f_1 x_1(t) - \frac{a_2}{a_4} x_2(t) - \frac{a_3}{a_4} e_1(t) \tag{2.20}$$

$$\dot{x}_1(t) = (a_1 - a_4 f_1)x_1(t) + a_4 \omega_1(t) \tag{2.21}$$

To create an input as well as cancel out the non-linearity of x_3, it is assumed that:

$$x_1(t)e_1(t) = \beta(t) \tag{2.22}$$

$x_1(t)$ in (2.21) is solved as (2.23).

$$x_1(t) = x_1(t_0)e^{(a_1 - a_4 f_1)t} + e^{(a_1 - a_4 f_1)t} \int_{t_0}^{t} e^{-(a_1 - a_4 f_1)t} a_4 \omega_1(\tau) d\tau \tag{2.23}$$

The required input, $\omega_1(t)$ is then calculated considering (2.22) and (2.23).

$$\omega_1(t) = \frac{\dot{\beta}}{a_4 e_1(t)} - \frac{\beta(t)}{a_4}\left(\frac{(a_1 - a_4 f_1)}{e_1(t)} + \frac{\dot{e}_1(t)}{e_1^2(t)} \right) \tag{2.24}$$

With the help of the value obtained for the new control input, state x_3 in (2.17) is rewritten as (2.25). As a consequence, the state now has a virtual input which can control its state directly. Among the many possibilities of input choice, a typical form of input signal is selected to control the response time, disturbance rejection, and command following as given in (2.26).

$$\dot{x}_3(t) = a_5\beta(t) + a_6 x_3(t) + a_7 e_3(t) \tag{2.25}$$

$$\beta(t) = -f_3 x_3(t) - \frac{a_7}{a_5} e_3(t) + t_3 x_{3ref} \tag{2.26}$$

$$\dot{x}_3(t) = -a_5 f_3 x_3(t) + a_5 t_3 x_{3ref} \tag{2.27}$$

The IFC structure (depicted in Figure 2-12) is different from conventional controller structures for HVDC systems. As shown, the load information and bus voltage are used in this structure to create a required control input. In Figure 2-12 K' is a function to determine *β(t)*.

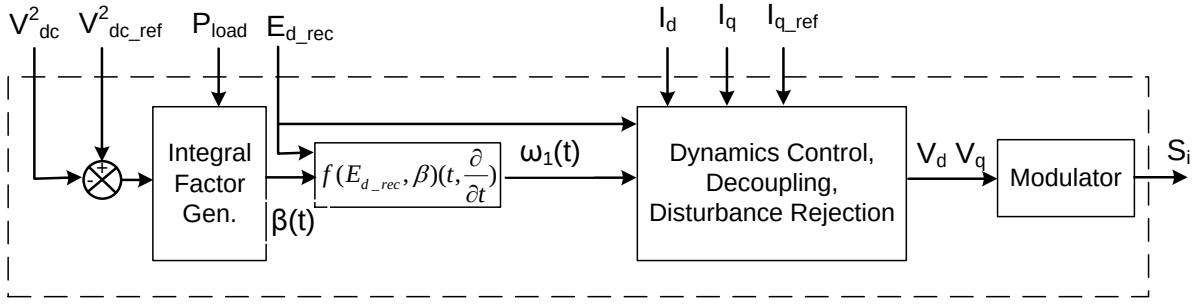

Figure 2-12. Proposed Integral Factor Control (IFC) structure for the DC link controller in VSC-based HVDC applications.

The control parameters for IFC are calculated and presented in (2.28) based on the response of the associated modes: λ_i and λ_c.

$$Para(IFC) = \left\{ \begin{array}{l} f_1 = f_2 = \dfrac{\lambda_i + a_1}{a_4} = R_s - L_s\lambda_i \;;\; f_3 = \dfrac{\lambda_c + a_6}{a_5} = \dfrac{1}{3}R_p C_{DC}\lambda_c - \dfrac{2}{3} \\ t_2 = -\dfrac{a_1 - a_4 f_2}{a_4} = -L_s\lambda_i \;; \qquad t_3 = -\dfrac{a_6 - a_5 f_2}{a_5} \end{array} \right\} \tag{2.28}$$

2.6.2 **Method II: BackStepping Control (BSC)**

In control theory, backstepping is a technique for designing controls for nonlinear systems developed around 1990, 42. It is a recursive technique in which one designs feedback controls and finds Lyapunov functions for a set of n-increasingly complex systems, the last system being of interest. Although it is not the intention of this section to deal with the non-linearity of the system now (the linear system has been derived and the fault is at the inverter side), the fundamental basis of the idea can be interpreted as the local control of the states that do not have access to the input. In other words, some states are used as a pseudo-control to stabilize others by introducing some virtual state variables representing the difference between the actual and virtual control.

Since the system considered is a three-state one introduced in (2.10) and $x_2(I_q)$ can be regulated independently by setting u_2 as (2.18), the design procedure is confined to a two state system , $x_1(I_d)$ and $x_3(V_{DC}^2)$. Thus, x_1 is used to control x_3 as shown in (2.29) and (2.30). The change of the coordinates here to z indicates that x_1 should take whatever value is necessary to make the error z_1 null corresponding to achieve the reference z_3.

$$z_3 = x_3 \tag{2.29}$$

$$z_1 = x_1 - \alpha(z_3, e_3) \tag{2.30}$$

This method is valid only at the level of the Lyapunov function. The candidate functions selected are based on the energy concept of the DC link capacitor and the interface inductor. Considering the state defined for the DC link voltage as $x_3=V_{DC}^2$, it is sufficient to propose the candidate functions as (2.31) and (2.32), which are positive definite functions.

$$V_3 = z_3 \tag{2.31}$$

$$V_1 = V_3 + \frac{1}{2} z_1^2 \tag{2.32}$$

It is remarkable that the key to ensuring the stability of the whole system is not choosing the virtual and actual controls but choosing the correct Lyapunov functions and generating their derivatives negative. The virtual control is chosen as (2.33) to meet the requirement.

$$\alpha(z_3, e_3) = -f_3 z_3 - \frac{a_7}{a_8} e_3 \qquad , \; a_8 = a_5 e_1 \tag{2.33}$$

The derivative of the proposed Lyapunov functions combining (2.21) and (2.29)-(2.33) results in:

$$\dot{V}_3 = a_8 z_1 + (-a_8 f_3 + a_6) z_3 \tag{2.34}$$

$$\begin{aligned} \dot{V}_1 &= \dot{V}_3 + z_1 \dot{z}_1 \\ &= a_8 z_1 + \left(-a_8 f_3 + a_6\right) z_3 + z_1 \left(a_4 \omega_1(t) + a_1 \alpha\left(z_3, e_3\right) - \dot{\alpha}\left(z_3, e_3\right)\right). \end{aligned} \tag{2.35}$$

Choosing the input signal $\omega_1(t)$ as (2.36) leads to having $\dot{V}_1$ in the form of (2.37).

$$\omega_1(t) = \left(-\frac{f_1}{a_4} - \frac{a_1}{a_4}\right) z_1 - \frac{a_1 \alpha\left(z_3, e_3\right)}{a_4} + \frac{\dot{\alpha}\left(z_3, e_3\right)}{a_4} \tag{2.36}$$

$$\dot{V}_1 = -f_1 z_1^2 + a_8 z_1 + (-a_8 f_3 + a_6) z_3 \tag{2.37}$$

It is not difficult to determine values for f_1 and f_3 that render all the derivatives in (2.34) and (2.35) negative definite. One can show that with positive values for the gains the

derivatives are negative for the circuit parameters which ensures the stability of the system in the selected bound. However, the response time is yet to be determined. The desired response time of the virtual states can be simply determined based on several linear methods since they have a simple form of (2.38). The proper consequence can be achieved when the error, z_1, goes to zero fast, so the constraint is that the mode associated with z_1 should be faster than that of z_3. This fact can be realized in that z_1 and z_3 have the nature of the current and DC link voltage respectively, which states that the controller follows the well-known rule in power electronics area to design the current regulator faster than the voltage one. However, there is a major difference in constructing the controller structure. The proposed BSC structure for voltage-sourced converters working as a rectifier of a VSC-based HVDC system is depicted in Figure 2-13. K in this figure is to determine α as shown in (2.33). In this structure the load information should be available to get the desired control input.

$$\begin{pmatrix} \dot{z}_1 \\ \dot{z}_3 \end{pmatrix} = \begin{pmatrix} -f_1 & 0 \\ a_8 & -a_8 f_3 + a_6 \end{pmatrix} \begin{pmatrix} z_1 \\ z_3 \end{pmatrix} \tag{2.38}$$

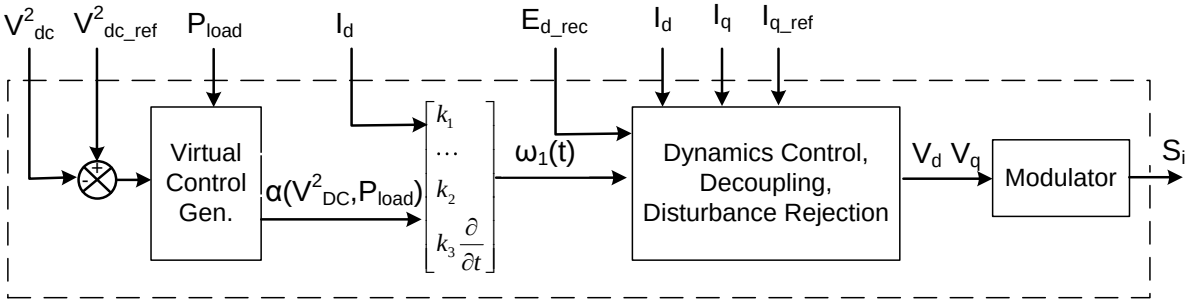

Figure 2-13. Proposed Back-Stepping Control (BSC) structure for the DC link controller in VSC-based HVDC applications.

The control parameters for this type of controller are calculated as (2.39) based on the response of the associated modes: λ_i and λ_c (current and voltage).

$$Para(BSC)=\left\{\begin{array}{c} f_1=\lambda_i\ ;\ f_2=\dfrac{\lambda_i+a_1}{a_4}=R_s-L_s\lambda_i\ ;\ f_3=\dfrac{\lambda_c+a_6}{a_8}=\dfrac{1}{3e_1}\left(R_pC_{DC}\lambda_c-2\right) \\ t_2=-\dfrac{a_1-a_4f_2}{a_4}=-L_s\lambda_i\ ;\ \ t_3=-\dfrac{a_6-a_8f_2}{a_8} \end{array}\right\} \quad (2.39)$$

2.6.3 **Performance Comparison with the Proposed Control Structures**

The system performance under different normal and fault cases is studied with the parameters indicated in Table I. To have a logical comparison, an identical response time is assumed for each mode in the respective controller structures to show the potential performance improvement.

The system performance under a single line to ground fault is shown in Figure 2-14 and Figure 2-15. The system starts to operate at V_{DC}=220V while the full rate of active power is acquired. The DC link voltage fall is unavoidable; however, as soon as the current reaches its reference the DC link voltage begins to achieve its reference. As can be seen, the states' dynamic variations for this step change of command are identical for all the proposed controllers. The SLG fault occurs at t=0.07 s and remains for 100 msec, then it is self-cleared. The power demand under the fault was reduced because the voltage at the bus was reduced by losing one line and has the behavior of (2.40). Full rate power can be provided if

the converter rating allows; this fact does not affect the controller performance. Another point to mention is that there is no need to consider the time-varying part as long as $I_q = 0$.

$$E_d = E_{dn}\left(\frac{2}{3} - \frac{1}{3}\cos(2\omega_s t)\right) \tag{2.40}$$

As could be expected, a 120 Hz component shows up in the DC link around the reference during an SLG fault, Figure 2-14. However, the performance improvement is obvious with the proposed controllers. As can be seen, the oscillations in the DC link voltage are hardly noticeable.

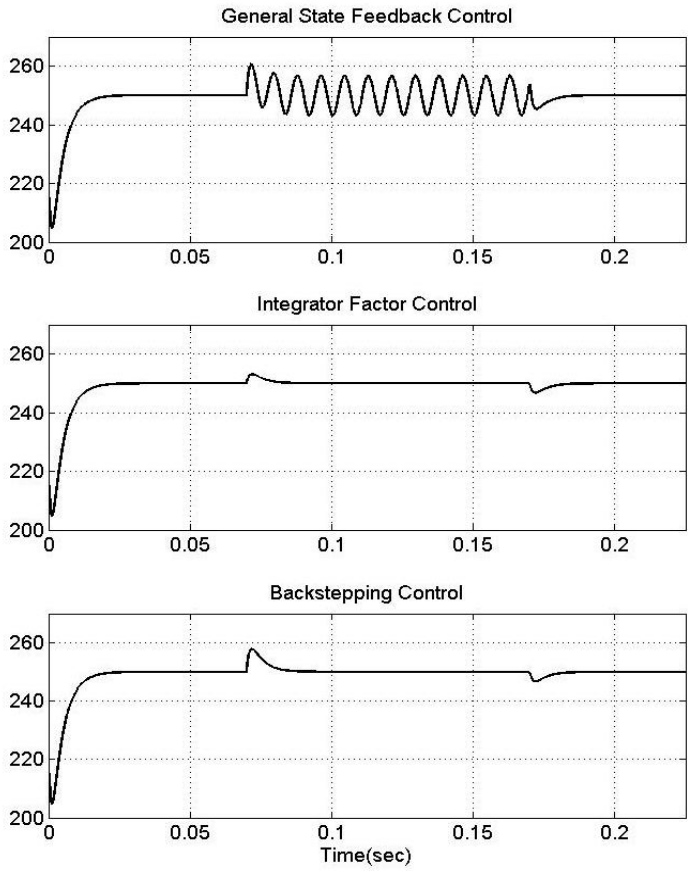

Figure 2-14. DC link voltage performance comparison with the proposed controllers under a single line to ground fault.

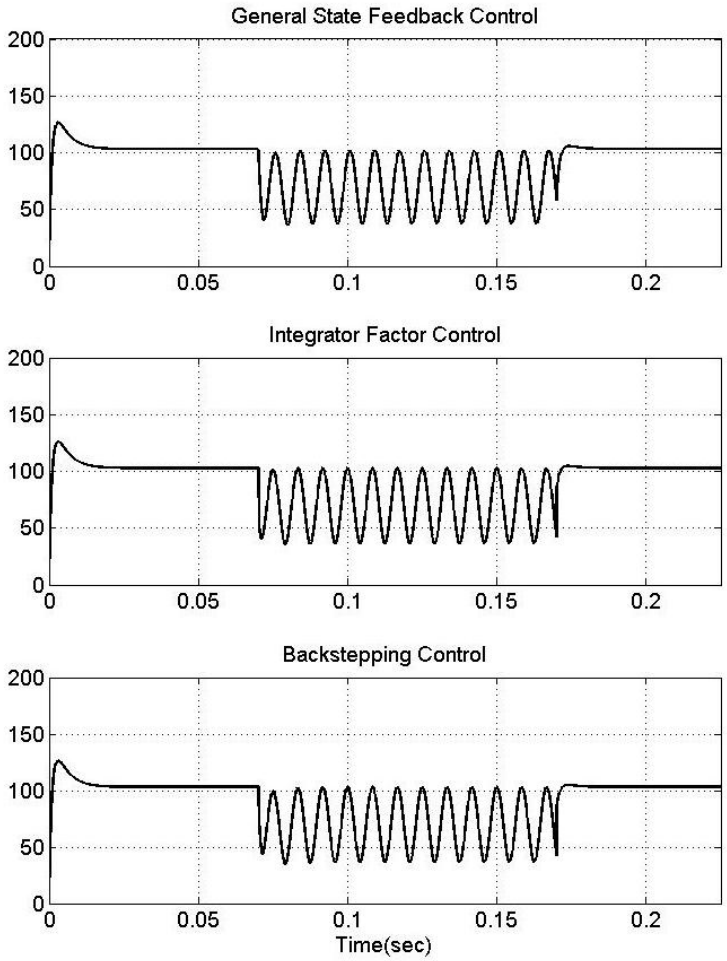

Figure 2-15. Effect of the proposed controllers on the d-component of the current under a single line to ground fault.

The case of phase reversal or generating a completely negative sequence is also examined as in Figure 2-16 and Figure 2-17. In this case, the DC link starts to reach its reference from V_{DC}=220 V at zero external current command. The phase reversal is initiated as before at t=0.07 s and self-cleared at t=0.17 s. Full rate of capacity is used to generate this negative sequence power. In this case, the oscillations in the DC link for the general state

feedback control mode have a much higher value than before. However, these oscillations do not appear in the last two proposed controllers.

For all the simulations and controllers the same modes are considered. The results show the same operational behavior under normal conditions.

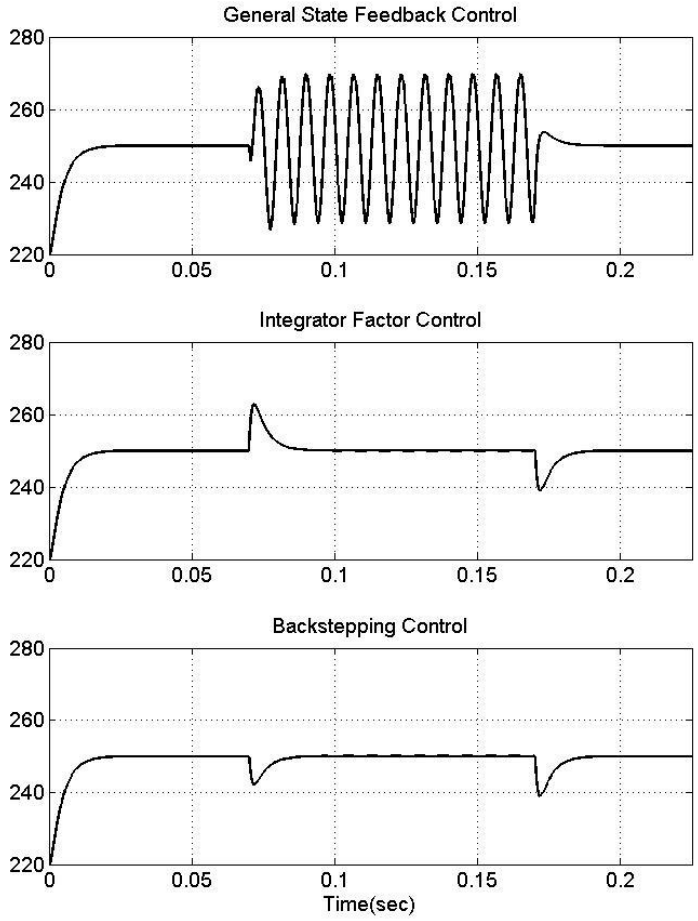

Figure 2-16. DC link voltage performance comparison with the proposed controllers under phase reversal.

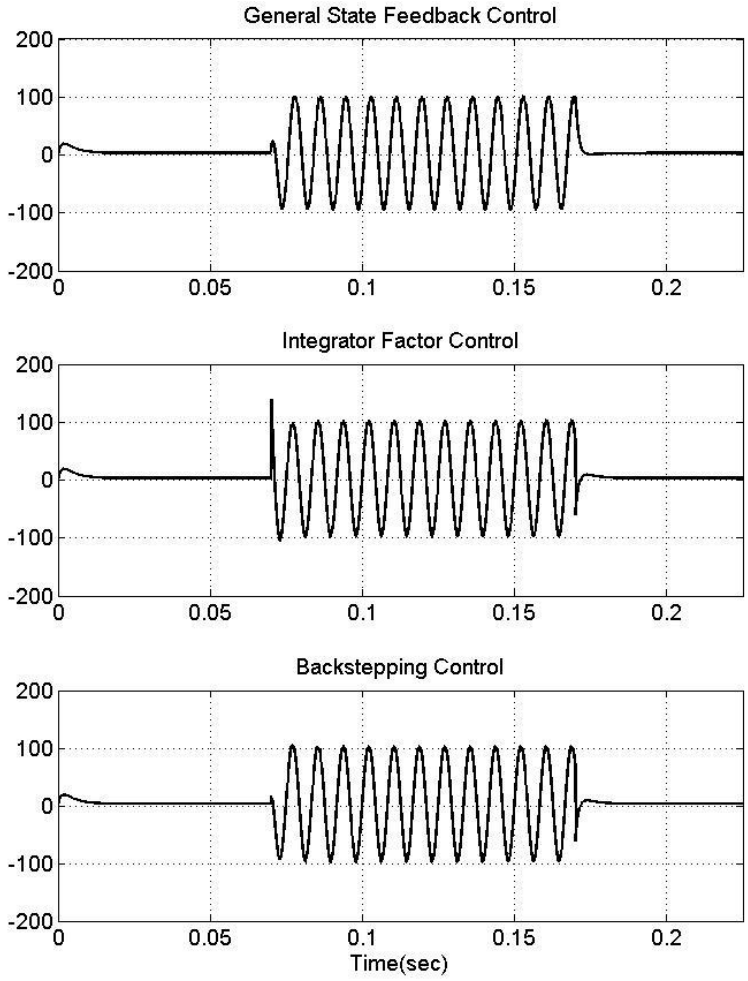

Figure 2-17. Effect of the proposed controllers on the d-component of the current under phase reversal.

In Figure 2-15 and Figure 2-17, a phase change in the current supplied by the converter is observed for different controllers. This phase compensation is a major contribution of the proposed controllers to suppressing the DC link voltage oscillations which is shown enlarged in Figure 2-18.

Comparing these proposed control structures shows that the Integrator Factor Control (IFC) and Backstepping Control (BSC) have superior performance to the more commonly used feedback control method for VSC-based HVDC systems. It is worth mentioning that this detailed mathematical analysis indicates a common point. The information on bus voltage rate, $\frac{dE_{bus}}{dt}$ or its respective estimated load information is essential to compensate for the conventional controllers. Therefore, this information can either be estimated or directly measured.

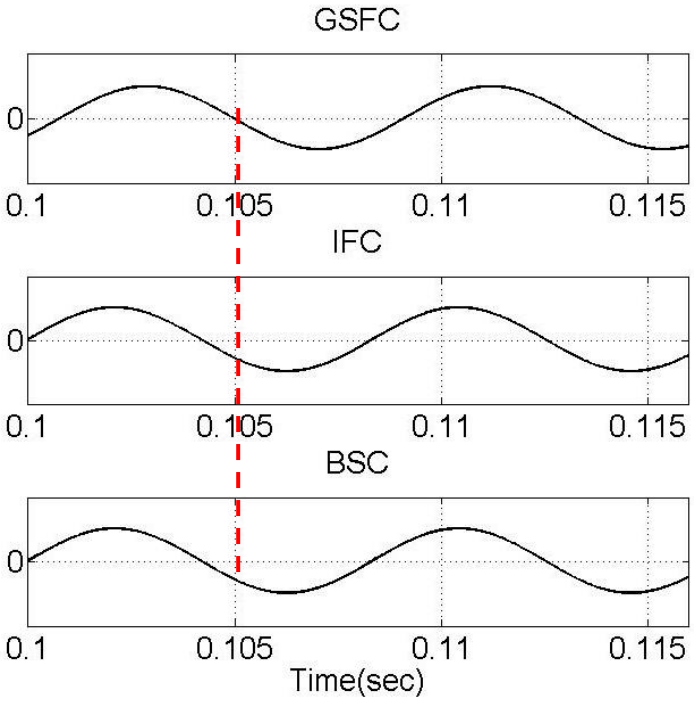

Figure 2-18. Phase compensation effect of the proposed controllers under phase reversal.

2.7 Generalized Controller for Back-to-Back Voltage-Sourced Converter under Power System Disturbance

It has been shown in the previous sections that the conventional control methods are not able to regulate the DC bus voltage of VSC-based "transmission" systems under power system disturbances. This failure is mainly due to the low switching frequency operation of these devices and limited bandwidth of the converter. Therefore, two structures are constructed here without sequence extraction based on local control of the converter states known as Back-Stepping Control (BSC) and Integral Factor Control (IFC), which mitigates the DC link voltage instability and oscillations. The issue is stated, following the work of 40, as a possible overvoltage in the DC link when the fault is incurred in the inverter side of the BTB VSC system in HVDC applications. However, with increasing applications of multi-MW converters in different applications, more transient capability is needed; i.e., the unbalanced condition can be in either converter in the BTB system. In this section, a unified control architecture is proposed that improves the transient performance of the VSC BTB system in current and emerging applications, denoted as HVDC, drive and hybrid power systems. The ground of the proposed controller will be explained in the following section specifically for the DC link voltage controller converter in the BTB system.

2.7.1 Modified Back-Stepping Control (BSC) for BTB VSC Systems

In this section, the proposed controller for the general case will be explained. The major difference from what has been explained in the previous sections is that the fault can be

either in the DC link controller or the power flow controller in the BTB system. This brings more dynamics to the DC link rather than the load seen in the previous section.

The reactive power, controlled by the q-component of the current, has a direct input V_q as shown in (2.3). This controller is desired to have decoupled and disturbance rejection characteristics while it achieving the required response time. This criterion is met if its input V_q has the form of (2.41), which is similar to (2.18). The first term in this equation is responsible for the response time of the state and the remaining terms are for decoupling, disturbance rejection and command following in order. The result of the first order system is shown in (2.42), also available in such literature as 7.

The direct input for the d-component of the current or active power controller term, V_d, is first designed to have decoupling and disturbance rejection terms as in (2.43). The additional term, Ψ_1, is used as the control input to regulate the DC link voltage and active power through a backstepping control method.

$$V_q = -f_q I_q + L_s \omega_s I_d + E_q + t_q I_{qref} \tag{2.41}$$

$$\dot{I}_q = \left(\frac{R_s + f_q}{L_s} \right) I_q - \frac{t_q}{L_s} I_{qref} \tag{2.42}$$

$$V_d = -L_s \omega I_q + E_d + \Psi_1 \tag{2.43}$$

$$\dot{I}_d = -\frac{R_s}{L_s} I_d - \frac{1}{L_s} \Psi_1 \tag{2.44}$$

As explained in the previous section, backstepping is a recursive technique in which one designs feedback controls and finds Lyapunov functions for a set of n- increasingly complex

systems, the last system being the one of interest. The fundamental idea can be interpreted as the local control of the states that do not access the input. In other words, some states are used as a pseudo-control to stabilize others by introducing some virtual state variables representing the difference between the actual and virtual control. Accordingly, β defined below is used to control DC link voltage which does not have direct control input as shown in (2.45) and (2.46) . The change of the coordinates here to *z* indicates that β should take whatever value is required to make the error z_1 null corresponding to achieving the reference z_3 (stable DC link Voltage).

$$z_3 = V_{DC}^2 \tag{2.45}$$

$$z_1 = \beta - \alpha\left(z_3, E_q, P_{load}\right) \tag{2.46}$$

where

$$\beta = \frac{3E_d I_d}{C_{DC}}.$$

This method is valid only at the level of the Lyapunov function. The selected candidate functions are based on the energy concept of the DC link capacitor and the interface inductor. If the defined state for the DC link voltage is considered to be V_{DC}^2, it is sufficient to propose the candidate functions as (2.47) and (2.48), which are positive definite functions.

$$V_3 = \frac{1}{2} z_3^2 \tag{2.47}$$

$$V_1 = V_3 + \frac{1}{2} z_1^2 \tag{2.48}$$

It is remarkable that the key to ensuring the stability of the whole system is not choosing the virtual and actual controls but choosing the correct Lyapunov functions and generating their derivatives negative. The virtual control input is chosen as (2.49) to meet these requirements.

$$\alpha\left(z_3, E_q, P_{load}\right) = -f_{VDC} z_3 - \frac{3}{C_{DC}} E_q I_q + \frac{2}{C_{DC}} P_{load} + t_{VDC} V_{DCref}^2 \tag{2.49}$$

The derivative of the proposed Lyapunov functions combining (2.7) and (2.45)-(2.49) results in:

$$\dot{V}_3 = z_3 \dot{z}_3 = z_3 \left(z_1 + \alpha + \frac{3E_q I_q}{C_{DC}} - \frac{2V_{DC}^2}{R_P C_{DC}} - \frac{2P_{load}}{C_{DC}} \right) \tag{2.50}$$

$$\begin{aligned} \dot{V}_1 &= \dot{V}_3 + z_1 \dot{z}_1 \\ &= \dot{V}_3 + z_1 \left(\beta \left(\frac{\dot{E}_d}{E_d} + \frac{-R_s}{L_s} \right) + \frac{-3E_d}{L_s C_{DC}} \Psi_1 - \dot{\alpha} \right) \end{aligned} \tag{2.51}$$

Choosing the input signal Ψ_1 *(t)* as (2.52) leads to having $\dot{V}_1$ and $\dot{V}_3$ in the form of (2.53) and (2.54), which ensures the stability of the virtual controllers, z_1, and consequently the system. In other words, the derivative functions become negative definite, assuring the stability of the system.

$$\Psi_1 = \frac{-L_s C_{DC}}{3E_d} \left(-f_d z_1 - z_3 - \left(z_1 + \alpha \right) \left(\frac{\dot{E}_d}{E_d} - \frac{R_s}{L_s} \right) + \dot{\alpha} \right) \tag{2.52}$$

$$\dot{V}_3 = -f_{VDC} z_3^2 + z_3 z_1 \tag{2.53}$$

$$\dot{V}_1 = -f_{VDC} z_3^2 - f_d z_1^2 \tag{2.54}$$

The proposed backstepping control structure for the DC link voltage controller converter is shown in Figure 2-19. From the top level view, a feedforward power measurement is added to the controller. The required input to insure the stability of the DC link, $\Psi_1(t)$, is generated through the manipulation of the virtual control input z_1, the PCC voltage and the converter current. The details of how the implemented controller generates the reference vectors are presented in Figure 2-20. As can be seen, the structure is fairly straightforward compared to Figure 2-3 and it has been implemented in the commonly used synchronous frame without a sequence extraction block or resonant compensator, compared to 23 and 25.

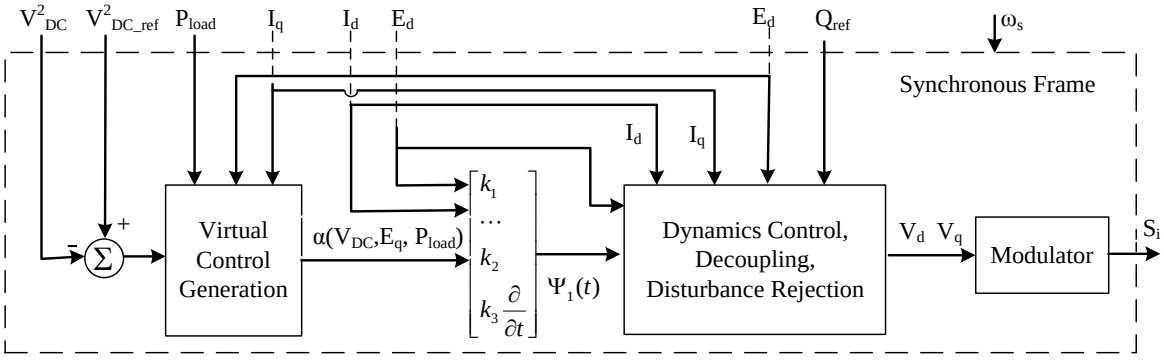

Figure 2-19. Proposed backstepping control structure for the DC link voltage controller converter in a BTB VSC system.

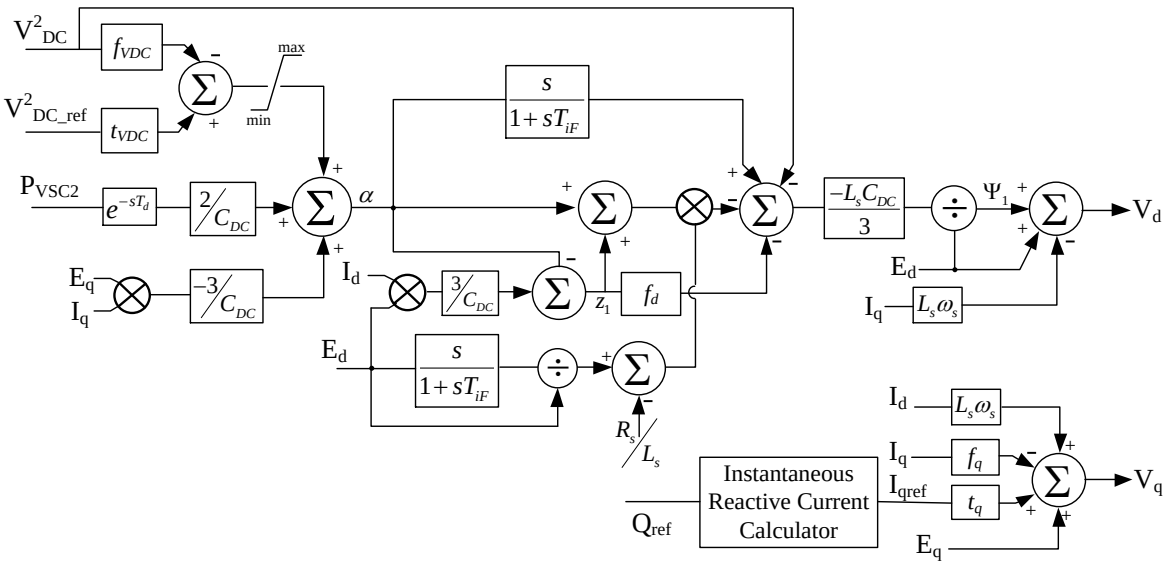

Figure 2-20. Implemented proposed control structure in the synchronous frame to generate the reference vectors for the DC link voltage controller converter.

The control parameters for this type of controller are calculated as in (2.55) based on the response of the associated modes: λ_i and λ_c for the current and DC link voltage respectively.

$$para = \begin{cases} f_d = \lambda_i \,;\, f_q = R_s - L_s\lambda_i \\ f_{VDC} = \lambda_c \\ t_q = -R_s + f_q \,;\, t_{VDC} = f_{VDC} + \dfrac{2}{R_p C_{DC}} \end{cases} \tag{2.55}$$

2.8 **Dynamic Performance Evaluation of BTB VSC Systems with the Proposed Generalized Control Architecture in RTDS**

This section presents and evaluates the dynamic performance of BTB VSC systems in different applications with the proposed generalized control architecture. Applications are

categorized as HVDC, drive (wind) and hybrid power system applications. The proposed controller has been implemented in an RTDS housed in the FREEDM Systems Center, Figure 2-21, and compiled on a GPC processor card with a controller sampling time of $50\mu s$ and key circuit parameters as tabulated in Table II. For reference, the performance comparison of the BTB VSC system (based on the average model) with the proposed control scheme and commonly used controller structures has been also presented. The PLECS package in the Matlab environment has been used to develop the average models.

In the following, certain assumptions have been made:

1. The system references are controlled based on the currents for the case studies under faults.
2. There is no change in control mode of the system pre-, during, and post-fault. Under unbalanced grid voltages, reactive power demand can dominate the available converter capacity. This demand imposes some limitations in regulating the DC link voltage.
3. Power systems have same short circuit capacity.

Figure 2-21. Real Time Digital Simulator (RTDS) facility at FREEDM Systems Center.

Table II. VSC BTB System Parameters with the Generalized Control Structure

Base Power	S	10 MVA
Line-to-line voltage (converter side)	E	1 PU = 13.8 kV
Line-to-line voltage for drive app.	E_w	1 PU = 3.3 kV
Line frequency (grid)	f	60 Hz
Leakage inductance	L_s	15% PU
Interface resistance	R_s	0.4% PU
DC link voltage	V_{DC}	1 PU = 1.65 V_{AC}
DC link capacitance	C_{DC}	0.66 PU
Unit capacitance constant	H	4.16 ms
Switching frequency	f_s	900 Hz (15xf)
Converter loss resistor (estimated)	R_p	1% PU
Continuous overcurrent capability	I	1.5 PU
Absolute overcurrent capability	I_{max}	2 PU
Current controller pole location	λ_i	-1000
Voltage controller pole location	λ_c	-250
Communication delay time for power measurement	T_d	10 ms
Time delay of the derivatives	T_{iF}	0.1 ms
Controller sampling time	t_s	50 us

2.8.1 **BTB VSC System for HVDC Applications**

BTB VSC systems in HVDC applications, represented in Figure 2-22, are used for power flow control. One converter operates in PQ mode and the other one is responsible for compensating for the losses and insuring a stable operation of the DC bus voltage while it supports its reactive power demands. In vector-controlled VSC systems, reactive power is regulated independent of active power.

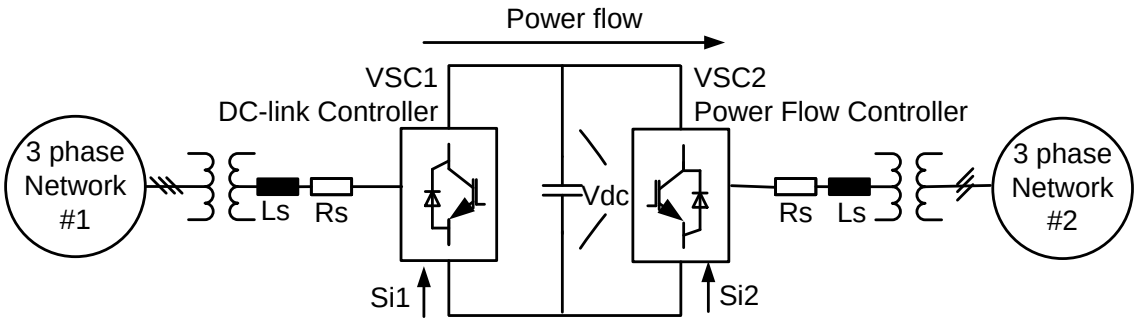

Figure 2-22. BTB VSC system for HVDC applications

The first group of results is presented in Figure 2-23 where system start-up dynamic performance is shown when 1PU of power is supplied to network #2. The converter system is charged naturally in some cycles and it reaches the reference voltage afterwards. In this set of results a unity power factor operation of converters has been verified and presented.

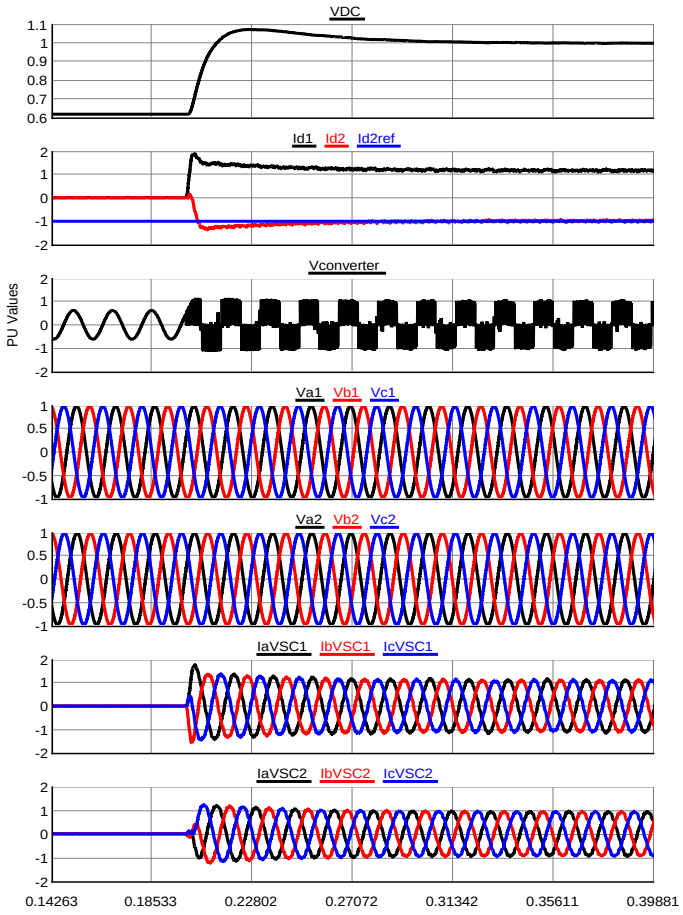

Figure 2-23 Start-up dynamic performance of the BTB VSC system as in HVDC applications and unity power factor operation of 1 PU power under balanced conditions- RTDS results.

Figure 2-24 shows the dynamic performance of the VSC BTB system in response to a change in power flow direction under balanced conditions. The system supplies 0.8 PU power and the VSC#1(DC link voltage controller) provides 0.2 PU capacitive and VSC#2 (power flow controller) 0.6 PU inductive reactive power. As can be observed the proposed controller for the BTB system operates satisfactorily and as well as the common control

structures. These values are considered in the following case studies to have consistency in the results obtained for unbalanced conditions.

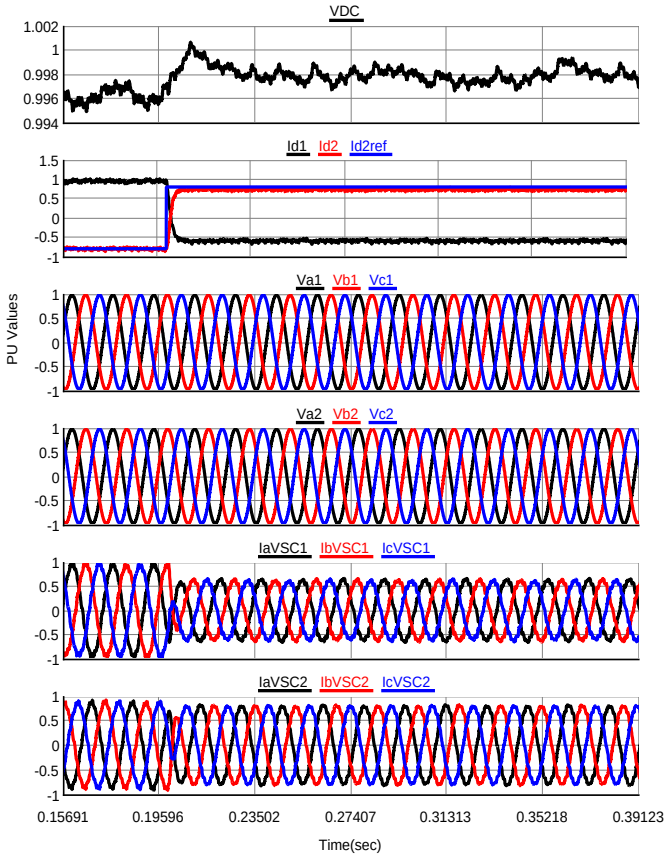

Figure 2-24. Dynamic performance of the BTB VSC system as in HVDC applications, changing power flow direction, with no change in reactive power reference under balanced conditions- RTDS results.

The dynamic performance of the VSC BTB system under an unbalanced condition in the inverter side (power flow controller converter) is presented in Figure 2-25 and Figure 2-26. The first figure, Figure 2-25 compares the performance of the BTB VSC system in the developed average model with the commonly used controllers and the proposed controller.

The second figure, Figure 2-26, presents the detailed switching model of the converter system developed in RTDS. The unbalanced system is represented by a 50% voltage drop in phase A of the inverter-side PCC voltages (V_{abc2}), which can be considered as a fault near the inverter station. The fault remains for 6 cycles. As can be observed, the DC link voltage remains practically stiff, and a harmonic measurement of the DC link voltage for the second and fourth harmonics shows a satisfactory level of compensation. This mode of operation is mainly of interest in the literature, 25, 40 and 41.

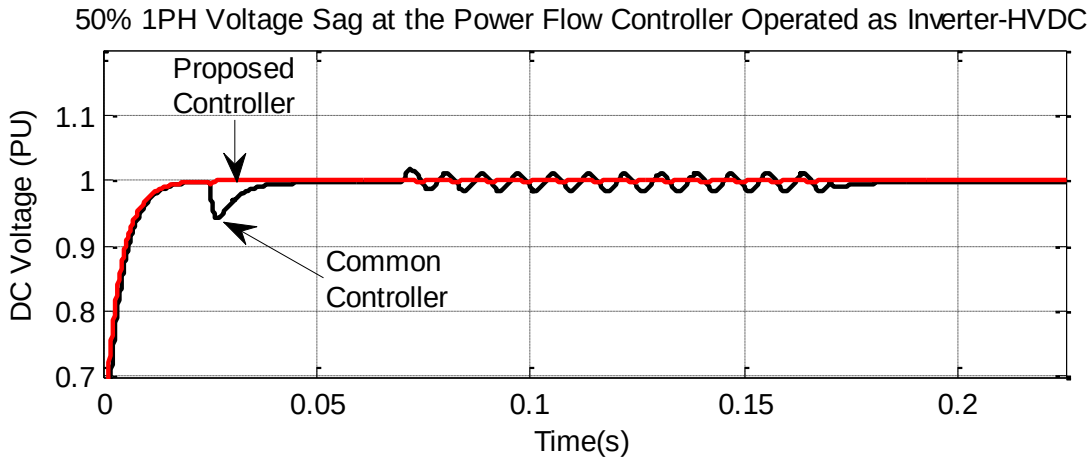

Figure 2-25. Performance comparison of the BTB VSC system with the proposed controller and commonly used control schemes for HVDC applications under an unbalanced condition of 50% single-line voltage sag in the power flow controller side (average model).

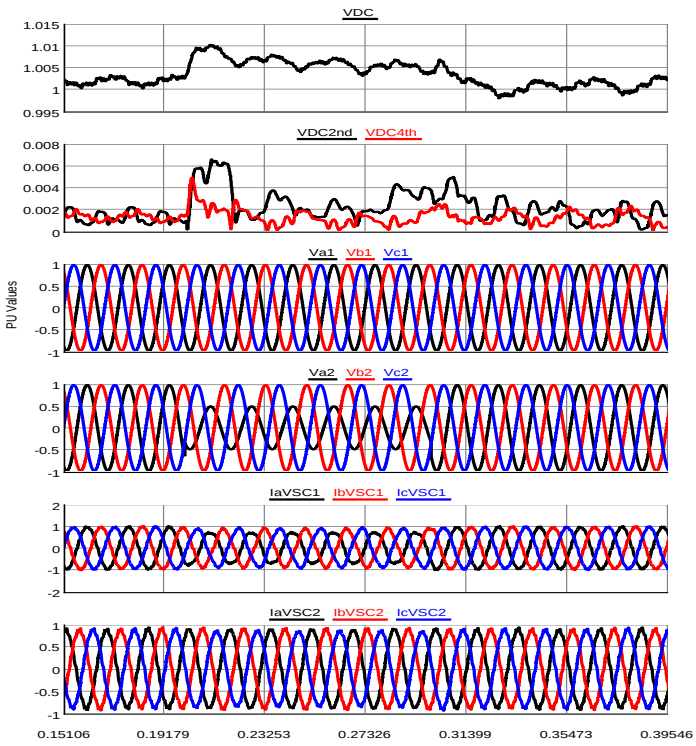

Figure 2-26. Dynamic performance of the BTB VSC system as in HVDC applications under an unbalanced condition of 50% single-line voltage sag in the power flow controller side- RTDS results.

Figure 2-27 and Figure 2-28 present the dynamic performance of the BTB system when a 50% voltage drop occurs in phase A of the rectifier side (DC link voltage controller). Due to the voltage drop, the rectifier carries higher currents to maintain the load power and regulate the DC bus voltage. It can be seen that the DC link voltage has a minor change of about 1% PU and the effect of negative sequence power is reduced to 1.5% PU presented in the DC link voltage. It can be also observed that the inverter current is hardly affected by the dynamics of the DC link under the unbalanced condition. This result represents a major performance improvement of the BTB VSC systems which has not been shown before.

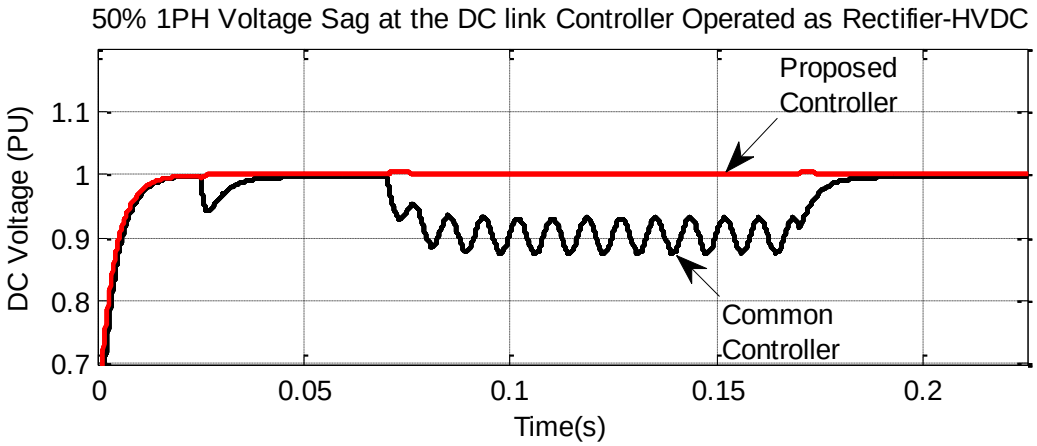

Figure 2-27. Performance comparison of the BTB VSC system with the proposed controller and commonly used control schemes for HVDC applications under an unbalanced condition of 50% single-line voltage sag in the DC link voltage controller side (average model).

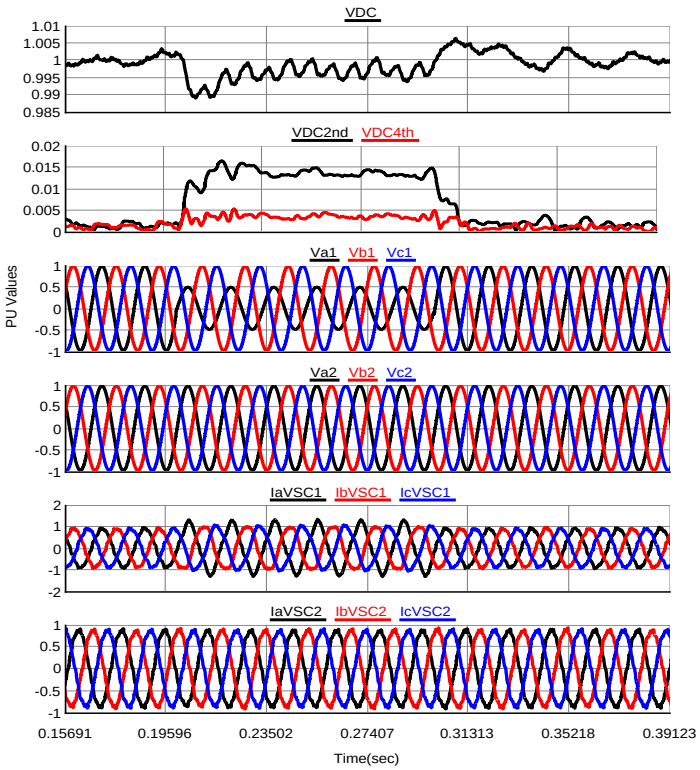

Figure 2-28. Dynamic performance of the BTB VSC system as in HVDC applications under an unbalanced condition of 50% single-line voltage sag in the DC link voltage controller side- RTDS results.

The dynamic performance of the VSC BTB system in HVDC applications while the DC link controller is operated as an inverter and the power flow controller as a rectifier is presented in Figure 2-29-Figure 2-32. This mode of operation may not be practiced in HVDC power transactions and it is presented to combine the problem and address the dynamics. In Figure 2-29 and Figure 2-30, the unbalanced system is represented by a 50% voltage drop in phase A of the PCC voltages (V_{abc1}). The fault remains for 6 cycles. As can be observed, the DC link voltage remains practically stiff, and a harmonic measurement of the DC link voltage for the second and fourth harmonics shows a satisfactory level of compensation. The inverter currents change (increase in phase A) to compensate for the unbalanced power flowing into the system; however, it remains within the safe operating area of the switches. In Figure 2-31 and Figure 2-32, the system performance under more severe imbalances is shown, represented by a 50% and 90% voltage drop in phase B and C of the power flow controller side respectively.

Based on the result obtained in different case studies, it can be concluded how effective the proposed controller is for HVDC applications under normal and unbalanced conditions. In other words, the deficiency of the high power VSCs in terms of control bandwidth is improved through a high bandwidth control architecture which does not require sequence extraction or any diminishing factors.

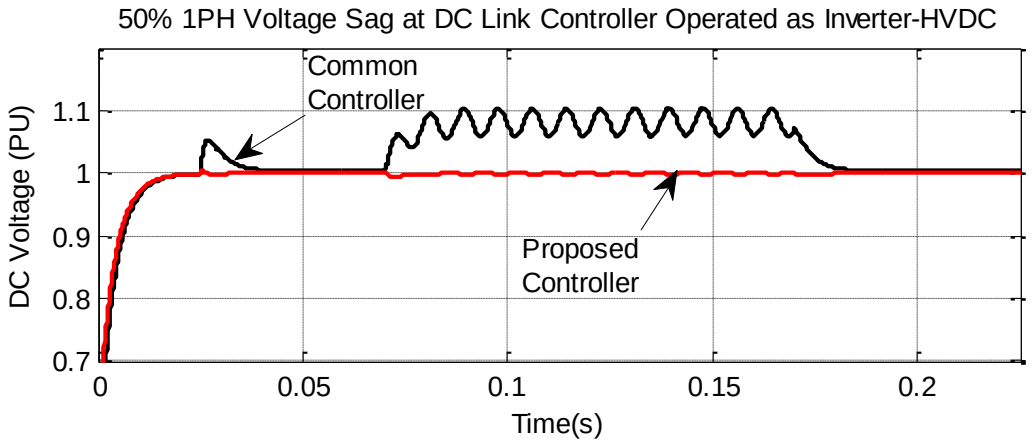

Figure 2-29. Performance comparison of the BTB VSC system with the proposed controller and commonly used control schemes for HVDC applications under an unbalanced condition of 50% single-line voltage sag in the DC link voltage controller side operated as an inverter (average model).

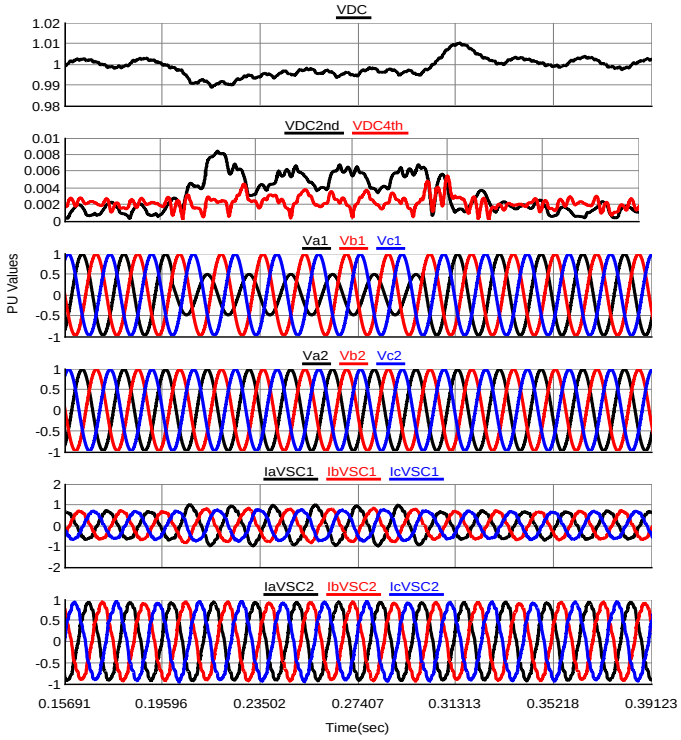

Figure 2-30. Dynamic performance of the BTB VSC system in HVDC applications under an unbalanced condition of 50% single-line voltage sag in the DC link voltage controller side operated as an inverter- RTDS results.

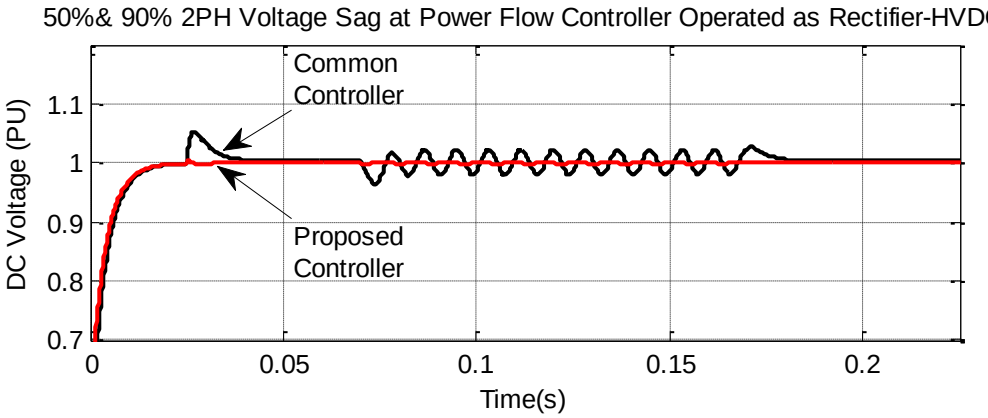

Figure 2-31. Performance comparison of the BTB VSC system with the proposed controller and commonly used control schemes for HVDC applications under an unbalanced condition of 50% in phase B and 90% in phase C voltage sag in the power flow controller side operated as the rectifier (average model).

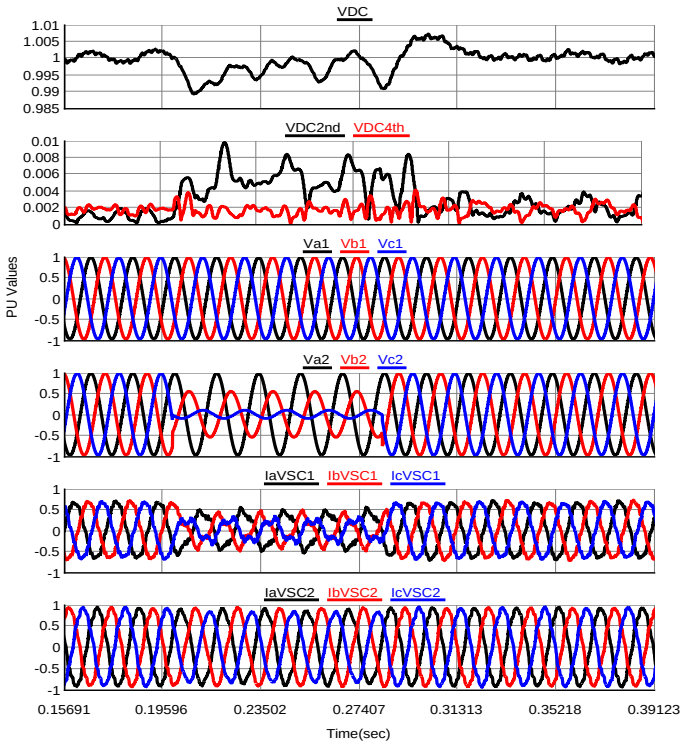

Figure 2-32. Dynamic performance of the BTB VSC system in HVDC applications under unbalanced condition of 50% in phase B and 90% in phase C voltage sag in the power flow controller side operated as the rectifier- RTDS results.

2.8.2 **BTB VSC System for Drive (Wind) Applications**

This section is provided to address emerging large capacity wind turbines (>10MW). These turbines are expected to use direct drive technologies shown in Figure 2-33 and the BTB VSC system as the enabling interface. A robust DC link voltage is considered to be the key factor that affects the turbine operation. In the following case studies, it is assumed that the turbine side converter (VSC#2) operates at 30 Hz and supplies 0.8 PU active power and absorbs 0.6 PU inductive reactive power while the grid side converter (VSC#1) regulates the DC link voltage and provides 0.2 PU capacitive reactive power. The dynamic performance of the VSC BTB system in the drive application under unbalanced conditions in the inverter side or grid side (DC link voltage controller converter) is presented in Figure 2-34- Figure 2-37. In Figure 2-34 and Figure 2-35 the unbalanced system is represented by a 50% voltage drop in phase B of the inverter side PCC. In Figure 2-36 and Figure 2-37 a more severe fault occurs which is represented by a 50% voltage sag in phase B in addition to a 30% voltage drop in phase C of the grid. From the results obtained, it can be concluded that the proposed control scheme is effective in maintaining a robust DC link voltage even under unbalanced grid conditions. In other words, the drive side in this case of high power wind generators with a BTB VSC interface can operate independently from the grid disturbances, translating to higher availability of the renewable resources.

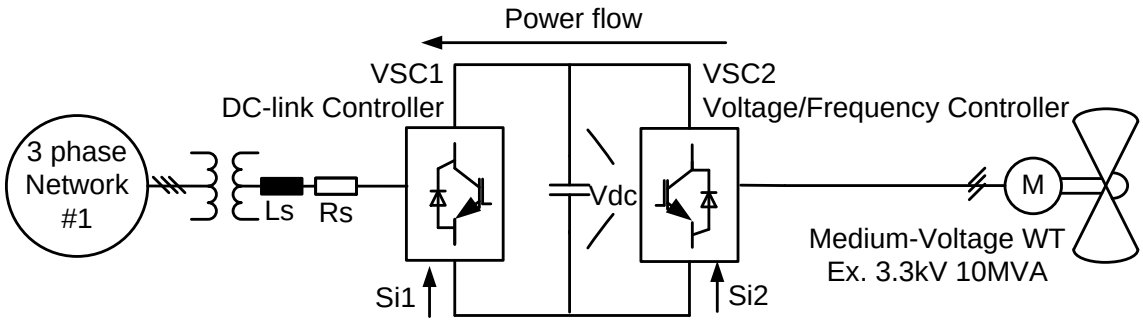

Figure 2-33. Simplified BTB VSC system in drive (wind) applications.

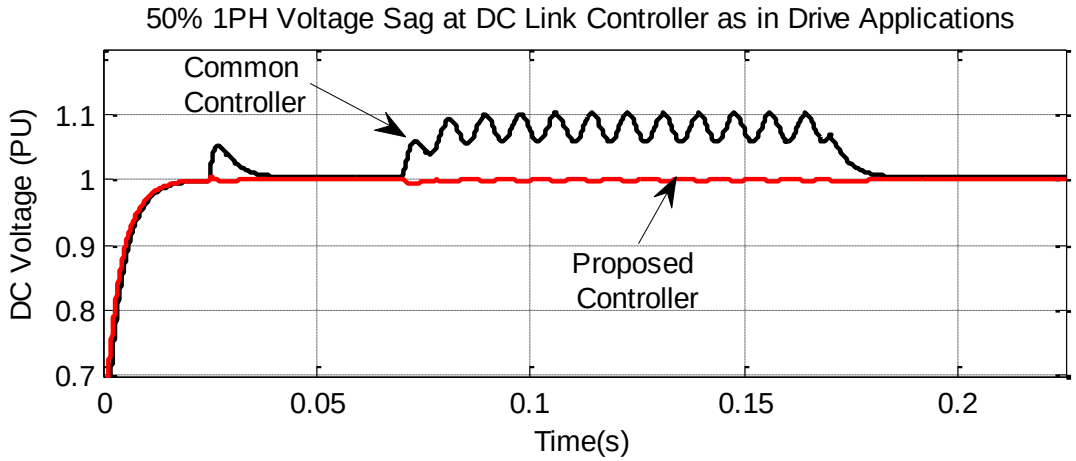

Figure 2-34. Performance comparison of the BTB VSC system with the proposed controller and commonly used control schemes under an unbalanced condition of 50% single line voltage sag in the DC link voltage controller for the drive application operated at 30 Hz (average model).

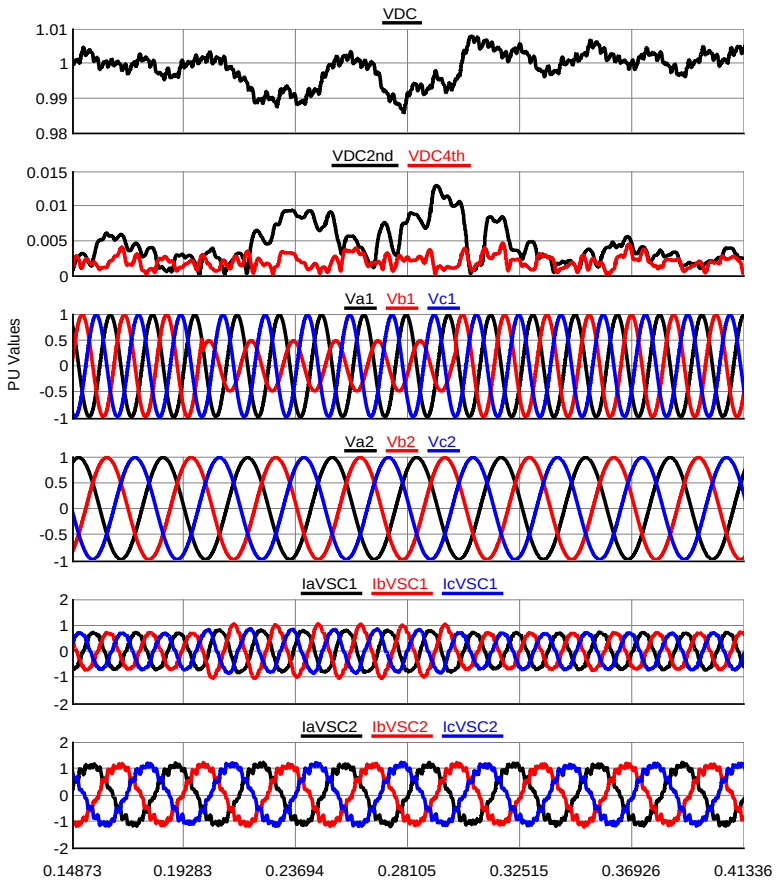

Figure 2-35. Dynamic performance of the BTB VSC system in drive (wind) applications under an unbalanced condition of 50% single-line voltage sag in the DC link voltage controller side and drive side operates at 30Hz- RTDS results.

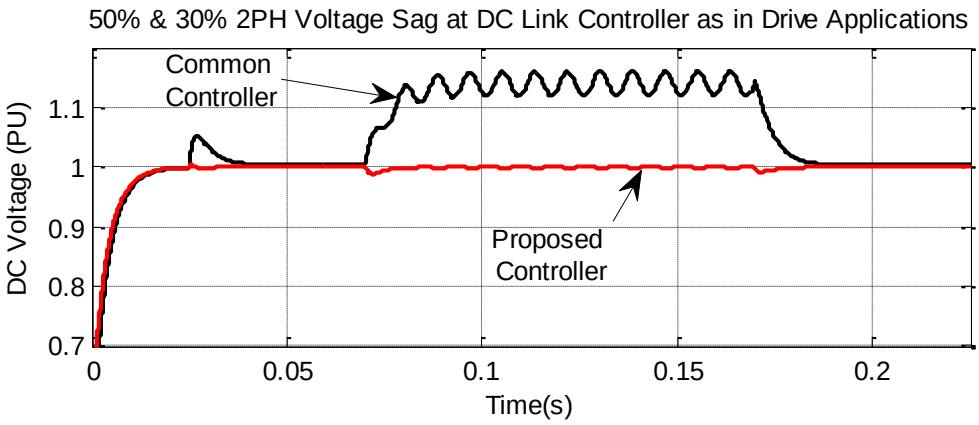

Figure 2-36. Performance comparison of the BTB VSC system with the proposed controller and commonly used control schemes under an unbalanced condition of 50% in phase B and 30% in phase C voltage sag in the DC link voltage controller for a drive application operated at 30 Hz (average model).

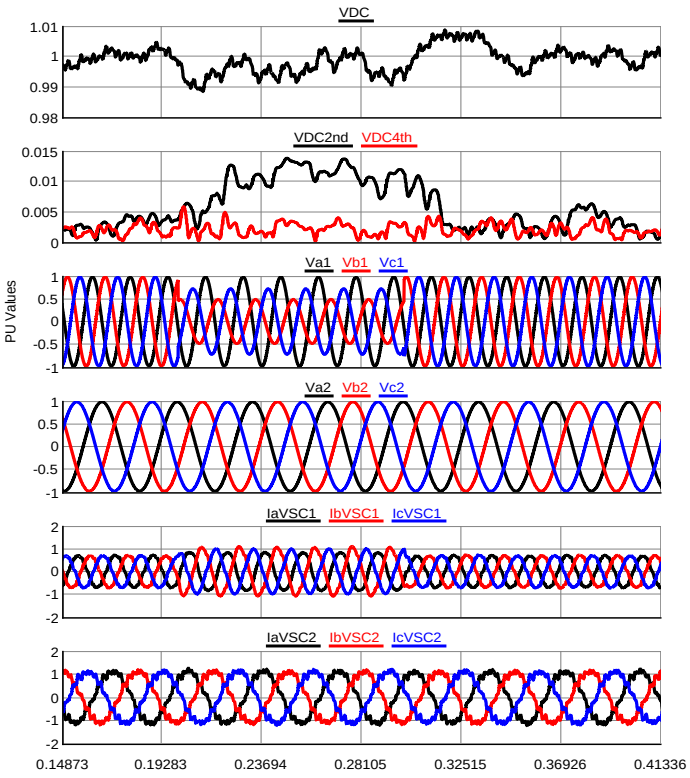

Figure 2-37. Dynamic performance of the BTB VSC system in drive (wind) applications under an unbalanced condition of 50% in phase B and 30% in phase C voltage sag in the DC link voltage controller side (grid) and drive side operating at 30 Hz- RTDS results.

2.8.3 **BTB VSC System for Transmission Transformer (Partial) Bypass**

With increasing demands of power electronics in the network, it is expected to have hybrid systems. One example of a hybrid system approach is known as the Modular Transformer Converter (MTC). An MTC as the transmission controller provides the flexibility of full or partial utilization for the transmission lines and power transformers. This flexibility thereby effectively increases the system's spare capacity and operating margins, and also provides back-up in case of substation transformer failure (or forced reduced rating operation) scenarios by providing real-time continuous power flow control. A simplified schematic of the MTC as the transmission controller connected in parallel to a transmission transformer is depicted in Figure 2-38. It is not the intention of this chapter to justify the applicability of the MTC approach for power systems and this topic will be covered in Chapter 4. Nevertheless, introducing the MTC as shown in Figure 2-38 brings remarkable effects on the dynamics of the system. In particular, any unbalance in the power system is seen by both converters which has been little appreciated in conventional applications of BTB VSC systems.

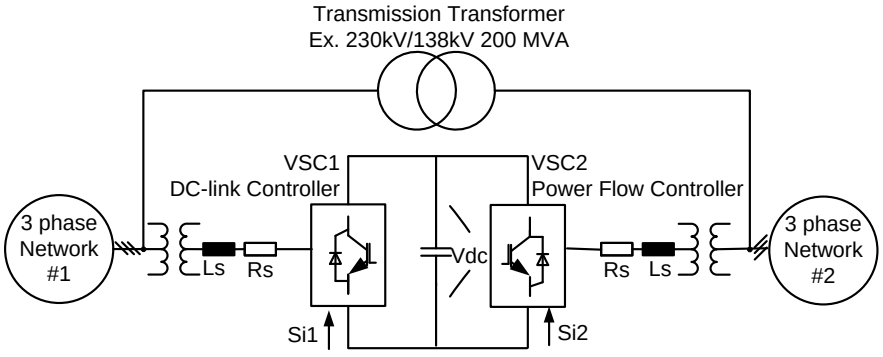

Figure 2-38. BTB VSC system in hybrid power system as transmission transformer (partial) back-up for life extension of the transmission transformer or contingencies.

The dynamic performance of the VSC BTB system with the proposed control structure for hybrid power system applications under balanced and unbalanced conditions is presented in Figure 2-39 and Figure 2-40. The first figure, Figure 2-39, presents the performance comparison of a BTB VSC system in the developed average model with the commonly used controllers and the proposed controller. The second figure, Figure 2-40 presents the detailed switching model of the converter system developed in RTDS. The power flow in the BTB system remains as stated in the previous case studies except that two networks have 5 degree phase difference for the natural power flow of the grid. The unbalanced system is represented by a 90% voltage drop in phase A of the PCC voltages. As can be observed, the DC link voltage remains practically stiff, and harmonic measurement of the DC link voltage for the second and fourth harmonics shows a satisfactory level of compensation under this severe fault case. Therefore, an MTC with the proposed control structure can be utilized even under the unbalanced conditions when it is needed the most.

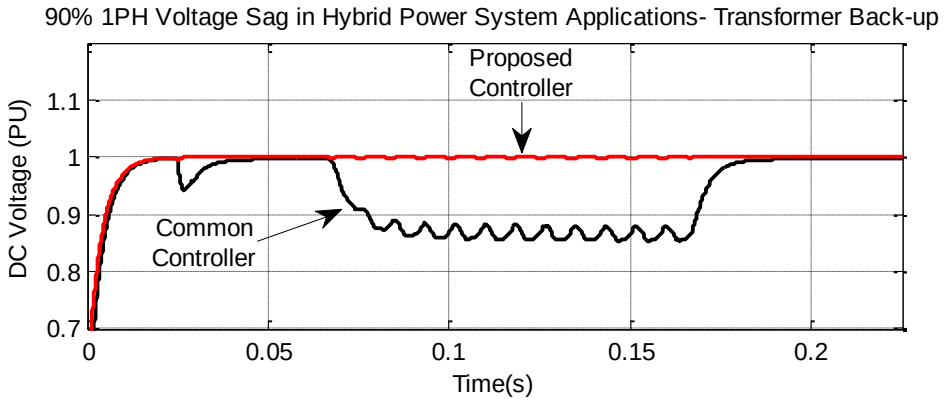

Figure 2-39. Performance comparison of the BTB VSC system with the proposed controller and commonly used control schemes under unbalanced condition of 90% voltage sage in phase A for hybrid power system applications (average model).

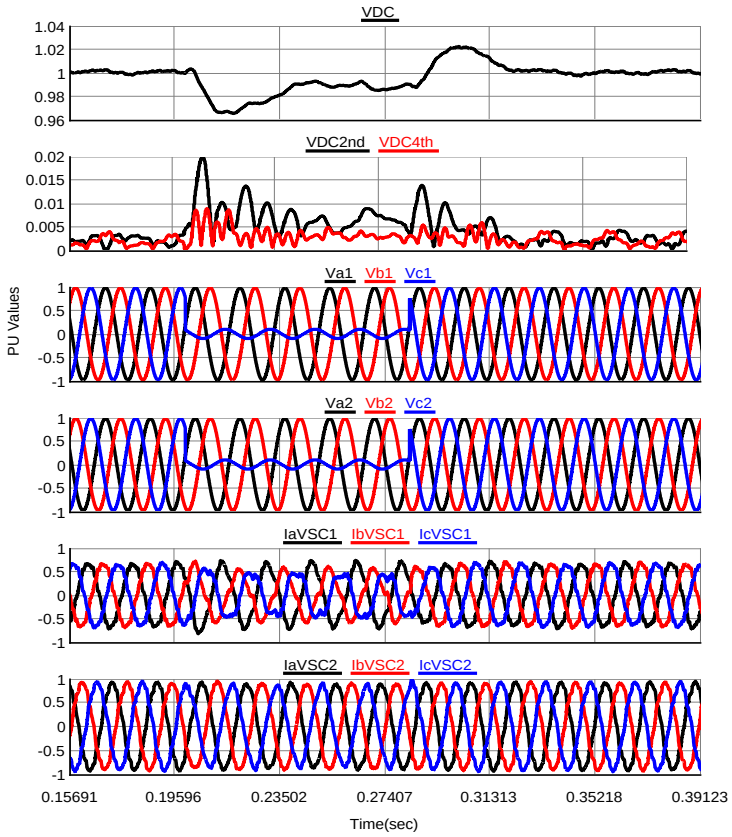

Figure 2-40. Dynamic performance of the BTB VSC system as in hybrid systems for transmission transformer (partial) back-up under unbalanced condition of 90% voltage sag in phase A- RTDS results.

2.9 **Summary**

VSC technology is the preferred building block for FACTS and HVDC controllers. VSC operates like a synchronous generator and therefore is well suited for transmission applications. However, performance of transmission level VSC technology under power system faults is one of the reasons that this technology may not be the first option for system

operators and utilities. In fact, if power system fault occur, VSC solutions are currently out of service just when they may be needed the most.

This chapter has addressed the DC link voltage control issues for vector-controlled back-to-back VSC-based transmission systems under power system disturbances which can be applied to a single VSC solution such as STATCOM. Having analyzed the state-of-the-art methods to mitigate the DC link voltage fluctuations under grid faults, this dissertation proposed control structures in the commonly used dq-synchronous frame. The proposed structures obviate the need for a sequence extraction block or resonant compensator. Therefore, there is no diminishing bandwidth factor, making them suitable for transmission applications for which the switching frequency is limited to a couple of hundred Hertz.

First, two control structures were proposed to address the possible overvoltage in BTB HVDC applications when the fault has occurred on the inverter side. The first scheme, Integrator Factor Control (IFC), was constructed by introduction of a non-linear virtual input to remove the inverter interaction from the DC link dynamics in the time domain. The other scheme was developed based on the Back-Stepping Control (BSC) method and the proper Lyapunov functions were introduced. The numerical results agreed with the theory developed to remove the varying load effect under network disturbances.

With increasing applications of multi-MW converters in different applications, more transient capability is needed; i.e., the unbalanced condition can be in either converter in the BTB system. In this chapter, a generalized control architecture was proposed that improves the transient performance of the VSC BTB system in current and emerging applications, denoted as HVDC, drive and hybrid power systems. The proposed controller structure is

designed based on regulating the converter system's states locally in the dq-synchronous frame without sequence extraction or a resonant compensator. The scheme; however, utilizes the interaction of the converters, the load, the bus voltage and their derivatives to compensate for the phase delay in the current regulator. The RTDS verification that the controller attains less than 1% DC link voltage deviation under most common faults ascertains the applicability and effectiveness of the proposed scheme for different transmission applications denoted as HVDC, drive and hybrid power systems. It is clear that for single VSC applications such as STATCOM, a lower number of measurements suffices for the effectiveness of the proposed control structure. For instance, no power measurement is needed. Therefore, it can be claimed that the proposed architecture is a generalized controller for the VSC technology.

Chapter 3. ANGLE-CONTROLLED VOLTAGE-SOURCED CONVERTER

3.1 Introduction

All Voltage-Sourced Converters (VSC), the building blocks of FACTS devices, regardless of their topology, can be divided into the two types shown in Figure 3-1. One type is the vector controlled or PWM-based inverter that has been explained in the previous chapter. The function of generating an arbitrary voltage vector is already known for this type of inverter, because the DC link voltage which is regulated to a fixed value, can be chopped with the PWM pulses to any arbitrary voltage vector. However, this type of converter system may not be suitable or may be uneconomical for many transmission level FACTS devices due to the output voltage quality and switching losses.

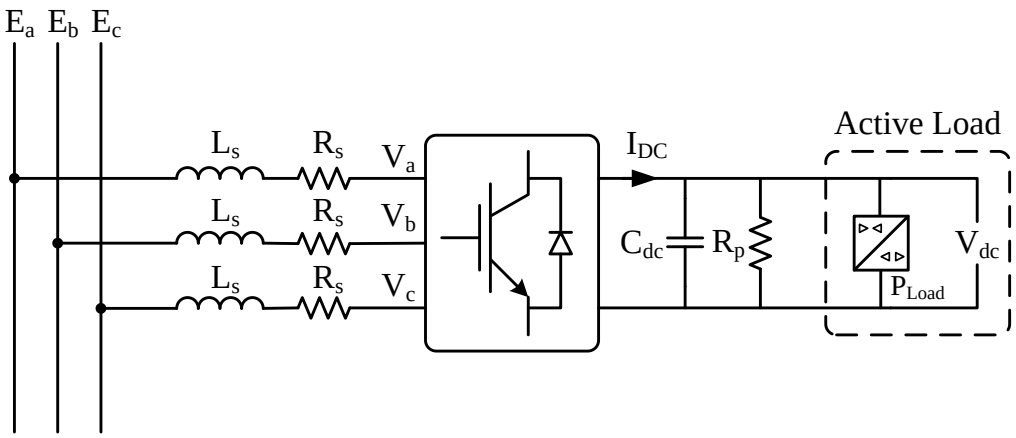

Figure 3-1. General schematic of voltage-sourced converter.

The other type of converter is based on output voltage angle control. So far, only reactive power transfer has been demonstrated, pioneered by Westinghouse (currently Siemens). An example of an angle control based converter is shown in Figure 3-2. It has been shown that by a slight change of angle the converter is able to provide inductive/capacitive reactive power as presented in Figure 3-3 , 7. Hence, very clean output voltage with a line switching frequency of 50/60 Hz could be achieved. However, with that scheme the active power is theoretically considered to be null except for the small fraction of power needed to compensate for the system losses. Consequently, there is an opportunity for research to investigate a complete angle controller for two converter systems which can be extended to HVDC applications or FACTS controllers such as IPFC or UPFC. On other hand, modular transformers can be connected in series to provide higher voltages applicable in transmission applications. The former solution has been studied in this dissertation and is covered in the next chapter called Modular Transformer Converter (MTC).

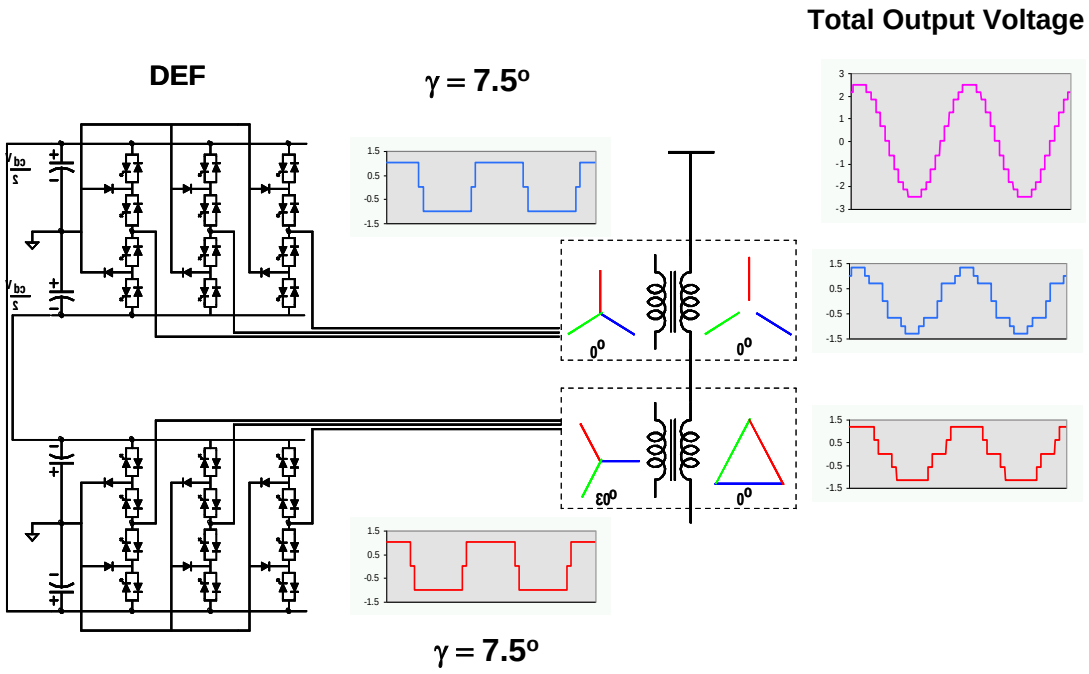

Figure 3-2. A 24 pulse angle-controlled VSC.

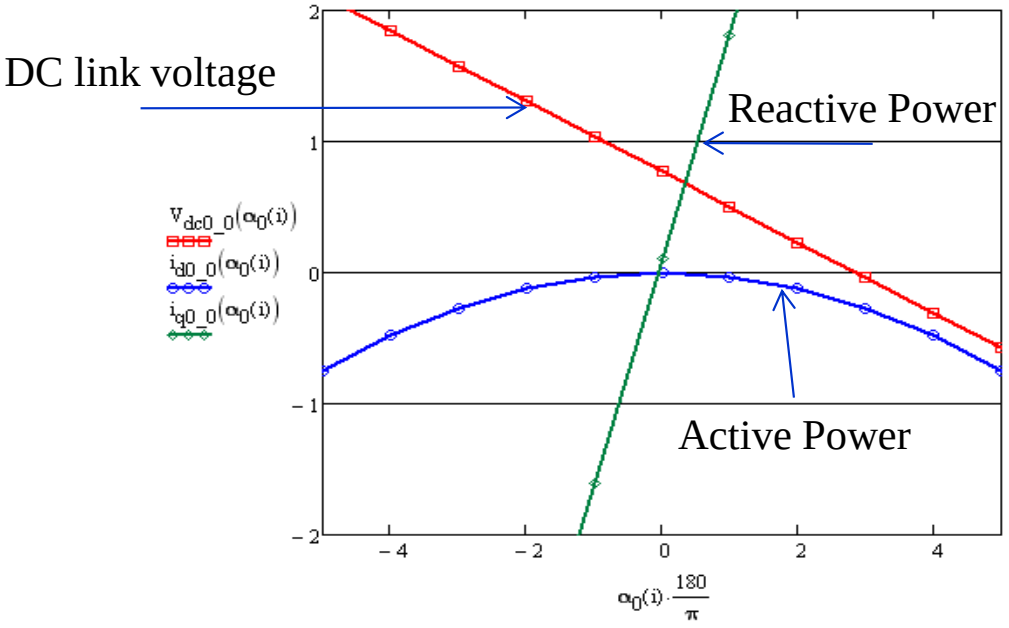

Figure 3-3. Operating characteristics of angle-controlled VSC as STATCOM.

It is important to note that in the pulse converters, optimum THD is achieved through a fixed phase delay, unlike complicated approaches for Selective Harmonic Elimination (SHE) for PWM converters. Figure 3-4 presents a general schematic of voltage construction in VSCs. For the pulse converters, one converter or a group of converters generates a voltage vector leading the other converter's voltage or a group of converters' voltages. To obtain optimum THD it can be proved that the leading (or lagging) angle should be fixed; shown as 2β in Figure 3-4. This fact has been also shown through (3.1)-(3.3). As a consequence, in pulse converters, there is only one degree of freedom shown as α in Figure 3-4. This limitation can be one of the grounds for not developing the vector-controlled pulse-converters. On the other hand, one degree of freedom is sufficient to achieve one objective. Therefore, STATCOM, which ultimately regulates the reactive power injection, is the best candidate for pulse-converters.

$$|V_{lead}| = |V_{lag}| = V \tag{3.1}$$

$$V_{Cd} = 2V\cos\beta\cos\alpha \tag{3.2}$$

$$V_{Cq} = -j2V\cos\beta\sin\alpha \tag{3.3}$$

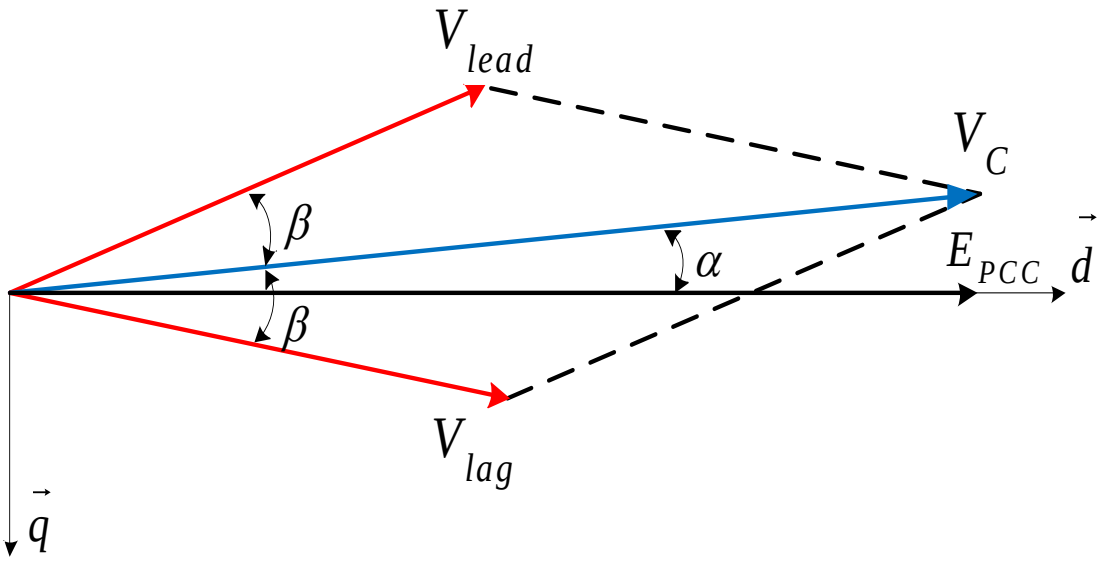

Figure 3-4. Output voltage vector construction in pulse-VSCs.

Besides reactive power, active power transfer capability has been shown in 44 and 45 by reconfiguration of the pulse converter system to achieve some level of freedom in control which may not be automatic. The contribution of the referenced work was the introduction of de-icer applications in transmission lines, where an angle controlled 48-pulse STATCOM was reconfigured to generate DC power to melt the ice on the lines. In 46, a unique converter topology is introduced. When there are two different voltage vectors, two independent variables are defined. These two variables are used to control active and reactive power independently. As mentioned in Figure 3-4, this approach suffers from the THD point of view and may not benefit from the basic nature of pulse converters. This chapter studies the feasibility and limitations of automatic control of the VSC with active power transfer capability based on angle control rather than PWM or vector control.

Until now, high power electronics converters that use linear or non-linear feedback control have been designed based on Single Input Single Output (SISO) systems. Although they can be sometimes interpreted as Multi Input Multi Output (MIMO) systems, the developed decoupled controllers mainly use the SISO principles. The main and original work in theory of inherent design limitations for SISO linear time-invariant feedback systems was developed by Bode, 47.

However, since one of the objectives of this dissertation is to regulate the active and reactive power of the converter through the converter output voltage angle, the converter system represents a single input two output system. Clearly, one actuator cannot be used to regulate two outputs to arbitrary setpoint values. Nevertheless, a one-dimensional class of setpoint values is feasible. As we shall see, the control signal used to force the outputs to a feasible setpoint may generate a transient disturbance in an orthogonal direction. In this chapter, the definition of "direction" of the plant and controller will be used to develop the feedback system.

The rest of this chapter is organized as follows. Section 3.2 presents the feasibility of active power transfer through angle control. In Section 3.3 the principle of single input two output feedback systems is introduced. The proposed feedback system and its verification through several cases are presented in Section 3.4 with an average model. Section 3.5 provides the verification of the proposed SITO control architecture for different BTB VSC applications in a PSCAD/EMTDC environment.

3.2 **Feasibility Study**

It is important to understand the operating area of the voltage- sourced converter when it is operated on either angle controller or vector control. On the other hand, the power system side can also affect the apparent power (VA) that can be transferred between two points. Figure 3-5 demonstrates the reactive power that can be delivered when the generated voltage can be altered so that a nominal active power is transferred. From this figure it can be concluded that if it is possible to generate a desired voltage vector, it is then possible to have a controlled active/reactive power theoretically. This is known through chopped PWM pulses or angle control for reactive power regulation.

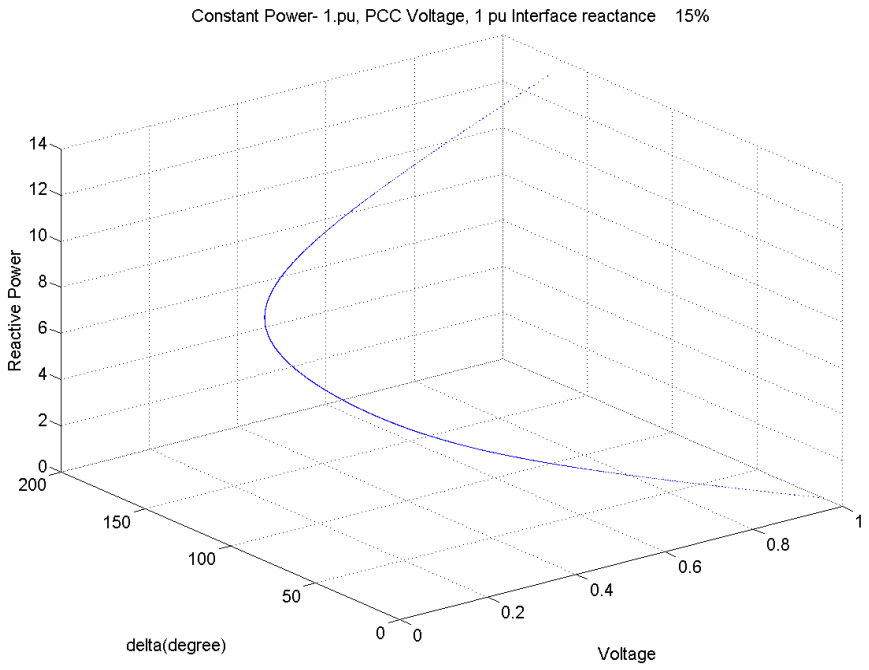

Figure 3-5. Reactive power transfer capability of the power system with constant active power.

The next step is to verify whether the voltage-sourced converter is able to provide the variable voltage vector to accommodate this apparent power range. The schematic of a voltage-sourced converter is depicted in Figure 3-1. Therefore, it is necessary to find out how VSC may operate with active power support capability if there is only one degree of freedom for the angle control.

(3.4) describes the current and voltage quantities of the VSC in the dq-synchronous reference frame, for which the d-axis is always aligned with the instantaneous bus voltage. Understanding of feasible the operating area is essential for the control concepts that will be developed. The set of equations is solved for a different power when only the angle is changed. The positive sign for power refers to the rectifier mode of operation and the negative sign for inverter mode. The parameters are listed in Table III.

TABLE III. Angle-Controlled System Parameters in P.U.

DC link capacitance	C'	0.88
AC side inductance	L'	0.3
AC side resistance	R'	0.01
DC/AC voltage factor	K	$4/\pi$
Converter loss resistance	R'_p	$100/k$
Frequency	$\omega = \omega_b$	377
Bus voltage	E'_d	1

$I_p^{'}$ is inserted to show the effect of the load in the DC link as the power source/sink. Figure 3-6-Figure 3-8 demonstrate the possible region in which VSC can supply or absorb power. As can be observed, there is the potential of using the angle as the only controller

input to achieve different values for active and reactive power while obtaining some stable values for the DC link voltage. *p* denote *d/dt*.

$$p\begin{bmatrix} i'_d \\ i'_q \\ v'_{DC} \end{bmatrix} = A\begin{bmatrix} i'_d \\ i'_q \\ v'_{DC} \end{bmatrix} + \begin{bmatrix} -\frac{\omega_b}{L'}E'_d \\ 0 \\ -\omega_b C' I'_p \end{bmatrix} \tag{3.4}$$

$$A = \begin{bmatrix} -\frac{R'_s\omega_b}{L'} & \omega & \frac{k\omega_b}{L'}\cos(\alpha) \\ -\omega & -\frac{R'_s\omega_b}{L'} & \frac{k\omega_b}{L'}\sin(\alpha) \\ -\frac{3}{2}kC'\omega_b\cos(\alpha) & -\frac{3}{2}kC'\omega_b\sin(\alpha) & -\frac{\omega_b C'}{R'_p} \end{bmatrix} \tag{3.5}$$

$$p\begin{bmatrix} i'_d \\ i'_q \\ v'_{DC} \end{bmatrix} = A\begin{bmatrix} i'_d \\ i'_q \\ v'_{DC} \end{bmatrix} + \begin{bmatrix} -\frac{\omega_b}{L'}E'_d \\ 0 \\ -\omega_b C' I'_p \end{bmatrix} \tag{3.6}$$

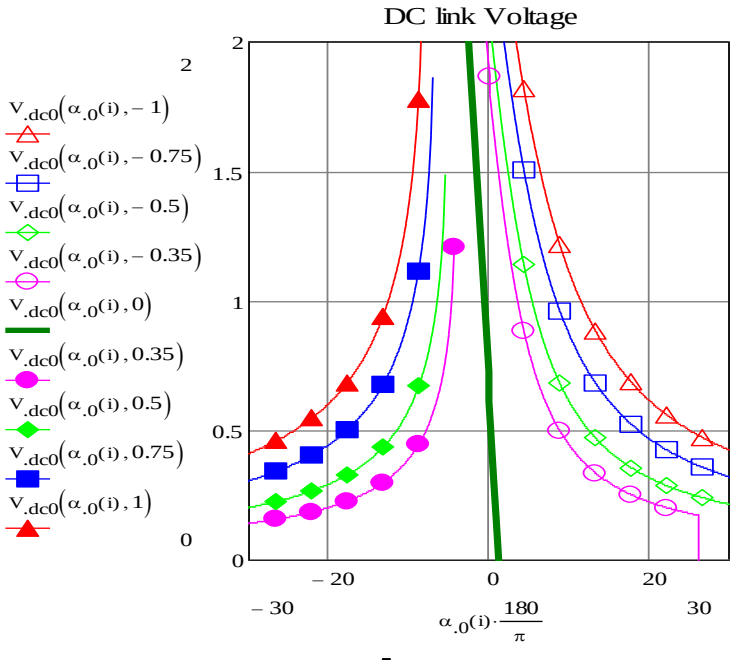

Figure 3-6. DC link voltage steady state operating points vs. output voltage angle.

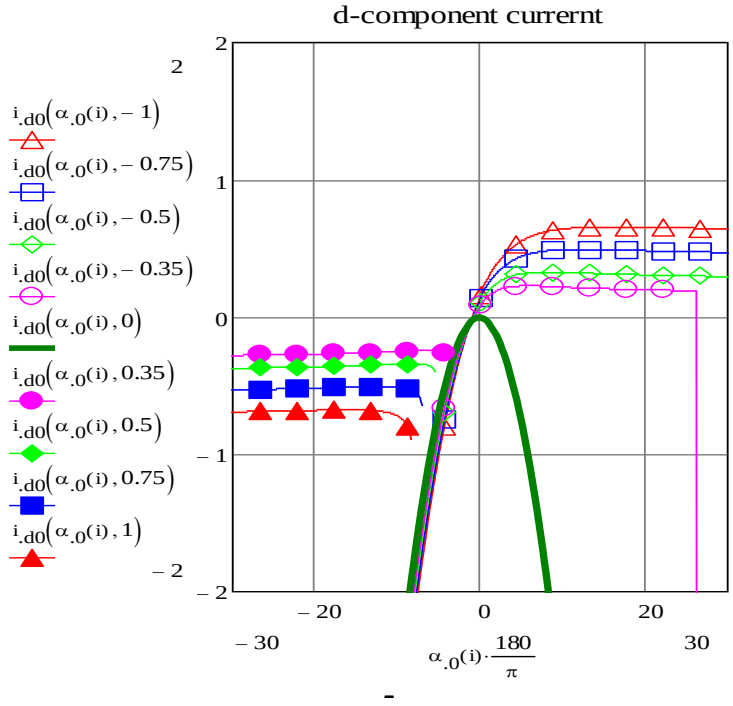

Figure 3-7. d-component of the current(representing the active power) steady state operating points vs. output voltage angle.

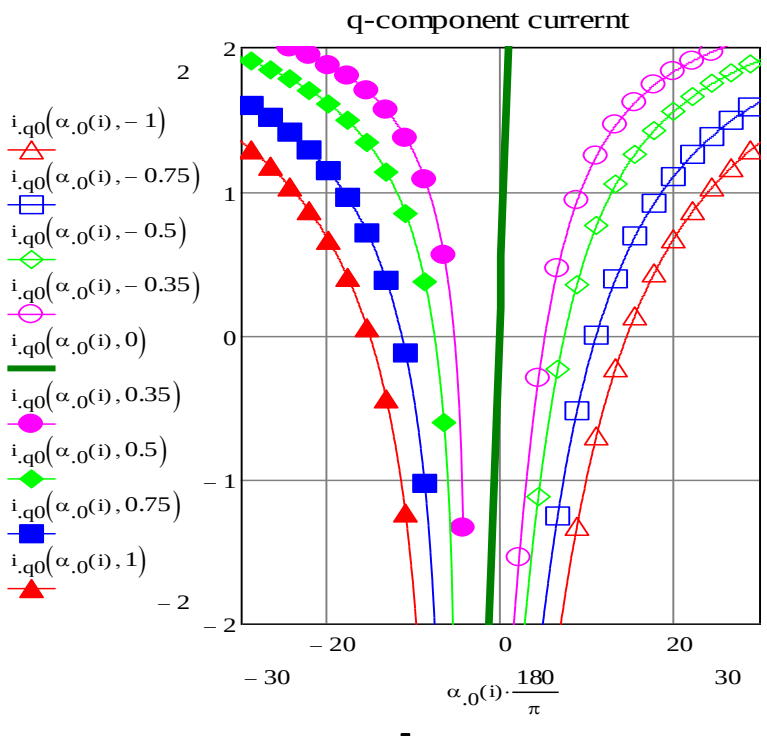

Figure 3-8. q-component of the current (representing the reactive power) steady state operating points vs. output voltage angle.

3.3 **Single Input Two Output (SITO) Feedback Systems**

3.3.1 **Introduction**

Since the objective of this chapter is to regulate the active and reactive power through output voltage angle control, a different framework for the feedback system must be developed. As is obvious by now, the considered scheme has the properties of single input two output systems as presented in Figure 3-9.

Given that the SITO feedback systems for VSC based FACTS devices have not been reported, it becomes essential to review the properties of SITO feedback systems. The main

body of this section uses the results stated in 48 and 49. Clearly, one actuator cannot be used to regulate two outputs to arbitrary setpoint values. Nevertheless, a one-dimensional class of setpoint values is feasible. As we shall see, the control signal used to force the outputs to a feasible setpoint may generate a transient disturbance in an orthogonal direction.

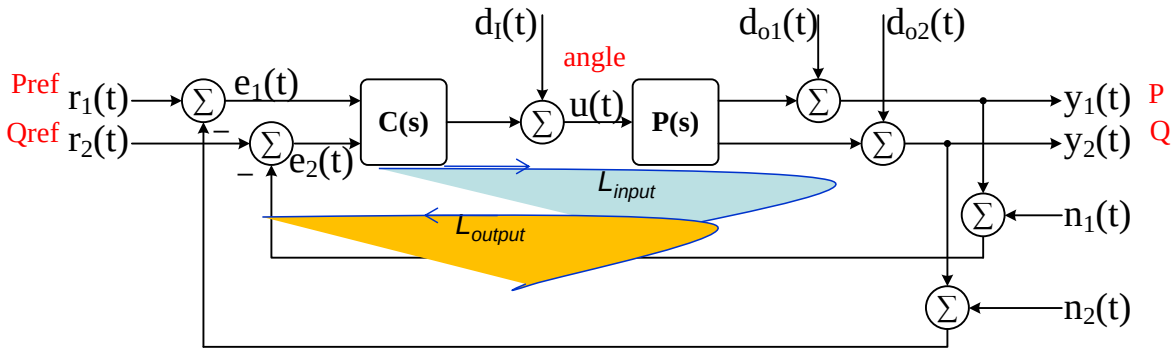

Figure 3-9. General Single Input Two Output (SITO) automatic feedback system.

3.3.2 **Preliminaries**

Give a vector $v \in C^n$, let $\|v\|$ denote the Euclidean vector norm. Denote the range of a matrix $M \in C^{m \times n}$ by $\Re(M)$, the rowspace of M by $\Re_{row}(M)$ and the nullspace of M by *N(M)*. We denote the matrix norm induced by the Euclidean vector norm by $\|M\|$. Let the open and closed right and left halves of the complex plane be denoted by ORHP, CRHP, OLHP, and CLHP, respectively.

Consider the feedback system depicted in Figure 3-9, where *P(s)* and *C(s)* are the transfer functions of the plant and the controller respectively, and their elements shown in (3.7) are rational and proper.

$$P(s)=\begin{bmatrix} P_1(s) \\ P_2(s) \end{bmatrix} \quad C(s)=\begin{bmatrix} C_1(s) & C_2(s) \end{bmatrix} \tag{3.7}$$

Associated with this feedback system are the input and output open loop transfer functions, $L_I \triangleq CP$ and $L_O = PC$, sensitivity functions, $S_I \triangleq (1+L_I)^{-1}$ and $L_O = PC$ and complementary sensitivity functions, $T_I \triangleq L_I(1+L_I)^{-1}$ and $T_O \triangleq L_O(1+L_O)^{-1}$. It is known that each closed loop transfer function characterizes the close loop response to a class of exogenous inputs.

Each pair of sensitivity and complementary sensitivity function must satisfy the identities:

$$S_I(s)+T_I(s)=1 \tag{3.8}$$

$$S_O(s)+T_O(s)=I \tag{3.9}$$

The latter one may be rearranged into the useful form:

$$S_O(s)=I-\frac{P(s)C(s)}{1+C(s)P(s)} \tag{3.10}$$

Many design criteria in the SISO case consider the high gain limit as $|L_I(j\omega)| \to \infty$, where we can conclude that

$$T_I(j\omega) \to 1 \quad S_I(j\omega) \to 0 \tag{3.11}$$

Here, the difference in SITO systems is that high gain properties of the output transfer functions are not so straightforward. In fact, note that the plant and controller transfer functions have non-trivial nullspaces. Considering (3.10), we can conclude that $\|S_O(j\omega)\| \geq 1$ independently of the gain of the system. Therefore, not all the disturbances can be attenuated and not all the commands can be tracked.

These are the facts that necessitate a framework within which the response of a SITO system can be described. Consequently, this framework should lead us to design stabilized controllers. This framework as 48 suggests, uses the roles of gain and direction of the controller which will be covered in the next subsections.

3.3.3 **Plant and Controller Directions**

Lemma 1. A $q \times p$ transfer matrix P of normal rank equal to p can always be factored as

$P(s) = N(s)K(s) = \underline{K}(s)\underline{N}(s)$

where N is a $q \times p$ polynomial matrix and K is a $p \times p$ transfer matrix.

Based on Lemma 1, we can factor the plant and controller as

$$P(s) = N_p(s)K_p(s) \quad N_p = \begin{pmatrix} n_{p1} & n_{p2} \end{pmatrix}^T \tag{3.12}$$

$$C(s) = K_c(s)N_c(s) \quad N_c = \begin{pmatrix} n_{c1} & n_{c2} \end{pmatrix}^T \tag{3.13}$$

Definition 1. (Transfer Matrix Direction)

a. Suppose that $P(j\omega) \neq 0$, and define the direction of the plant at that frequency ω by $\Re\left(N_p(j\omega)\right)$. If $j\omega$ is not the pole of $P(s)$, then $\Re\left(N_p(j\omega)\right) = \Re\left(P(j\omega)\right)$.

b. Suppose that $C(j\omega) \neq 0$, and define the direction of the plant at that frequency ω by $\Re_{row}\left(N_c(j\omega)\right)$. If jω is not the pole of $C(s)$, then $\Re_{row}\left(N_c(j\omega)\right) = \Re_{row}\left(C(j\omega)\right)$.

It is straightforward to verify that the directions depend only on the ratios:

$$P_{rat} \triangleq \frac{n_{p2}}{n_{p1}}$$

and

$$C_{rat} \triangleq \frac{n_{c2}}{n_{c1}}.$$

As mentioned in 48, several interesting properties of SITO systems are described in terms of plant and controller alignment.

3.3.4 **Plant/Controller Alignment**

Definition 2. (Plant/Controller Alignment Angle): Assume that both $P(j\omega)$ and $C(j\omega) \neq 0$. Suppose that ω is neither a pole of *P(s)* nor *C(s)*. Then define the alignment angle between the plant and controller by (3.14).

$$\phi(j\omega) \triangleq \arccos\left(\frac{|C(j\omega)P(j\omega)|}{\|C(j\omega)\|\|P(j\omega)\|}\right) \tag{3.14}$$

If $j\omega$ is a pole of *P(s)* and/or *C(s)*, then define the alignment angle by (3.15).

$$\phi(j\omega) \triangleq \arccos\left(\frac{|N_c(j\omega)N_p(j\omega)|}{\|N_c(j\omega)\|\|N_p(j\omega)\|}\right) \tag{3.15}$$

If $\phi(j\omega) = 90^\circ$ then the plant and controller are completely misaligned. We say loosely that the controller and plant are well aligned if $\phi(j\omega) \approx 0^\circ$, and poorly aligned if $\phi(j\omega) \approx 90^\circ$.

If the plant and controller are significantly misaligned, then the magnitude of the output sensitivity function and complementary sensitivity function may be much larger than their counterparts at the plant input as is clear from the following proposition. It must be added that alignment is critical to closed loop performance at frequencies within the closed loop bandwidth.

Proposition 1. The output complementary sensitivity function satisfies

$$\|T_O(j\omega)\| = \frac{|T_I(j\omega)|}{\cos(\phi(j\omega))} \tag{3.16}$$

where $\phi(j\omega)$ is defined by (3.14).

3.3.5 **Plant Direction vs. Frequency**

It has been shown in 48 that a perfectly aligned controller will achieve the minimum possible level of interactions given the limitations imposed by the plant. To define those

limitations, 49 introduces a coordinate system that describes how the plant varies with frequency.

Definition 3. (DC Coordinates) Let $M \in R^{2\times 2}$ be an orthonormal matrix whose first column spans $\Re\left(N_p(0)\right)$. Define transformed coordinates $\tilde{N}_p = M^T N_p$. Define $\tilde{n}_{p1}$ and $\tilde{n}_{p2}$ as in (3.12). By construction $\tilde{n}_{p2} = 0$, and if $\Re\left(P(j\omega)\right)$ is constant, then $\tilde{P}_2(j\omega) = 0$. A similar transformation yields $C = \tilde{C}M^T$.

It is easy to show that transformation to DC coordinates preserves the transfer function at the plant input transfer functions and the norm of the transfer functions at the plant output.

By analogy to (3.12), we can factor the plant in transformed coordinates as

$$\tilde{P}(s) = \begin{pmatrix} \tilde{n}_{p1}(s) \\ \tilde{n}_{p2}(s) \end{pmatrix} \tilde{K}_p(s) \tag{3.17}$$

In 50, integral constraints on the output complementary sensitivity function are developed in DC coordinates. Here, we focus on one integral constraint that helps to define the range of the stabilizing controllers.

Define the desired input loop gain like a first order system. Suppose that:

$$\tilde{P}(s) = \begin{pmatrix} \tilde{n}_{p1}(s) \\ \tilde{n}_{p2}(s) \end{pmatrix} \tilde{K}_p(s) \tag{3.18}$$

$$\left\| T_O(j\omega) \right\| \le \left| T(j\omega) \right| = \left| \frac{\omega_0}{j\omega + \omega_0} \right| \tag{3.19}$$

$$\phi(0) \le \phi_{\max} \tag{3.20}$$

Then,

$$\log \frac{\|T_O\|_\infty}{|T_I(0)|} \geq \left\{ \omega_0 F(P) - \omega_0 \int_0^{\omega_0} \log \left| \frac{\omega_0 / j\omega}{1 + \omega_0 / j\omega} \right| \frac{d\omega}{\omega^2} - \frac{\pi}{2} \omega_0 \tan(\phi_{\max}) \left| \lim_{s \to 0} \frac{d}{ds} \tilde{P}_{rat}(s) \right| \right\} \tag{3.21}$$

where,

$$F(P) \triangleq \frac{\pi}{2} \left(\sum_{i=1}^{N_\delta} \frac{1}{\delta_i} + \sum_{i=1}^{N_\rho} \frac{1}{\rho_i} + \sum_{i=1}^{N_\lambda} \frac{1}{\lambda_i} + 2 \sum_{i=1}^{N_\alpha} \frac{1}{\alpha_i} \right). \tag{3.22}$$

Denote

a. NMP zeros of $\Delta^*(s) = \tilde{N}_P^T(-s)\tilde{N}_P(s)$ by δ_i,

b. NMP zeros of $\Delta^*(s) = \tilde{N}_P^T(-s)\tilde{N}_P(s)$ by ρ_i,

c. OLHP zeros of $\tilde{n}_{p1}$ by λ_i,

d. NMP zero of $\tilde{n}_{p1}$.

The measure introduced in (3.21) can show the lower bound for the peak of the output complementary sensitivity function.

3.3.6 **Perfect Plant/Controller Alignment**

Based on what we have seen, it is tempting to suppose that perfect alignment, $\phi(j\omega) = 0$ is an optimal choice. However, in this subsection it will be shown that it is not desirable to make $\phi(j\omega) = 0, \forall \omega \in \mathbb{R}$.

Proposition 2. The plant and controller are perfectly aligned at all frequencies if and only if the controller can be expressed as

$$C(s) = K_c(s)\begin{pmatrix} n_{p1}(-s) & n_{p2}(-s) \end{pmatrix} \tag{3.23}$$

where $n_{p1}(s)$, $n_{p2}(s)$ are given in (3.12) and $K_c(s)$ is a rational transfer function.

Corollary 1. (NMP Zeros of $n_{p2}(s)$) Suppose that $P(s)$ and $C(s)$ are perfectly aligned at all frequencies. Then unless the direction of the plant is constant with frequency, the input open loop transfer function $L_I(s)$ must necessarily possess at least one NMP.

The significance of Corollary 1 is that NMP zeros of $L_I(s)$ will impose design limitations on $S_I(s)$. In fact, the lower bound in (3.21) can give some hints on how to design the input open loop transfer function. This limitation is specifically important for the plant whose direction does not change significantly with frequency. This fact has no counterpart in SISO systems.

3.3.7 **Disturbance Rejection**

We can use the high gain limit to present the response of the system to a disturbance. With the help of the high gain proposition of 48, the following results can be obtained.

Corollary 2. Let $S_O^{HG}(s)$ be the high gain output sensitivity transfer function, then

$$N\left(S_O^{HG}(j\omega)\right) = \Re\left(P(j\omega)\right) \tag{3.24}$$

$$\Re\left(S_O^{HG}(j\omega)\right) = N\left(C(j\omega)\right) \tag{3.25}$$

By Corollary 2, use of high gain at a given frequency will attenuate the effects of a disturbance at that frequency if and only if the disturbance is aligned with the plant. The response to a disturbance that is aligned with the plant will not be zero; however, by (3.25) the response will be confined to $\Re\left(S_O^{HG}(j\omega)\right) = N\left(C(j\omega)\right)$. For instance, for a stable $S_O(s)$, a step disturbance can be rejected with integral control if and only if it is aligned with the zero frequency gain of the plant. The response to other step disturbances is confined to $N(C(0))$.

A similar definition for the alignment angle between the output disturbance and the plant/controller can be written.

Suppose that the output disturbance has the form

$$D_O(s) = P_d(s)D(s) \tag{3.26}$$

Definition 4. Define the angle between the plant/controller and the disturbance by

$$\phi_{pd}(j\omega) \triangleq \arccos\left(\frac{\left|P^H(j\omega)P_d(j\omega)\right|}{\left\|P^H(j\omega)\right\|\left\|P_d(j\omega)\right\|}\right) \tag{3.27}$$

$$\phi_{cd}(j\omega) \triangleq \arccos\left(\frac{\left|C(j\omega)P_d(j\omega)\right|}{\left\|C(j\omega)\right\|\left\|P_d(j\omega)\right\|}\right) \tag{3.28}$$

Then, in the limit as $\left|S_I(j\omega)\right| \to 0$.

$$\frac{\left\|S_O(j\omega)P_d(j\omega)\right\|}{\left\|P_d(j\omega)\right\|} \to \frac{\sin\left(\phi_{pd}(j\omega)\right)}{\cos\left(\phi(j\omega)\right)} \tag{3.29}$$

The result of (3.29) is consistent with (3.16) and (3.24).

3.4 **Feedback System Design for VSC as a SITO Closed-Loop System**

The VSC state space equations, (3.4) are nonlinear if α is regarded as an input variable. The small signal modeling of the converter system leads to the following.

$$p\begin{bmatrix}\Delta i_d' \\ \Delta i_q' \\ \Delta v_{dc}'\end{bmatrix} = A_\Delta \begin{bmatrix}\Delta i_d' \\ \Delta i_q' \\ \Delta v_{dc}'\end{bmatrix} + B_\Delta \Delta\alpha + K_\Delta \begin{bmatrix}\Delta E_d \\ \Delta P_L\end{bmatrix} \tag{3.30}$$

where

$$A_\Delta = \begin{bmatrix} -\frac{R_s'\omega_b}{L'} & \omega & \frac{k\omega_b}{L'}\cos(\alpha) \\ -\omega & -\frac{R_s'\omega_b}{L'} & \frac{k\omega_b}{L'}\sin(\alpha) \\ -\frac{3}{2}kC'\omega_b\cos(\alpha) & -\frac{3}{2}kC'\omega_b\sin(\alpha) & \frac{-\omega_b C'}{R_p} - \omega_b C'\frac{P_{L0}}{V_{DC0}^2} \end{bmatrix}$$

$$B_\Delta = \begin{bmatrix} \frac{-k\omega_b V_{DC0}}{L'}\sin(\alpha_0) \\ \frac{k\omega_b V_{DC0}}{L'}\cos(\alpha_0) \\ \frac{3}{2}kC'\omega_b(i_{d0}\sin(\alpha_0) - i_{q0}\cos(\alpha_0)) \end{bmatrix}$$

$$K_\Delta = \begin{bmatrix} \frac{-\omega_b}{L'} & 0 \\ 0 & 0 \\ 0 & \frac{-\omega_b C'}{V_{DC0}} \end{bmatrix}. \tag{3.31}$$

The plant and output disturbance can be calculated as follows:

$$P(s) = C(sI - A_\Delta)^{-1} B_\Delta \tag{3.32}$$

$$D_o(s) = C(sI - A_\Delta)^{-1} K_\Delta \tag{3.33}$$

where

$$C = \begin{bmatrix} 1 & 0 & 0 \\ 0 & 1 & 0 \end{bmatrix}.$$

Transfer functions have been numerically computed for two operating points: a complete power sink of 1 p.u (rectifier mode) and power source of 1 p.u.(inverter mode). The corresponding steady state p.u. values for 1 p.u. of power sink are

$$i_{d0} = -0.677, i_{q0} = 0, V_{dc0} = 0.796, \alpha_0 = -11.55^\circ.$$

To study the direction of the plant vs frequency, a new coordinate is introduced as mentioned in the previous section. Using Definition 3, the M matrix is determined to be (3.34).

$$M = \begin{pmatrix} 0.391 & -0.92 \\ 0.92 & 0.391 \end{pmatrix} \tag{3.34}$$

The integral of (3.21) is calculated for both operating points. For both operating points *F(P)=0.019*. The plot for the lower bound of (3.21) is presented in Figure 3-10. It can be seen that the range of ω for which (3.18)-(3.20) are satisfied is limited. Although it might be desirable to have perfect alignment, it has been shown that this implies a bandwidth constraint on the closed loop system. This constraint is more critical for SITO systems if the plant direction does not change significantly. Figure 3-11 depicts the plant direction in two

coordinates. It can be seen that the plant direction does not change significantly in any of these coordinates with frequency within the required bandwidth.

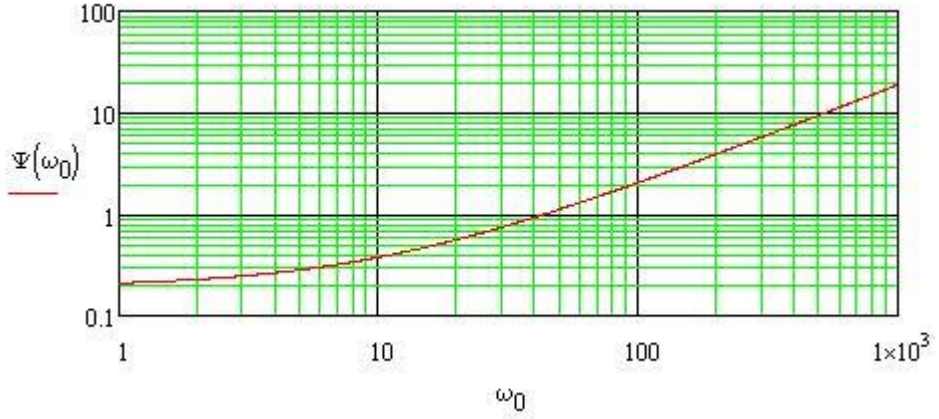

Figure 3-10. Low bound on $\frac{\|T_o\|_\infty}{|T_I(0)|}$

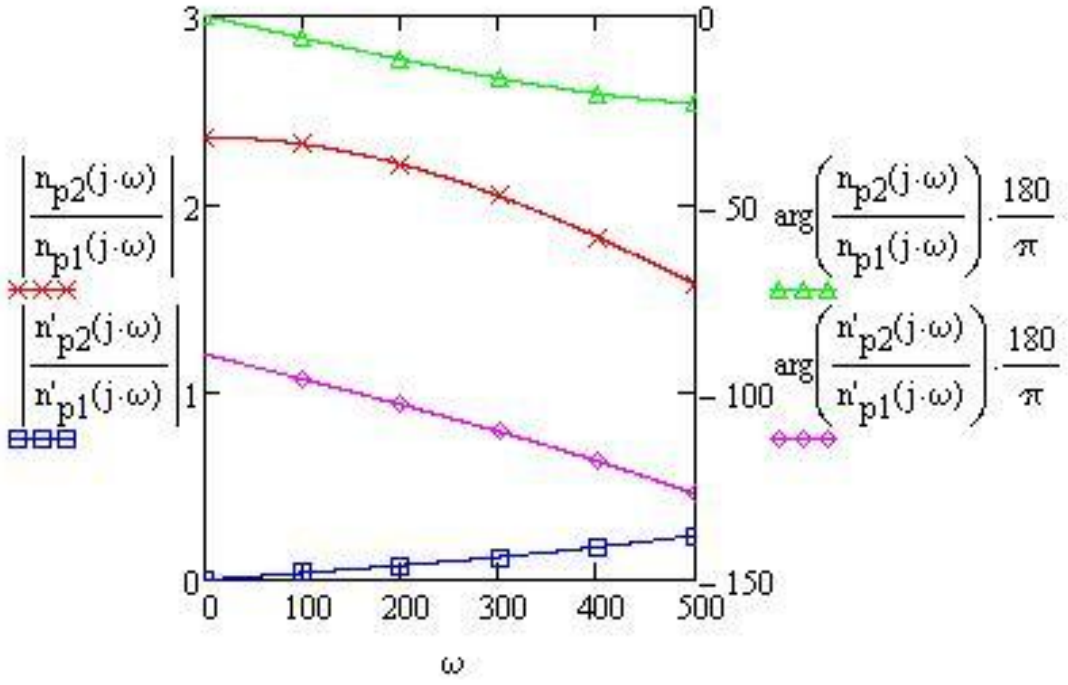

Figure 3-11. Plant (converter system) direction vs. frequency.

It can be also shown that with this particular example, perfect alignment cause the system to become unstable. This can be proved by several methods, such as the Routh-Hurwitz stability criteria.

From Figure 3-10, Figure 3-11 and what has been explained in the previous section, there is a family of stabilizing controllers that should not be perfectly aligned with the plant.

Suppose that the considered plant has a major disturbance of DC load power which can be considered as the energy storage system or another converter forming a BTB system. It has been shown that if the plant is aligned with the output disturbance, by using an integral controller, that effect of the disturbance to the output can be rejected in steady state. This point is worth mentioning, since it can supply additional criteria for designing the power converter. The alignment angle between plant and this disturbance is calculated as (3.14) and plotted in Figure 3-12. It has been shown that at low frequency the disturbance is aligned with the plant and can be rejected.

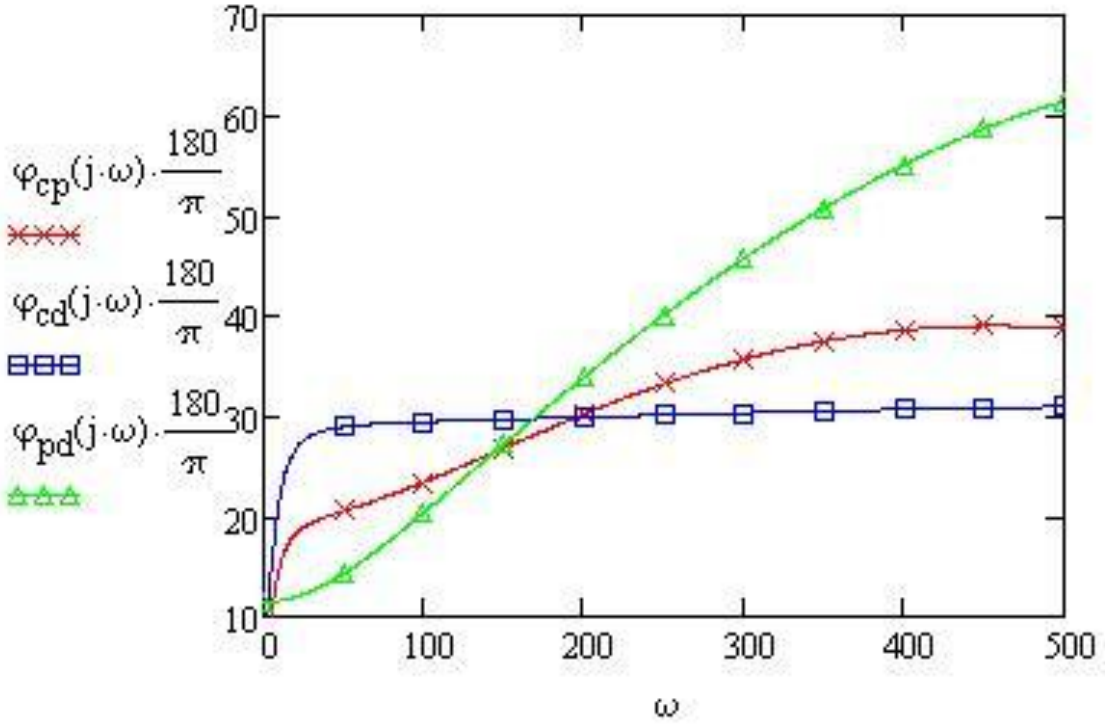

Figure 3-12. Alignment angles variations vs frequency.

Therefore, from a family of stabilizing controllers for this SITO system, the following controllers are selected that are slightly misaligned with the plant and the second disturbance (DC load) to satisfy the output sensitivity and complementary sensitivity transfer functions requirements. The corresponding input complementary sensitivity function is plotted in gain/phase diagram, Figure 3-13, which can be interpreted as in the SISO case.

$$C_1(s) = \frac{61}{s+200} + \frac{7.876}{s} + 1.5 \tag{3.35}$$

$$C_2(s) = \frac{143.2}{s+200} + \frac{23.59}{s} + 0.5 \tag{3.36}$$

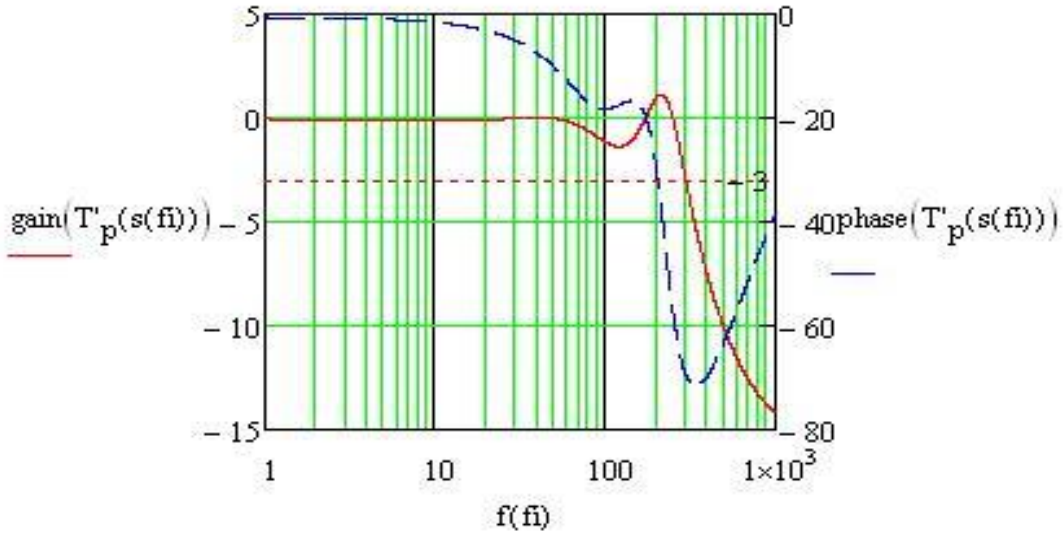

Figure 3-13. Gain/phase plot of the input complementary sensitivity function.

The performance of the average mode of the converter for the designed feedback system is shown in Figure 3-14 with certain regions expanded in Figure 3-15-Figure 3-17. In the first second, the converter absorbs a ramp of active power up to 1 p.u. while the reactive power is null. As can be seen, the DC link does not undergo a major change due to this active power change. Different operation modes are shown in this figure. An interesting mode is at 2.5s: when the reactive power has a step change to -0.8, the DC link voltage reaches a new point as expected. From 3s onward the inverter mode is shown.

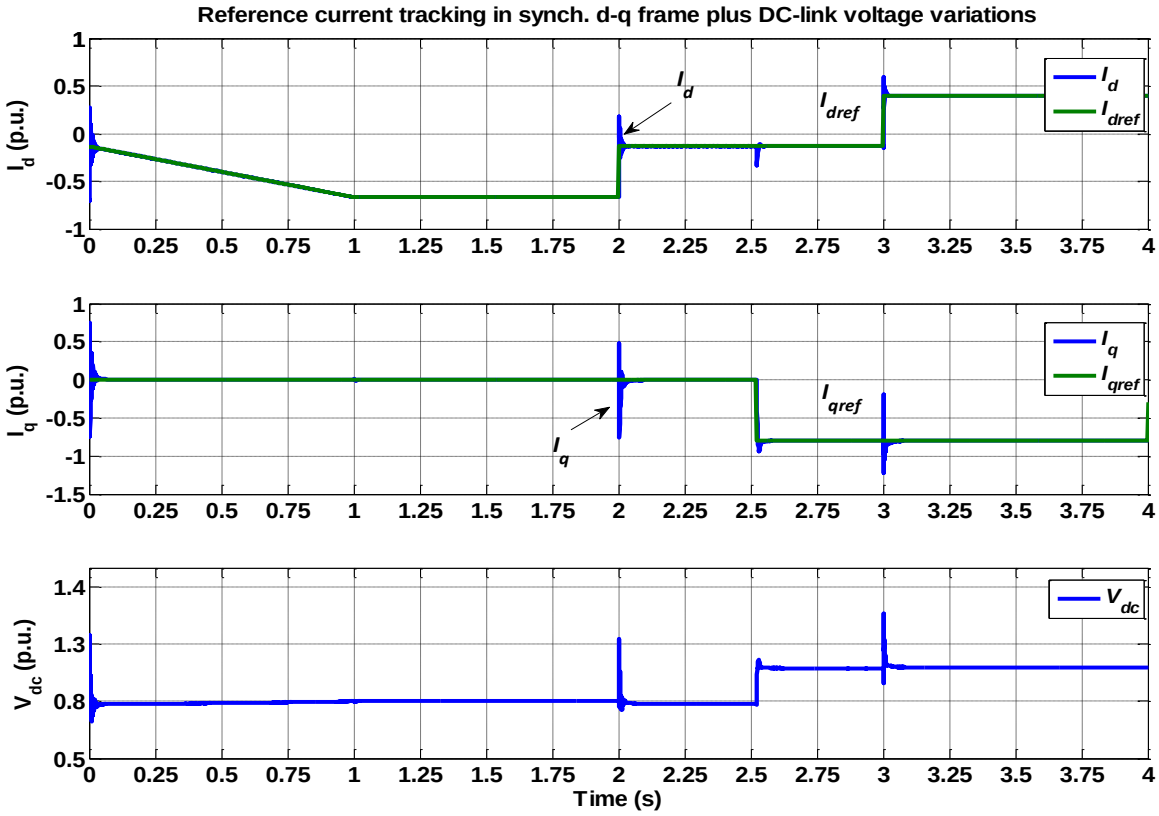

Figure 3-14. Converter performance when it is controlled with just the output voltage angle.

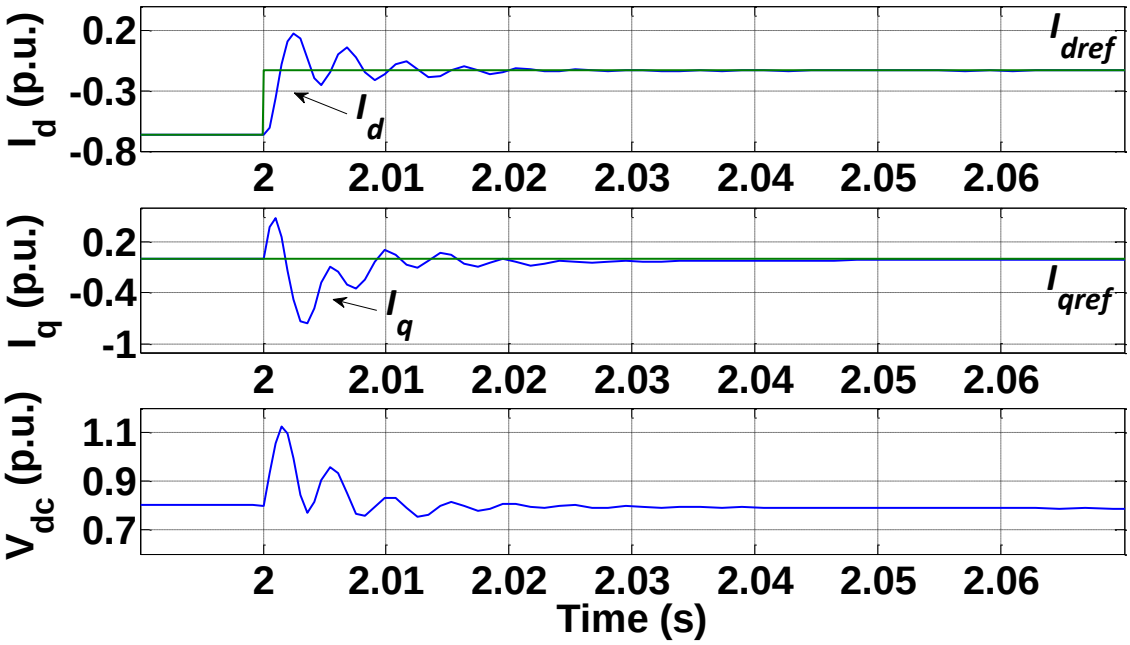

Figure 3-15. Transient response of the angle-controlled VSC for a change in active power in rectifier mode.

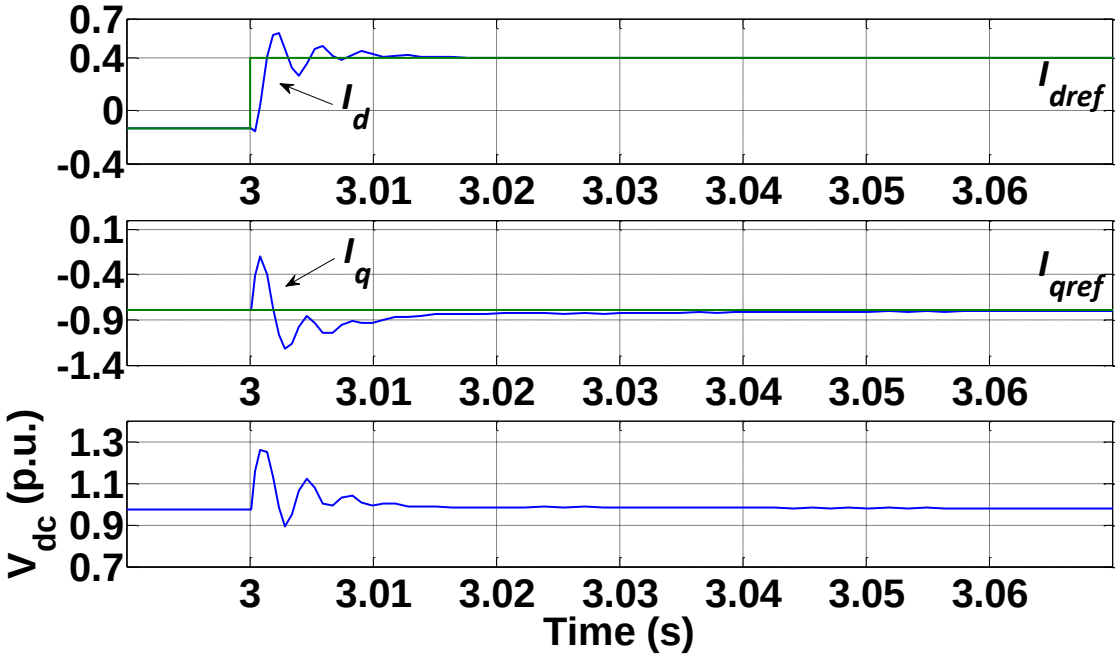

Figure 3-16. Transient response of the angle-controlled VSC for a change in active power in inverter mode.

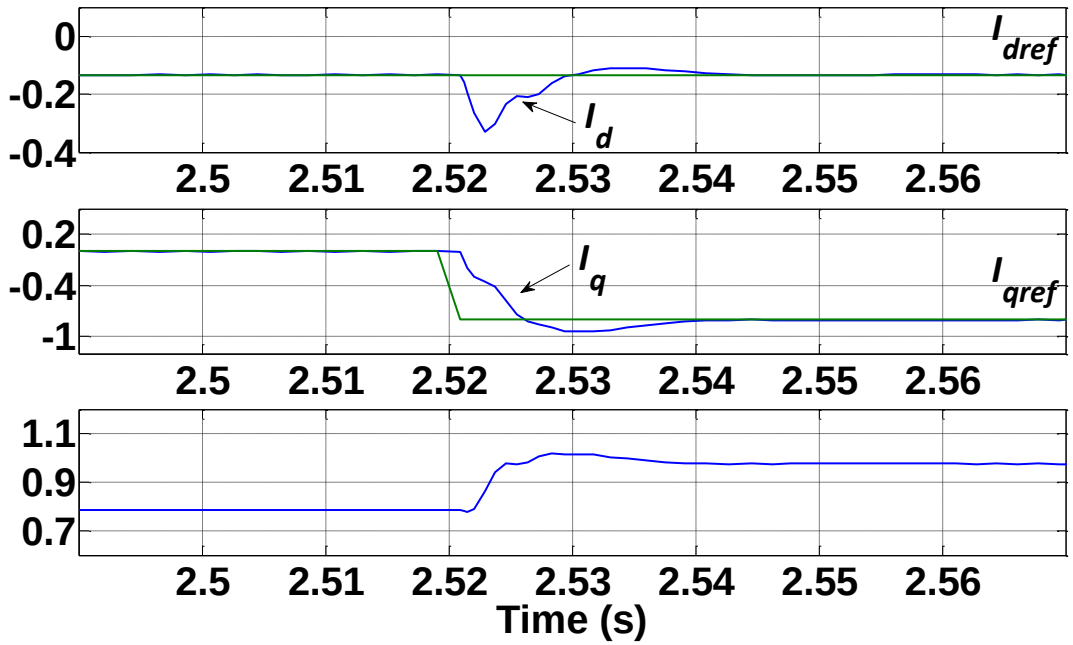

Figure 3-17. Transient response of the angle-controlled VSC for a change in reactive power.

3.5 **Verification of the Proposed SITO Control Structure for VSC**

3.5.1 **Unified Power Flow Controller**

It has been shown in the previous section that a shunt VSC is able to provide regulated active and reactive power while it is controlled only by the output voltage angle and switched at line frequency. In order to realize the load for the shunt converter, another VSC is connected to the DC link forming a back-to-back configuration. The added converter is either connected in series or shunt to the line through an interfacing transformer. The first group of results is presented for substation power flow control schemes where one VSC is connected in shunt and the other one is connected in series. The whole system is constructed in a PSCAD/EMTDC environment for a 20 MVA BTB VSC system. Figure 3-19-Figure 3-21

present the EMTDC simulation results of a BTB VSC system as the substation power flow controller. Each converter consists of two 10MVA 3-level NPC converters connected with a 138kV interfacing transformer to provide 24-pulse operation. The shunt converter in this mode is operating with angle control similar to STATCOM while the series converter is operaring based on vector control. The BTB VSC as the power flow controller controls the transformer active and reactive power while it regulates the substation sending end voltage.

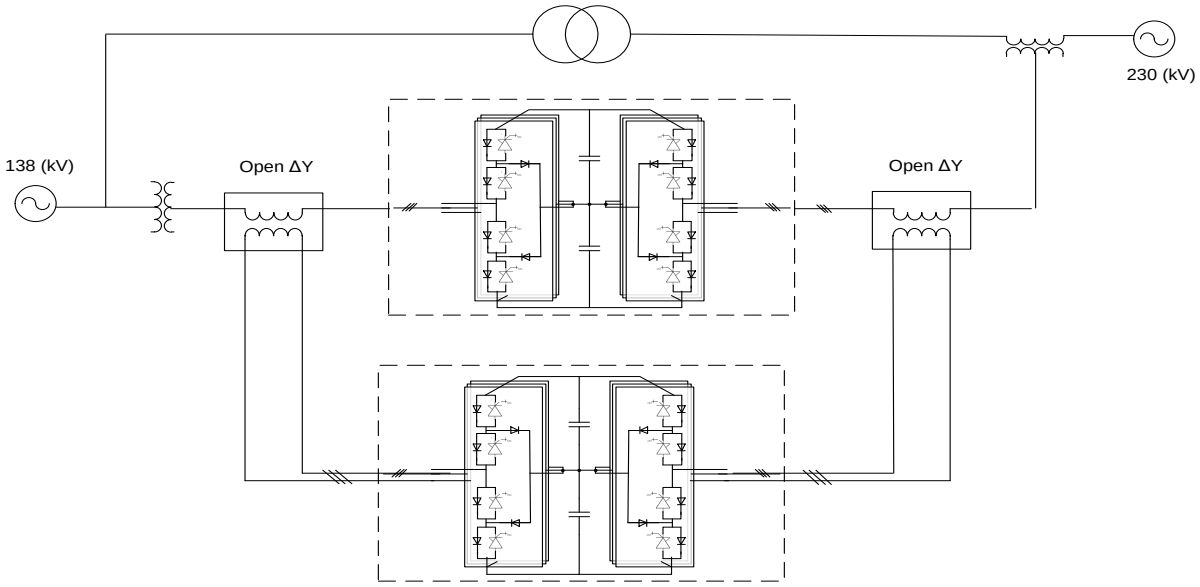

Figure 3-18. Hybrid-controlled BTB VSC for power flow control.

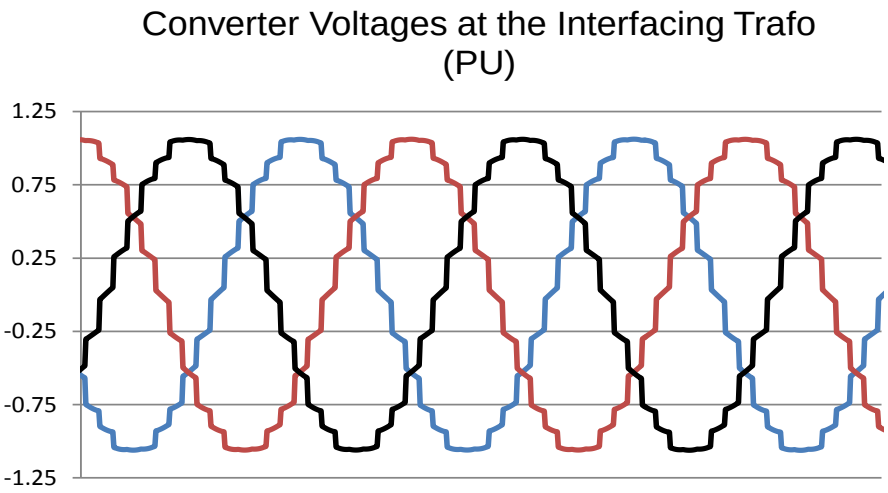

Figure 3-19. 24-pulse shunt converter output voltage with angle control.

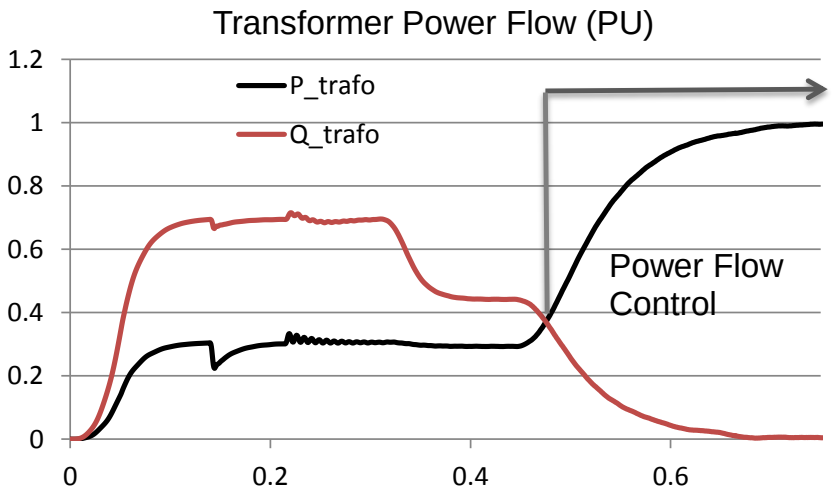

Figure 3-20. Substation transformer power flow dynamics with hybrid-controlled BTB VSC.

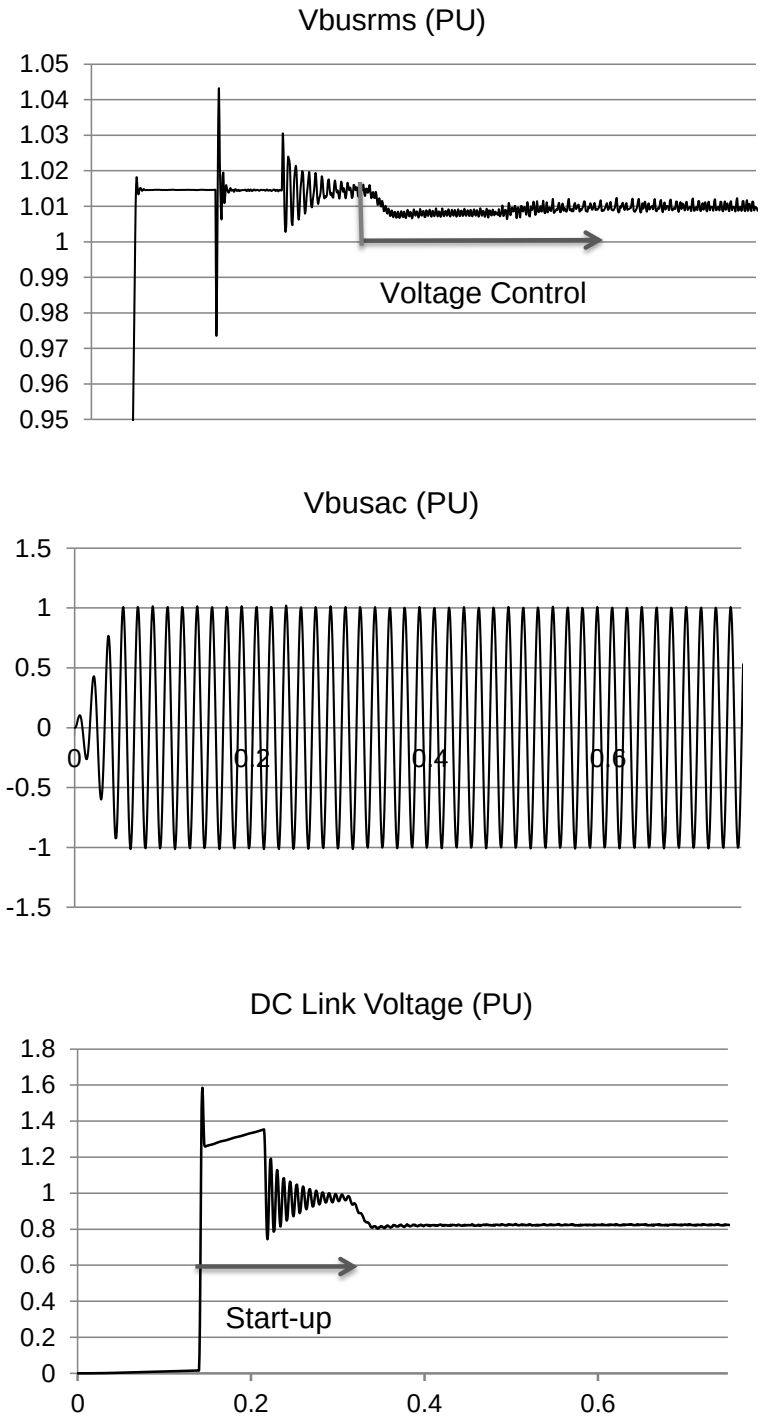

Figure 3-21. Operational performance (voltages) of the BTB VSC system as the power flow controller.

3.5.2 **Point-to-Point BTB HVDC Applications**

This study is further conducted to operate two converters in a BTB configuration with angle control. Although there is the possibility of reactive power compensation at both sides, the controller design can be cumbersome for the whole range of operation. Therefore, the proposed BTB system in the shunt-shunt mode currently has one set point for the reactive power. In other words, both converters provide the same reactive power. In fact, this mode of operation is quite acceptable for a hybrid AC and DC system where it is used as the back-up in case of emergency or forced reduced transformer rating operation scenarios. A comprehensive simulation has been conducted in the PSCAD environment for the 20MVA angle-controlled BTB VSC system shown in Figure 3-22. Different case scenarios have been created and the results are presented in Figure 3-23-Figure 3-25. As shown, different active and reactive power can be controlled perfectly without controlling the DC link voltage through the advanced angle control. The variation in the DC link voltage comes with the main concept of a DC link voltage according to the reactive power support for the grid.

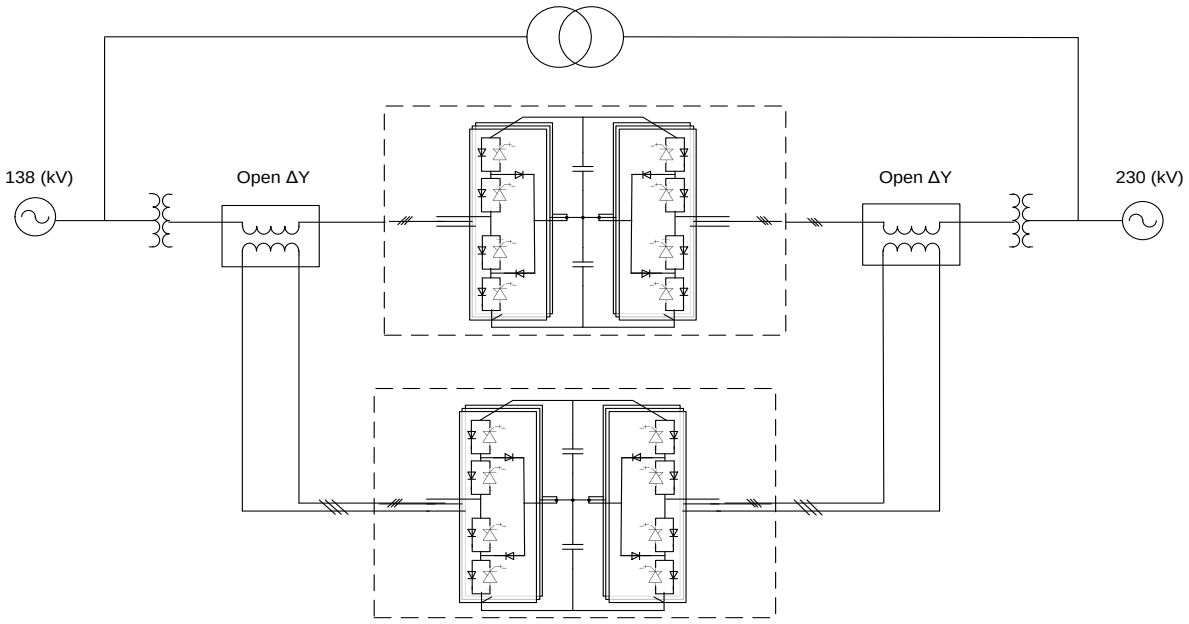

Figure 3-22. Angle-controlled BTB VSCs for HVDC applications.

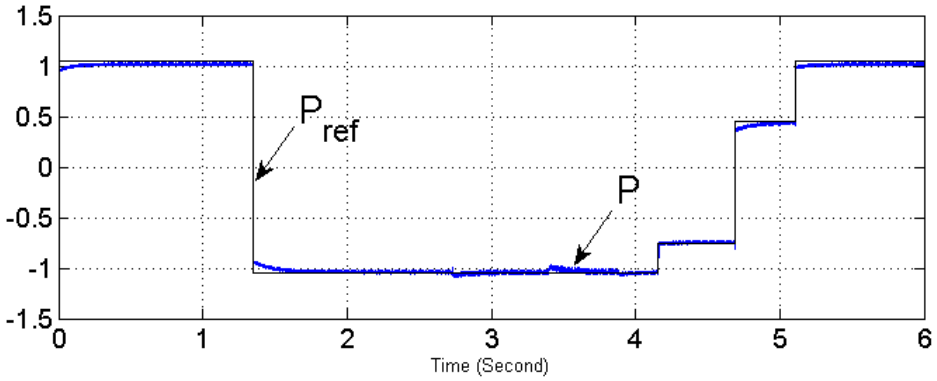

Figure 3-23. Active power dynamic performance of the angle-controlled BTB VSC system.

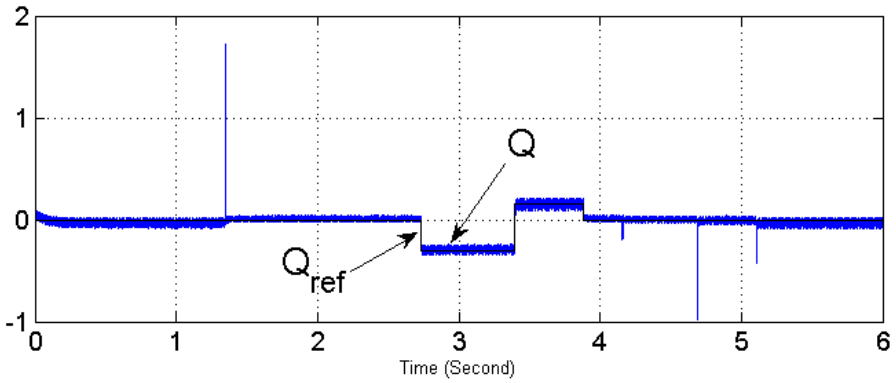

Figure 3-24. Reactive power dynamic performance of the angle-controlled BTB VSC system.

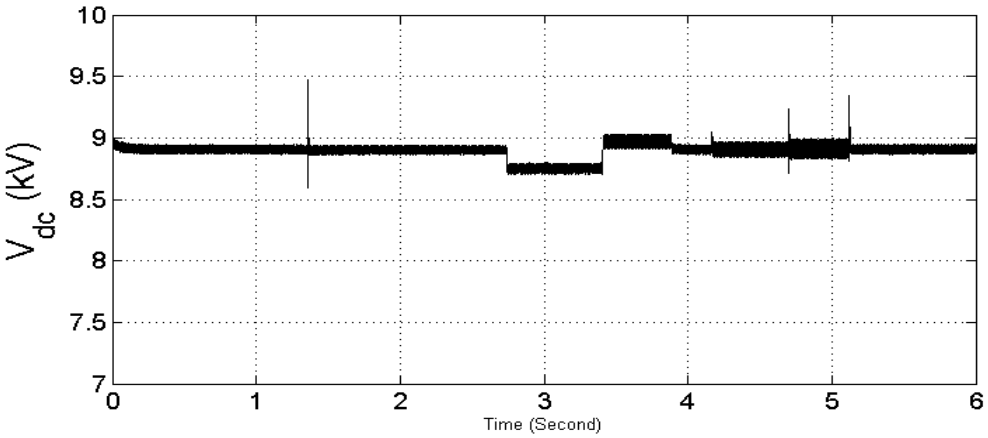

Figure 3-25. DC link voltage dynamic performance of the angle-controlled BTB VSC system.

3.5.3 **Discussion of Component Design in Angle-Controlled Converters**

Unlike vector-controlled converters, the operation of angle-controlled converters is highly dependent on the physical components, in particular the interfacing inductors. This dependence has been well documented for angle-controlled STATCOM by Schauder et al.

in 7 where the authors showed that the DC link voltage steady state operation depends on the interfacing inductor, and the inductive power dynamic is affected by the DC link capacitor. These relationships are shown in (3.37) and (3.38). The parameters and notations are the same as used in this chapter except i_{q0x} which in 7 defined as the maximum reactive power regulation amendable by linear feedback control.

$$V_{DC0} = \frac{1}{k}\left(\left|E_d'\right| - i_{q0}L'\right) \tag{3.37}$$

$$i_{q0x} = \frac{2V_{DC0}}{3kC_{DC}} \tag{3.38}$$

Including active power transfer in angle-controlled converters brings new dynamics that have been addressed in this chapter. It was emphasized that the controller, the converter components, and the disturbances and their interactions affect the dynamic of the whole system. These interactions were addressed through the definition of the direction among different spaces which were defined as (3.14) and (3.27). Here, some constraints and limitations in designing the interfacing inductance are presented mainly based on the angle between the plant and disturbance, which in this case is the load. The first constraint is presented in (3.39). This inequality in any feasible operating point must be conserved to avoid a completely misaligned condition at steady state between the disturbance and the plant.

$$L' \neq \frac{kV_{DC0}}{i_{d0}\sin\left(\alpha_0\right) - i_{q0}\cos\left(\alpha_0\right)} \tag{3.39}$$

While the direction definition provides a strong tool with which to design the controller, it may be difficult to change or redesign the components, in particular the inductance value.

Therefore, another metric has been developed which relates the inductance value to a parameter called D_t directly. This parameter D_t , which has been derived from (3.27) and (3.29), determines the capability of angle-controlled converters to reject the effect of the load regardless of the controller design. Perfect alignment or complete load rejection capability is defined as 1 for the factor, D_t and zero implies completely misalignment or no capability to reject the load. (3.40) presents the relationship taking into account the operating points. In (3.40), for the sake of simpler terms, the values for the terms $k = 4/\pi$ and $\omega = 377$ have been inserted and no loss in the interface transformers and the converter has been considered; i.e., $R_s' = 0$ and $R_p' = \infty$. Different feasible operating points for different values of inductance were calculated to transfer 1.5PU active power and the result of (3.40) are presented in Figure 3-26. Observing the result obtained, one can conclude that increasing the interface inductance reduces the control range for the angle-controlled converter.

$$L' = \frac{V_{DC0} i_{q0} \left[\left(D_t^2 - 1 \right) \left(1 - 2\sin\left(\frac{\alpha_0}{2} \right) \right) \right] + i_{d0} \left[\left(1 - D_t^2 \right) V_{DC0} \sin\left(\alpha_0 \right) + 0.785 D_t \sqrt{1 - D_t^2} \right]}{-0.785 \left(i_{q0}^2 \left[\left(D_t^2 - 1 \right) \left(\sin\left(\alpha_0 \right) - 1 \right) \right] + i_{d0}^2 \left[\left(D_t^2 - 1 \right) \sin\left(\alpha_0 \right)^2 + 0.616 / V_{DC0}^2 \; D_t^2 \right] - i_{do} i_{q0} \sin\left(2\alpha_0 \right) \left(D_t^2 - 1 \right) \right)} \tag{3.40}$$

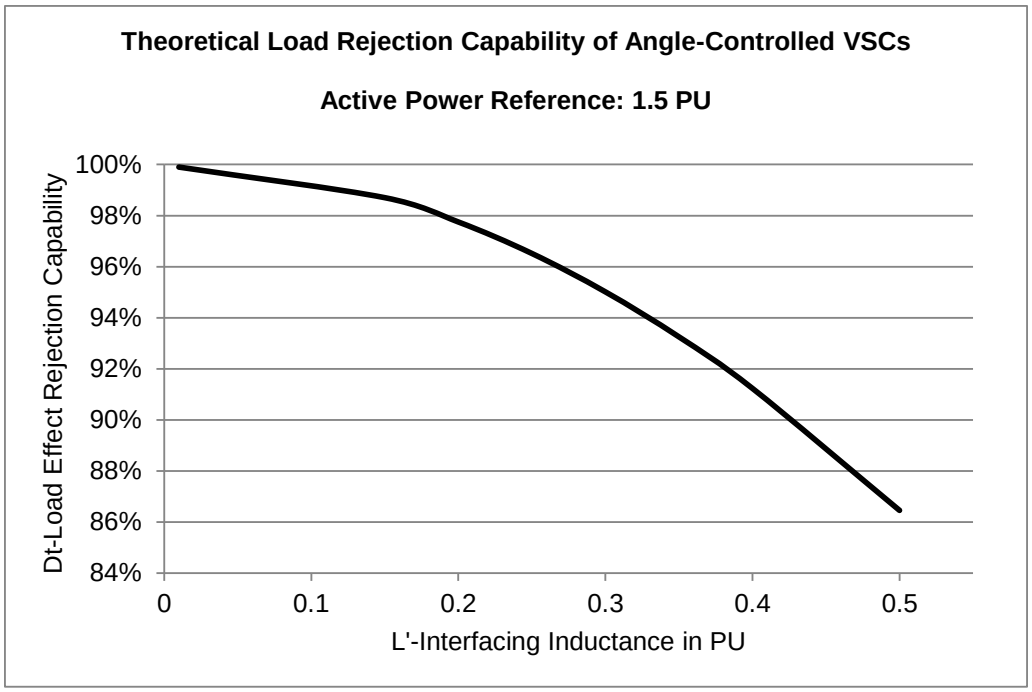

Figure 3-26. Theoretical load rejection capability of an angle-controlled VSC vs. interfacing inductance value for an active power reference of 1.5PU.

To examine the effectiveness of the proposed design tool as shown in Figure 3-26, the same angle-controlled BTB VSC system as shown in the previous section for point-to-point HVDC applications is simulated in a PSCAD environment with different inductance values for the interfacing transformers. It might be worth mentioning that the converter was initially designed for 1 PU power and 1.5 PU has not been considered in the component design of the converter. The results of the simulation for inductance value of 15% PU are presented in Figure 3-27. As can be seen, the required power is transferred with a small steady state error (insignificant) but the converter is stable and the performance is acceptable for this small inductance. The simulation results for an inductance value of 50% PU are presented in Figure 3-28. The same 1.5 PU power set point is applied to the angle-controlled converter

system. As can be observed, not only can it not reach the required power, but it also has unacceptable DC link voltage oscillations. From the results, it can be concluded that the converter components in particular interfacing inductors highly affect the performance of the angle-controlled converters in transferring active power as predicted and shown in Figure 3-26.

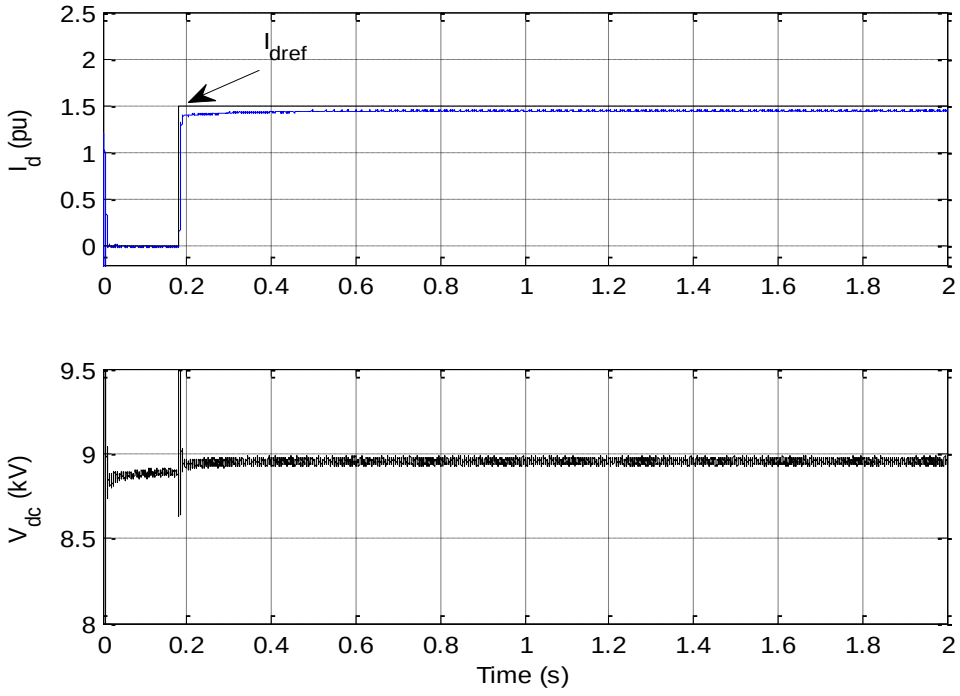

Figure 3-27. Dynamic performance analysis of the angle-controlled BTB VSC system to show the converter system disturbance rejection capability with interfacing inductance of 15% PU.

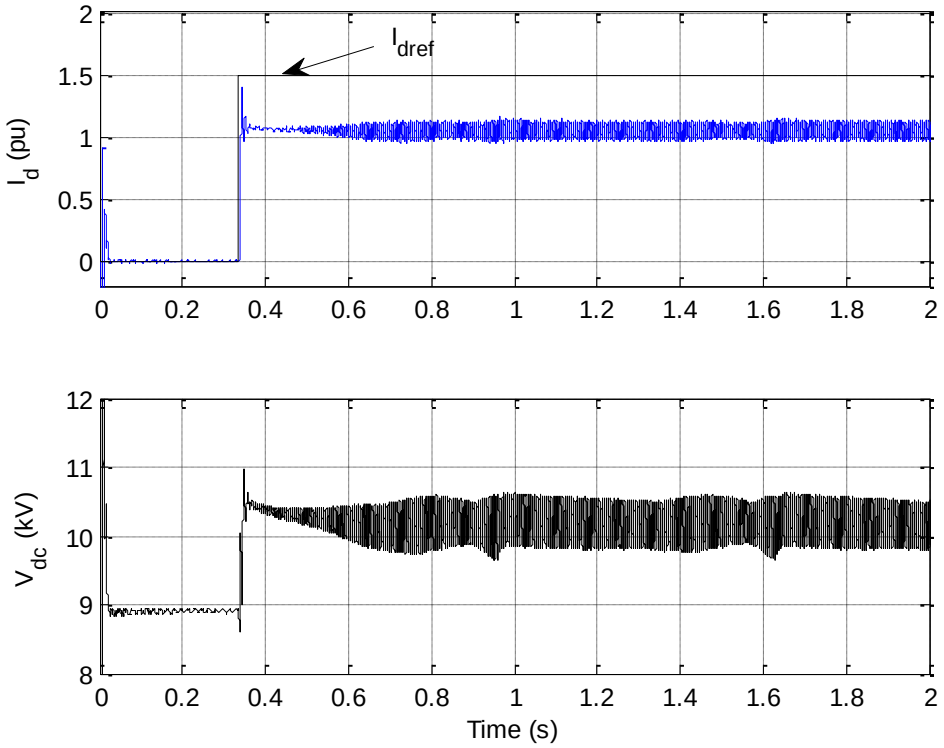

Figure 3-28. Dynamic performance analysis of the angle-controlled BTB VSC system to show the converter system disturbance rejection capability with an interfacing inductance of 50% PU.

3.6 **Summary**

This chapter has introduced the possibility of automatic control of active and reactive power for voltage-sourced converters through an angle-control structure. A new control framework which uses the properties of an SITO feedback system is developed for voltage-sourced converters. Clearly, one actuator, in this case the angle, cannot be used to regulate two outputs (active and reactive power) to arbitrary setpoint values. Nevertheless, this chapter showed that a one-dimensional class of setpoint values is feasible for the VSC technology. Design limitations and tradeoffs imposed by the plant and controller for such a

system have been explained. In the proposed control structure, the definition of “direction” has been used to determine the control parameters. It has been shown that although the intention might be to have the controller completely or perfectly aligned with the converter dynamics, this level of alignment can make the converter system unstable. In fact, it has been shown that if the plant and controller are perfectly aligned at all frequencies, the input open loop transfer function must necessarily possess at least one NMP zero, which imposes some limitations on the sensitivity functions of the closed-loop system. Since a VSC with basic component design criteria has the properties of a plant whose direction does not change significantly with frequency, the perfectly aligned condition has been rejected in this research. On the other hand, any VSC system has major disturbances of DC load power. These DC load disturbances can be considered to constitute another converter forming a back-to-back system. It has been shown that if the plant is aligned with the output disturbance, by considering an integral controller, that effect of the disturbance to the output can be rejected in steady state. This point is worth mentioning, since it can provide additional criteria for designing the power converter. The selected designed criterion has been implemented by making the plant (VSC) aligned with the disturbance at low frequency or within the bandwidth of the converter. In addition, the effect of the components in particular, the interfacing inductors have been studied and formulated as a design tool and a constraint for the proposed angle-controlled VSC system with active and reactive power transfer capabilities. This research work enhances the operational region of existing shunt family of FACTS devices which can also be extended for transmission level VSC-based HVDC systems through advanced angle control with superior performance.

Chapter 4. MODULAR TRANSFORMER CONVERTER

4.1 Background

Today it goes without saying that electricity serves as one of the key resources in every country. Its role is so obvious in our lives that many take its availability and reliability for granted. However, for many techno-economical reasons, every year society encounters power interruption. Figure 4-1 presents the effects of disturbances on power loss and the affected number of customers, showing data that has been collected through the work of the U.S. Energy Information Administration (EIA) within the past few years, 51. It can be seen that each year a considerable amount of generating capacity is lost for some period affecting large numbers of customers. Although it is difficult to exactly determine the affected number of customers, the scale is in millions of customers affected each year just in the US.

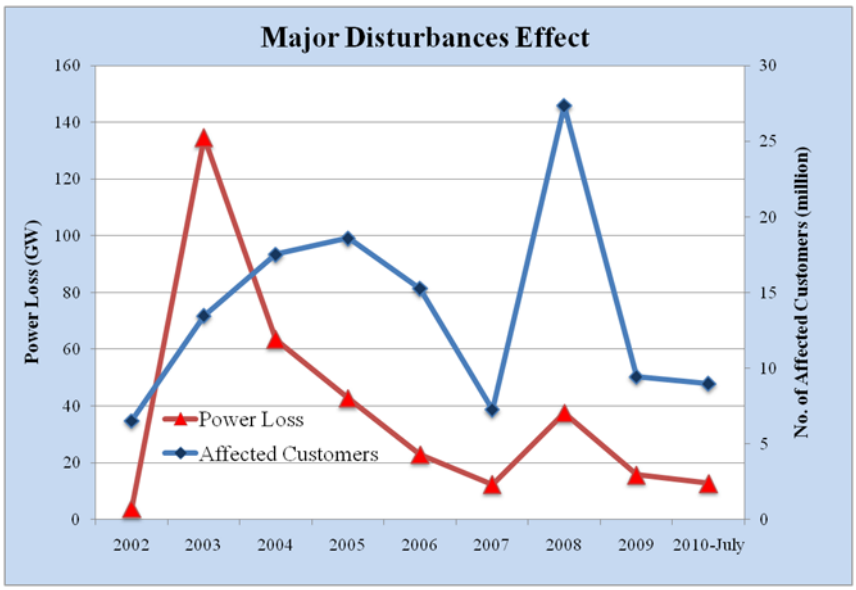

Figure 4-1. Power interruption effects on power loss and number of affected customers.

Utility customers are usually categorized as: residential, industrial, and commercial. Obviously, the effects of power loss are different for each sector. Many agencies are working to estimate the loss in dollar value of power interruption. Figure 4-2 shows a study conducted by Lawrence Berkeley National Lab in 2002, with a total loss of $79 billion for power interruptions in 2002, 52. Others, such as Electric Power Research Institute (EPRI), estimated even more for the same period ($119 billion per year), 53.

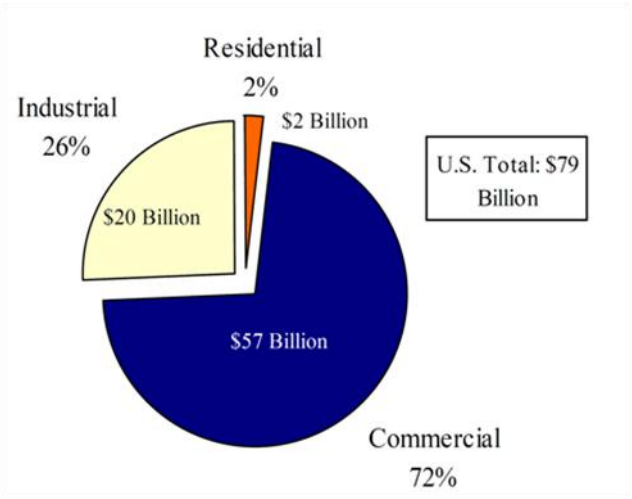

Figure 4-2. Cost of power interruptions for U.S. customers in 2002.

New energy policies requiring higher penetration of renewable sources are fast moving the electricity market towards a higher degree of deregulation and competition. In order to cope with the situation electric utility companies, in the short run, to push their systems to their rated power handling capabilities, and in the long run, to invest heavily in grid infrastructure to provide for the required extra capacity. The former reduces system reliability and the latter, albeit a heavy investment, does not guarantee to efficiently remove bottlenecks in the system, i.e. congestion problems that might arise due to new variability in power generation. One hurdle that impedes investment in grid infrastructure and transmission capacity is the intermittent[2] nature of these sources. A generation availability index is defined as in (4.1) and determined based on the data available from US Energy Information Administration (EIA) for wind and solar generation. A selected set of results for the year 2009 is depicted in Figure 4-3, in which the limited availability of these sources can be

[2] Intermittency of renewables throughout this chapter is defined in more than a day time-frame

followed. Similar results can be obtained by observing the renewable generation capacity of specific regions. Figure 4-4 shows the wind-generated power in the Midwest with no significant summer generation. Consequently, Transmission Owners (TO) are reluctant to invest in the available technologies for UPFC and Phase Shifting Transformers (PST) that may not have enough economic benefits for their systems. Power flow controllers, such as UPFCs, have been well studied to help relieve the situation by regulating power over transmission lines, but the complexity of coordinated control has prevented their extensive usage. This chapter introduces a transformer power flow controller enabling the system operators control power flow, effectively increase their spare capacity, and also provide back-up in case of substation transformer failure modes. Because this latter problem constitutes the majority of power outage occurrences, the system reliability can also be considerably increased.

$$\text{Generation Availability Index (GAI)} = \frac{\text{Generation Energy}}{\text{Generation Capacity} \times 8760(h/yr)}(\%) \qquad (4.1)$$

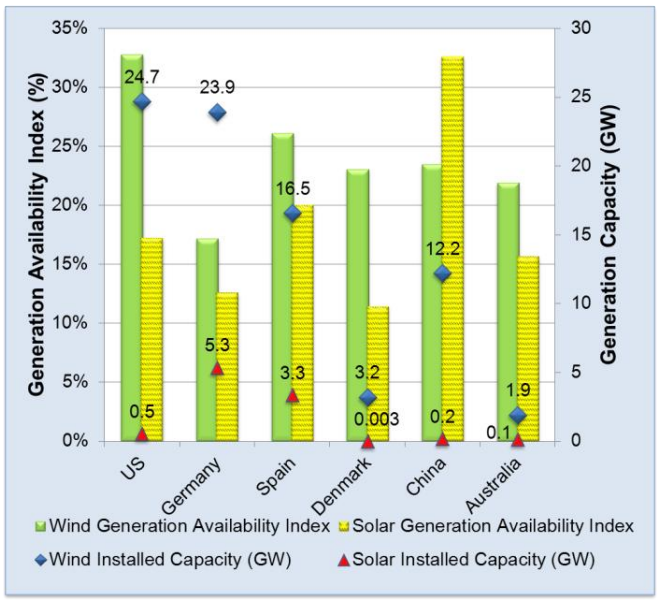

Figure 4-3. Wind and solar generation availability for selected countries.

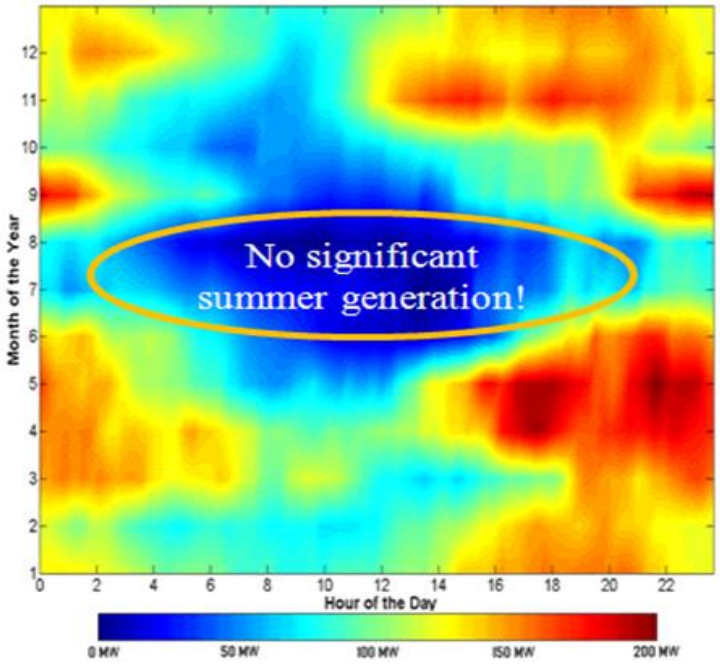

Figure 4-4. US Midwest region wind generation capacity profile.

4.1.1 **Transformer Outages**

The transmission grid and its assets, especially those on American soil, are aging. Thus the asset owners and system operators are to managing their properties and services with more concern than that of some decades ago. On the other hand, the new market environment is driving transmission and distribution companies to find ways to improve their competitive position. Increased equipment utilization, deferral capital expenditure and reduced maintenance expense are among the few key factors for today's T&D grid owners. Although tighter budgets are nothing new for engineers, today's increased need to leverage more out of existing equipment must be achieved with a majority of T&D assets nearly at and even past the end of their life cycles. A very familiar example of such assets is the power transformer, a very robust component of power systems. Power transformers are the single most expensive component of the equipment installed in high voltage substations, comprising up to 60% of the total investment, 54, and therefore, utilities and system operators tend to push their utilization time. It has been reported that the average age of power transformers in the US is now approaching 40 years. This result seems reasonable considering the rates of transformer installations during the last 40 years, as shown in Figure 4-5, 55.

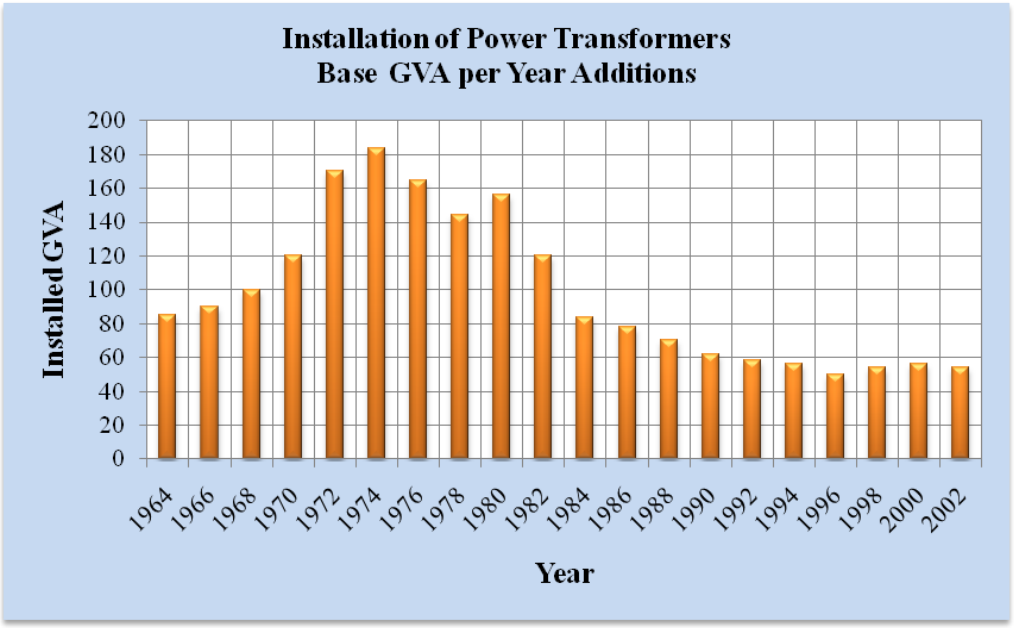

Figure 4-5. Installation of power transformers base GVA per year additions in US.

The North American Electric Reliability Corporation (NERC) through the Transmission Availability Data System (TADS) Working Group (WG) began to collect outage data from 2008; at present reporting is mandatory for all US Transmission Owners (TOs) on the NERC Compliance Registry, and all of the NERC TOs complied, 56. The published reports include only automatic outage data, which is considered Phase I of the study. Phase II, which covers the non-automatic outage data, will be available from 2011 on annually. The scope of the TADSWG report is the outage data of every transmission asset, AC and DC, which sits on a minimum 200 kV level (low voltage side).

By definition from NERC, an automatic outage is an outage which results from the automatic operation of switching device, causing an element to change from an in-service

state to a not in-service state. Since this study is focused on the transformer related outages, associated definitions are provided here.

- The outage initiation codes are either Element-Initiated or Other-than-Element Initiated.
- An automatic outage with an outage duration of a minute or greater is a "sustained" outage.
- The Outage Mode Codes are one of the following: (a) Dependent Mode Initiating (one outage) and Dependent Mode (second outage); (b) Common Mode Initiating and Common Mode (two outages); or (c) both Common Mode (two outages).
- Event type No. 10 is an automatic outage of an AC circuit or transformer with normal clearing.

The NERC data is processed with attention to the transformer outages for the past two years (only available in public data before now). Figure 4-6 and Figure 4-7 show the duration of the transformer sustained outages with the voltage level (high side) of the element also shown. As predicted, without many transformer installations, 688 as of 2008 to a total of 705 units in 2009, the outage duration increased significantly in just two years. The results are classified into two main groups as "element (transformer)-initiated only" and "other than element-initiated." It can be observed that the transformer operational mechanism takes the majority of the outages. Another point is that the 300-399 kV class, which mainly covers 345 kV transformers needs immediate attention and revised management.

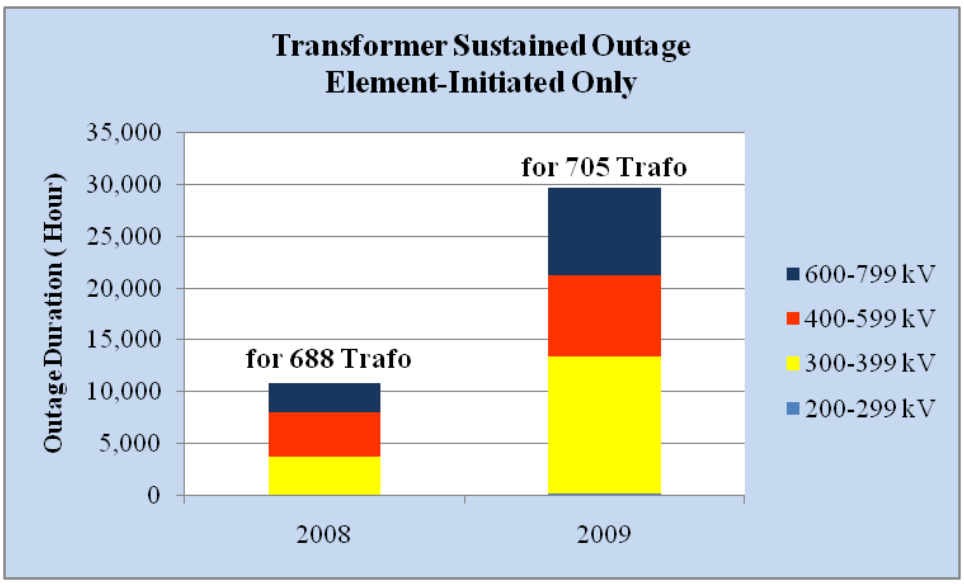

Figure 4-6. Transformer "Element-Initiated Only" sustained automatic outage data based on different transmission voltage levels.

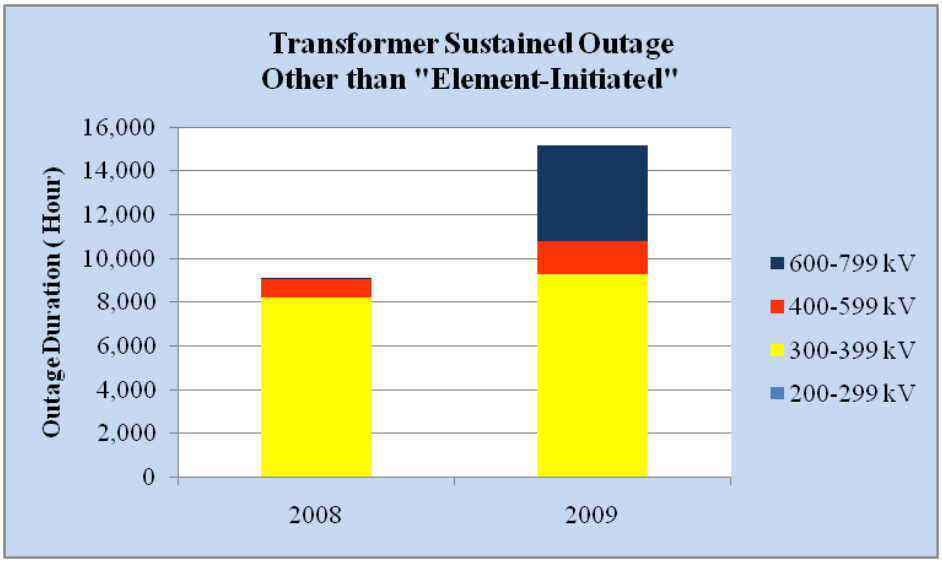

Figure 4-7. Transformer other than "Element-Initiated Only" sustained automatic outage data based on different transmission voltage levels.

The exact causes of outages are currently considered confidential to NERC TOs. However, examining the outage mode code and event type, presented in Figure 4-8 and Figure 4-9, leads to some helpful conclusions. It can be seen the single mode outage has the highest value in the two years resulting from overloading (not because of other elements' outage), internal faults, etc. Transformer outages initiate other elements' outages, which can be also affect the grid availability and reliability.

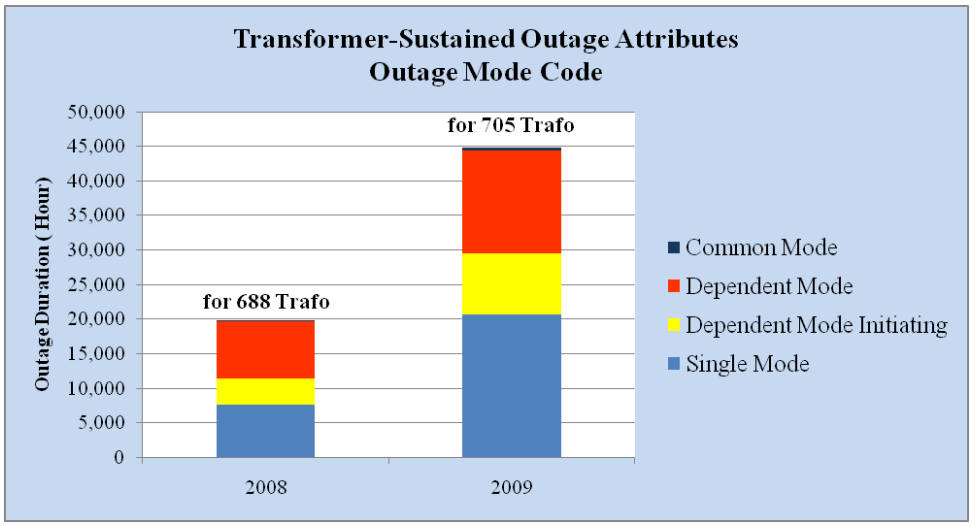

Figure 4-8. Transformer sustained automatic outage attributes-Outage Mode code.

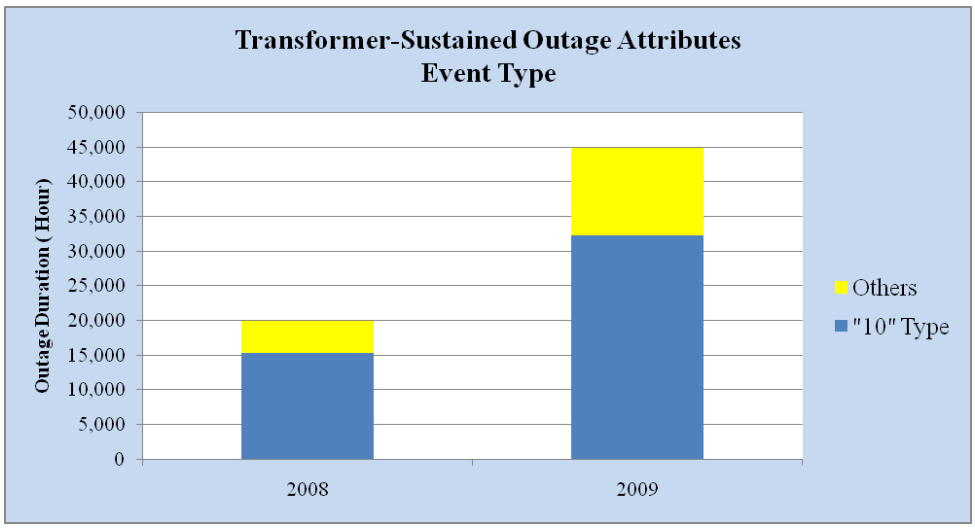

Figure 4-9. Transformer sustained automatic outage attributes-Event Type.

Although it is expected to see 99.999% reliable operation for the transformers, transmission transformers in 2010 were just 97.009% reliable, Figure 4-10. Considering the long lead time for power transformer manufacturing and installation and rising concerns related to natural disasters, one can expect worse figures in the near future. In summary, transmission transformers, with specific attention to the 300-399 kV class which mainly covers 345 kV transformers, need immediate attention and revised management.

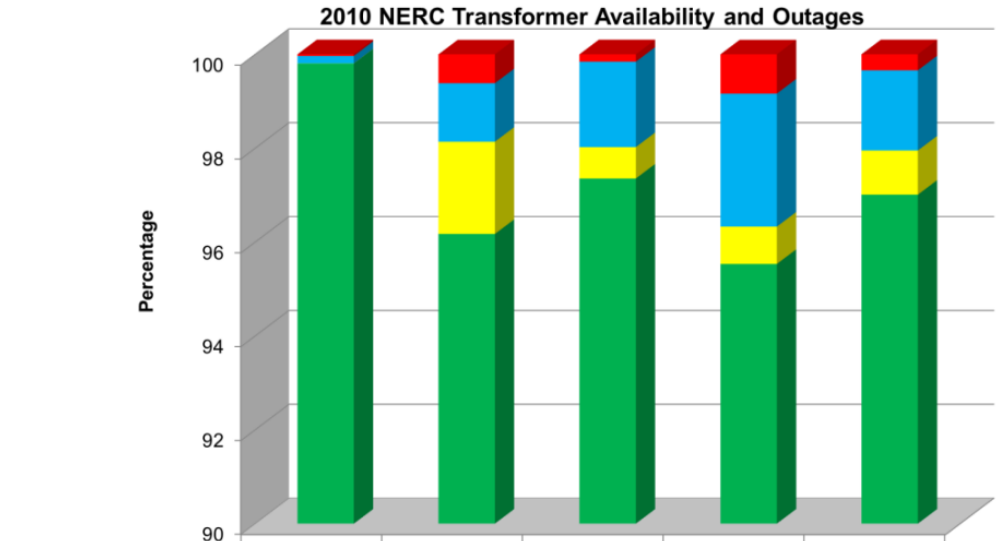

	200-299 kV	300-399 kV	400-599 kV	600-799 KV	Transformers
Operational Outages	0.034	0.616	0.159	0.836	0.342
Planned Outages	0.159	1.246	1.819	2.835	1.708
Auto Sustained Outages	0.004	1.965	0.669	0.795	0.941
Availability	99.803	96.172	97.354	95.5335	97.009

Figure 4-10. US Transmission transformer (>200 kV) availability in 2010.

4.1.2 **Effect of New Intermittent Distributed Generation on Existing Assets**

There is an increasing demand for new generation units, especially renewable ones, throughout the country. The very evidence of such sources are wind farms, 8500 MW of which were installed just in 2008. These plants are usually distributed over a vast area due to their low power density compared to that of conventional fossil fuel based plants. Therefore, their connection to the grid itself is an optimization problem. On the other hand, according to U.S. Federal Energy Regulatory Commission (FERC) proposal in June, the 2010 connection cost allocation is with the TOs and utilities, 57. However, investment in the grid infrastructure and transmission capacity has failed to keep up with the rising pace of new wind energy installations. With high penetration of distributed renewable generation, a huge

upgrade in transmission assets can be foreseen. Currently, voltage regulation and Var support for renewable generations are becoming standard to improve the operation and reliability of the power system. With further renewable penetration as high as 40% to 60%, the operation of the grid must be revised. One hurdle that impedes investment in grid infrastructure and transmission capacity is intermittent nature of these sources. Consequently, Transmission Owners (TO) are reluctant to invest in the available technologies such as UPFC and Phase Shifting Transformer (PST) that may not have enough economic benefits for their systems.

The National Renewable Energy Laboratory (NREL) has published a report that highlights the growing problem of wind energy curtailment, which occurs when wind plants are required to or choose to reduce their generation output. Based on NREL investigation, one of the main reasons for wind curtailment is the lack of available transmission capacity during a particular time to incorporate some or all of the wind-generated power, 58.

As an example, we conducted intensive research with our industry partner (Quanta Technology) on one of the potential regions in the country for wind generation. It was observed that the power due to the newly installed wind farms flows in a 138 kV network, which can overload the network, while there is a noticeable capacity margin in the 345 kV system, substation and transmission lines, Figure 4-11. In order not to avoid curtailing generation and to reroute the power to increase the utilization time of the 345kV asset, multiple new HV substations were proposed, as shown in Figure 4-12. However, this solution was regarded as too expensive an option considering the availability factor of the wind farms presented in Figure 4-3 . Therefore, it was concluded that not only is there a possible severe

underutilization of upstream assets due to newly installed variable generation units, but also the connection of these units should be revised and modified.

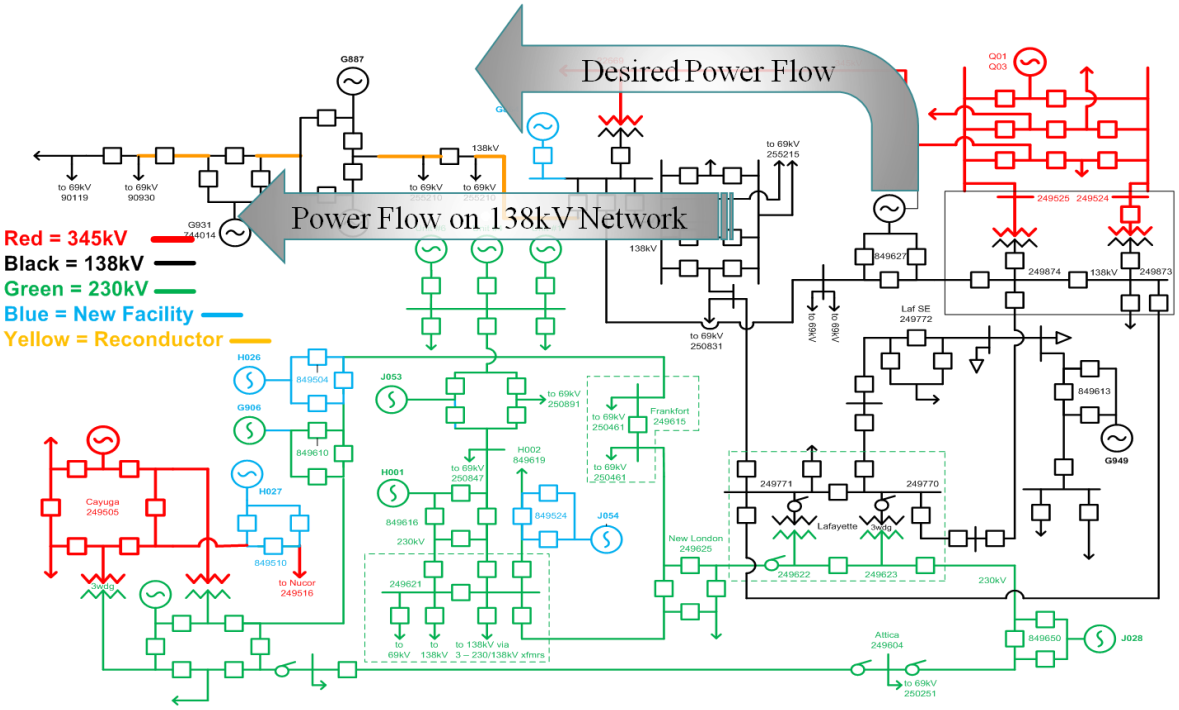

Figure 4-11. New generation effects on existing assets - wind generation, State level.

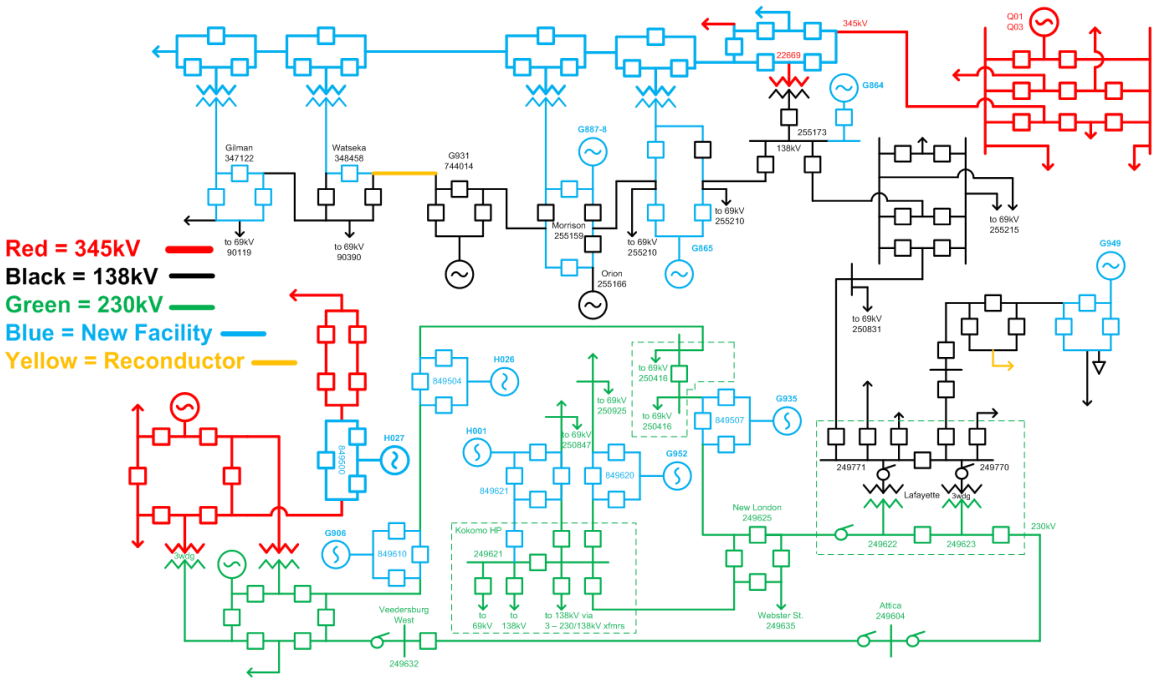

Figure 4-12. Alternative solution to reroute the power flow for new wind generator output (expensive solution, yet ineffective).

4.2 **Towards Smart Transmission Substations**

Currently, power delivery through substations is almost completely uncontrolled. In other words, power is mainly regulated through controllers at the generation units' controllers, and substations are considered as the nodes in power flow analysis. At locations away from power plants, Phase Shifting Transformers (PSTs) and Unified Power Flow Controllers (UPFC) are considered to be feasible approaches to regulating the power flow in transmission lines, especially in the tie-lines between areas. It is expected that more power flow controller will be installed in grids in the future to insure economical and reliable operation. In the following, the current state of the art technologies will be explained briefly.

4.2.1 **Controllable Transformers**

Controllable transformers or hybrid transformers have been proposed recently and are under investigation to add dynamic control to regular or existing power transformers and possibly to also reduce the overall costs by integrating a fractionally rated converter into the main transformer, 62, and 63. Although several functions such as active and reactive power control can be obtained, direct connection of power converters with high dv/dt and harmonics is typically not possible. One potential issue is associated with the secondary B-H loops and increased losses due to high frequency switching. Consequently, an overrated or even a special power transformer, and/or a more complex power converter must be used. All of these factors affect the reliability, efficiency and cost of the overall system and not only of the power converter itself. It can be concluded that the application map of the proposed approaches, if successful, is limited to distribution grids with custom designed *new* 60 Hz transformers which may be replaced with the advent of Solid State Transformers, 65-71.

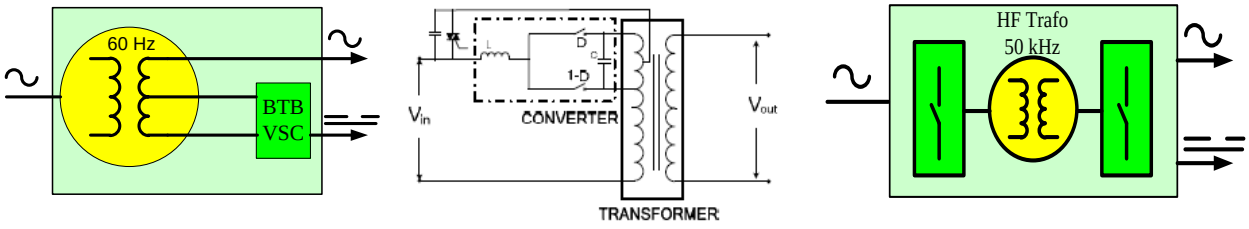

Hybrid Transformer | Controllable Transformer, 63 | Solid State Transformer

Figure 4-13. Recent advances in active transformers (simplified schematics) - not commercialized yet.

4.2.2 **Recovery Power Transformer**

In the previous section, the necessity for immediate attention to transformers was clarified. However, due to the de-regulated and tight market, system planners and TOs are reluctant to renovate their entire facilities, thus they push their transformers' nameplate life time. Nonetheless, adding value and flexibility to a common engineering solution may be an approach to bridge into the market. For the transformers, a multi-purpose device is beneficial and attractive for system planners and TOs.

The polytransformer is an approach that adds value and flexibility to conventional power transformers. A polytransformer's main application is its use as a universal spare. It is a compact (autotransformer structure), multi-voltage power transformer that helps utilities to secure the transmission grid. It has multiple voltage ratings for high, low and tertiary voltages. Designed with internal taps, the polytransformer can be connected to a variety of ratings – for instance, 400 kV to 230 kV, 400 kV to 138 kV, 400 kV to 115 kV, 230 kV to 138 kV, 230 kV to 115 kV, and with 33 kV, 26.4 kV and 24 kV in the tertiary system. The voltage rating is selected by changing connections internally prior to moving the transformer to a new location. The compactness of the design stems from a magnetic core enclosing the windings and horizontal lay-down operation to match transportation and hauling restrictions. The flexibility in voltage range, connections and compact design allows the TOs to provide a spare transformer for their region of interest (system) and even lease their spare transformers when they do not need them. An example of such a transformer manufactured by ABB in 2005 is shown in Figure 4-14, operating in parallel with the main transformer. This

transformer has been rented by the owner to another utility, once interconnecting systems from 400/230 kV and later from 400/132 kV. Reinstallation of a polytransformer is expected to take about 15 days within the utility.

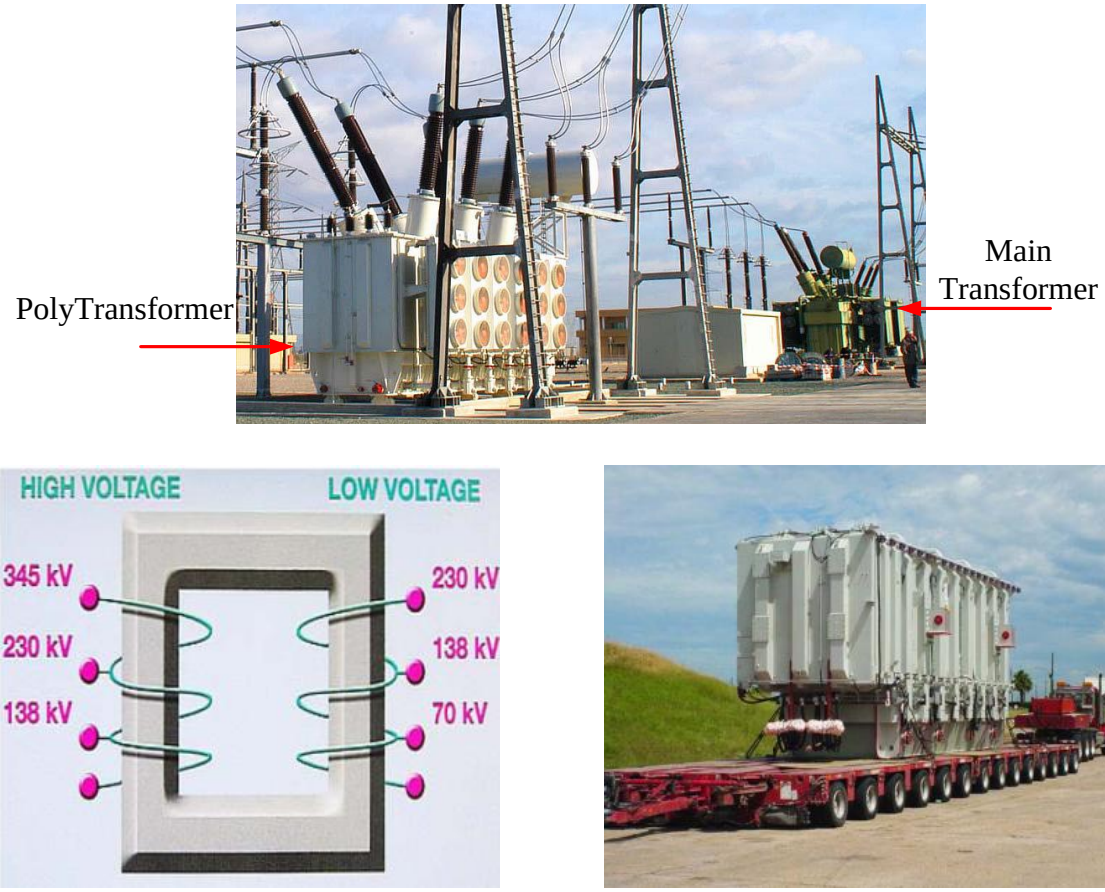

Figure 4-14. An example of an ABB polytransformer installation in Spain, 2005, 64.

4.2.3 **Phase Shifting Transformer (PST)**

In a de-regulated market, electrical power generation capacity will be installed and scheduled following purely financial incentives, which often results in transmission

bottlenecks. Transmission capacity- becoming a sometimes scarce good - will be traded. Some means is needed to guard transmission assets from unscheduled use. Phase angle control allows the determination of the amount and the direction of power exchanged over lines connecting two networks. The very first phase angle controller was realized with a combination of two transformers with multiple taps, one transformer in shunt and the other in series with the line as shown in Figure 4-15, and several mechanical switches, back in 1932 (Siemens). Since then there have been several installations up to 1400MVA throughput power. Conventional PSTs cannot regulate the reactive power flow through the lines. Combined with capacitor and reactor, a hybrid PST, called Interphase Power Controller (IPC), can control the reactive power. The other approach in the PST class is introduced by Sens as the Sen Transformer, 60 . This transformer consists of multiple windings in the shunt and series parts, providing the required voltage vector. Hence, the Sen transformer can control both the active and reactive power in the line.

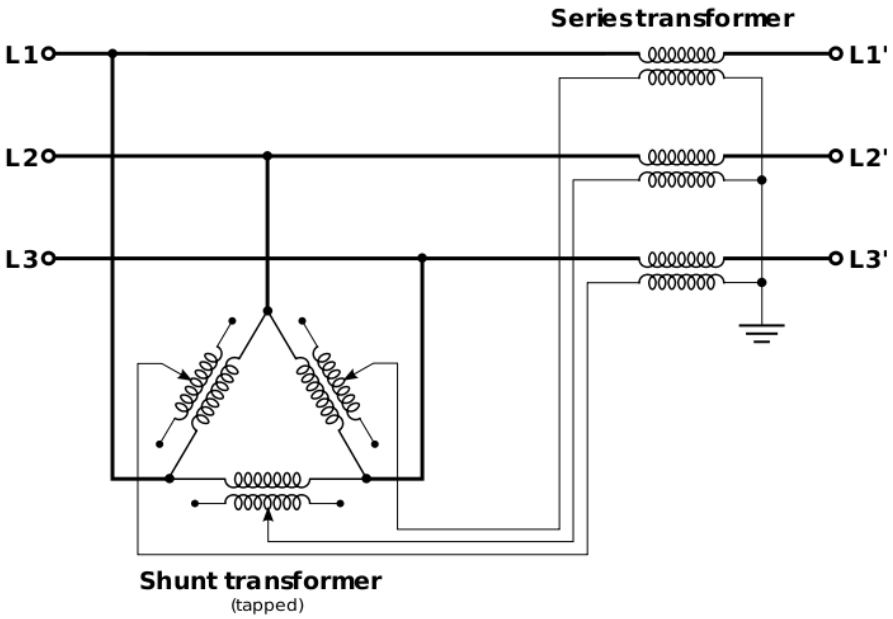

Figure 4-15. Simplified circuit diagram of phase shifting transformer, 82.

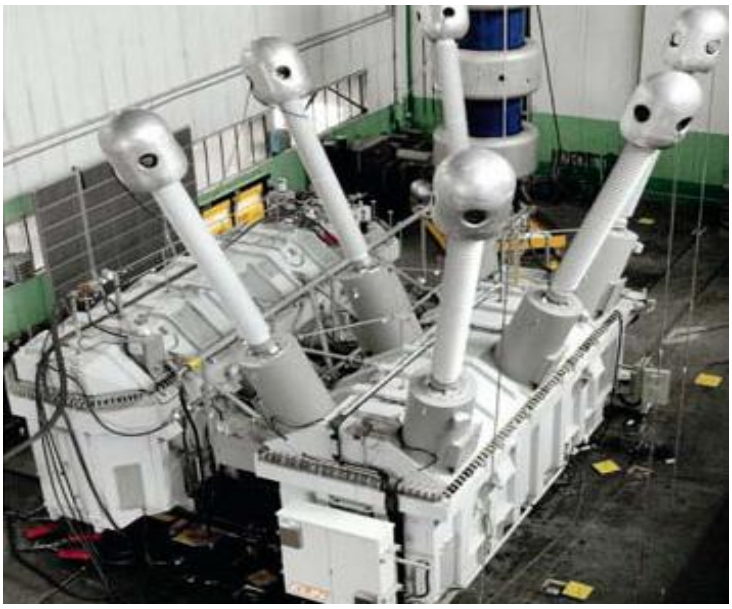

Figure 4-16. Two phase-shifting transformers, 525kV, 650 MVA throughput power, angle variations =+/-24º, Siemens.

4.2.4 **Unified Power Flow Controller (UPFC)**

The UPFC concept was proposed by Gyugyi in 1991. Compared to PSTs, the UPFC is a solid state approach that adds the capability for reactive power support. In addition, the UPFC is much faster than the PST in terms of control, making it ideal for dynamic control of the system. The Unified Power Flow Controller (UPFC) is the most comprehensive FACTS Controller, invented and developed in the US at the Westinghouse R&D center (now Siemens). A UPFC not only regulates active and reactive power through the transmission line but also provides VAR support for the connecting bus. A very successful albeit costly project is the Convertible Static Compensator (CSC) which is the most versatile FACTS Controller in the world, installed by the New York Power Authority, NYPA, at their Marcy substation as shown in Figure 4-17. For the NYPA CSC, eleven modes of operation, including the UPFC, have been operating since 2003. The *custom designed* CSC helps NYPA to mitigate congestion issues so that not only has it recovered its investment cost, but it also provides revenue as a spinning VAR reserve and as a power flow controller for contingency management for NY-ISO, 61.

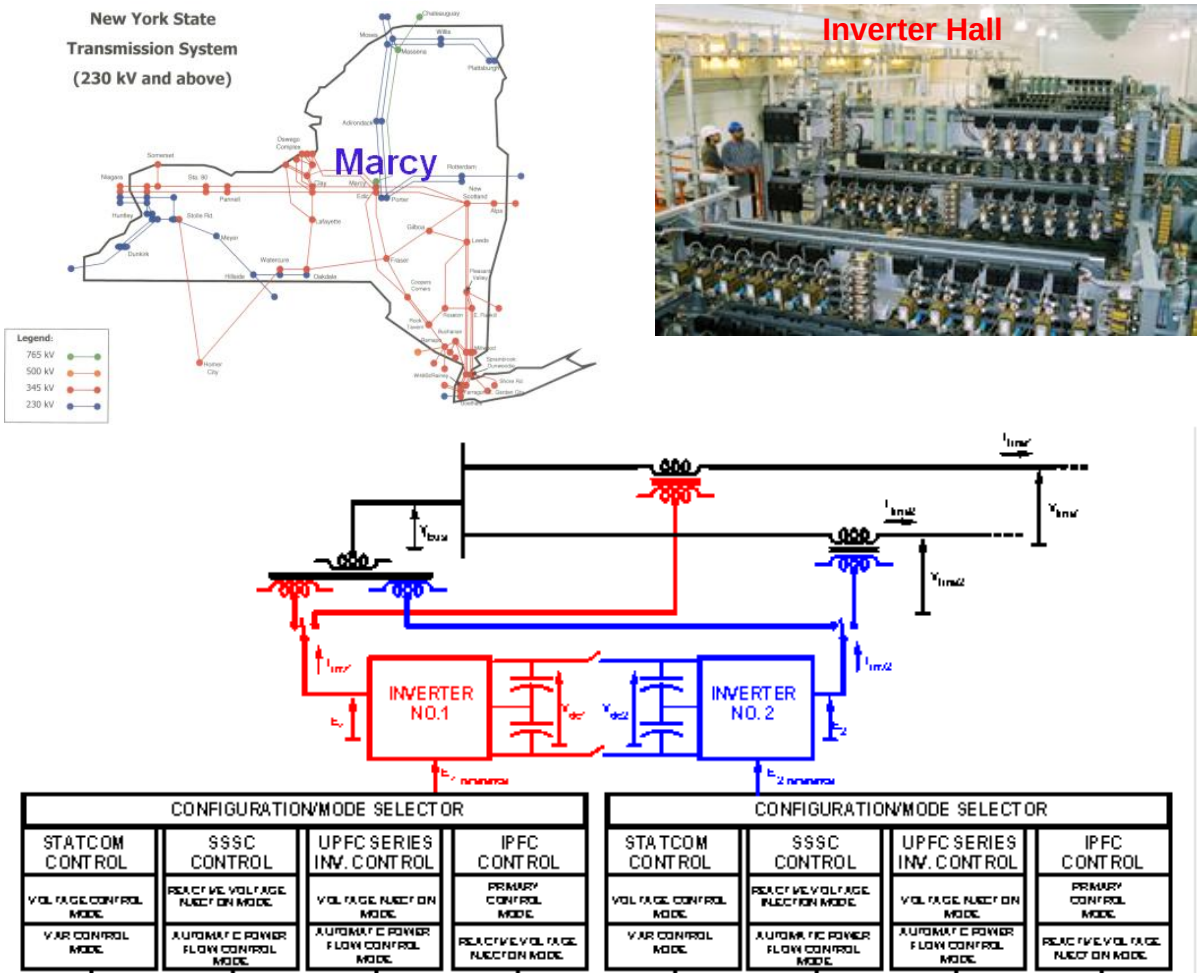

Figure 4-17. 2x100 MVA NYPA CSC at Marcy on 345kV Transmission lines.

4.2.5 **Power Flow Control at Transmission Substations**

PSTs and UPFC applications are considered to control the power flow in the major tie-lines where the Back-To-Back (BTB) HVDC option becomes too expensive. Until now, complex coordinated (supervisory) control of power flow prohibits extensive utilization of UPFCs except for a very few projects (only three worldwide). Although the UPFC has superior dynamic and steady state function, it is clear that coordinating it is quite complex in

a meshed transmission network, such as the IEEE 30 bus system shown in Figure 4-18. Although several methods have been proposed for finding the optimum locations for UPFC installation and the supervisory controls, they were not sufficiently successful and convincing for system planners and dispatchers to benefit from it. Consequently, a PST becomes the device of choice for power flow control, which is practical suited for major inter-area connections.

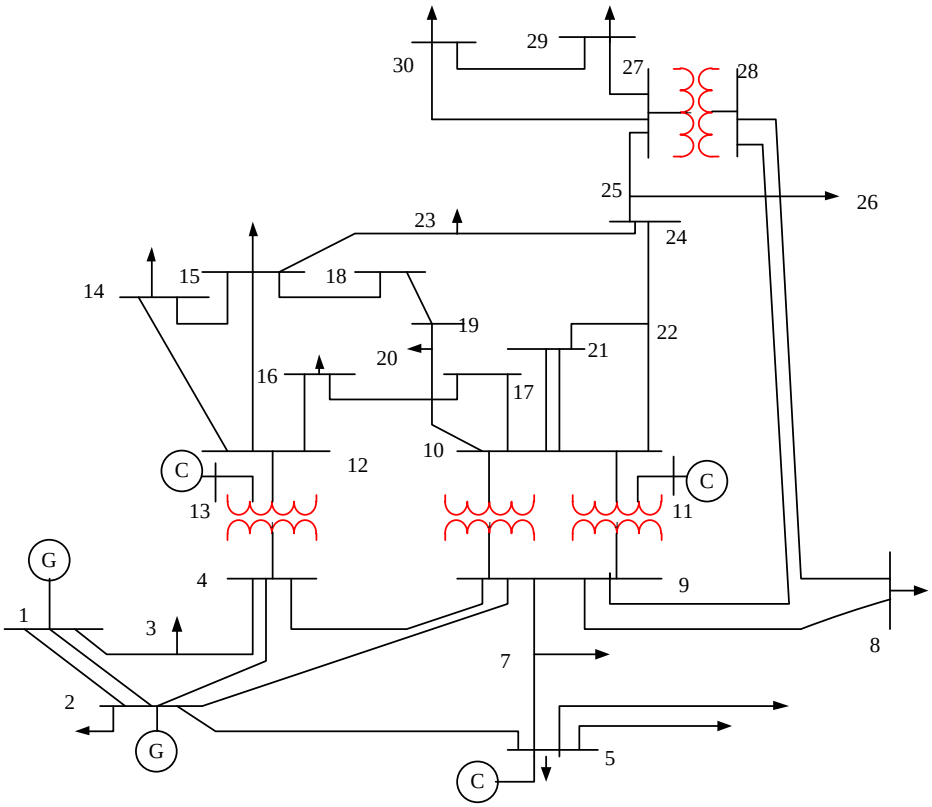

Figure 4-18. IEEE 30 bus test system; it is less complex to install in substations rather than lines, 83.

The PST with mechanical switches is far too slow to be considered for the dynamics of the power system, thus it is considered under steady state conditions. On the other hand, the

UPFC has not gotten the attention of system planners due to its coordination complexities, which involve not the power electronics but the system controls. Power flow control at substations rather than directly at the lines can provide a unique approach for system planners to dispatch power with much less complexity in a meshed network.

A dynamic power flow controller at a substation that includes a recovery transformer function is a valuable asset for system planners. The benefits are:

- Is a less complex solution for system operators to (re)dispatch power in system contingencies and normal operation
- Offers hardware-based solution in asset management for TOs
- Provide an alternative solution to transmission curtailment methods due to the new intermittent generation sources including large wind and solar farms
- Adds degrees of freedom in a de-regulated market.

On the other hand, conventionally, FACTS controllers like the NYPA CSC have been developed and inspired mainly for improving power transfer capability or allowing investment deferral on transmission lines. However, due to the aging of transmission transformers and the effects of high penetration of renewables on flow-gates, more controls on transformers may be needed right at the substations. Consequently, this dissertation also introduces a Convertible Static Transmission Controller (CSTC) which is installed across the transmission transformer to increase the system's spare capacity and operating margins. This offered solution with added values for mesh systems provides the following functions and benefits:

- Transmission or distribution transformer life extender

- Recovery transformer for disaster management
- Seasonally renewable transmission controller

Figure 4-19 presents the general schematic of the proposed power flow controller at the substation. In this approach solid state switches have been used as in the UPFC to insure real time control and dynamic compensation of the transmission systems. In addition to the UPFC/PST functions, this solution can provide back-up to its controlling transformer as well.

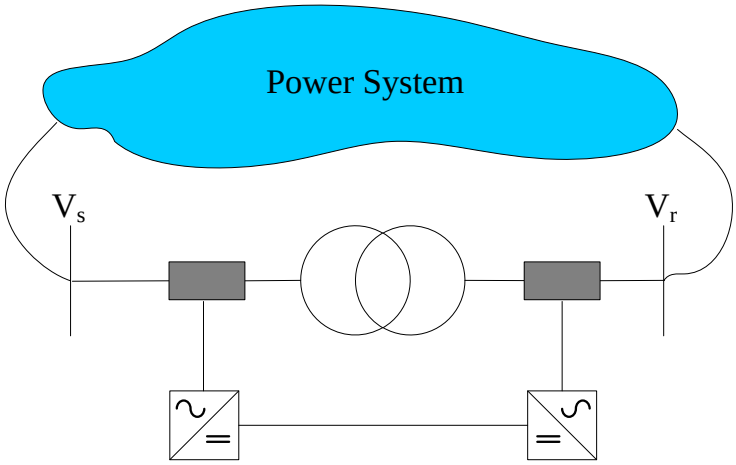

Figure 4-19. Schematic of introduced power flow controller at substation.

Based on the general structure of the proposed power flow controller at the substation shown in Figure 4-19, different connecting configurations can be used. These configurations are presented in Figure 4-20 and as shown, Figure (a) is for shunt-shunt, (b) for series-shunt, and (c) is for series-series connection. In the following, the effect of each configuration will be discussed. This multi-functionality represents a significant paradigm shift and performance improvement over the CSC implementation.

The desired flexible framework is enabled and proposed with a modular solution called a Modular Transformer Converter (MTC), and its benefits and characteristics are presented in Figure 4-21. Should the circuit be developed through advanced control and semiconductor switches, a versatile transmission controller can be realized and will be introduced as the CSTC presented in Figure 4-22. This system meets all the grid code standards for integration into the network.

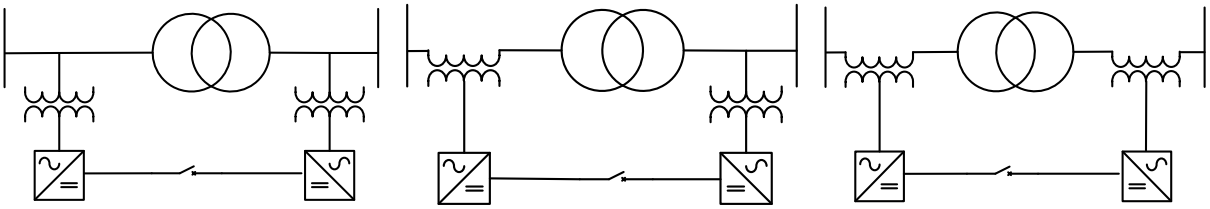

Figure 4-20. Possible connecting configurations of the proposed power flow controller.

- Versatile asset
- Power flow router
- Asset management hardware
- Transportable
- Scalable
- Different voltage compatible
- High efficiency
- Distributed DC link
- Retrofit into substations
- Modular for Utilities

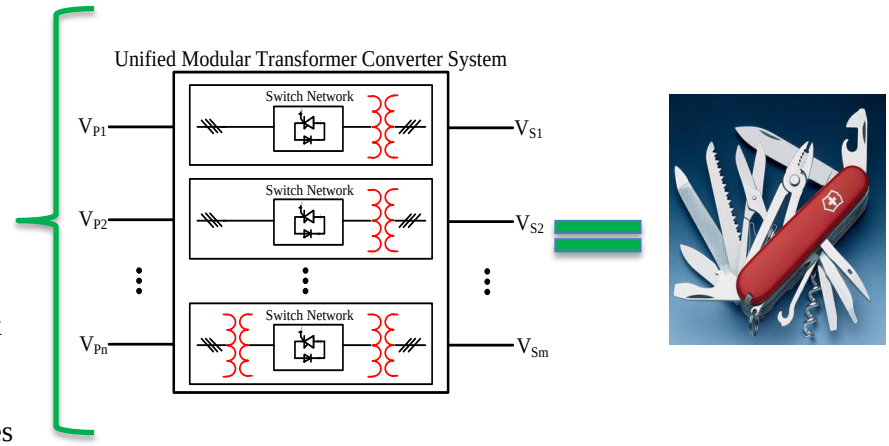

Figure 4-21. Flexible transmission controller frame with Modular Transformer Converter (MTC).

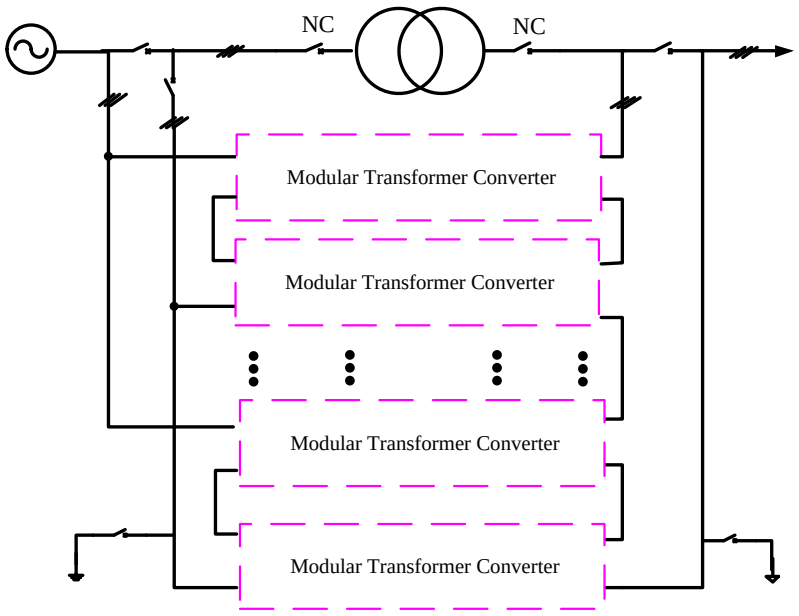

Figure 4-22. Representative schematic of MTC-based Convertible Static Transmission Controller (CSTC).

4.3 Substation Power Flow Controller Connecting Configurations

4.3.1 Shunt-Shunt Connecting Configuration - Substation Voltage/Phase Angle Controller

The shunt-shunt connecting configuration, shown in Figure 4-20-(a), can be interpreted differently.

1. The only configuration for the main transformer back-up
2. Active power controller independent of the main transformer operation -parallel operation with the transformer
3. Reactive power support at the substation sending and receiving end buses to increase the transmittable active power

4. Transformer power flow controller

One of the motivations of this section is to propose a unique power electronics (active) based solution that provides back-up in case of substation transformer failure or forced reduced transformer operation scenarios. Figure 4-23 presents the proposed approach as the preferred hardware-based asset management solution, in which a fractionally rated CSTC bypasses the existing main transformer. If the CSTC has sufficient control bandwidth, it can provide damping and active filtering functions as well. It is worth noting that the required control can be embedded in the CSTC, thus simplifying the power system operation (node power flow does not change), if the necessary commands are received from the main transformer. This mode of operation is called distributed control vs. the centralized control that may be requested in contingencies. In addition, the CSTC is desired to be transportable and compatible with different voltage levels and therefore operates as a recovery transformer. A recovery transformer sometimes known as a "ReX Transformer" with high voltage SiC devices, compact design and light weight, has gained the attention of the Department of Homeland Security (DHS) for disaster situations and indeed is an option for CSTC development. Figure 4-24 shows a representative application of transportable CSTCs associated with an appropriate control mode. In the normal mode of operation, CSTCs extend the life time of existing transformers by partially bypassing and conditioning the substation throughput power. In case of transformer failure, CSTCs can be aggregated or dispersed to meet power, voltage, VAR and configuration requirements. It is essential to distinguish this mode of operation from the BTB HVDC control functions, explained below.

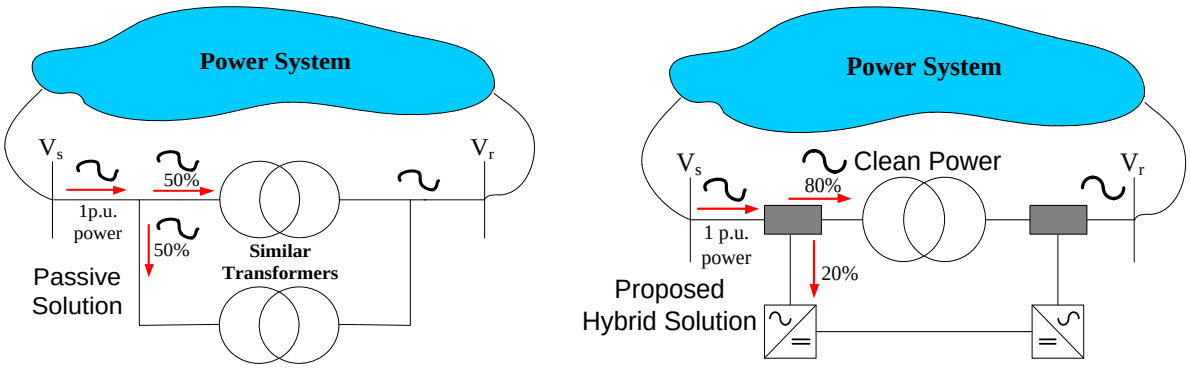

Figure 4-23. Two hardware-based asset management approaches for life time extension of a transformer under forced reduced operation and distorted power throughput.

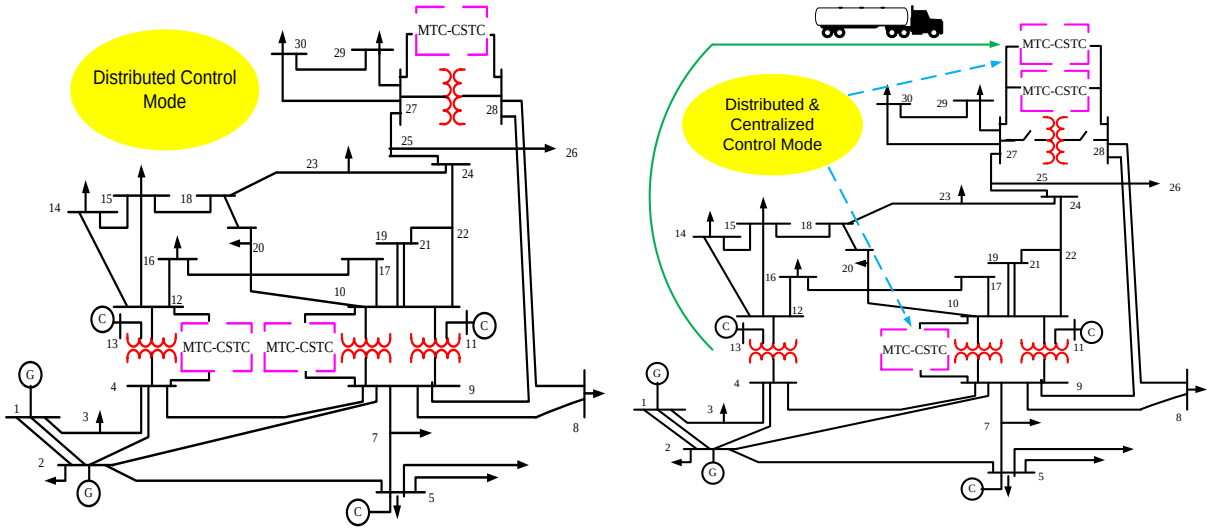

Figure 4-24. Distributed CSTC application in normal forced reduced operation of transformers and distributed and aggregated CSTCs under contingencies on IEEE 30 bus mesh AC system.

This configuration can be utilized as an active back-up for the main transformer up to its rating. While this solution can operate similarly to a BTB HVDC, the desired control functions are completely different and should not be compared to HVDC applications. An important feature of shunt-shunt mode is its capacity to operate locally without changing the substation power flow or, consequently the meshed power system. This capability of the

CSTC, based on an MTC, enables the equipment to be dispersed in the meshed network to extend the life-time of the transmission or distribution transformers without complicating the power system operation. The MTC-based solution in this case can also be aggregated to meet the power and voltage requirements for disaster management, serving as a recovery transformer.

A representative vector analysis of the CSTC in shunt-shunt mode for (partial) back-up purposes is presented in Figure 4-26 based on the test system shown in Figure 4-25. As mentioned earlier, a CSTC in the shunt-shunt mode should not change the substation power flow. In order to accomplish the desired function, the CSTC regulates the substation's sending end voltage, V_{sub}, such that active power leaving the substations remains constant while reducing the transformer power flow. In fact, the CSTC acts like a voltage/phase angle regulator which is totally different from the BTB HVDC converters' functions. The governing relationships have been derived as (4.2)-(4.4). There are two control variables, k_1 and k_2, to determine the required substation voltage (vector). k_1 assures constant substation output power and k_2 relates the power that is required to bypass the transformer with the CSTC. Consequently, the output voltage magnitude and phase angles are set as two references for the MTC converters. To measure the phase, it is expected that Phasor Measurement Units (PMUs) will be utilized instead of using model-based phasor prediction methods in the CSTC structure.

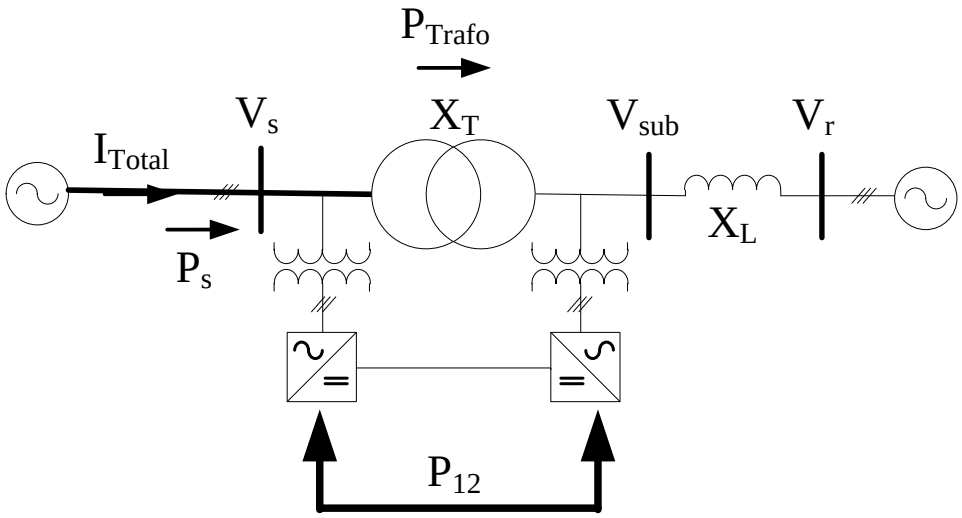

Figure 4-25. Test system to analyze the CSTC in a shunt-shunt connecting configuration.

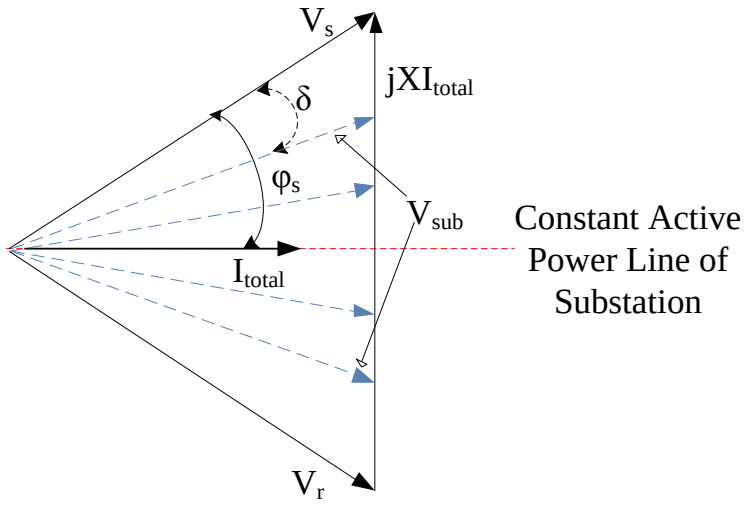

Figure 4-26. Vector analysis of the CSTC for shunt-shunt configuration operated as voltage/phase-angle regulator for transformer back-up as shown in Figure 4-25.

$$V_{sub}\cos\left(\overset{\varphi_{sub}}{\varphi_s-\delta}\right)=\frac{P_s}{I_{total}}\equiv k_1 \tag{4.2}$$

$$V_{sub}\sin(\delta)=\overset{P_{new-Trafo}}{k_n P_s}\left(\frac{X_t}{V_s}\right)\equiv k_2 \tag{4.3}$$

$$\delta = \arctan\left(\frac{\cos\varphi_s}{k_1/k_2 - \sin\varphi_s}\right) \tag{4.4}$$

Reactive power support increases the transmittable active power (item number 3). This is not a new concept and can be found in several literature sources, 3. In fact, the proposed system consists of two STATCOMs at the substation buses shown in Figure 4-27. By making the substation buses the PV type and taking into account the Short Circuit Ratios (SCRs) of the connecting system and the impedance of the shunt transformers, we can define the amount of reactive power injection (converter rating) needed to increase the transmittable power.

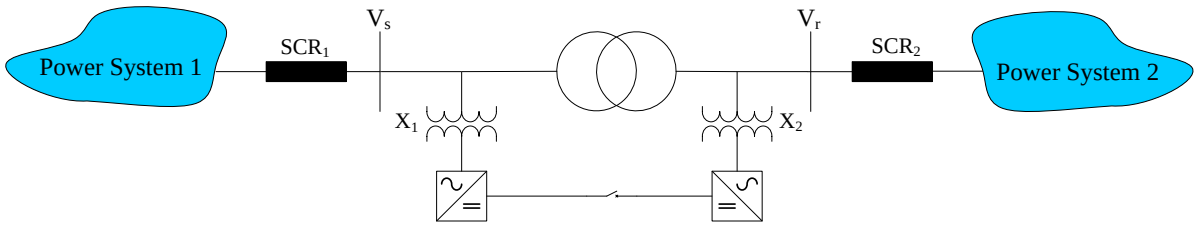

Figure 4-27. Shunt-shunt connecting configuration for supporting only reactive power injection to increase the transmittable power.

Up to now, we have explained indirect power flow control of the substation with a shunt-shunt configuration. It is of interest to actively utilize the transformer capacity. To accomplish that, all the voltages and angles of the two substations' busses must be regulated. The IEEE 30 bus system is chosen as a reference with attention to the transformer connected between bus 4 and 12. A power flow program has been run to find the active and reactive

power through the transformer. The values are called P_0 and Q_0. Figure 4-28 shows the effect of the shunt-shunt controller on the transmitted power through the transformer relative to the case without the controller. In this example the receiving end voltage is set to 1 pu. As can be seen, the power can change by a factor of more than ten for various angles and voltages. The voltage magnitude of the sending end voltage does not affect that much of the transferred active power, as expected; however, its effect on the reactive power is significant. Figure 4-29 presents the relative PQ operating region of the transformer with the controller. It has been observed that increasing the voltage magnitude at the sending end (often preferred) reduces the reactive power throughput capability of the transformer.

A shunt-shunt connecting configuration is a new concept for power flow controllers that needs further investigation. One interesting, yet challenging, problem is how to determine power flow through the converter. It can be shown that the power can change by a factor of more than ten for various angles and voltages. However, the reactive power throughput capability of the transformer is reduced.

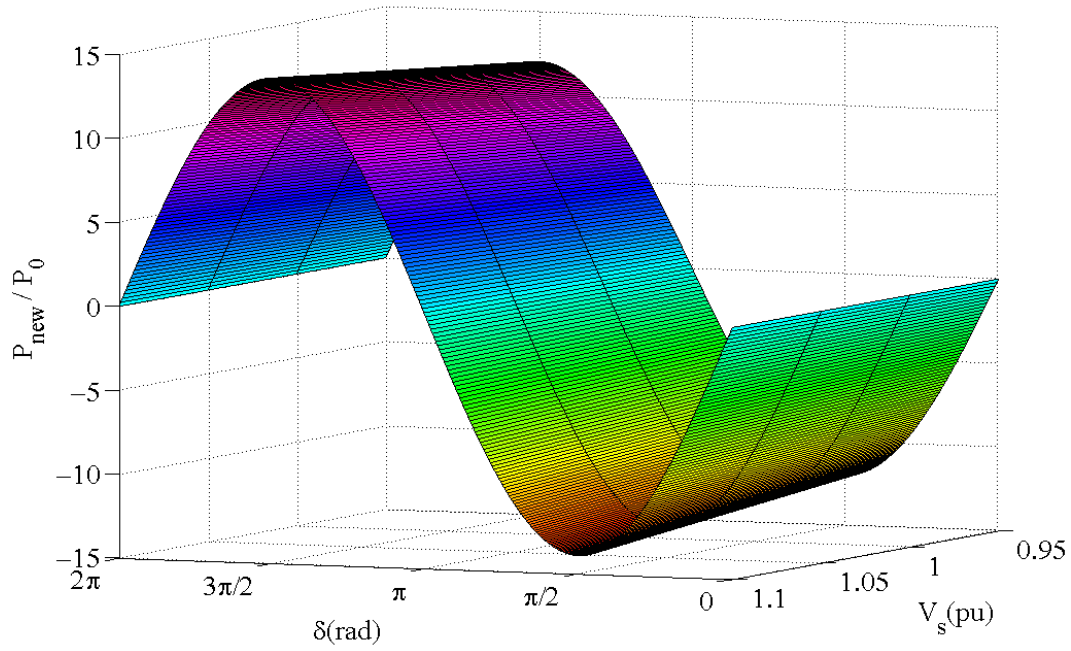

Figure 4-28. Range of active power through the transformer relative to the initial power, shunt-shunt configuration.

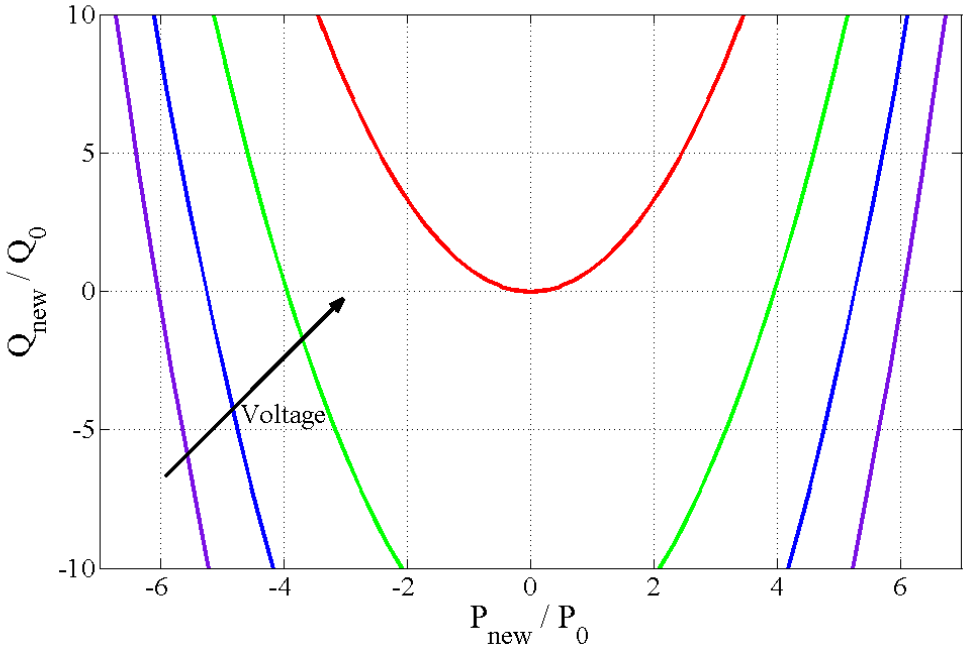

Figure 4-29. Relative PQ effective operating region of a shunt-shunt controller.

4.3.2 **Series-Shunt Connecting Configuration – Substation Power Flow Controller**

Although the shunt-shunt option is necessary for back-up operation, there are unsolved issues and constraints regarding the power flow control during the normal operation of the transformer. The solid state-based series compensator is conventionally referred to as the power flow controller. When this compensator is equipped with an active power source, it can control the active and reactive power independently. One approach is the one that has been shown in Figure 4-20(b). An example of vector analysis of a series-shunt configuration is shown in Figure 4-30. The shunt converter, by providing the reactive power to the receiving end bus, maintains the voltage magnitude. Meanwhile, it can transfer the active power to the series converter to provide a different voltage and angle. Hence, this configuration can control the active and reactive power flow through the transformer while maintain the bus voltage magnitude. It is important to understand that there are multiple points for each of the controlled values. One example is shown qualitatively in Figure 4-31. In this example, multiple active power values can be transferred through the transformers while zero reactive power is delivered.

To show the effect of the series-shunt configuration on the transformer throughput power, consider an IEEE 30 bus system with the transformer connected between bus #4 and bus #12 is considered as shown in Figure 4-34. This MTC system is shown in Figure 4-32 where the active and reactive power without the controller is called P_0 and Q_0. A steady state model of the proposed power flow controllers is necessary for the power flow analysis.

Figure 4-33 presents the desired power model, which can be used in any power flow program. This model includes the transformer in every run of the power model which makes it unique. It is worth noting that the active power required to supply variable series voltages is supplied through the transformer. Hence, all the active power entering the substation flows through the transformer. The result is shown in Figure 4-35 and Figure 4-36. As can be seen, with a fraction of the rated power, the transformer throughput power changes significantly. This option, unlike the shunt-shunt option shows a wider operational area for reactive power.

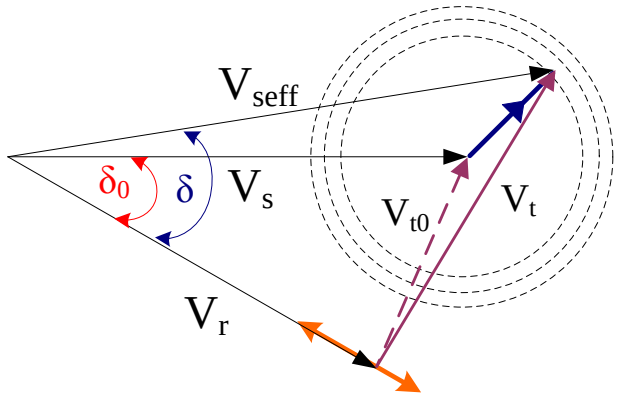

Figure 4-30. Vector analysis of the transformer power flow controller for a series-shunt configuration.

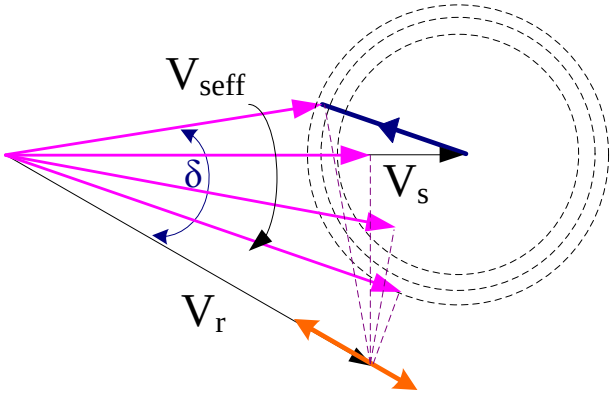

Figure 4-31. Example of a series-shunt option vector analysis for zero reactive power transfer.

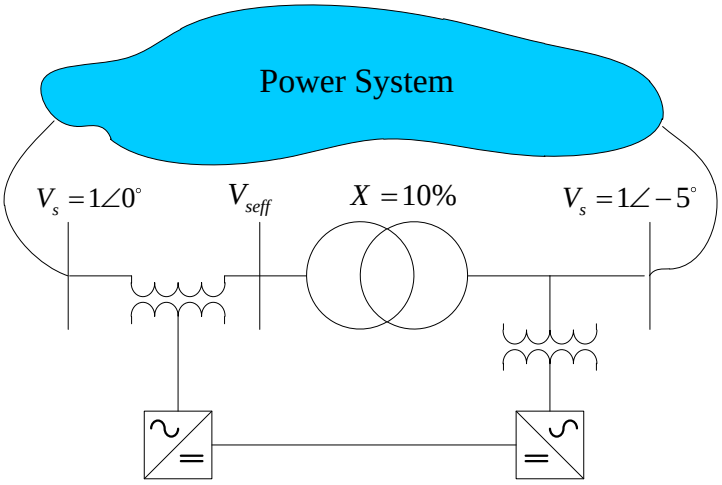

Figure 4-32. MTC based CSTC test system values in series-shunt mode of operation in IEEE 30 bus.

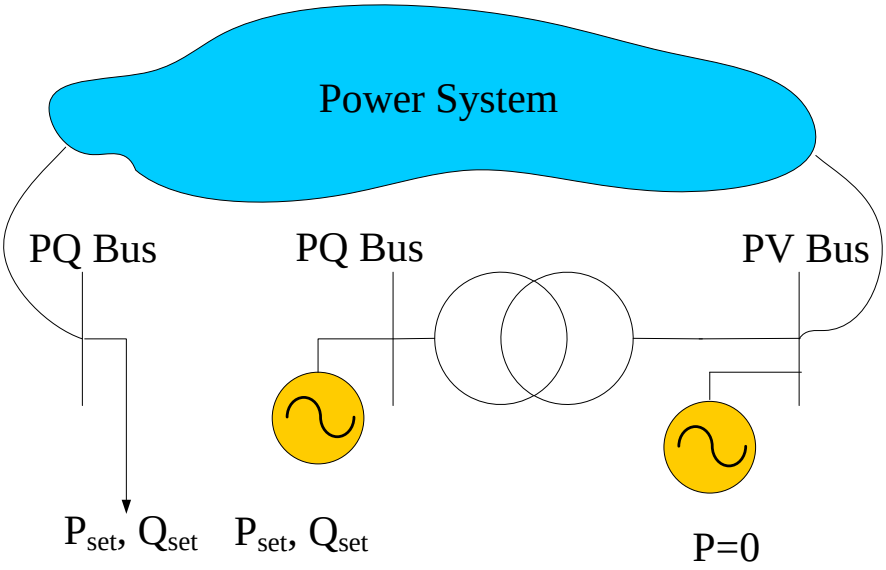

Figure 4-33. Power flow model for the series-shunt connecting configurations.

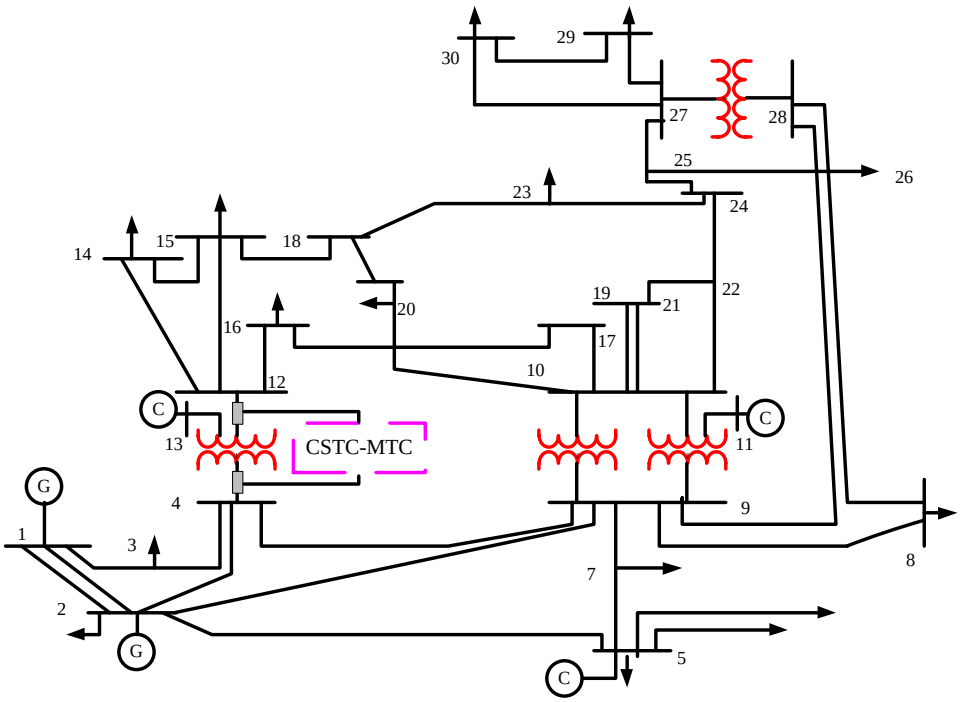

Figure 4-34. MTC-based CSTC as the substation power controller in the IEEE 30-bus system.

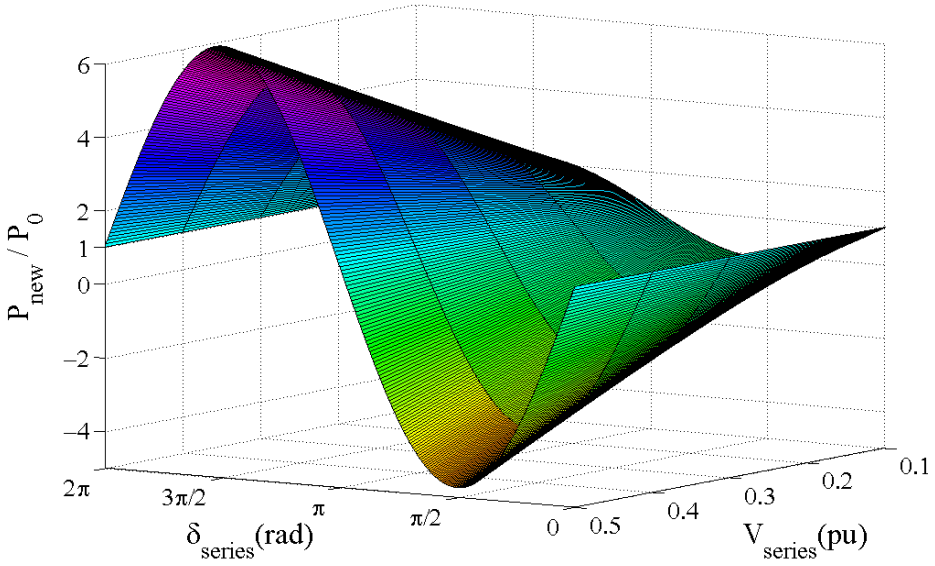

Figure 4-35. Range of active power through the transformer relative to the initial power, series-shunt configuration.

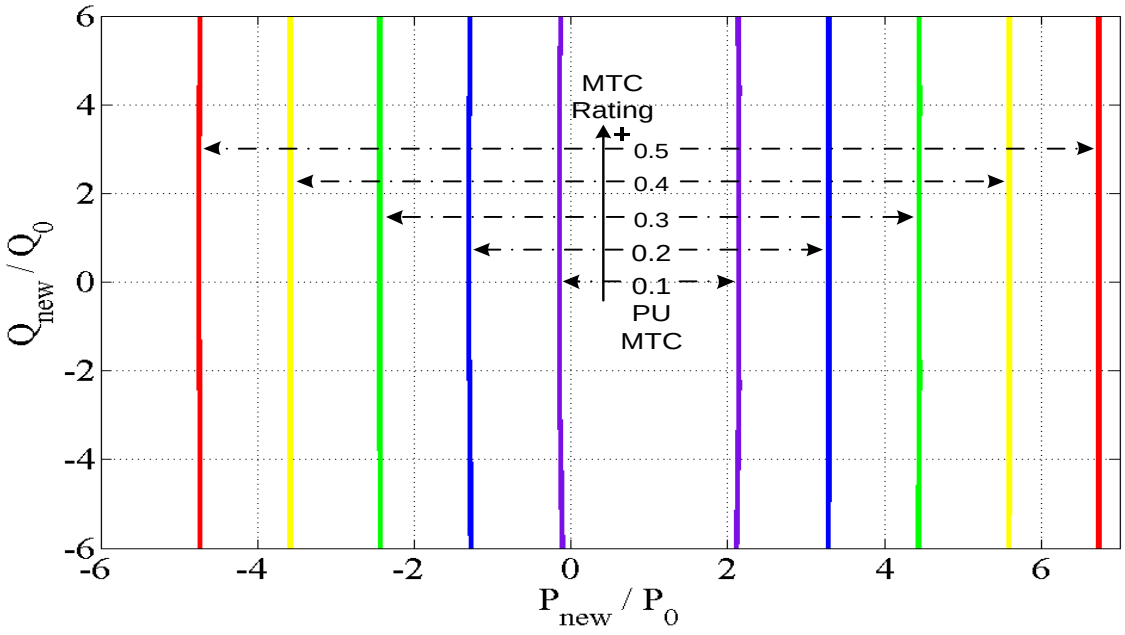

Figure 4-36. Relative PQ effective operating region of the series-shunt controller.

4.3.3 **Series-Series Connecting Configuration – Dual Series Static Compensator**

The presence of the transformer makes it possible to connect two series converters across the transformer, which is quite unique in the FACTS controllers. It is important to distinguish this approach from the IPFC (Interline Power Flow Controller) and vector analysis of this mode is presented below. This mode of operation is called a Dual Series Static Controller (DSSC). This configuration is presented in Figure 4-20-(c) and, the single-phase equivalent circuit diagram in Figure 4-37 is proposed for vector analysis.

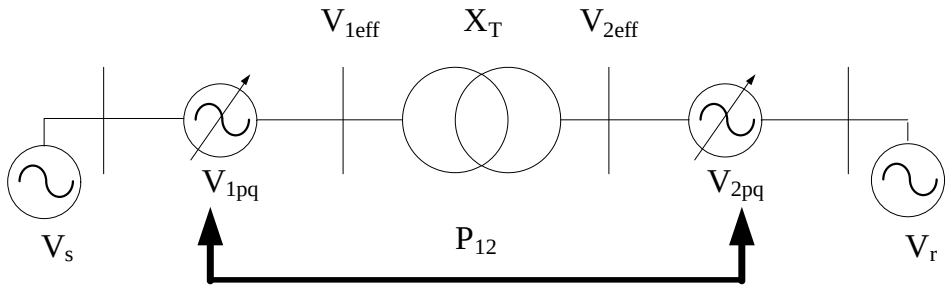

Figure 4-37. Single phase equivalent circuit of MTC in series-series mode.

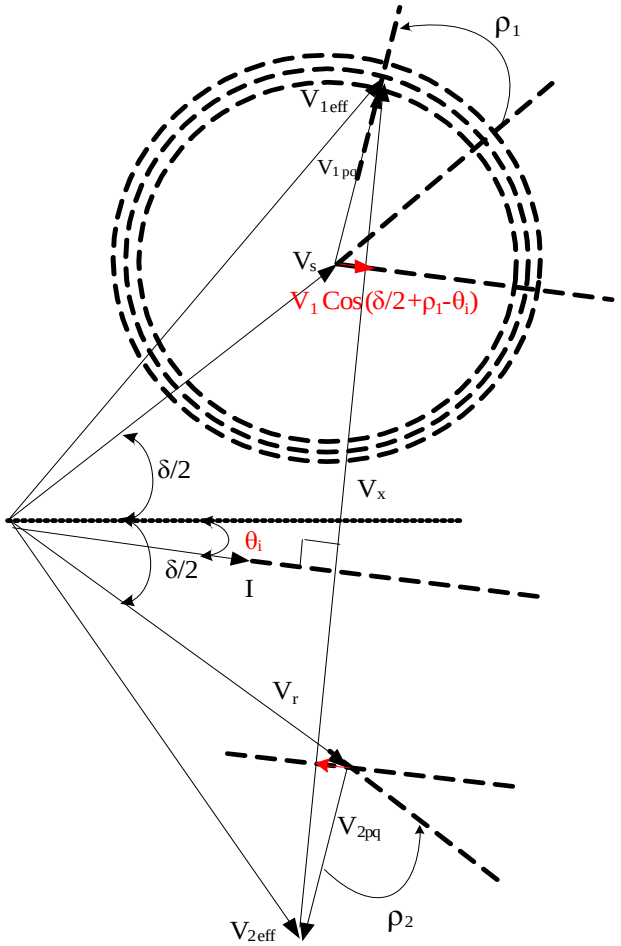

Figure 4-38. Vector analysis of transformer power flow controller for series-series configuration.

With reference to Figure 4-38 based on the test system shown in Figure 4-37, the active power P and the reactive power Q supplied by the receiving end can be written as (4.7) and (4.8).

$$\overrightarrow{V_{1pq}} = V_1 e^{j(\frac{\delta}{2}+\rho_1)} = V_1(\cos(\frac{\delta}{2}+\rho_1) + j\sin(\frac{\delta}{2}+\rho_1)) \tag{4.5}$$

$$\overrightarrow{V_{2pq}} = V_2 e^{-j(\frac{\delta}{2}+\rho_2)} = V_2(\cos(\frac{\delta}{2}+\rho_2) - j\sin(\frac{\delta}{2}+\rho_2)) \quad (4.6)$$

$$P = \frac{V_s V_r}{X_T}\sin\delta + \frac{V_r V_1}{X_T}\sin(\delta+\rho_1) + \frac{V_r V_2}{X_T}\sin(\rho_2) \quad (4.7)$$

$$Q = \frac{V_r(V_s\cos\delta - V_r)}{X_T} + \frac{V_r V_1}{X_T}\cos(\delta+\rho_1) - \frac{V_r V_2}{X_T}\cos(\rho_2) \quad (4.8)$$

In order to maintain the power balance on the DC side, the constraint shown in (4.9) must be taken into account leading to a governing relationship for the converters' voltage outputs in the form of (4.10).

$$\mathrm{Re}\left\{\overrightarrow{V_{1pq}} \times \vec{I}^{*}\right\} = -\mathrm{Re}\left\{\overrightarrow{V_{2pq}} \times \vec{I}^{*}\right\} \quad (4.9)$$

$$V_1(\cos(\frac{\delta}{2}+\rho_1-\theta_i)) = -V_2(\cos(\frac{\delta}{2}+\rho_2+\theta_i)) \quad (4.10)$$

4.3.4 Comparison of the Proposed CSTC- and Conventional FACTS-Based Power Flow Controllers

In order to evaluate the proposed CSTC in the power flow control mode, conventional FACTS controllers such as SSSC, UPFC and IPFC have been compared in a test system shown in Figure 4-39. This 4-bus system with one transmission substation can represent a flowgate of power delivery from renewable resources. It should be mentioned that the SSSC and UPFC are inserted into the incoming or outgoing lines of the substation due to the benefits of having the power flow control at the substation and not the lines. The comparison has been made through three different case scenarios with different natural power flow as follows:

Case I: (P0=0.9174 (pu), Q0=0.0401(pu))
Case II: (P0=0.9248 (pu), Q0=1.0351(pu))
Case III: (P0=0.9195 (pu), Q0=-1.0099(pu))

The results of this comparison have been presented in Figure 4-40-Figure 4-42 for a 10% series voltage injection for each controller (a 20% voltage injection is assumed for SSSC). As can be observed, the SSSC is the device of choice for the network with low reactive power loadings. However, going to the systems with natural higher reactive power, the improved characteristics for DSSC and UPFC become apparent. The results also show that the controllable range of the DSSC is much wider than that of UPFC, and it can independently control both real and reactive power over a broad range. In addition, its control region in terms of real and reactive power is independent of the line current whereas the control ranges of the IPFC and SSSC depend on system operating points.

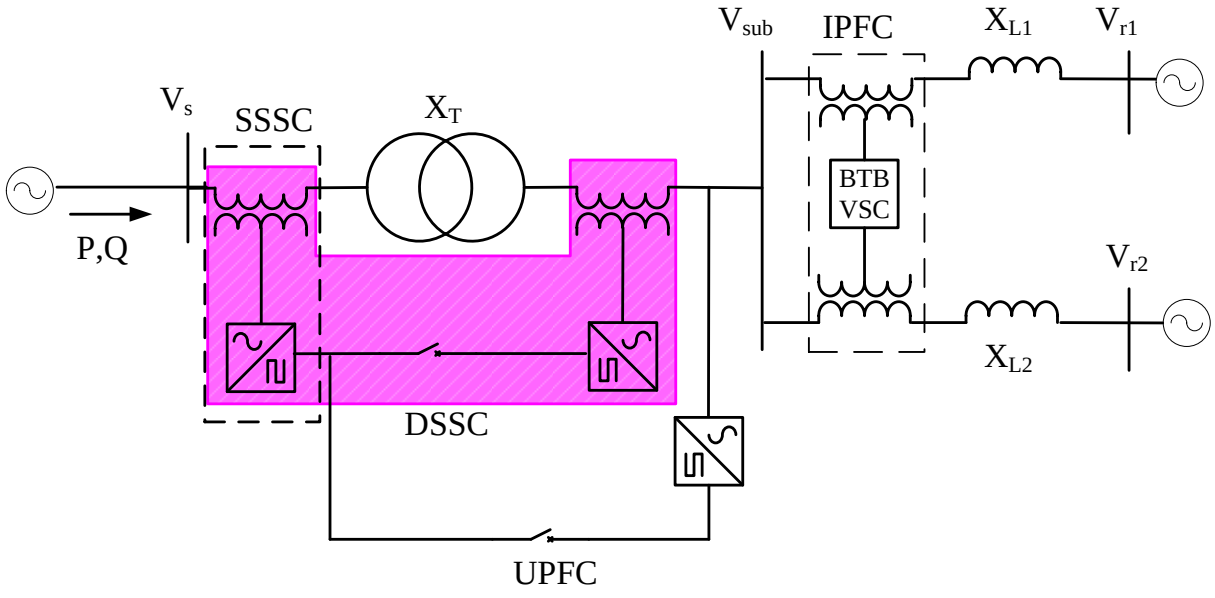

Figure 4-39. Test system to compare different modes of the CSTC and common FACTS.

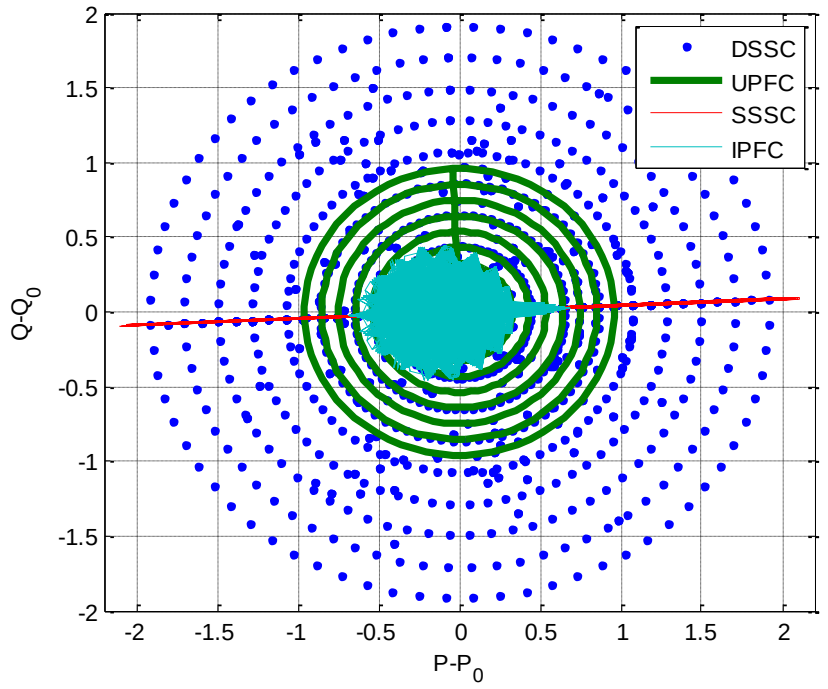

Figure 4-40. P-Q operating characteristics with DSSC, UPFC, IPFC, and SSSC (*Natural Power Flow: P_0=0.9174 (pu), Q_0=0.0401(pu)*).

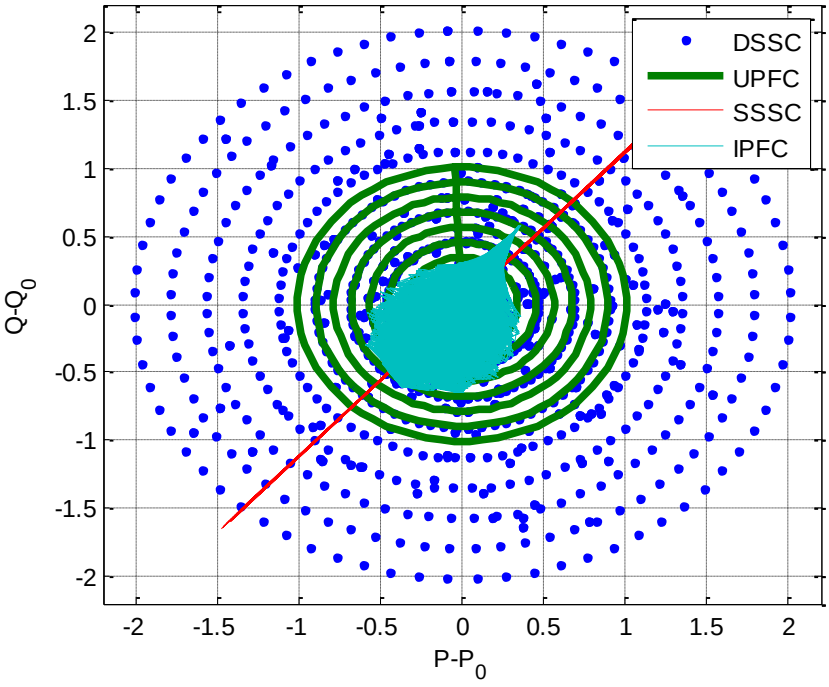

Figure 4-41. P-Q operating characteristics with DSSC, UPFC, IPFC, and SSSC (*Natural Power Flow: P_0=0.9248 (pu), Q_0=1.0351(pu)*).

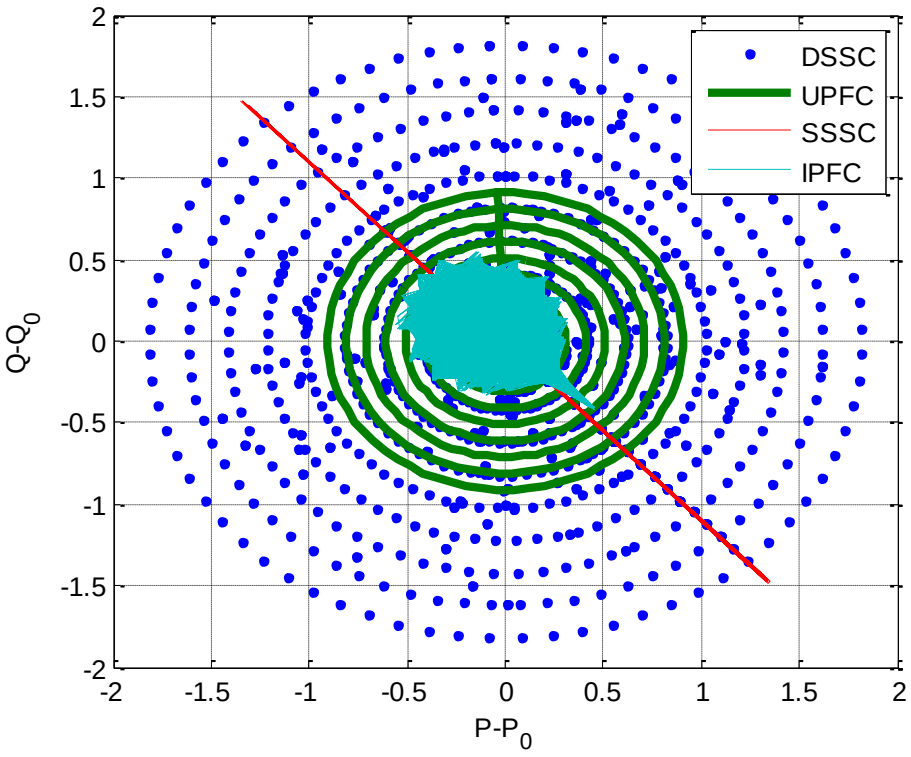

Figure 4-42. P-Q operating characteristics with DSSC, UPFC, IPFC, and SSSC (*Natural Power Flow: P_0=0.9195 (pu), Q_0=-1.0099(pu)*).

4.4 **Modular Transformer Converter (MTC) System**

Modularity gives a flexible platform for developing multiple products with wide range of ratings. The level of modularity can be defined very differently from the switch to the converter system level. At high power level the semiconductor switch is often considered as the module. Recently, a fairly new multi-level converter topology (so called Modular Multilevel Converter (MMC or M2C)) has been implemented in an HVDC project, 84. In

this topology a set of complementary switches (half bridge) and a DC capacitor are included in its structure.

Clearly, the module rating and its structure are the most important factors to define. The module rating is important because it must be completely (or with minimal effort) compatible with the system when they are stacked and the limitations of the scaling must be determined. The structure is important because it affects the cost, efficiency, harmonics and many other performance criteria. Consequently, as explained, the T&D application levels where the modules are to be deployed must be clearly defined. On the other hand, for all the proposed options the insulation limits must be clearly investigated.

When the power electronics are integrated into the grid, utilities and TOs often require electrical isolation. Hence, the transformer availability, size and many other factors cannot be ignored. As the results shown from the IEEE 30 bus exemplify, a fraction of the transformer power rating is sufficient to change the loading of the substation. In other words, 10 to 100 MVA will be the power flow controller range for typical transmission level transformers (800kV~138kV). With attention to higher voltage levels especially 345kV transformers, this power range is not common and requires custom-designed transformers, if one unit is delivered.

The Modular Transformer Converter (MTC) concept is developed to provide the following benefits:

1. Transportable modules or groups of modules
2. Scalable to meet different voltages and powers
3. High efficiency

4. High reliability
5. Commonly used semiconductor switches
6. Commonly used transformers
7. Low switching stress

Considering the power and voltage range, the M2C topology requires a number of modules in series (IGBT), a non-conventional transformer (in terms of power) and at least twice as many energy storage elements compared to the 3-level NPC with the same rating. In fact, M2C is a quite adequate for high power (>100MW) HVDC and a transformerless MW-range motor-side drive. Figure 4-43 presents the proposed three-phase module which includes IGCT switches in a 3L-NPC converter, and a 69kV/4.16kV (or 63 kV) transformer. To achieve a compact design, it can use one side autotransformer. This approach regardless of the semiconductor technology is called a Modular Transformer Converter (MTC). An MTC is a transportable bidirectional AC/AC conversion unit. If several MTC building blocks are combined they can be considered to be transmission or distribution level equipment or assets.

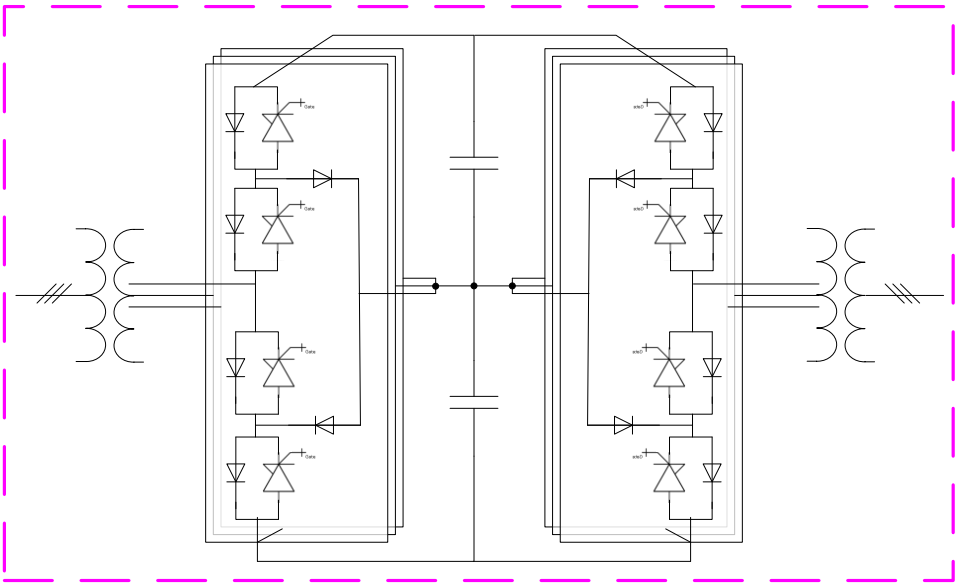

Figure 4-43. 10~15 MVA IGCT based back-to-back three phase module.

An MTC is potentially cost effective since it utilizes standard power electronics converter systems, for instance, standard medium voltage drive converters. This approach is totally different from that of commercial FACTS or HVDC controllers. Currently, standard medium voltage drive systems are commercially available up to 10 MVA with IGCT-based three-level NPC converters and up to 2 MVA with IGBT which are more than 97% energy efficient. With the advent of new high voltage SiC based semiconductor switches such as 15kV SiC IGBT and 10kV SiC JBS diode technologies higher power and higher efficiency can be foreseen for MTC building blocks. An example of an MTC with available technology is shown in Figure 4-44. As explained earlier, the MTC can be up to 10 MVA with no need for series connection of semiconductor switches. While in the shunt connection, the current flowing in the converter is controlled, although this is not true for the series connection.

Therefore, split-winding transformers are considered for one or both sides of the MTC. This is the preferred topology for an MTC.

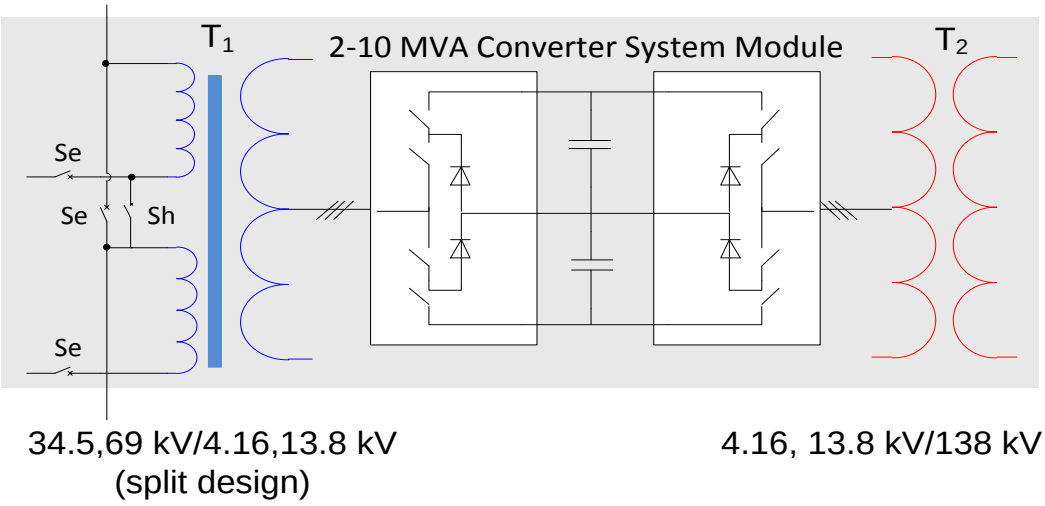

Figure 4-44. An example of MTC based on three-level NPC MV drive converters- Medium Risk.

SiC devices such as a 15kV SiC IGBT potentially enable high bandwidth MW range converters and present higher voltage blocking capability than that of Si-based devices. Therefore, transformerless approaches become attractive in MTC structure. Transformerless solutions especially for series injections are applied to single phase and not three phases. Two examples of single phase MTCs are presented in Figure 4-45. Further improvement in the MTC building block can be obtained through cross modulated bridges has shown in Figure 4-45. This module uses the floating point of a DC link for the next connection level and it can inject a floating series voltage of about 15kV for each phase, equivalent to more than 10% for a 230kV transmission voltage. The other side of the module consists of two more half bridges with advanced modulations that can be connected with an interfacing

transformer (34.5kV/69kV/115kV) to match the transmission grid voltages. Two 15kV SiC-IGBT based MTC units with a device yet to be developed can provide a power flow controller for 200MVA, 230kV/115kV transformers.

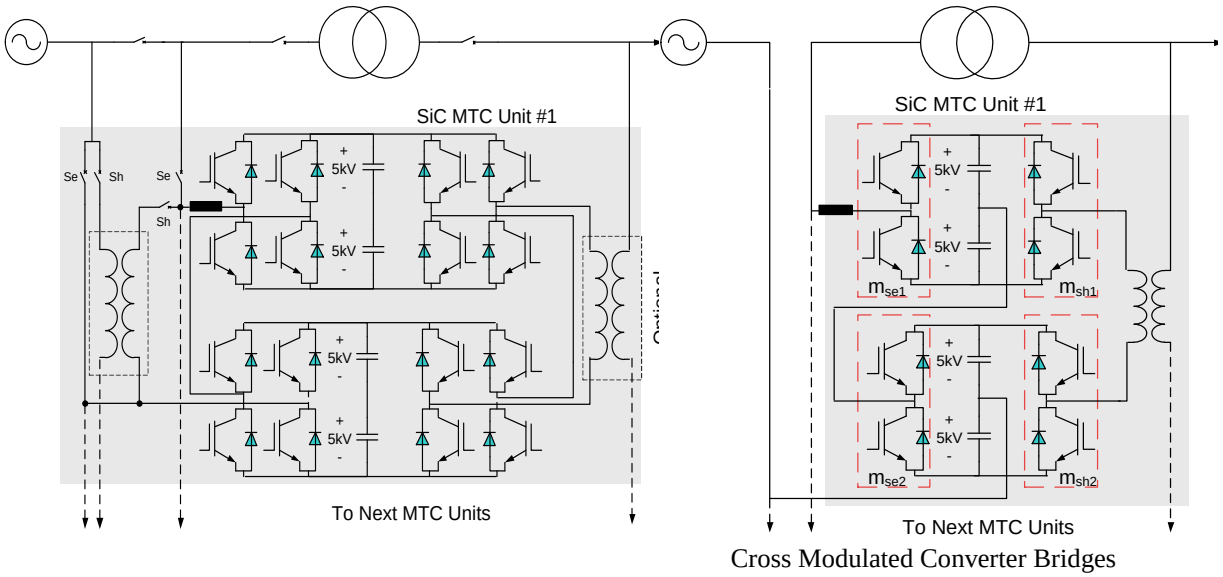

Figure 4-45. Single phase approaches for some transformerless integrations, more applicable for large transformers- High Risk.

The key component of MTC converters is the semiconductor switch and better performance can also be obtained through a hybrid semiconductor configuration (such as a Si switch and SiC diode), and modified circuit topology and control. An efficiency evaluation of the MTC in terms of the semiconductor technology and applied control is presented in Figure 4-46 for a 2 MVA MTC building block shown in Figure 4-44. In addition to more common benefits, high efficiency is one of the key factors that enables the transportability of the MTC system. As can be observed, the combination of available Si IGBTs and SiC diodes in the MTC provides superior efficiency compared to the commonly used Si IGBT and Si

PiN diodes. These results are based on the detailed PSPICE simulation and methods developed in Bhattacharya's group, 85. From a control point of view, three different control structures have been considered denoted as angle, vector, and hybrid control. A simplified advanced angle-control structure is shown in Figure 4-47. In the angle control structure, the output voltage magnitude is determined naturally by the operation of the converter; i.e., the constant ratio between AC output and DC output is considered. Consequently, the control objectives are determined by regulating only the output voltage angle. In addition, the angle-control structure in multi-pulse converters (ex. 24-pulse shown in Figure 4-48) ensures a superior harmonic spectrum which is essential for transmission level equipment. It should be mentioned that this method is well adapted for commercial STATCOMs and Parkhideh et. al. have shown the possibility of extending this method for active and reactive power control. The other control structure is the so-called vector control which is typically applied to PWM converters, Figure 4-49. This control structure presents higher controllability compared to the angle-control structure. However, this controllability is obtained through higher switching frequencies than in angle-controlled converters being operated at line frequency (50/60 Hz). Another approach is to combine the two control structures to create a hybrid control structure in a BTB system. In this scheme, one converter or a group of converters operates with angle control and the others operate with vector control.

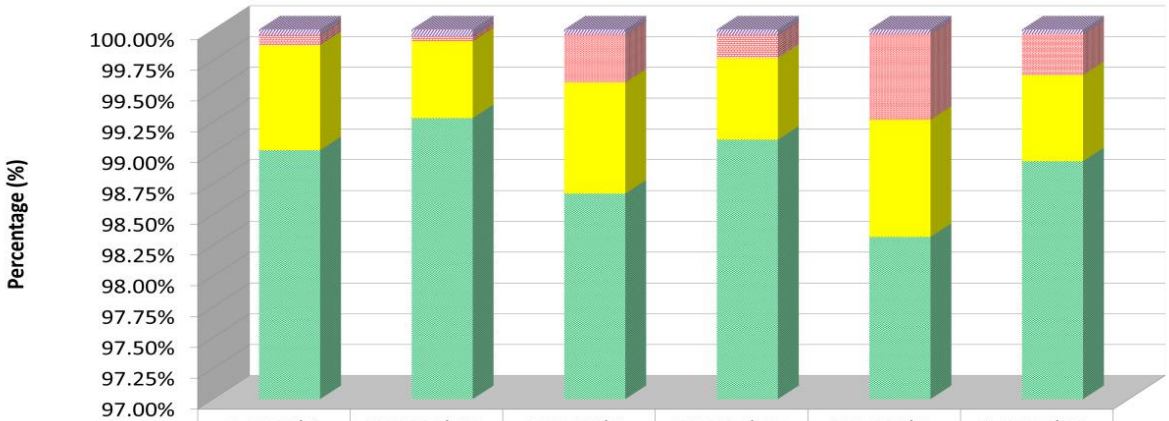

	Si-IGBT/Si-PiN diode Angle Control 60Hz	Si-IGBT/SiC-JBS diode Angle Control 60Hz	Si-IGBT/Si-PiN diode Hybrid Control 540Hz	Si-IGBT/SiC-JBS diode Hybrid Control 540Hz	Si-IGBT/Si-PiN diode Vector Control 540Hz	Si-IGBT/SiC-JBS diode Vector Control 540Hz
Parasitics Loss	0.05	0.05	0.04	0.05	0.04	0.04
Switching Loss	0.08	0.04	0.39	0.19	0.69	0.33
Conduction Loss	0.85	0.63	0.90	0.66	0.95	0.70
Efficiency	99.02	99.28	98.67	99.11	98.32	98.93

Figure 4-46. Efficiency comparison of an MTC shown in Figure 4-44 with different semiconductor devices and controls (no passive filters).

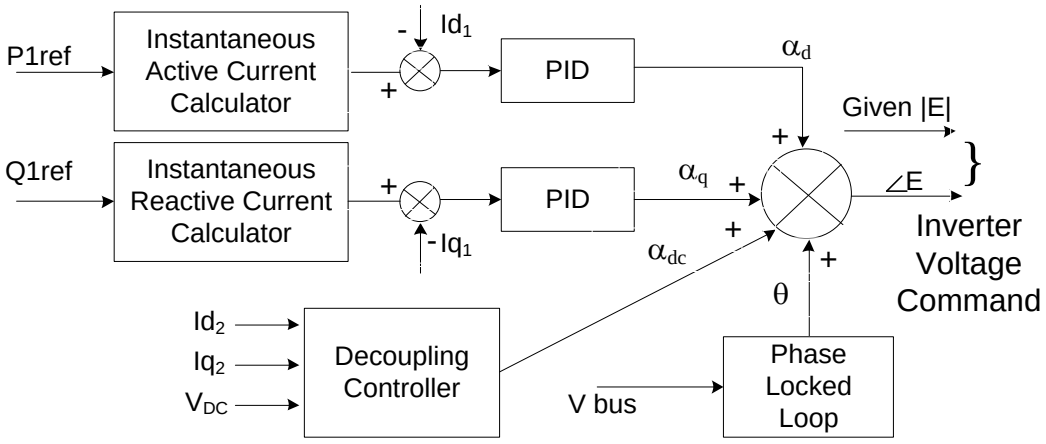

Figure 4-47. Advanced angle-control structure for a VSC.

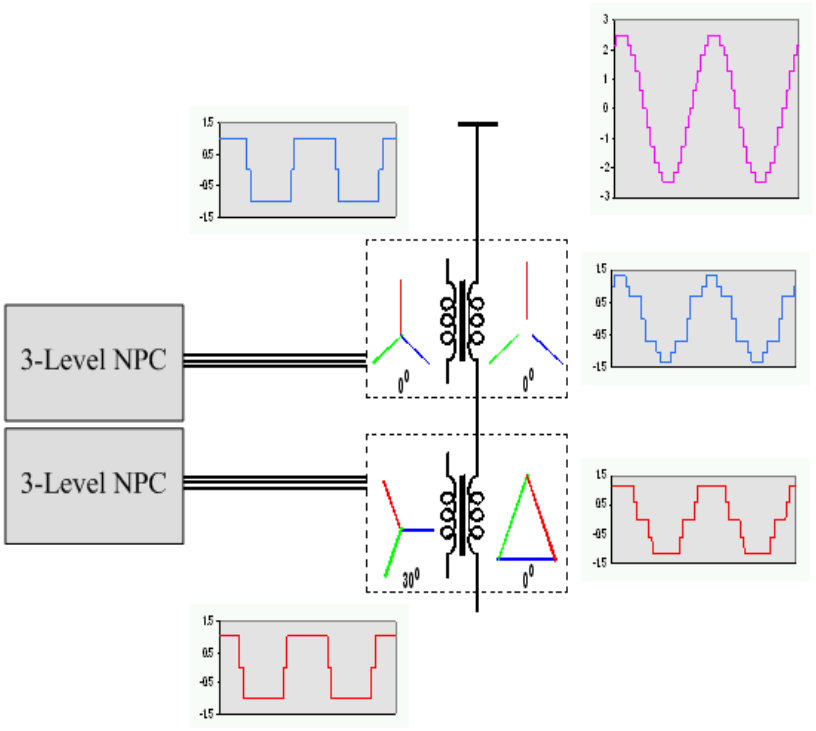

Figure 4-48, A 24-pulse angle-controlled VSC.

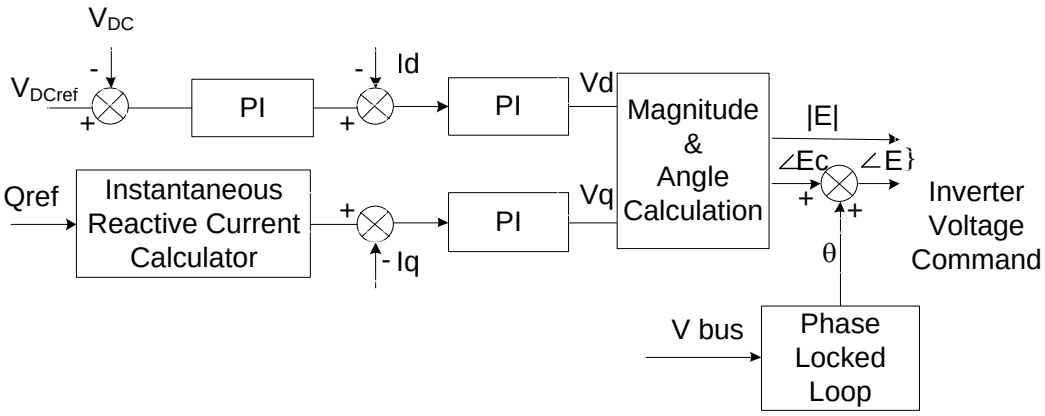

Figure 4-49. Generalized vector-control structure for VSC

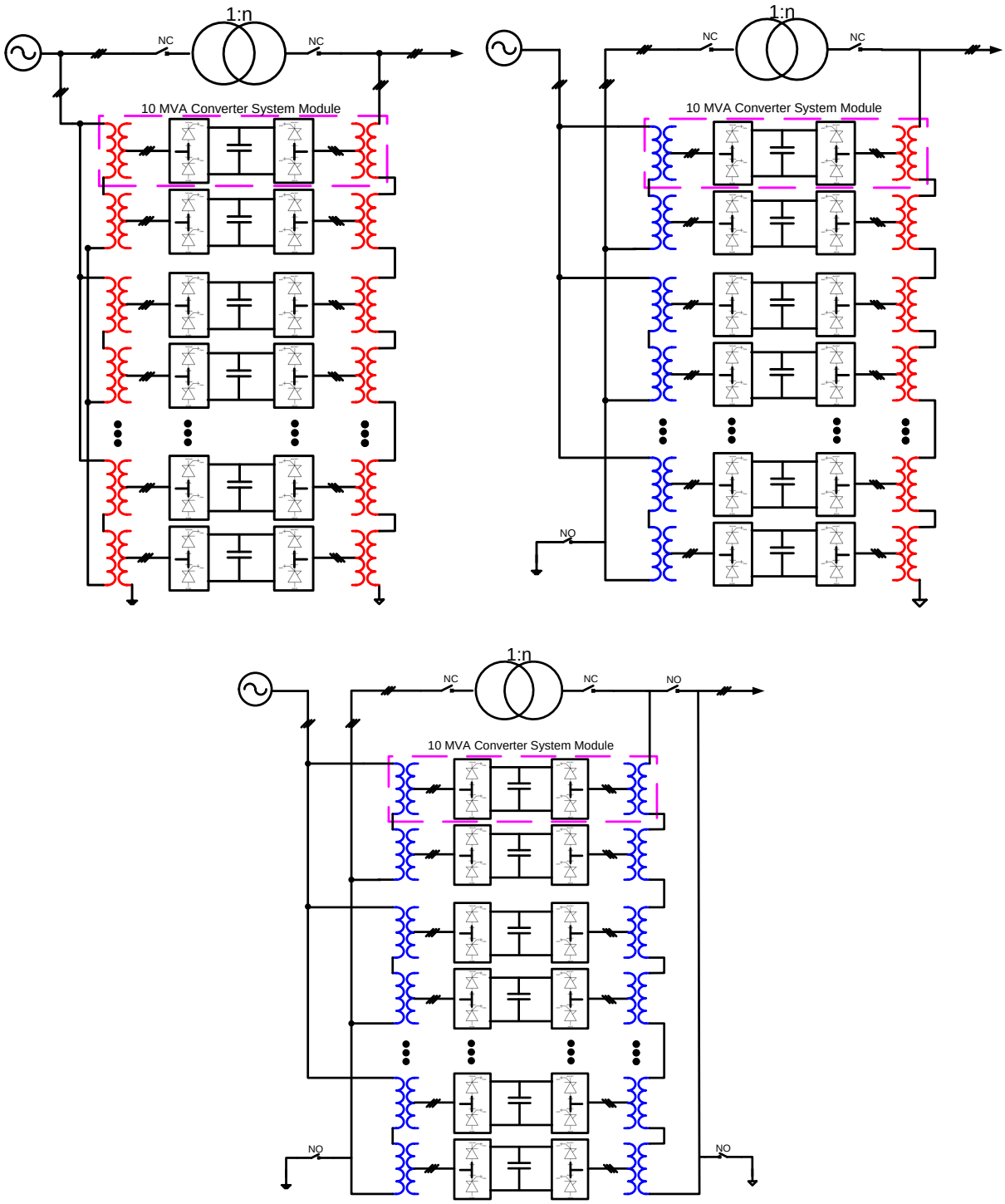

Figure 4-50. Representative Modular Transformer Converter (MTC)-based systems (red lines indicate parallel integration and blue ones show series integration).

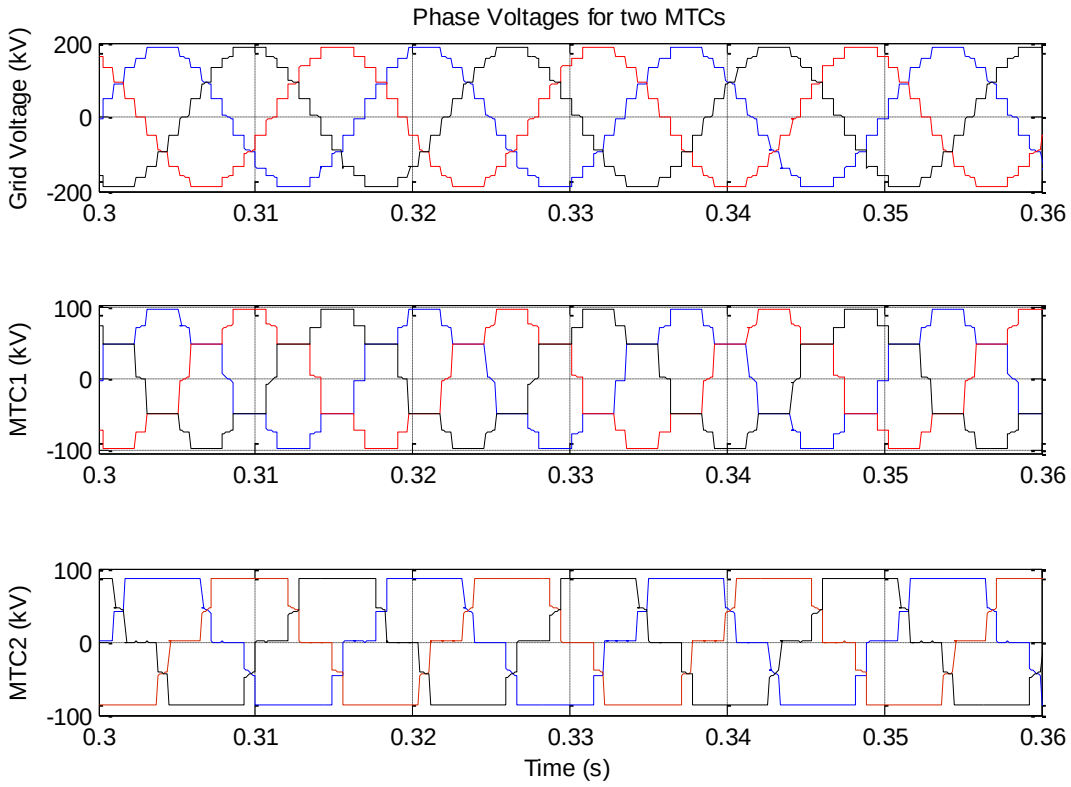

Figure 4-51. Representative voltage construction and scale-up in two series MTCs.

Once these modules are designed, they can be connected to scale up the voltage and current. A representative example for different connecting configurations is presented in Figure 4-50 and Figure 4-51 presents an example of voltage scale-up in two series MTCs that use 115kV interfacing transformers to connect to a 230kV grid with acceptable THD. In these configurations, the converters are intended to be used for power quality and back-up purposes with minimal reconfiguration (auxiliary devices) effort. It may be of interest to use an autotransformer instead of a regular transformer on one side of the MTC system. With this approach, volume and cost savings for each module are evident, whereas isolation is still

maintained with the other transformer. As a reference to a 345kV/138 kV, 600MVA transformer, six modules are connected in series and parallel. The 60 MVA MTC system is able to double the loading of the transformer actively.

The control structure is crucial for reliable and efficient operation of an MTC system. As has been shown, the converters can operate at line frequency (60Hz) while providing low THD. Different B-H curves for transformers, their effect under power systems faults, and switch stresses are among the challenges that should be addressed.

4.5 Dynamic Performance of MTC-Based CSTC

In this section the dynamic performance of the CSTC is presented in different modes for two medium-voltage 10 MVA MTCs connecting to a 230kV/138kV transmission transformer in the test system shown in Figure 4-39. Each MTC is a standard medium voltage drive converter system which is capable of switching at 9~15 times the line frequency (60Hz). Although it is possible to control the MTCs with advanced angle-control structure to achieve an improved harmonic spectrum and efficiency, this study is confined to vector-controlled MTCs where each DC link voltage is regulated to a fixed value.

4.5.1 Shunt-Shunt Connecting Configuration – Substation Voltage/Phase Angle Regulator

As mentioned earlier, a CSTC in the shunt-shunt mode should not change the substation power flow. In order to accomplish the desired function, the CSTC regulates the substation's sending end voltage, V_{sub}, such that active power leaving the substations remains constant while reducing the transformer power flow. In fact, a CSTC acts like a voltage/phase angle

regulator which is entirely different from the BTB HVDC converters' functions. The governing relationships have been derived as (4.2)-(4.4). There are two control variables, k_1 and k_2, that determine the required substation voltage (vector). k_1 assures the constant substation output power and k_2 relates the power that is required to bypass the transformer to the CSTC. Consequently, the output voltage magnitude and phase angles are set as two references for the MTC converters. The control structure to realize the concept has been developed and presented in Figure 4-52. This control structure is constructed on the assumption of constant current in the substation incoming and outgoing power. A more accurate reference generator for the controllers can be proposed by forcing the active power to be constant. The proposed control structure for the CSTC shunt-shunt mode of operation is presented in Figure 4-53. In the proposed controller, a V_r / X_L term representing the substation outgoing network characteristics is used.

The PSCAD/EMTDC simulation results for MTC operation in shunt-shunt mode are presented in Figure 4-54. As explained in the previous section, this mode is different from common BTB HVDC applications where the receiving end converter is operated in PQ control mode. In this case, the receiving end converters in the MTCs directly regulate the voltage and phase angle of the substation outgoing bus to control transformer throughput power in order to extend the transformer lifetime. As can be seen in Figure 4-54, the active power flow through the transformer can be controlled by the CSTC without affecting the power systems natural power flow. This point is essential in developing active mobile

substations. The DC link voltages in the MTCs in this mode are controlled by the sending end converters and 1PU represents 25kV.

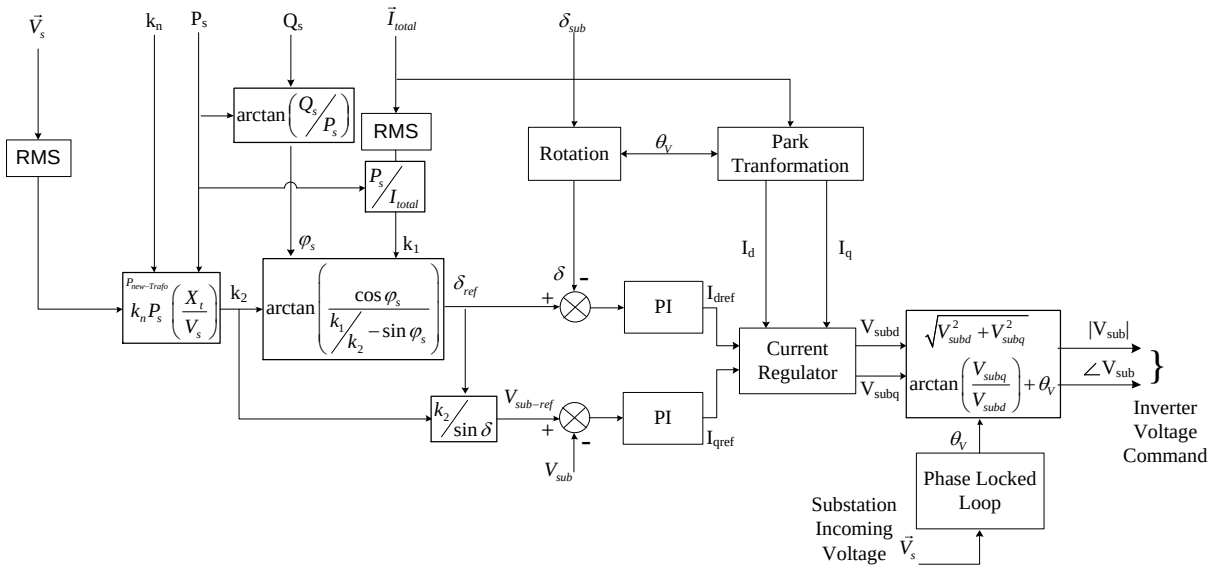

Figure 4-52. Control structure of the CSTC in the shunt-shunt mode of operation with an approximately constant substation power line.

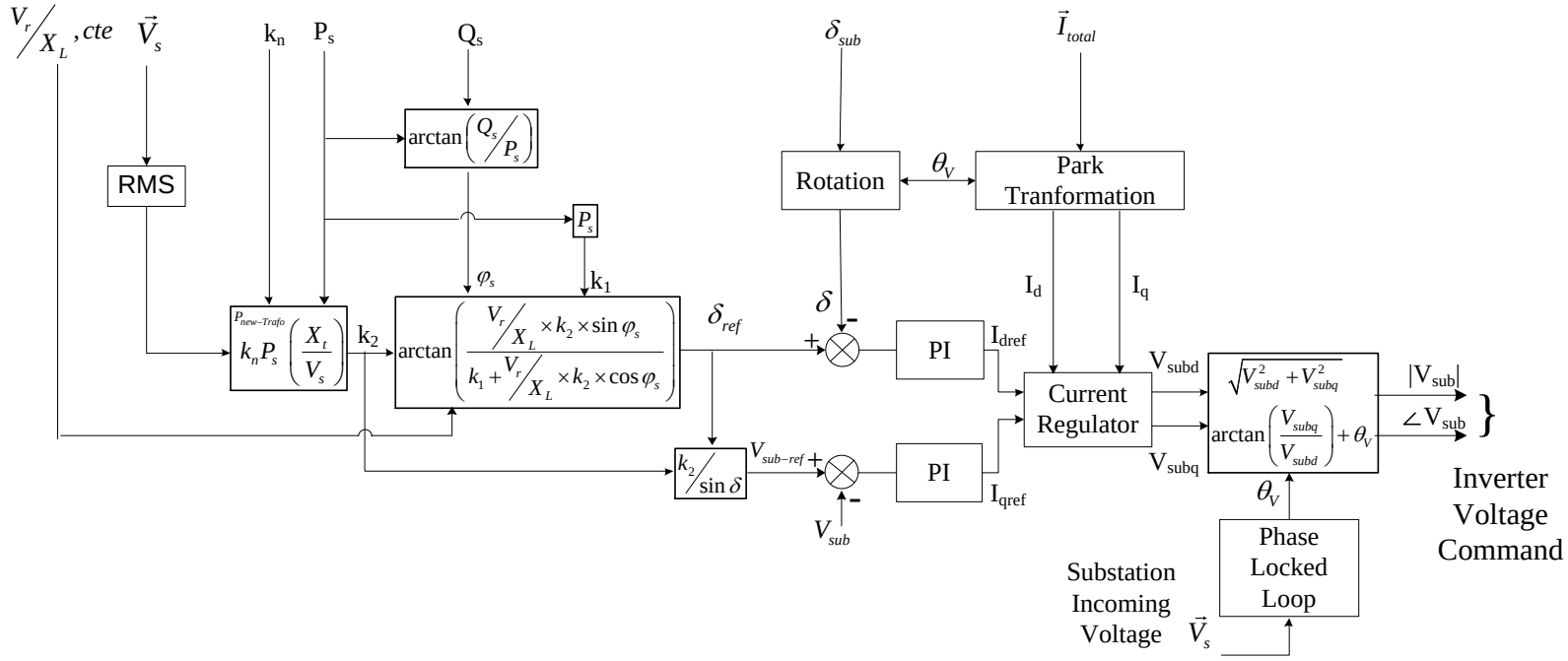

Figure 4-53. Proposed control structure of the CSTC in the shunt-shunt mode of operation as a substation voltage/phase angle regulator.

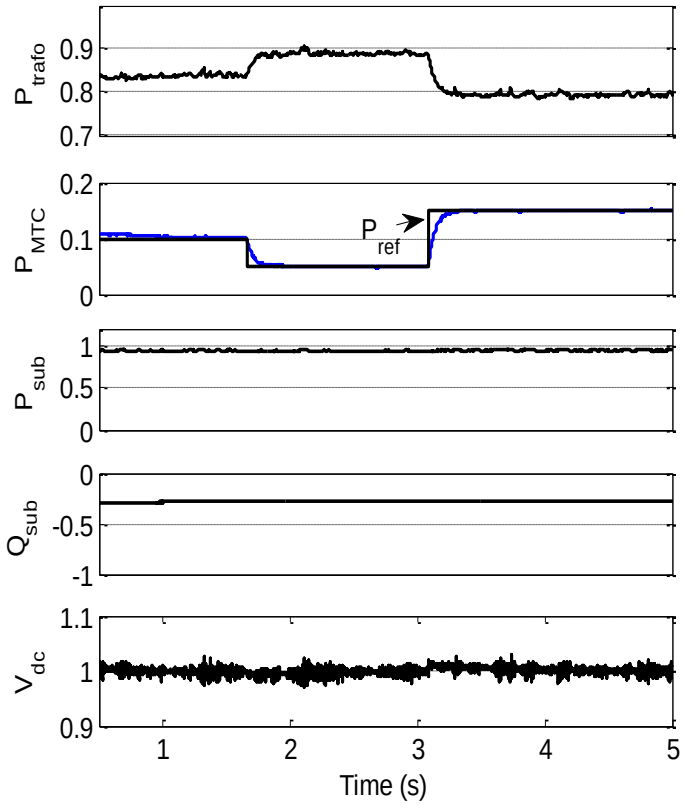

Figure 4-54. PSCAD simulation results in per unit for the shunt-shunt mode of operation for transformer partial bypass or power flow control without changing the power system power flow shown in Figure 4-39.

4.5.2 **Series-Shunt Connecting Configuration – Substation Power Flow Controller**

Figure 4-55 presents the PSCAD/EMTDC simulation results of the MTC-based CSTC system as the substation power flow controller in the series-shunt mode of operation. The series converter is used to control active power flow and reactive power flow through the transformer, and the shunt converter maintains the bus voltage magnitude at the desired value by injecting or absorbing reactive power. The control structure in this mode is similar to the

one used in conventional UPFCs as presented in 86. It should be mentioned that this mode of operation can be well adapted to a hybrid controller structure where one converter in the MTC system operates at line frequency with enhanced THD and efficiency as explained in Figure 4-46.

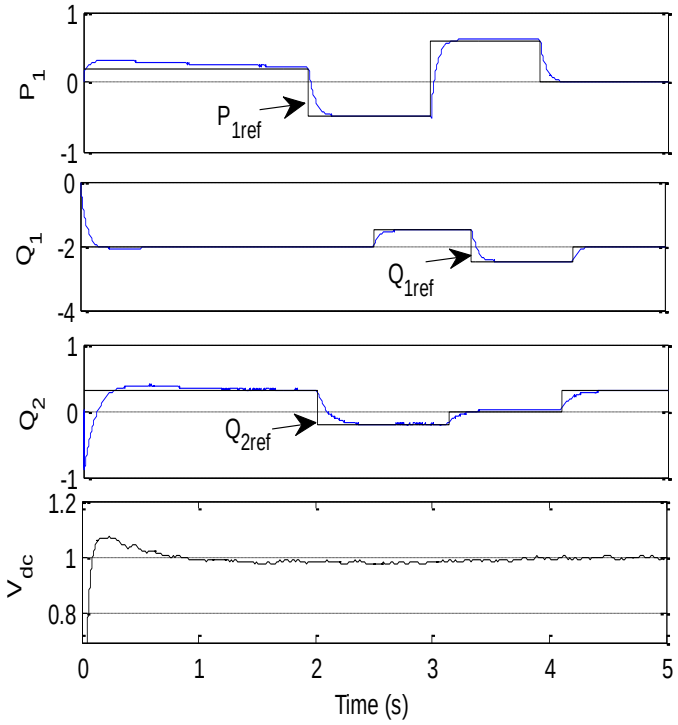

Figure 4-55. PSCAD simulation results in per unit for the CSTC series-shunt mode of operation in the test system shown in Figure 4-39.

4.5.3 Series-Series Connecting Configuration – Substation Power Flow Controller

This configuration is similar to the series-shunt configuration in terms of control objectives. The presence of the transformer, make it possible to connect two series converters to the line which is quite unique in the FACTS devices and is called DSSC (Dual Series

Static Compensator). In this mode of operation, active power and reactive power through the transformer can be controlled independently. The proposed control philosophy is that one converter regulates the DC bus voltage. The governing relationships to construct the control structures have been derived in (4.11)-(4.13).

The DSSC controllers belong to the family of dq-synchronous frame controls; however, unlike in conventional methods, they are synchronized with the line current rather than the bus voltage. In other words, the phase A current is always aligned with the d-axis. The significance of this work is to have inherently decoupled control of active and reactive power as can be seen in (4.11) and (4.12). Due to the changing nature of the line current, a proper control mechanism should be achieved through adaptive gain or feedforward control approaches.

$$P_s = \frac{3}{2}\left(V_{sd} I_d + V_{pq1d} I_d - V_{pq2d} I_d\right) + P_{loss} \tag{4.11}$$

$$Q_s = \frac{-3}{2}\left(V_{sq} I_d + V_{pq1q} I_d - V_{pq2q} I_d\right) \tag{4.12}$$

$$\frac{dV_{DC}^2}{dt} = \frac{3}{C_{DC}}\left(V_{pq1d} I_d + V_{pq2d} I_d\right) - \frac{2V_{DC}^2}{R_p C_{DC}} \tag{4.13}$$

Since no literature, to the best knowledge of the author, is available for the control structure based on line current PLL, the basic equations, transfer functions and their bode plot representations are presented with specific attention to DSSC dynamics.

The small-signal state-space representation of the DSSC can be written as in (4.14). It is obvious in the proposed current-based PLL that no I_q term exists.

$$\frac{\partial}{\partial t}\begin{bmatrix} i_d \\ i_q \\ V^2_{DC} \end{bmatrix} = A\begin{bmatrix} i_d \\ i_q \\ V^2_{DC} \end{bmatrix} + B\begin{bmatrix} V_{1d} \\ V_{1q} \\ V_{2d} \\ V_{2q} \\ V_{sd} \\ V_{sq} \\ V_{rd} \\ V_{rq} \end{bmatrix} \tag{4.14}$$

$$\begin{bmatrix} P_s \\ Q_s \\ V^2_{DC} \end{bmatrix} = C\begin{bmatrix} i_d \\ i_q \\ V^2_{DC} \end{bmatrix} + D\begin{bmatrix} V_{1d} \\ V_{1q} \\ V_{2d} \\ V_{2q} \\ V_{sd} \\ V_{sq} \\ V_{rd} \\ V_{rq} \end{bmatrix} \tag{4.15}$$

where

$$A = \begin{bmatrix} -\frac{R_s}{L} & \omega & 0 \\ -\omega & -\frac{R_s}{L} & 0 \\ \frac{3}{C_{DC}}(V_{1d0} - V_{2d0}) & 0 & -\frac{2}{R_p C_{DC}} \end{bmatrix}$$

$$B = \begin{bmatrix} \frac{1}{L} & 0 & -\frac{1}{L} & 0 & \frac{1}{L} & 0 & -\frac{1}{L} & 0 \\ 0 & \frac{1}{L} & 0 & -\frac{1}{L} & 0 & \frac{1}{L} & 0 & -\frac{1}{L} \\ \frac{3I_{d0}}{C_{DC}} & 0 & -\frac{3I_{d0}}{C_{DC}} & 0 & 0 & 0 & 0 & 0 \end{bmatrix}$$

$$C = \begin{bmatrix} 1.5(V_{sd0} + V_{1d0} - V_{2d0}) & 0 & 0 \\ -1.5(V_{sq0} + V_{1q0} - V_{2q0}) & 0 & 0 \\ 0 & 0 & 1 \end{bmatrix}$$

$$D = \begin{bmatrix} \frac{3I_{d0}}{2} & 0 & -\frac{3I_{d0}}{2} & 0 & \frac{3I_{d0}}{2} & 0 & 0 & 0 \\ 0 & -\frac{3I_{d0}}{2} & 0 & \frac{3I_{d0}}{2} & 0 & -\frac{3I_{d0}}{2} & 0 & 0 \\ 0 & 0 & 0 & 0 & 0 & 0 & 0 & 0 \end{bmatrix}.$$

Developing the state-space representation of the DSSC, we can now derive different transfer functions which are presented in (4.16)-(4.27). Variable current because of different power requirements is apparent in the transfer functions and should be taken into account.

$$\frac{\Delta P_s(s)}{\Delta V_{1d}(s)} = \frac{3I_{d0}}{2} + \frac{(R_s + Ls)(\frac{3V_{1d0}}{2} - \frac{3V_{2d0}}{2} + \frac{3V_{sd0}}{2})}{L^2 s^2 + 2LR_s s + \omega^2 L^2 + R_s{}^2} \tag{4.16}$$

$$\frac{\Delta P_s(s)}{\Delta V_{1q}(s)} = \frac{\omega L(3V_{1d0} - 3V_{2d0} + 3V_{sd0})}{2(L^2 s^2 + 2LR_s s + \omega^2 L^2 + R_s{}^2)} \tag{4.17}$$

$$\frac{\Delta P_s(s)}{\Delta V_{2d}(s)} = -\frac{3I_{d0}}{2} - \frac{(R_s + Ls)(\frac{3V_{1d0}}{2} - \frac{3V_{2d0}}{2} + \frac{3V_{sd0}}{2})}{L^2 s^2 + 2LR_s s + \omega^2 L^2 + R_s{}^2} \tag{4.18}$$

$$\frac{\Delta P_s(s)}{\Delta V_{2q}(s)} = -\frac{\omega L(3V_{1d0} - 3V_{2d0} + 3V_{sd0})}{2(L^2 s^2 + 2LR_s s + \omega^2 L^2 + R_s{}^2)} \tag{4.19}$$

$$\frac{\Delta Q_s(s)}{\Delta V_{1d}(s)} = -\frac{(R_s + Ls)(\frac{3V_{1q0}}{2} - \frac{3V_{2q0}}{2} + \frac{3V_{sq0}}{2})}{L^2 s^2 + 2LR_s s + \omega^2 L^2 + R_s{}^2} \tag{4.20}$$

$$\frac{\Delta Q_s(s)}{\Delta V_{1q}(s)} = -\frac{3I_{d0}}{2} - \frac{\omega L(\frac{3V_{1q0}}{2} - \frac{3V_{2q0}}{2} + \frac{3V_{sq0}}{2})}{L^2 s^2 + 2LR_s s + \omega^2 L^2 + R_s{}^2} \tag{4.21}$$

$$\frac{\Delta Q_s(s)}{\Delta V_{2d}(s)} = \frac{(R_s + Ls)(\frac{3V_{1q0}}{2} - \frac{3V_{2q0}}{2} + \frac{3V_{sq0}}{2})}{L^2 s^2 + 2LR_s s + \omega^2 L^2 + R_s{}^2} \tag{4.22}$$

$$\frac{\Delta Q_s(s)}{\Delta V_{2q}(s)} = \frac{3I_{d0}}{2} + \frac{\omega L(\frac{3V_{1q0}}{2} - \frac{3V_{2q0}}{2} + \frac{3V_{sq0}}{2})}{L^2 s^2 + 2LR_s s + \omega^2 L^2 + R_s{}^2} \tag{4.23}$$

$$\frac{\Delta V_{dc}(s)}{\Delta V_{1d}(s)} = \frac{3I_{d0}R_p}{C_{DC}R_p s + 2} + \frac{3R_p(R_s + Ls)(V_{1d0} - V_{2d0})}{(C_{DC}R_p s + 2)(L^2 s^2 + 2LR_s s + \omega^2 L^2 + R_s{}^2)} \tag{4.24}$$

$$\frac{\Delta V_{dc}^2(s)}{\Delta V_{1q}(s)} = \frac{3R_p \omega L(V_{1d0} - V_{2d0})}{(C_{DC}R_p s + 2)(L^2 s^2 + 2LR_s s + \omega^2 L^2 + R_s{}^2)} \tag{4.25}$$

$$\frac{\Delta V_{dc}^2(s)}{\Delta V_{2d}(s)} = \frac{-3I_{d0}R_p}{C_{DC}R_p s + 2} - \frac{3R_p(R_s + Ls)(V_{1d0} - V_{2d0})}{(C_{DC}R_p s + 2)(L^2 s^2 + 2LR_s s + \omega^2 L^2 + R_s{}^2)} \tag{4.26}$$

$$\frac{\Delta V_{dc}^2(s)}{\Delta V_{2q}(s)} = -\frac{3R_p \omega L(V_{1d0} - V_{2d0})}{(C_{DC}R_p s + 2)(L^2 s^2 + 2LR_s s + \omega^2 L^2 + R_s{}^2)} \tag{4.27}$$

A DSSC open loop Bode plot represents the system outputs; active power, reactive power, and DC link voltage for three different cases are plotted as follows:

1. High line current, high active power and low reactive power, Figure 4-56 and Figure 4-57
2. Low line current, low active power, and low reactive power, Figure 4-58 and Figure 4-59
3. High line current, high active power and high reactive power, Figure 4-60 and Figure 4-61

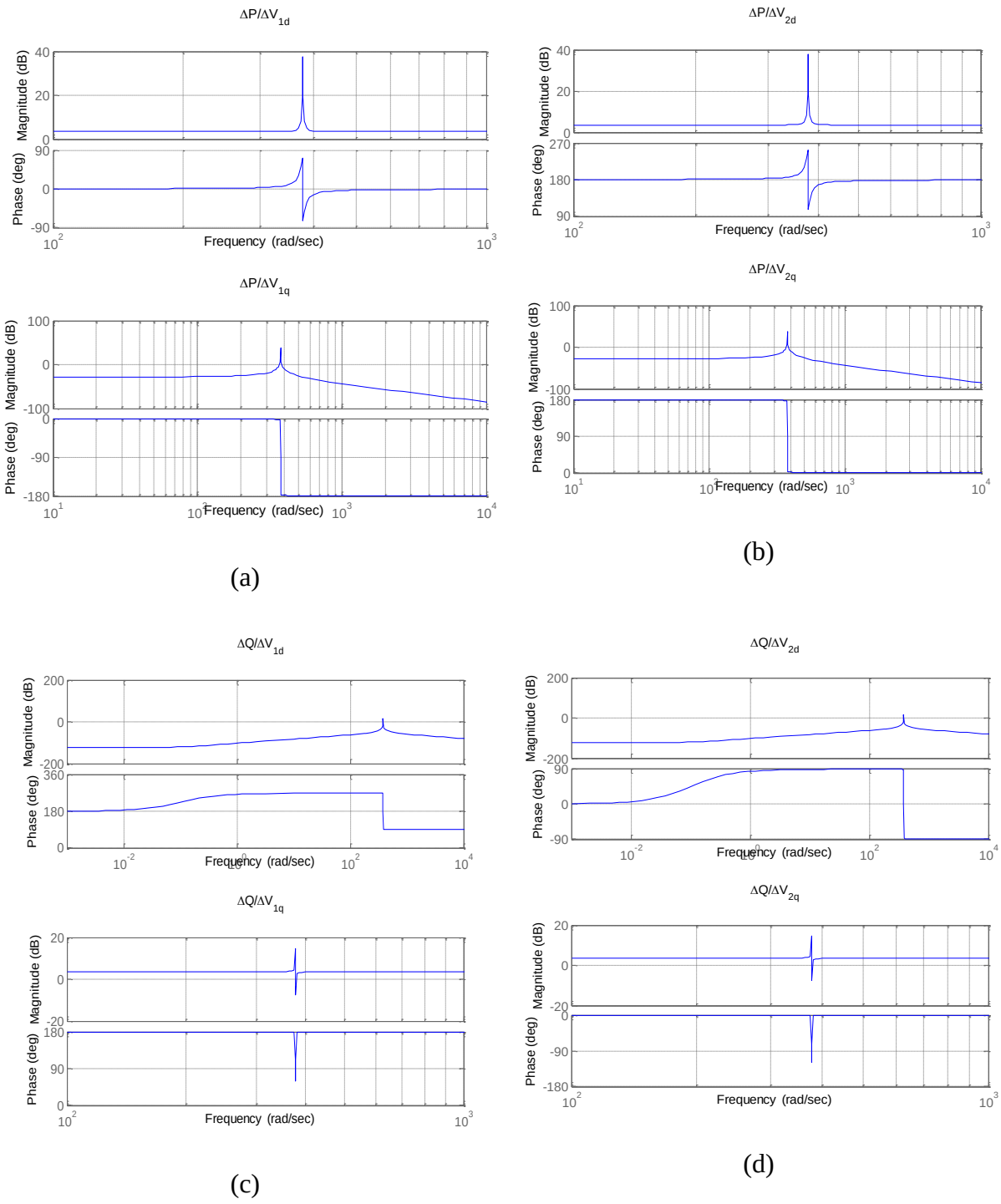

Figure 4-56.Active and reactive power Bode plot representation of the DSSC with operating points of P=1.0024, Q=0.02, and Id0=1.0026 PU (High current, high active power, and low reactive power case).

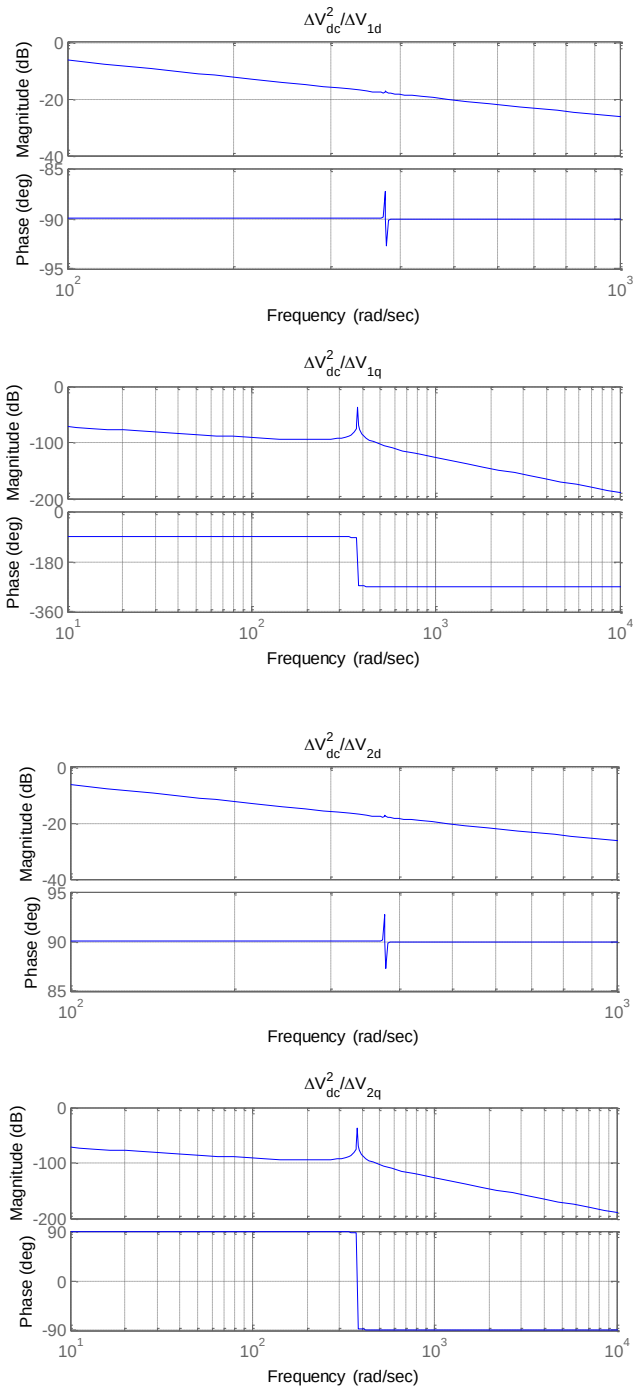

Figure 4-57. DC link voltage (V_{dc}^2) Bode plot representation of the DSSC with operating points of P=1.0024, Q=0.02, and Id0=1.0026 PU (High current, high active power, and low reactive power case).

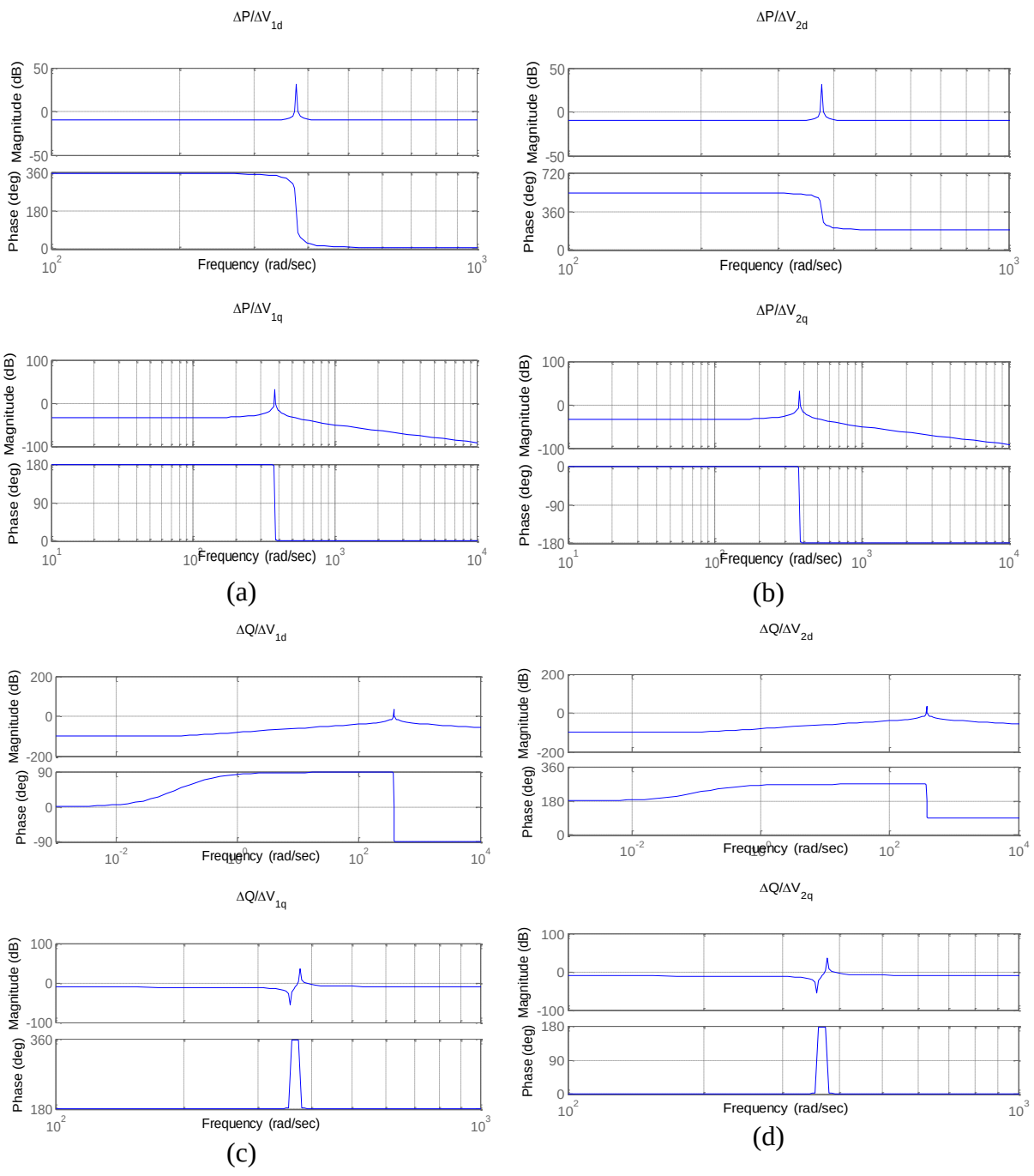

Figure 4-58.Active and reactive power Bode plot representation of the DSSC with operating points of P=-0.0912, Q=-0.1986, Id0=0.2186 PU (Low current, low active power, and low reactive power case).

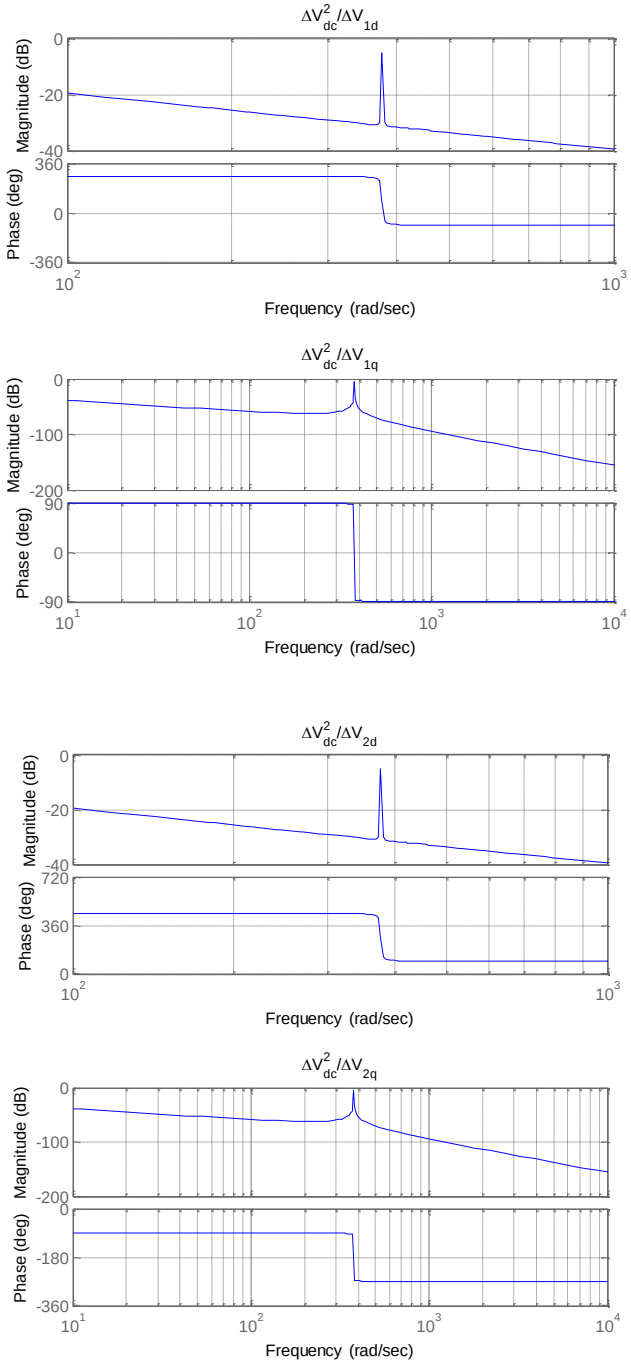

Figure 4-59. DC link voltage (V_{dc}^2) Bode plot representation of the DSSC with operating points of P=-0.0912, Q=-0.1986, Id0=0.2186 PU (Low current, low active power, and low reactive power case).

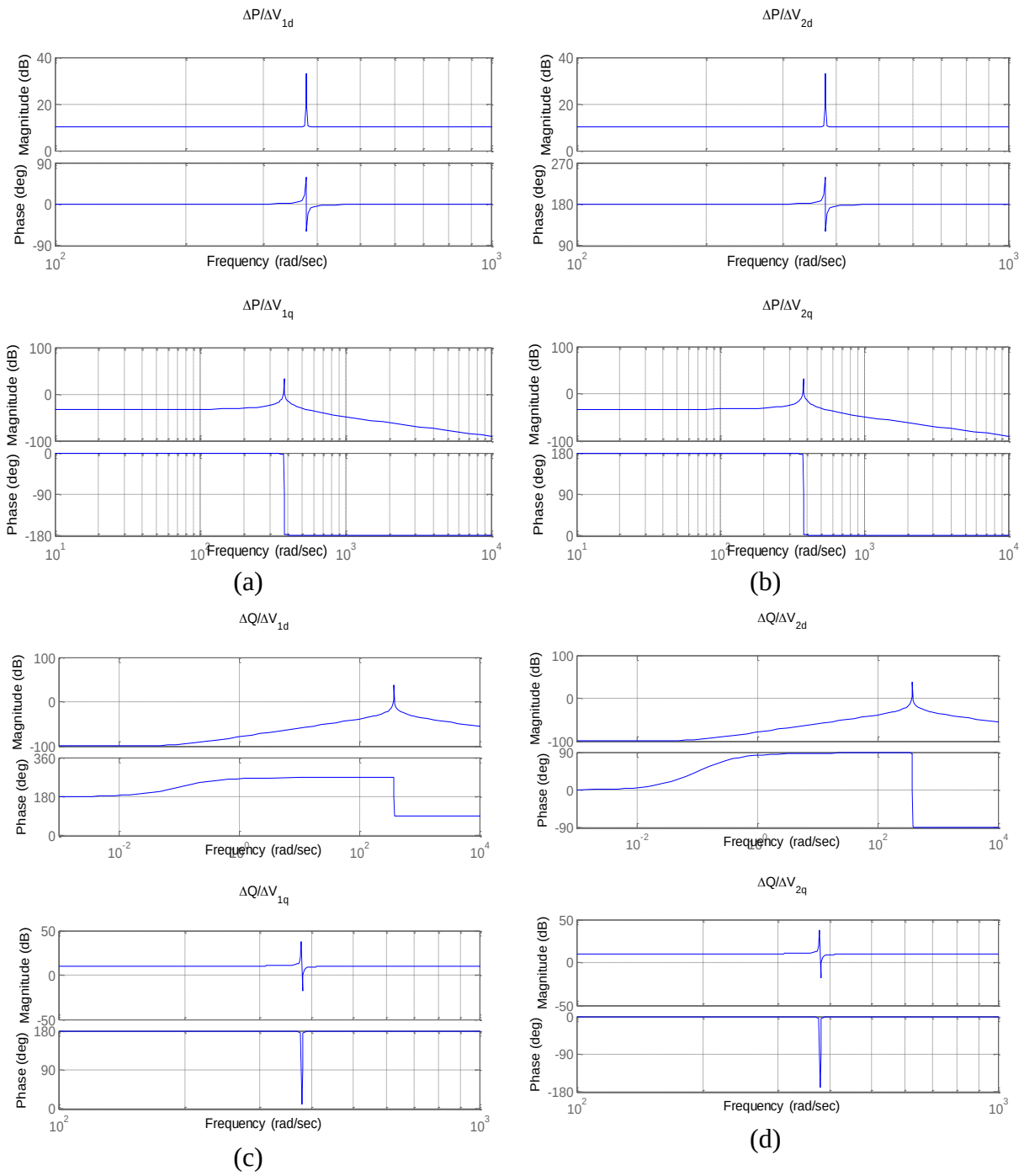

Figure 4-60.Active and reactive power Bode plot representation of the DSSC with operating points of P=1.0925, Q=1.8177, Id0=2.1208 PU (High current, high active power, and high reactive power case).

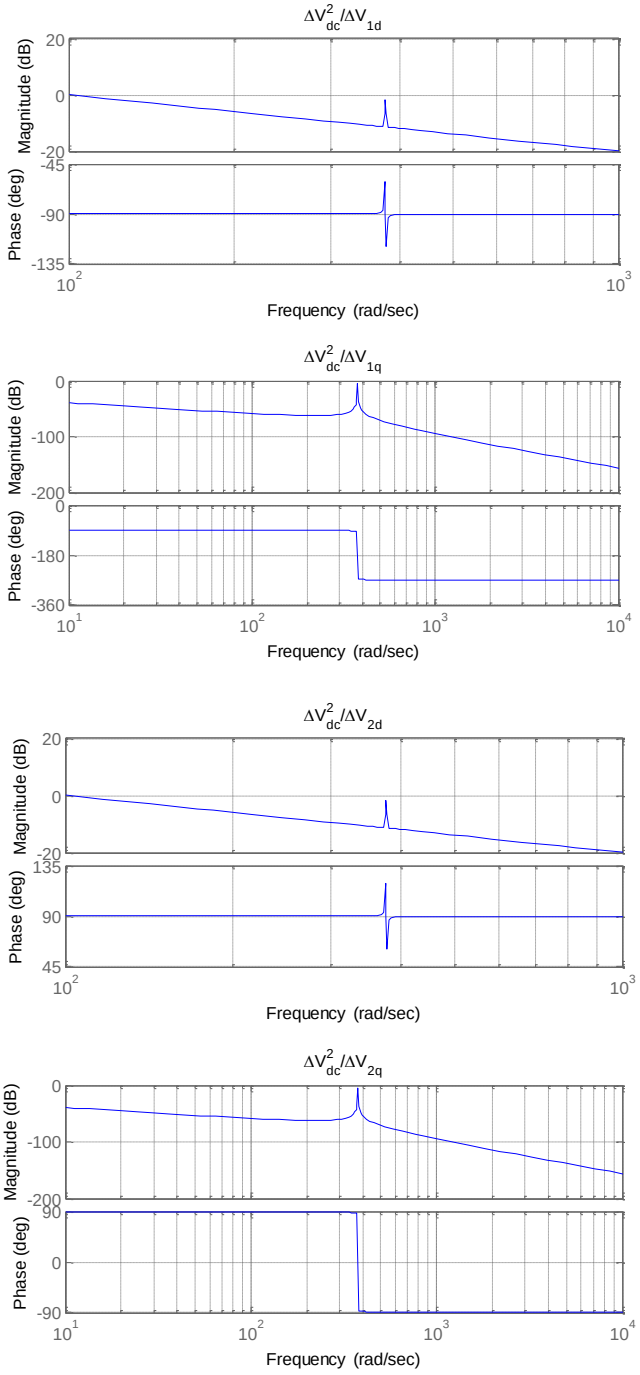

Figure 4-61. DC link voltage (V_{dc}^2) Bode plot representation of the DSSC with operating points of P=1.0925, Q=1.8177, Id0=2.1208 PU (High current, high active power, and high reactive power case).

From the Bode plot analysis of the DSSC in different cases, it was concluded that the DSSC dynamics are amendable to linear feedback control. The proposed control structures for DSSC converters based on line current PLL are presented in Figure 4-62 and Figure 4-63. Another important feature of the proposed controller is the substation reactive power control for which the required power is equally distributed between the two inverters without any controller fight. This requirement is obtained by measuring the respective voltage vector of inverter one (in this case the power flow controller inverter) and inserting it as the reference for the other inverter as shown in Figure 4-63.

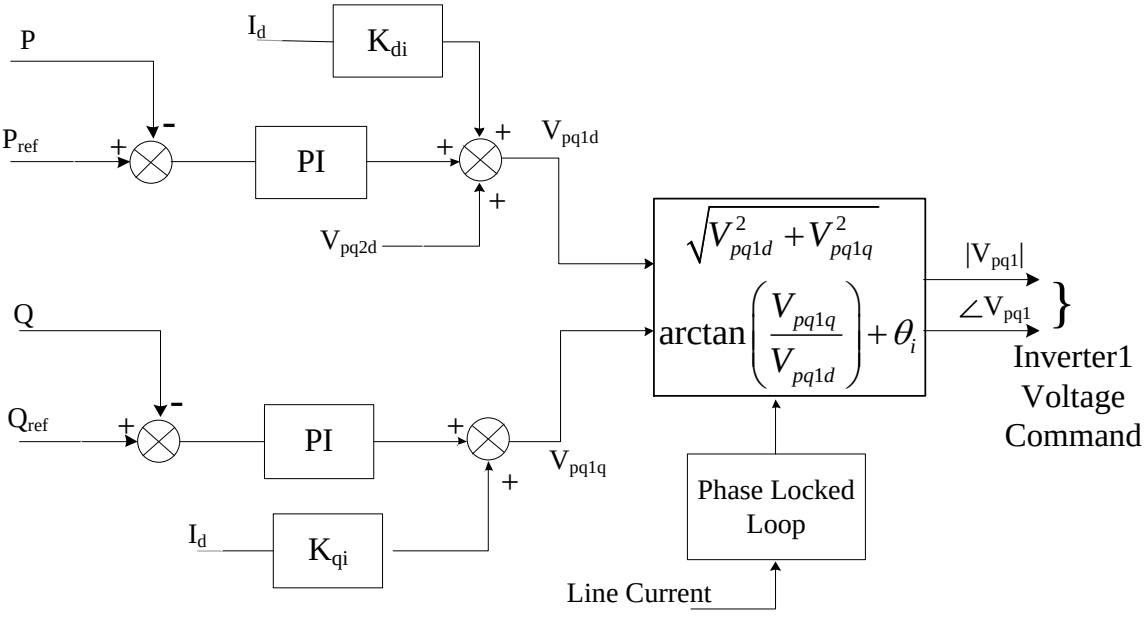

Figure 4-62. Power flow controller inverter control structure of DSSC.

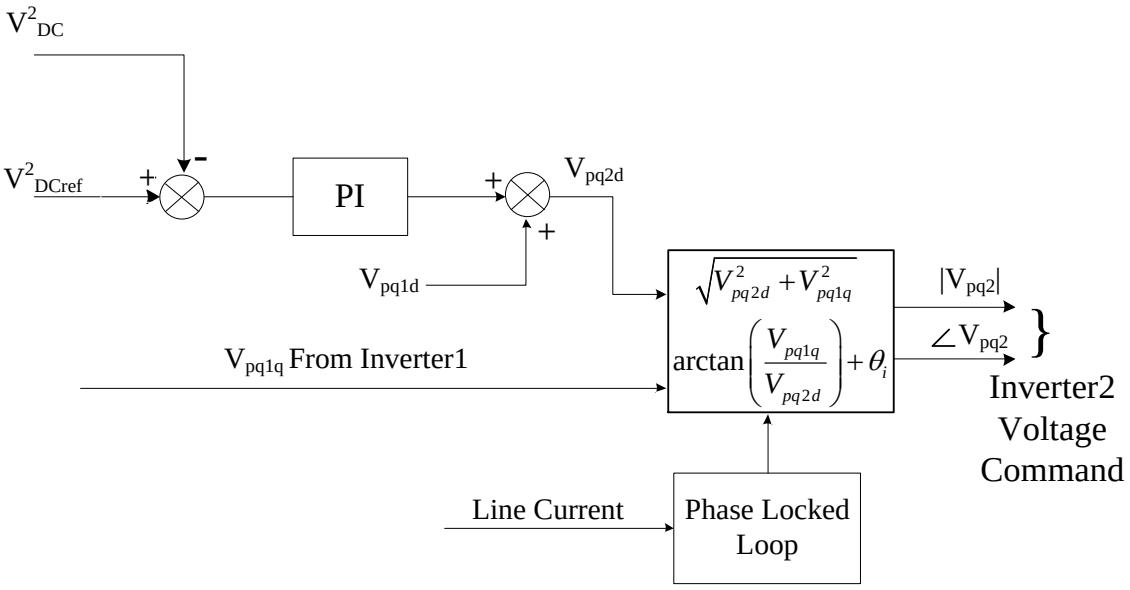

Figure 4-63. DC link controller inverter control structure of DSSC.

A DSSC EMTDC-based simulation has been carried out to verify the control structure under two different natural power flows denoted as low and high reactive power. Figure 4-64 and Figure 4-65 present the simulation results of the dynamics for DSSC under low reactive power flow. As can be seen, different active and reactive power can be controlled independently with insignificant coupling as expected, due to the proposed PLL based on the line current. A case with high natural reactive power is also tested to present the effectiveness of the DSSC compared to SSSC. The dynamics of the power flow control under high reactive power loading are presented in Figure 4-66-Figure 4-67. Control of active power is shown in Figure 4-66 and as can be seen, the active power can be controlled up to twice the natural power flow. The change of reactive power and its associated dynamics are shown in Figure 4-67 demonstrating the strength of DSSC compared to SSSC. Meanwhile, DSSC also

provides a wider active power control range than UPFC. The stiffness of the DC link voltage is also highlighted in this case.

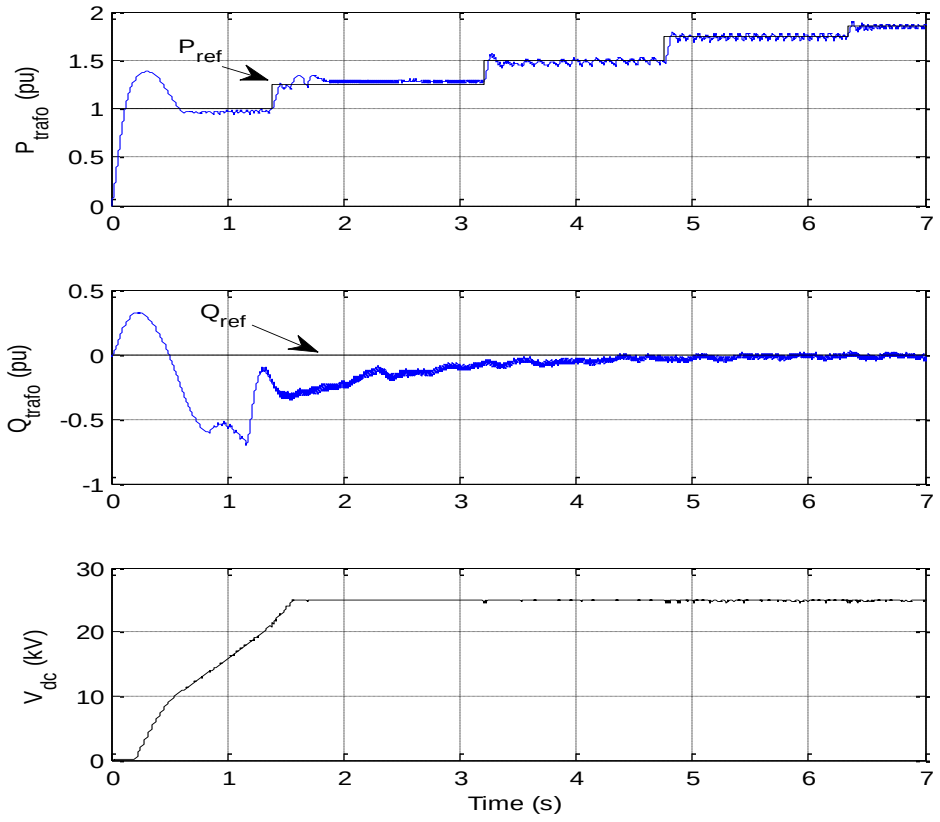

Figure 4-64. Dynamics of active power flow control in a DSSC under low reactive power loading.

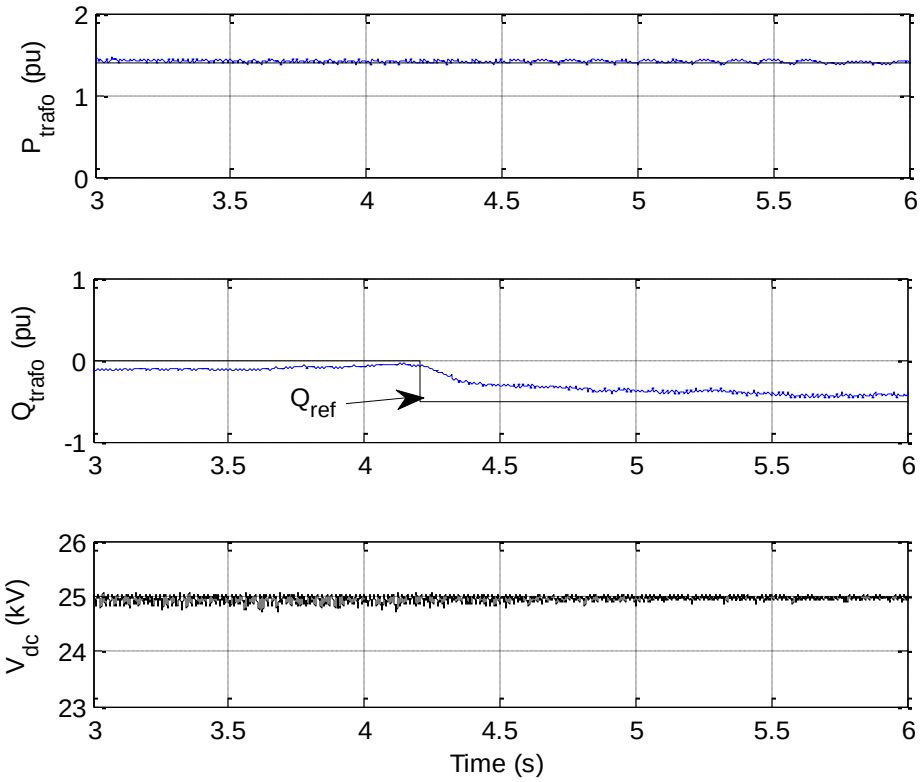

Figure 4-65. Dynamics of reactive power change in a DSSC under low reactive power loading.

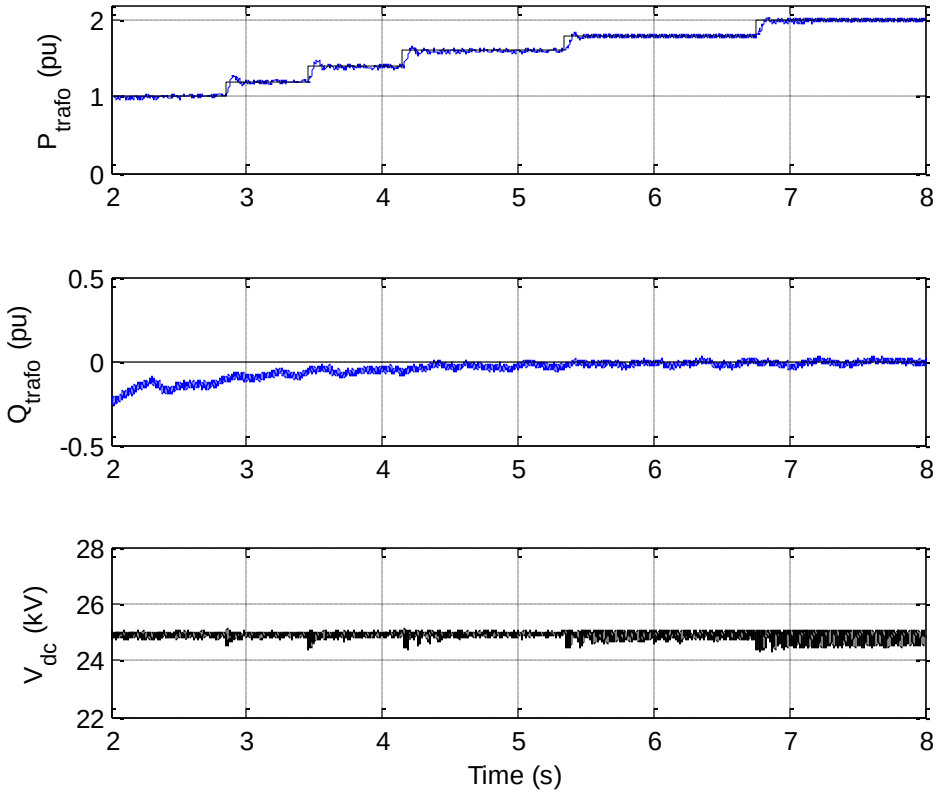

Figure 4-66. Dynamics of active power control in DSSC under high reactive power loading.

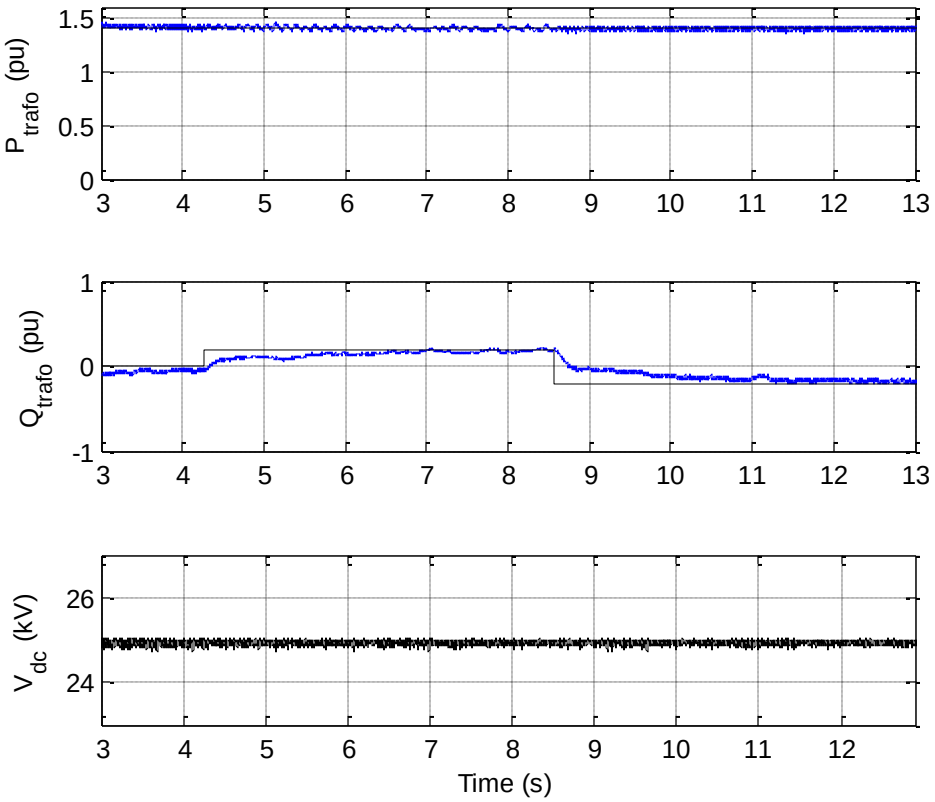

Figure 4-67. Dynamics of reactive power control in a DSSC under high reactive power loading.

4.6 **Summary**

Currently, transmission level power electronics use custom-designed converter structures to meet power system requirements including increased efficiency and a good harmonic spectrum. This requirement for the VSC technology typically requires an extensive engineering effort, which makes the power electronic solution costly and therefore precludes broad deployment of technology such as FACTS controllers.

This chapter proposed the concept of a Modular Transformer Converter (MTC) based on VSC technology to develop transmission level power electronic systems such as FACTS controllers. An MTC is a bidirectional AC/AC conversion unit that can be used as a standard drive converter with a much wider market, including sources such as the emerging 10MW wind generator drive system. The MTC concept has been initially perceived to reduce the cost of transmission level power electronics which can be retrofit into the AC network. As a consequence, utility-scale high power electronics may not require detailed custom power converter design and engineering and, system costs may benefit from the economies of scale.

Through development of an MTC, this research identified and introduced several applications including the *Recovery Transformer*, *Transformer Life Extender*, *Re-locatable Transmission Controller,* and *Seasonally Renewable Transmission Controller*. In fact, the MTC approach enables a versatile transmission controller, Convertible Static Transmission Controller (CSTC). Existing FACTS solutions enable dynamic control for the transmission lines; however, the MTC-based CSTC concept provides the flexibility of full or partial utilization for transmission lines and power transformers. This flexibility effectively increases the system's spare capacity and operating margins, and also provides back-up in case of power transformer failure (or forced reduced transformer rating operation) scenarios by providing real-time continuous power flow control and thereby, increased transfer capacity of existing transmission systems.

For transformer life extension or partial bypass purposes, the CSTC operates as the substation voltage/phase angle regulator which is different from conventional BTB HVDC applications. The proposed function enables the *locally controlled* CSTC which does not

complicate power system operation and can be utilized to inspire an active mobile substation or recovery transformer.

For power flow control with specific attention to renewable generation transmission in the meshed network, less complex coordinated control can be obtained with the CSTC concept. This chapter therefore, introduced the Dual Series Static Controller (DSSC) as a new FACTS controller that provides significantly superior performance in terms of operating characteristics compared to conventional power flow controllers. This chapter also proposed a control structure to operate the DSSC. In particular, the control structure was implemented in the dq-synchronous fame which is locked to the current rather than the voltage. The significance of this change is to decouple the control of the active and reactive power.

Finally, it is believed that a 10 to 100 MVA MTC-based CSTC that can be retrofitted into existing transmission substations and transformers has a strong potential to improve the reliability, controllability and efficiency of the grid.

Chapter 5. SUPPLEMENTARY ENERGY STORAGE AND ADVANCED ARCHITECTURES FOR GRID-CONNECTED HIGH POWER AC MULTI-MOTOR APPLICATIONS

5.1 Introduction

All-AC gearless drive systems have become popular in the mining industry because they increase the production rate of mines by almost 20% compared to DC drives. To supply the AC drive systems several Active Front Ends (AFE) with DC choppers are used to ensure a reliable and acceptable harmonic spectrum operation. Recently, integration of the energy storage system with the mining equipment has attracted attention from the industry especially for peak load shaving and smarter energy management of the mine. The energy storage system can capture the regenerative energy and reuse it for the motoring operation of the drive. However, the regenerative energy is currently either burnt into the choppers or fed back to the grid without billing for the reverse power. The industry is motivated since this regenerative power can be as high as 60% of the motoring power which is as high as 24 MW. Therefore, there is a possibility of cost reduction and component downsizing. However, the present status of development does not seem to be very promising mainly because energy storage systems, here ultracapacitor are still considered to be add-on parts to the existing products. In this chapter, we propose a new yet straightforward configuration for

development of the all-AC gearless mining equipment that has encouraging incentives for both the manufacturer and the mine operator.

Figure 5-1. 24MW AC-drive dragline in an open-pit mine, 89.

In addition, this chapter provides a methodology for comparing different energy storage technologies. There are different battery technologies with different technical and economical characteristics. Therefore, how to choose a proper technology is not straightforward. In this research, potential energy storage systems are sought out for peak-shaving for mining converters based on the annuity method.

5.2 All-AC Drive System for High power Mobile Mining Applications

Surprisingly, it has not been very long since AC drive systems were developed for the nearly a century old electrified mining industry. A particular class of mining apparatus , excavation machines, is used for material removal in surface mining applications; these are

typically classified as shovels, bucket wheel excavators and draglines,. The objective of the mines is to achieve the movement of the highest possible payload per hour while minimizing operating costs over the lifetime of the machines. The AC drive system for mining applications could not have succeeded without showing this improved performance factor which translates to a higher production rate compared to traditional, well-understood DC alternative. In particular, this transition from a DC to an AC drive system has led to about a 20% increase in production rate, while the equipment efficiency rises to around 86-89% compared to 74% for a DC drive, 87. Figure 5-2 represents an AC-drive dragline deck plan. Currently, draglines of up to 24 MW are built and shovels are manufactured up to 3MW.

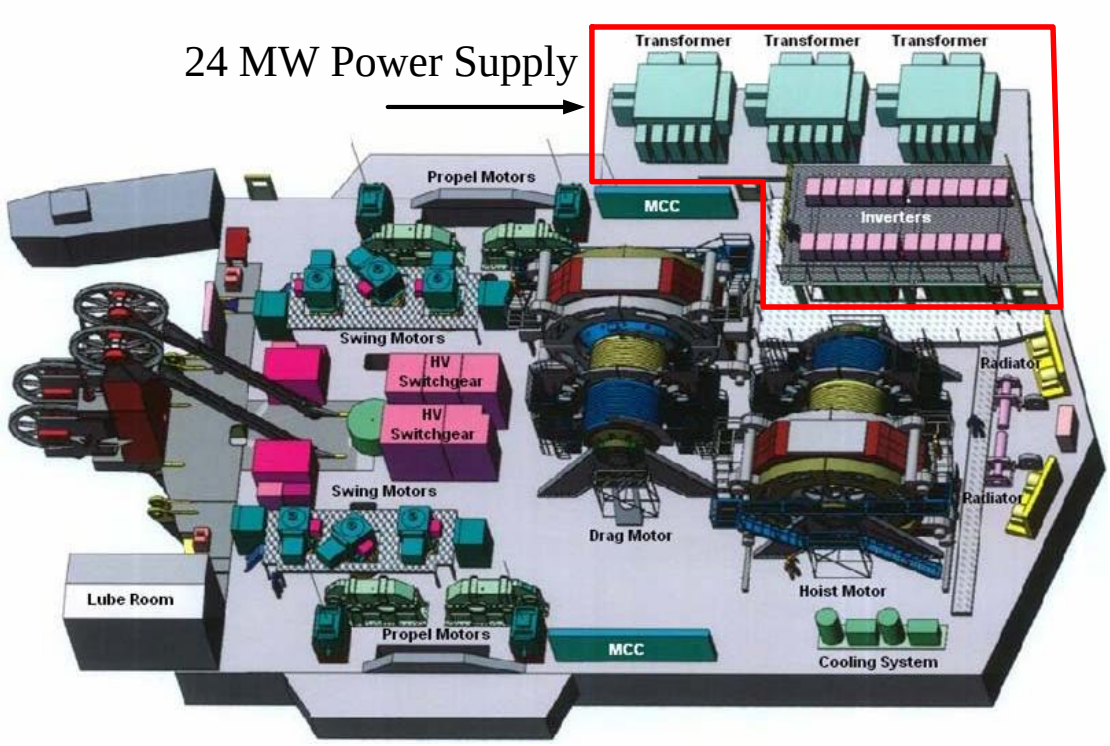

Figure 5-2. An example of a 24MW AC-drive dragline deck plan, 87.

5.3 **Front-End Converters for Mobile Mining Equipment**

Large mines are often located in areas with limited infrastructures, meaning that commercial or grid connected power is typically not available and mostly generated on site. Therefore, to comply with utility or on-site generation plant requirements especially with respect to harmonics, active front-end rectifiers have been chosen as the preferred front ends for mining converters, 90. However, the limited controller performance capability of the AFEs and the reliability requirements lead to an increased number of converters (there can be more than 40 AFEs in parallel) and the overdesign of each converter, 87. Figure 5-3 shows the electric circuit diagram where two or more AFEs are staggered to supply the AC drive system. On the other hand, there are sites where the regenerative power cannot be fed back to the mining distribution system, such as the Pribbenow mine located in Colombia S.A. with a generation capacity of 24MW, 92. The practical solution currently is simply to dissipate the excess energy into the resistive chopper banks to keep the DC link voltage of the AFEs within the acceptable range. It has also been observed that in electrical contracts with utilities this regenerative power does not reduce the energy bill. In all cases, this energy dissipation occurs in every load cycle, where the regenerated energy is sufficient to supply as much as 60% of the peak motoring power. Figure 5-4 presents a representative example of load cycles in two major motoring and regenerative regions of a typical operation window.

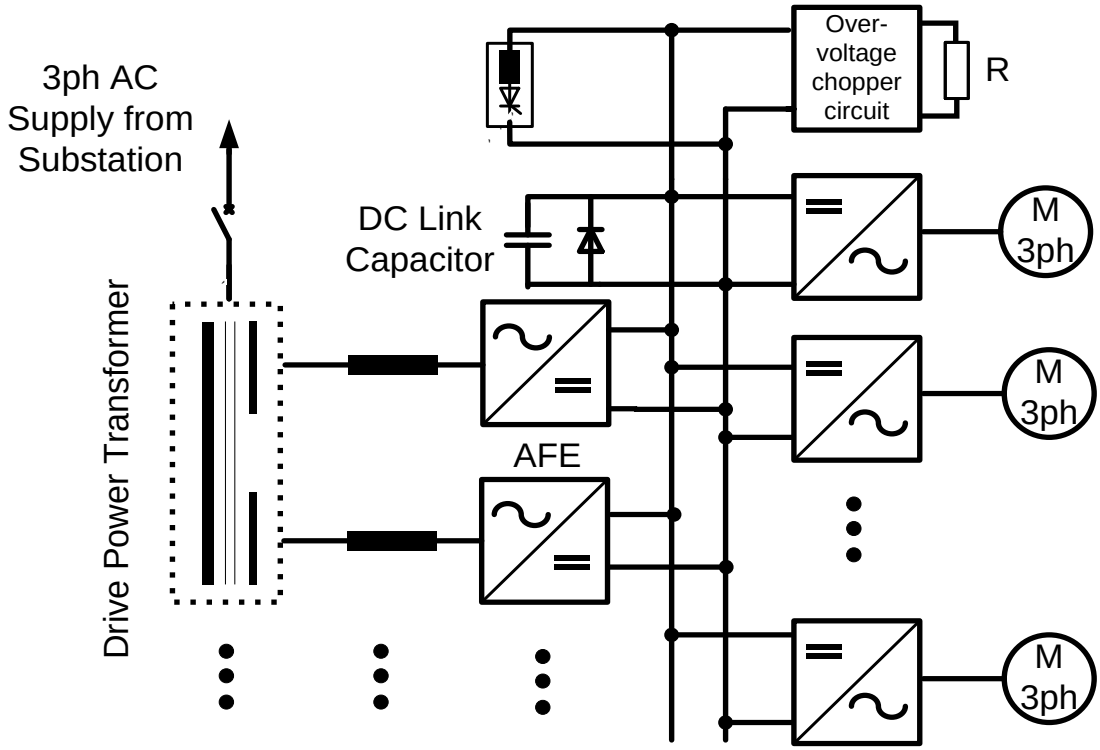

Figure 5-3. State-of-the-art high power AC drive system.

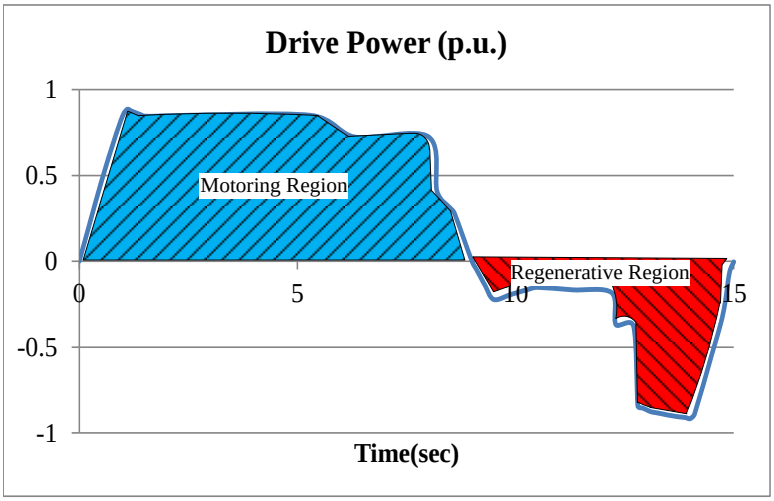

Figure 5-4. Example of a typical mining load profile.

5.4 The Current State-of-the-Art Active Front End Performance for Mobile Mining Equipment

Today mobile mining equipment, including shovels and draglines consists of several AFEs operating in parallel to ensure reliability, low current harmonic distortion, and the Var requirements of the mines. These AFEs are interfaced with several drive transformers to provide voltage matching, electrical isolation and current accumulation of the converters. The first is important since if AFEs are staggered with different switching angles, the current at the PCC becomes more sinusoidal. For instance, the PCC current for 32 staggered AFEs has a THD of less than 1% without using extra passive filtering. It is important that any improvement due to the topology or change in the controller must be benchmarked with the current state-of-the-art technology. In the following, a detailed analysis is presented of the dynamic performance of the AFE converters for mobile mining equipment.

One of the most important tasks of the front end converter system is to provide a stable and robust DC link voltage to the drive systems. The DC link in large multi-motor machines can be distributed among the front ends. The generalized DC link closed loop transfer function of the shovel systems including the controller is derived and presented in (1). This model is based on the linear derivation of the voltage source converter that has been introduced in Chapter 2; therefore, there is no need to have adaptation blocks for dynamic adjustments in the control structure. These adjustments are due to the non-linearity of the converter system. The details of this derivation are provided in 91 and the parameters are presented in Table I.

On the other hand, a varying load profile and the low switching frequency operation of the AFE side converters of mining AC drive systems prohibit the controller from having a high enough bandwidth to achieve the required response for the DC link voltage. Hence, an external compensator is considered and designed to reject disturbance. Here, the disturbance is the load power which is available for protection; therefore, the feed forward compensator with the required load as the input can be inserted into the voltage loop of the whole controller. The feedforward compensation term has been designed as in (2).

$$G_{V_{DC}^2}(s) = \frac{V_{DC}^2(s)}{V_{DCref}^2(s)} = \frac{\dfrac{3E_d K_{pV}}{C_{DC}\tau_i}}{s^2 + s/\tau_i + \dfrac{3E_d K_{pV}}{C_{DC}\tau_i}} \tag{5.1}$$

$$M(s) = \frac{2}{3E_d K_{pV}}\left(\frac{\tau_i s}{1+T_d s} + 1\right) \tag{5.2}$$

The current regulator is typically designed based on decoupled active and reactive power controls and behaves like a first order system. The current controller in mining applications is desired to have a response time in the range of 2 to 5 milliseconds. In addition to the PI controller, the current regulator nullifies the circulating current seen in parallel AFEs operating with different switching angles. The firing angles are preferably generated through the space vector PWM method. The simplified schematic of the implemented controller is presented in Figure 5-5. Detailed simulation studies have been conducted based on the parameters given in Table IV and the load profile shown in Figure 5-4. The simulation platform for the current study is the Matlab/Simulink SimPower package.

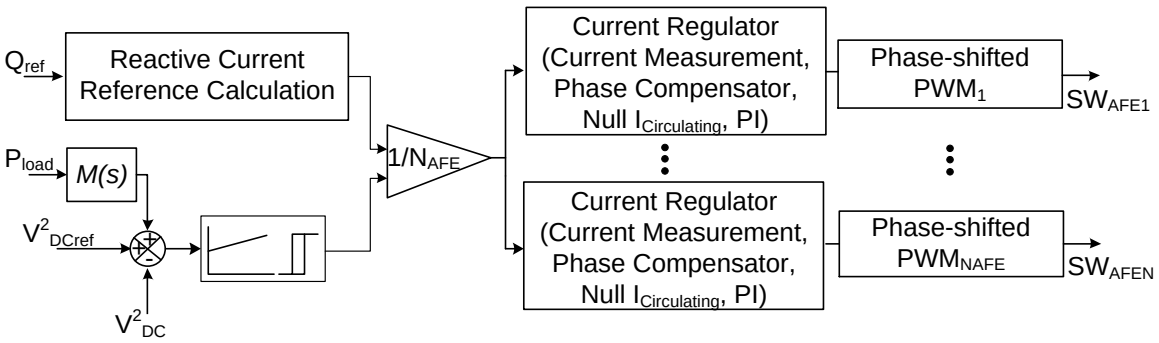

Figure 5-5. Simplified synchronous frame-based controller implementation for staggered Active Front Ends (AFE).

Table IV. High Power Mobile Mining System Parameters

Line-to-line voltage (AFE side)	E_d	900 V rms
Line frequency (grid)	f	60 Hz
Leakage inductance	L_s	16% PU
Interface resistance	R_s	0.4% PU
Each converter rated power	S_n	1 MVA
Number of AFEs	N_{AFE}	2, 4, 32
Nominal DC link voltage	V_{DC}	1.8 kV
Chopper circuit threshold	V_{ch}	2 kV
Crowbar circuit threshold	V_{cr}	2.2 kV
DC link capacitance	C_{DC}	12 mF
Required Ultracapacitance/300 kW	C_{Ucap}	1.5 F
Practical Ultracapacitance/300 kW	C_{Ucapp}	7.1 F
Switching frequency	f_s	540 Hz
Converter loss resistor (estimated)	R_p	1% PU
Absolute overcurrent capability	I_{max}	2 PU
Current regulator response time	τ_i	2~5 msec
Voltage loop proportional gain	K_{pV}	0.0014~ 0.00054
Time delay of the derivatives	T_d	0.1 ms
Controller sampling time	t_s	50 us

Figure 5-6 presents the simulation results for a 1.5MW shovel based on two staggered IGBT-based converters (IGBT 3.3kV, 1700A). The improved PCC currents in terms of harmonic distortions can be obtained through phase shifted PWM methods. In this

configuration the best performance is achieved with either 90° or 180° degree phase shift resulting in a THD of around 4.87% at nominal current. As mentioned earlier, no extra passive filtering is required. Nevertheless, three winding drive transformers are used in the shovel front end converters. These shovels are typically operated with unity power factor.

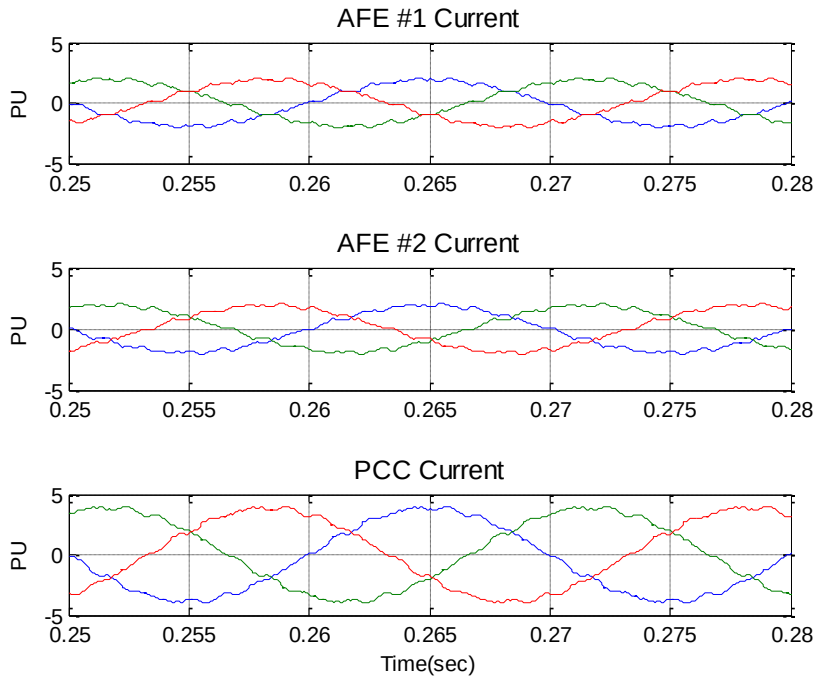

Figure 5-6. Simulated 1.5MW shovel currents with two staggered AFEs.

Figure 5-7 0presents the simulation results for a 3MW shovel based on four staggered active front ends. Due to more control over the phase shift angles, improved current waveforms are obtained in this shovel compared to the 1.5MW shovel. The staggering angle in the four AFE-based shovel is selected as 45° and two three-winding Dyy transformers are used.

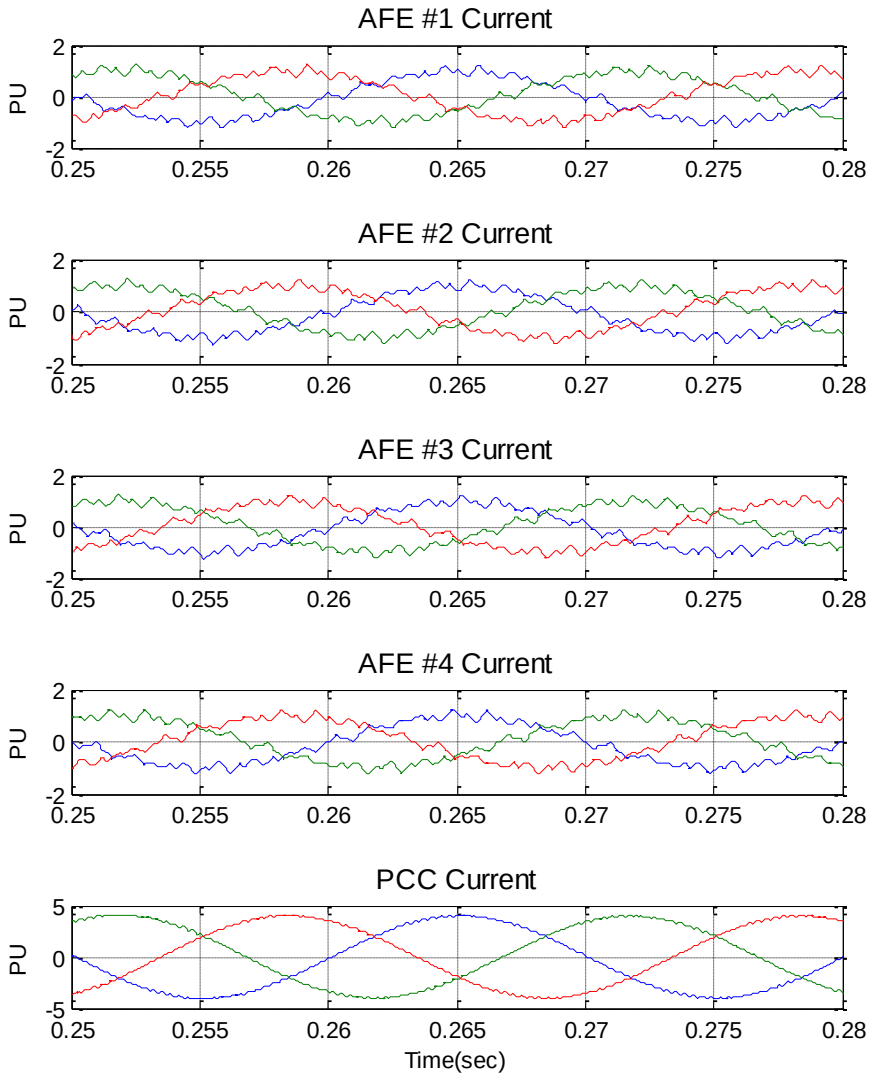

Figure 5-7. Simulated 3MW shovel currents with four staggered AFEs.

Draglines are the most complex and the most costly mobile equipment in the mines. Therefore, their reliability must be maintained with the highest priority. The draglines are currently manufactured up to 24MW with an AFE technology similar to what is are used in the shovels. To ensure reliability, the dragline can consist of 32 AFEs in addition to several

spare converters. In this study, a 32-AFE-based dragline with 8 split DC links is considered. One potential issue regarding the parallel AFEs with phase-shifted PWM and split DC link is emergence of circulating current among the converters and low order voltage harmonics in the DC voltages. To avoid these problems zero-sequence blocking control must be included in the current regulator of each AFE. In addition, draglines are required to provide a leading power factor (~2% PU VAR) while shovels operate with a unity power factor. Figure 5-8 presents the dragline operation performance showing almost sinusoidal PCC currents and eight DC link voltages. The staggering angle is chosen as 11.25° degrees resulting in a THD of less than 0.2% at the nominal current.

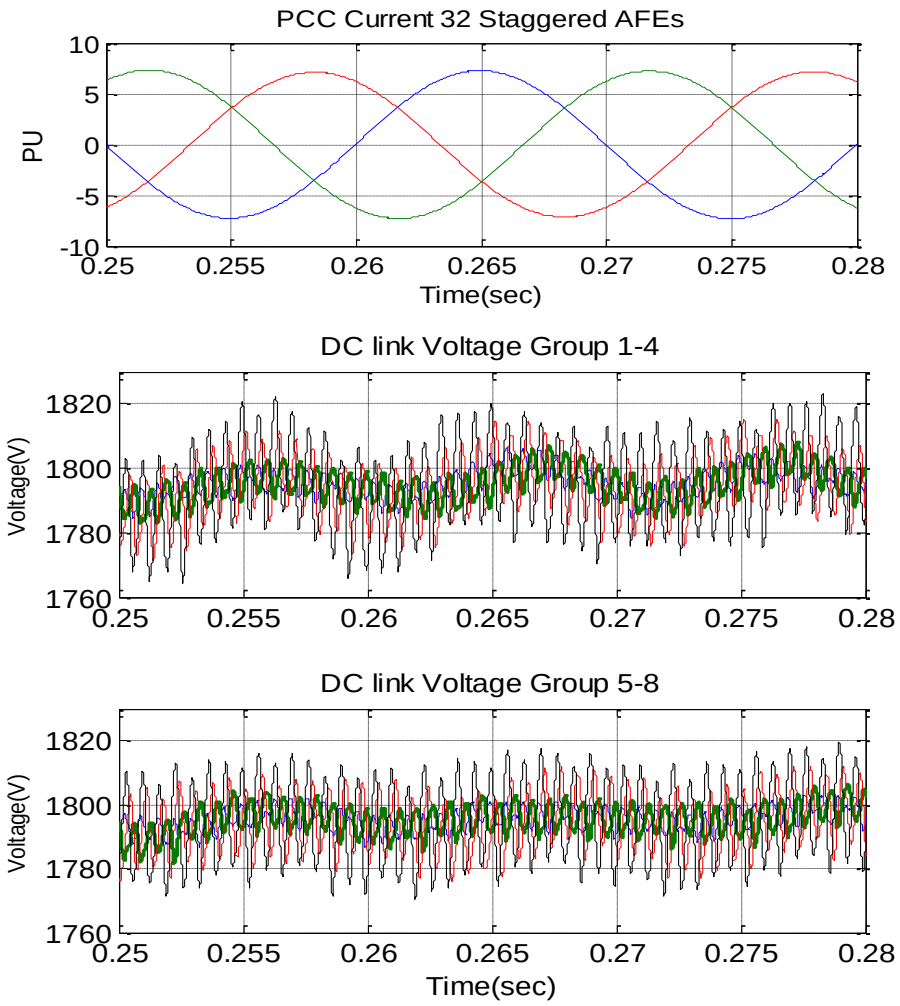

Figure 5-8. Simulated PCC currents in the 24MW dragline with 32 staggered (11.25° degree) AFEs and 8 split DC link voltages.

5.5 Supplementary Energy Storage System for Mobile Mining Equipment

5.5.1 Energy Storage Technology Selection

To solve the issues posed by the peak power demand or improve the performance and smart energy utilization and lessen dependency on fossil fuels, a peak shaving strategy is proposed in 91. The regenerated power produced by the excavator is stored in an energy

storage system and is used to reduce the peak demand of the drive system. Reduced peak demand not only reduces the energy costs but also provides a significant reduction in investment as the power rating of the system components can be reduced - applications for smaller machines such as wheel loaders are reported in 93. Energy storage systems have different characteristics and properties. Some comparative examples provided by the Electricity Storage Association (ESA), are presented in Figure 5-9-Figure 5-11. These make it difficult to apply one technology to every application including the mining ones. To choose the proper energy storage technology, several economic and technical criteria are considered, including weight, volume, and temperature.

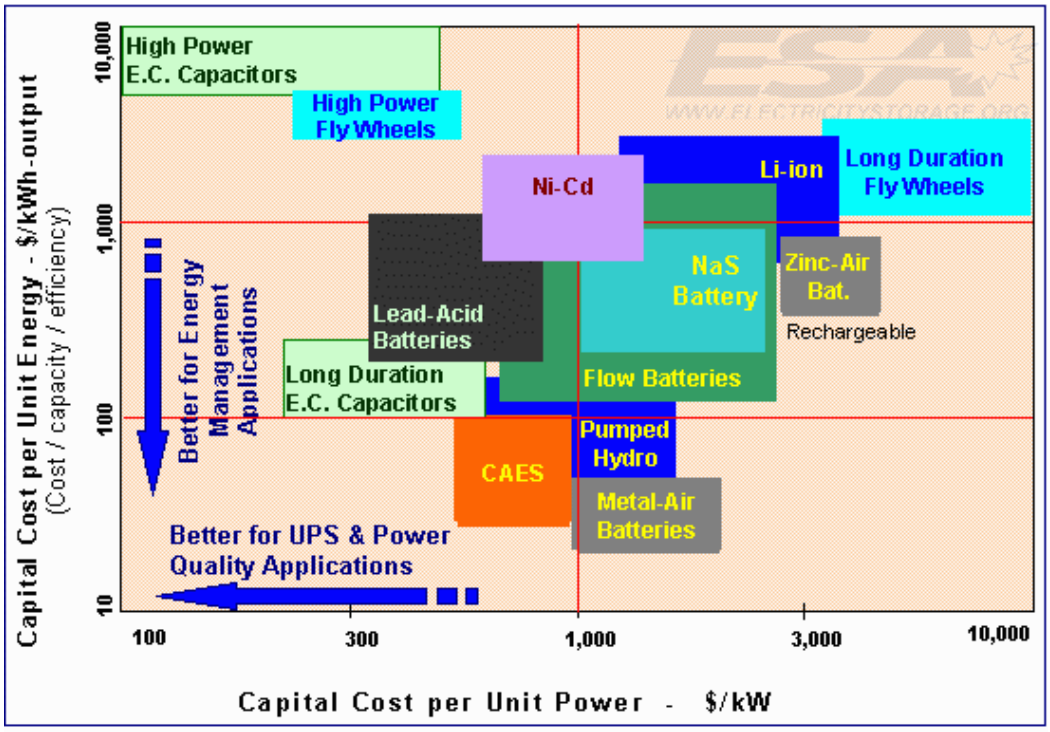

Figure 5-9. Capital cost comparison of selected energy storage technologies, 94.

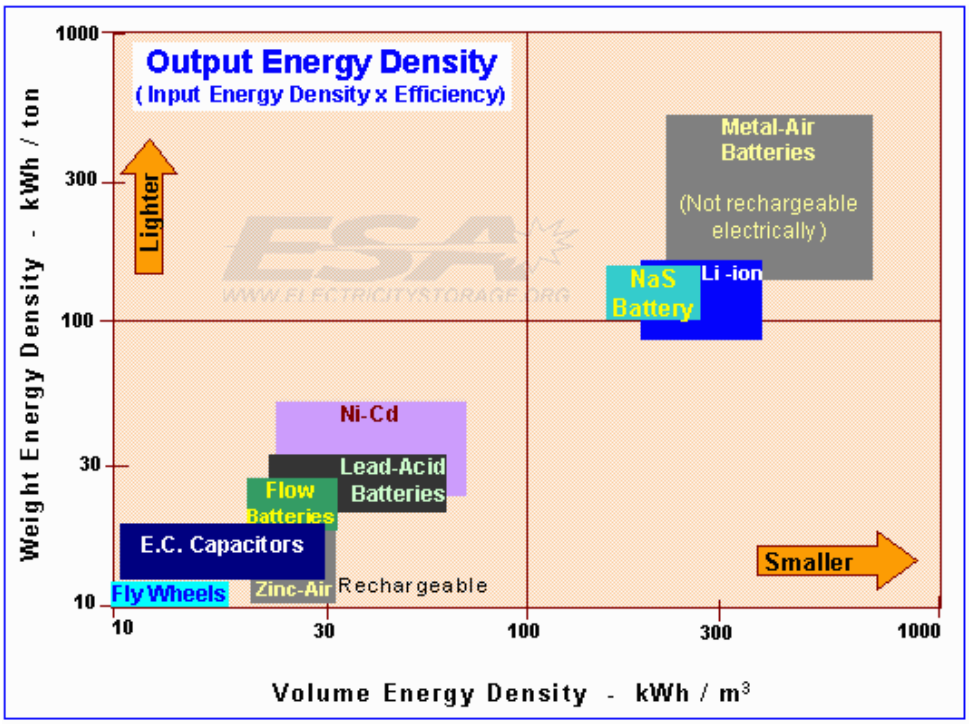

Figure 5-10. Energy density comparison of selected energy storage technologies, 94.

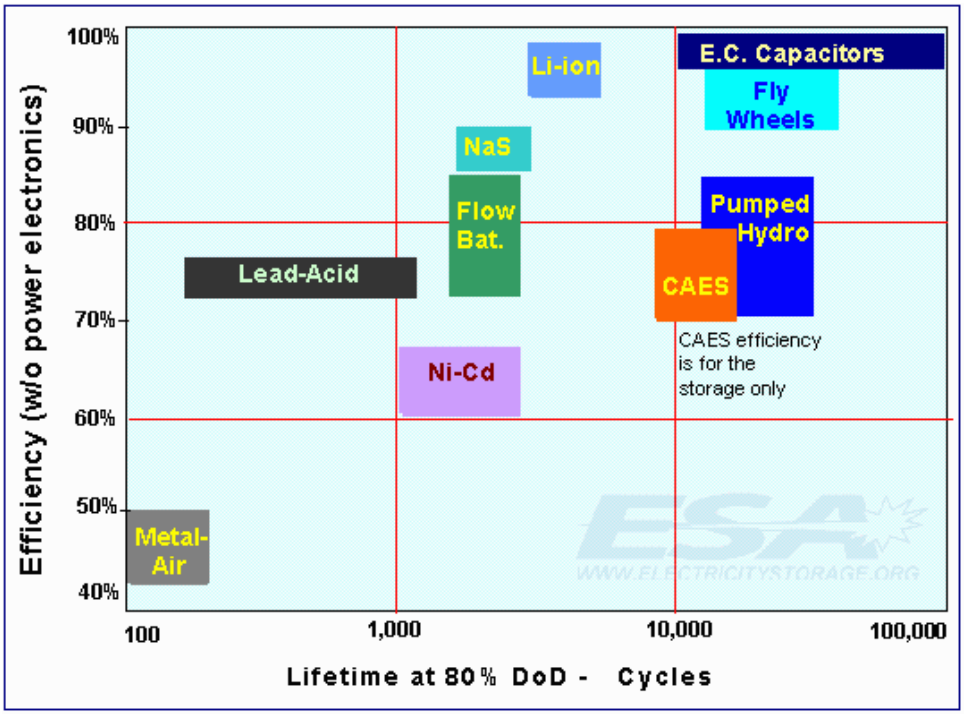

Figure 5-11. Efficiency comparison of selected energy storage technologies, 94.

5.5.2 **Energy Storage System Factors**

There are two primary criteria for identifying potential battery technologies.

1. Project requirements
2. Battery characteristics

Project requirements are those parameters that should be fulfilled with any type of battery. The following items are considered to be the project requirements:

- Power (kW)
- Energy (kWh)
- Voltage level (kV)
- Cycle (#/d)
- Life time (yr)
- Capital cost (%/yr)

Energy storage characteristics are those parameters that are unique for each battery technology and manufacturer. The following parameters are identified as the factors most affecting selection of the technology selection.

- Energy Price ($/kWh)
- Gravimetric energy density (Wh/kg)
- Volumetric energy density (Wh/L)
- Nominal cycles @ 80% DOD (#)
- Efficiency (%)
- Self-discharge (%/d)

- Maintenance (%/kW)

In addition to the battery characteristics, the power interface cost and its efficiency are considered -The interface should take care of the battery system conditions; therefore, each battery has custom designed power interface. Figure 5-12 summarizes the factors influencing battery comparison. The orange circles define the project requirements and the yellow ones shows the energy storage characteristics.

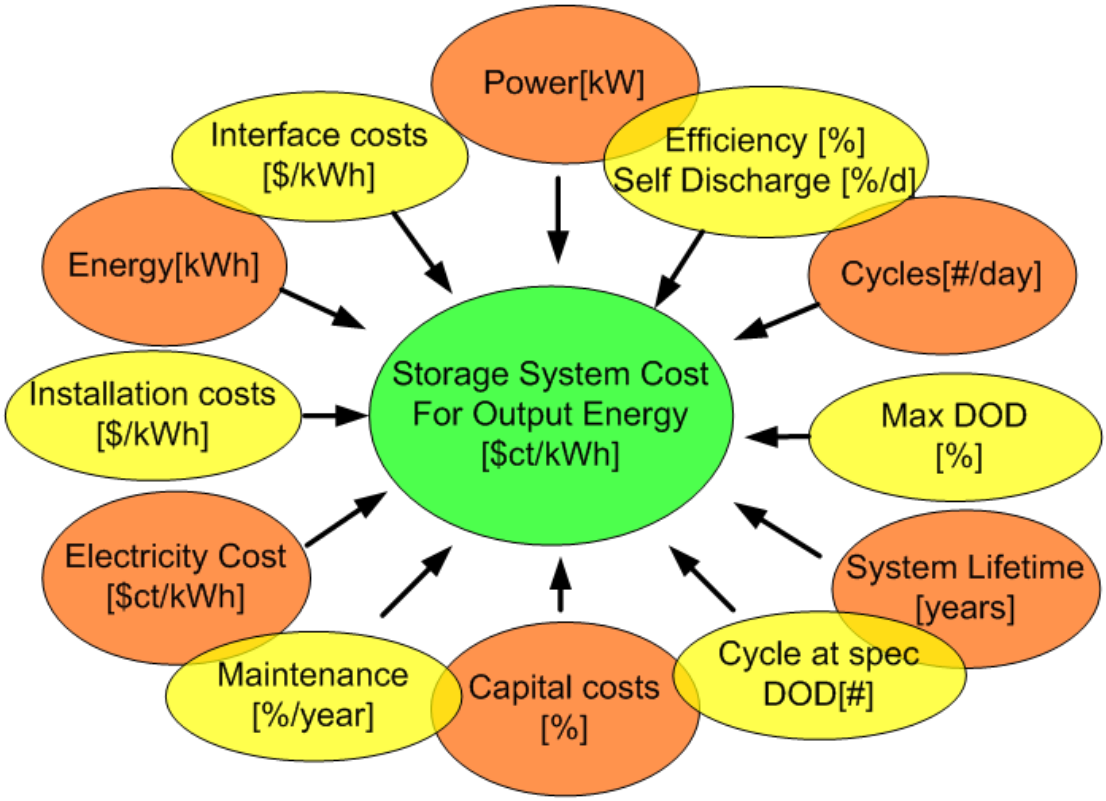

Figure 5-12. The factor influencing battery technology comparison.

5.5.3 **Annuity Method to Select Energy Storage Technology**

To compare energy storage technologies, the annuity method is used to convert all dollar values to a unique value of the interest. With the help of the annuity method, it is possible to determine the annual rate of the present value cash flows. Therefore, it is possible to compare several technologies with different characteristics.

The principle of the annuity method is described briefly as follows. In this method, the cash flows are estimated and all of them are re-evaluated in terms of present time. In other words, the present value of the project can be seen over the life of the project. A simple diagram of cash flow is demonstrated in Figure 5-13. It is very common to include the compound interest rate in the present value calculations. Therefore, the general formula for the present value calculation of a future cost/profit becomes

$$P = F\left(1+i\right)^{-n} \tag{5.3}$$

where P = present money, F = future money, i = interest(discount) rate, n = number of interest period.

(5.3) is extended to calculate all future costs in present value.

$$P_{cycle} = P + A\left[\frac{\left(1+i\right)^{n}-1}{i\left(i+1\right)^{n}}\right] \tag{5.4}$$

where P_{cycle} is the present value for the cash flow in every cycle, and *As* are the future payments.

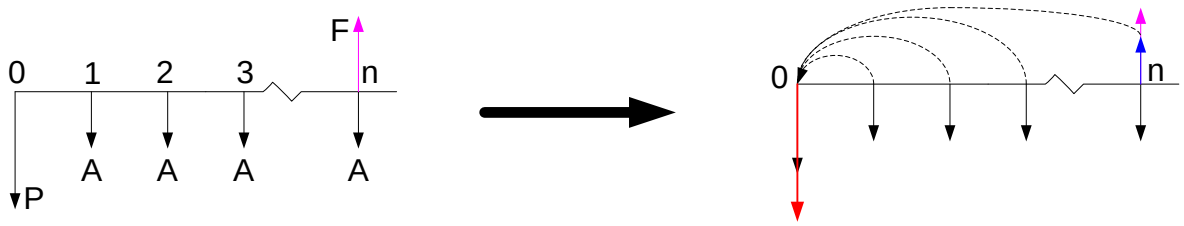

Figure 5-13. An example of a cash flow diagram.

In some projects, there are also some replacement costs. Under these conditions, the cash flow is calculated for every period reflected to its starting point. Finally, all the accumulated cash flows for every period/cycle are reflected to the present time. This principle is shown in Figure 5-14. The equation to calculate total cash flow remains the same as (5.4) except for the effective interest rate as shown in (5.5).

$$i_{eff} = (1+i)^{n'} - 1 \tag{5.5}$$

In (5.5), i_{eff} is the effective interest rate, i is the project interest rate, n' is the number of years between each replacement.

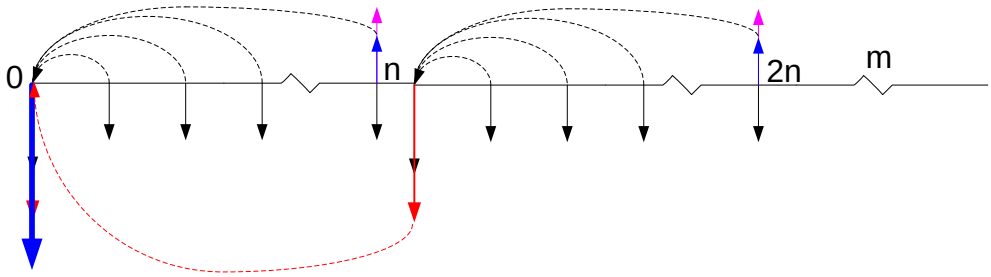

Figure 5-14. Cash flow model with multiple replacements.

When all the cash flows with different characteristics are estimated, it is possible to calculate the annual cash flow (A_n \$/yr) throughout the project time line (n) as in (5.6).

$$A_n = P_{total}\left[\frac{i(1+i)^n}{(1+i)^n - 1}\right] \tag{5.6}$$

This value can be used as a measure to compare different technologies with different characteristics especially life-time characteristics. In the following section, with the help of recently collected data, different energy storage technologies are compared using this annuity method.

5.5.4 **Energy Storage Properties and Assumptions**

It is desirable to have a unique number to use to compare different technologies; however, due to multiple data and many uncertainties we usually have a range. In carrying out the study, the following assumptions have been made:

- The storage system is considered to be an add-on device in a bigger project; hence service costs are taken over by the project regardless of the battery integration.
- Average price per kWh for all the battery technologies is considered.
- Average interface cost is considered for all the batteries.
- Average nominal cycles are considered for batteries.
- Round trip efficiency will change based on the SOC but we considered the average efficiency.
- Maintenance cost is assumed based on the power level of the plant not the energy.

- System efficiency is the product of battery efficiency and interface efficiency. This value can be modified to include self-discharge.
- Energy and power density are not considered as part of the dollar value.
- Life time of the battery is equal to the cycle life of the battery.
- Replacement cost for new batteries is assumed to be equal to the initial investment cost of the battery. Hence, no cost decrease in any technology is considered yet.
- Used energy storage systems do not have any value.

Based on the factors that have been identified for any project with an energy storage system, project requirements and properties for each technology have been collected. Table V shows the project requirements that have been determined for two pieces of mobile mining equipment: dragline and shovel. In these pieces of equipment, a 20% peak-shaving benefit has been considered. The major difference in these pieces of equipment is the load cycle duration. Draglines are much slower than shovels. In particular, this study is based on a 30-second load cycle for a dragline and a 15-second load cycle for a shovel. Table VI- Table VIII present the energy storage technology properties used in this study.

Table V. Project Requirements for Integrating Energy Storage Systems

Project Req.	Power (kW)	Energy (kWhr/cycle)	Voltage (kV)	Cycle (#/d)	Life time (yr)	Cycle time (hr)
Dragline	4800	20	0.48	2880	20	0.00416
Shovel	300	0.416	0.48	8640	20	0.00139

Table VI. Energy Storage Technology Properties-I

Properties	Energy Price ($/KWhr)		Interface Price ($/KW)		Gravimetric Density (Whr/Kg)	
Technologies	Low	High	Low	High	Low	High
Lithium ion	400	1000	30	50	170	500
Lead acid (flooded)	150	150	30	50	15	40
Lead acid (VRLA)	250	250	30	50	15	30
NaS/NasCl	250	1000	30	50	150	150
ZnBr	300	400	30	50	70	190
NiMH	300	1000	30	50	30	110
NiCd	400	700	30	50	35	60
Ultracapacitor	32,692	69,930	30	50	2.4	3.1

Table VII. Energy Storage Technology Properties-II

Properties	Volumetric Density (Whr/L)		Nominal cycles @ 80% DoD		Roundtrip Efficiency (%)	
Technologies	Low	Low	High	Low	Low	High
Lithium ion	250	4000	10000	85	4000	500
Lead acid (flooded)	108	800	1200	70	800	40
Lead acid (VRLA)	100	1800	3000	80	1800	30
NaS/NasCl	180	12500	18750	80	12500	150
ZnBr	15	2500	2500	60	2500	190
NiMH	140	2000	2500	60	2000	110
NiCd	50	5000	10000	60	5000	60
Ultracapacitor	2.59	750000	1250000	95	750000	3.1

Table VIII. Energy Storage Technology Properties-III

Properties	Self-discharge (%/d)	Maintenance (%/KW)	System Efficiency (%)
Technologies	Estimated	Estimated	
Lithium ion	0.01	1	87.29
Lead acid (flooded)	0.33	3	74.92
Lead acid (VRLA)	0.07	1	79.97
NaS/NasCl	0	3	84.88
ZnBr	0.07	1	63.01
NiMH	1	1	62.42
NiCd	0.33	1	62.84
Ultracapacitor	0.33	1	93.30

5.5.5 **Energy Storage Comparison for High Power Mining Equipment**

This section presents this dissertation's view on energy storage selection for high power multi-motor, particularly mining equipment. The first set of results is generated for a 24 MW dragline for which peak-shaving of 20% has been assumed. Figure 5-15 presents the projected cost of electricity for the dragline based on the data provided in Table V-Table VIII.

As can been seen, there are significant differences among the technologies for the dragline, and it is easy to eliminate some technologies such as flooded lead-acid batteries. Therefore, four technologies have been identified as potential technologies for dragline: Lithium-ion, NiCd, NaS, and ultracapacitor. The comparison in terms of projected energy price based on the annuity method for these technologies is presented in Figure 5-16. As can be seen, NaS technology presents a significantly better energy price compared to other technologies.

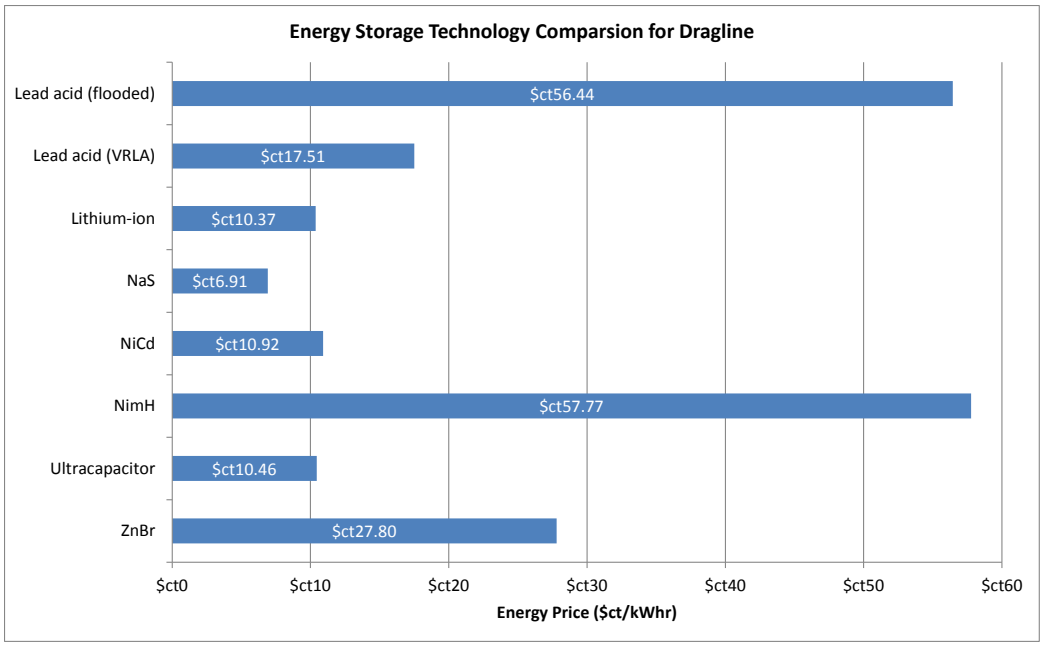

Figure 5-15. Comparison of commercially available energy storage technology for a dragline.

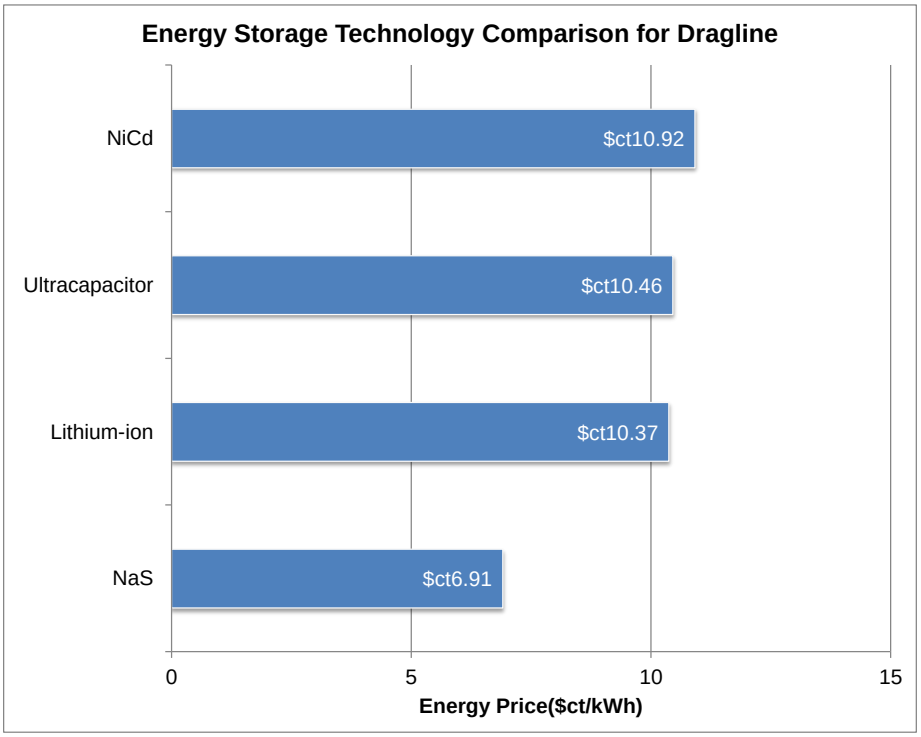

Figure 5-16. Comparison of energy prices for selected energy storage technologies for a dragline.

Shovels are typically faster than draglines with a duty cycle from 10 to 30 seconds. In this study a 1.5 MW shovel with a 15 second duty cycle is considered with the project requirements shown in Table V. The result of an energy price comparison for the same technology as selected for the dragline is presented in Figure 5-17. As can be seen, for the shovel, an ultracapacitor is the technology of the choice in terms of projected energy price. It is worth noting that the result obtained is different from what has been shown for the dragline, for which NaS batteries show better economical values.

There are several indirect factors that affect the whole system and not only the energy storage one f which is energy density. Despite the long life time of the ultracapacitor compared to other technologies, it suffers from low gravimetric and volumetric energy density compared to other technologies presented in Table VI. Figure 5-18 shows the magnitude of this effect, despite the superior energy price of the ultracapacitor for shovels. As can be observed, an ultracapacitor is about 100 times less dense in terms of volume and heavier than lithium-ion technology.

Another factor is the temperature characteristics of the energy storage technology. This factor is important since the ambient temperature of mines can vary significantly throughout the year. The Hei Dai Gou coal mine in China is one of the many examples where the temperature ranges from -35 ºC to +38 ºC. From the point of view of temperature characteristics, ultracapacitor have superior properties compared to other technology. On the other hand, it has recently been announced that sodium-based (Ni(M)x) batteries are under "low risk-type" practical research because of temperature properties for mining

apparatus, 93. These research activities emphasize the importance of the temperature properties of the energy storage system for future mining environments.

In the economic evaluation of the technologies, the number of replacement units has been considered. Figure 5-19 presents the estimated required energy storage units over 20 years of operation of mining equipment. As can be seen, the required number of replacement units for the ultracapacitor is significantly lower than the ones for other technologies, increasing the feasibility and applicability of the solution.

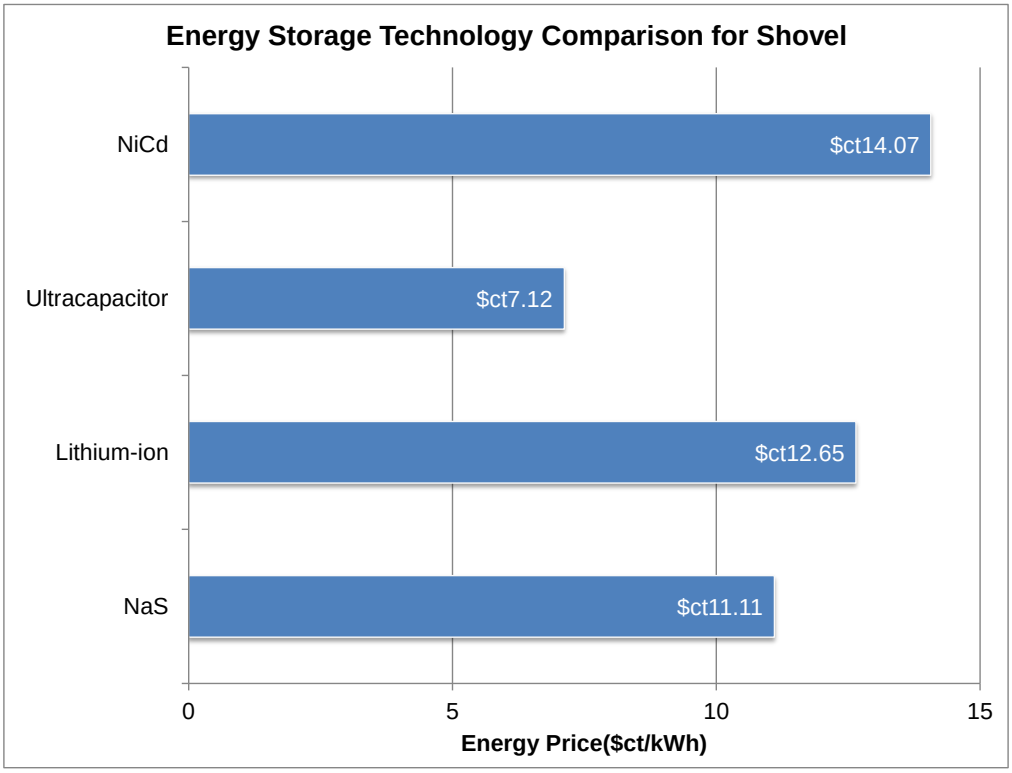

Figure 5-17. Comparison of energy prices of selected energy storage technologies for shovels.

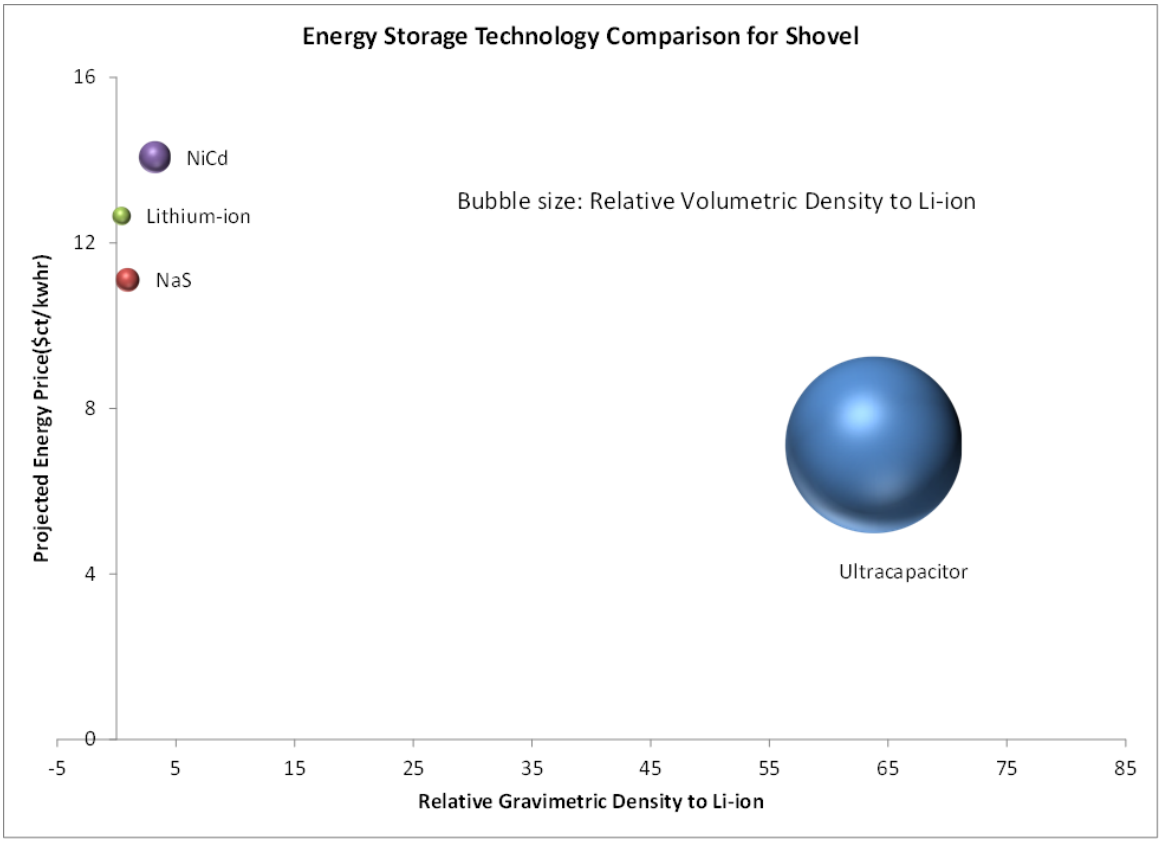

Figure 5-18. Comparison of selected energy storage technologies for shovel.

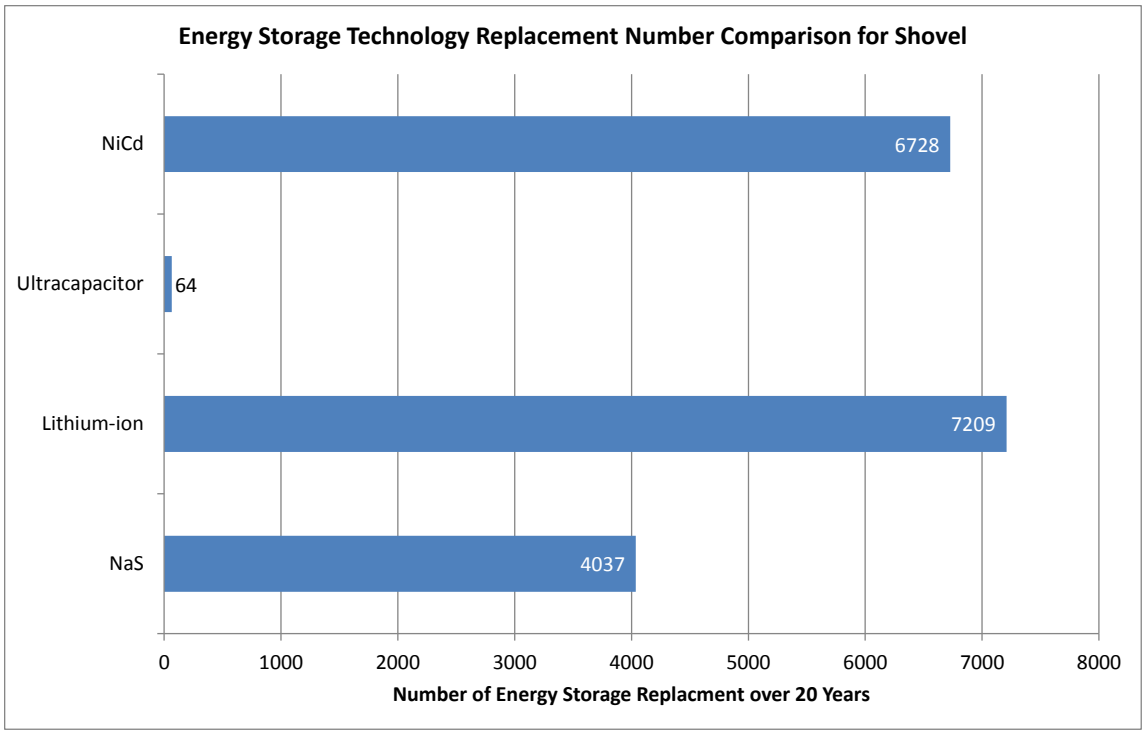

Figure 5-19. Replacement of selected energy storage technologies for shovel.

5.6 Ultracapacitor Integration into Existing Mobile Mining Converters

Based on the obtained results from the annuity method and feasibility analysis, the ultracapacitor has been selected as the technology of choice. Integration of ultracapacitors into shovels and draglines provides benefits from the system rating, system operation, life time, reliability, and many other factors and is at the same time economically viable. There are two options for ultracapacitor integration; direct and indirect through a separate DC/DC converter. Obviously, direct integration requires a flexible DC link voltage that must be tolerated in the drive side. On the other hand, the power flow is completely controlled by the internal current controller's parameters, i.e. current limit and time constant τ_i. An example of

a 1.5 MW converter performance integrated directly with ultracapacitor and different power contributions is presented in Figure 5-20. In this example several 125V ultracapacitor modules are arranged in series and parallel providing about 7F. In the other approach, a separate DC/DC converter is considered (unless drive inverters with high enough bandwidth are used) to exchange power from the DC bus to the ultracapacitor modules. The schematic of this approach is shown in Figure 5-21. A boost converter topology is chosen as shown in Figure 5-22 which is connected to strings of 7F ultracapacitors. In this example, the DC/DC converter also contributes in controlling the DC link voltage of the shovel. Therefore, special care has been taken in order to avoid any fight between the controllers of the AFEs and the DC/DC converter. The proposed control structure to meet the mentioned requirement is presented in Figure 5-23. Due to more controllability, the maximum motoring power to be supplied by the AFE is simply selected as P_{MAX}=950kW, while the maximum regenerated power that can be fed back by the AFE to the grid is selected as P_{MIN}=-200kW. The extra regenerated power is used to charge a stack of ultracapacitors as presented in Figure 5-24. It has been observed that the rating of this equipment could be reduced to 0.73 PU due to the proposed peak-shaving.

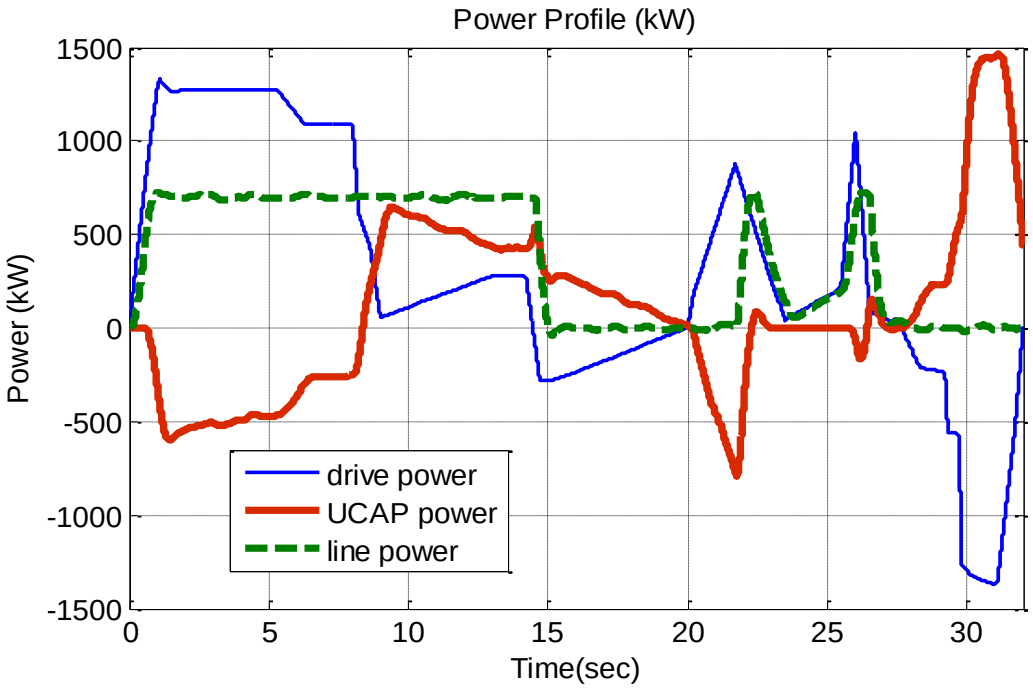

Figure 5-20. Simulated dynamic performance of the 1.5MW shovel integrated with an ultracapacitor directly at the DC link.

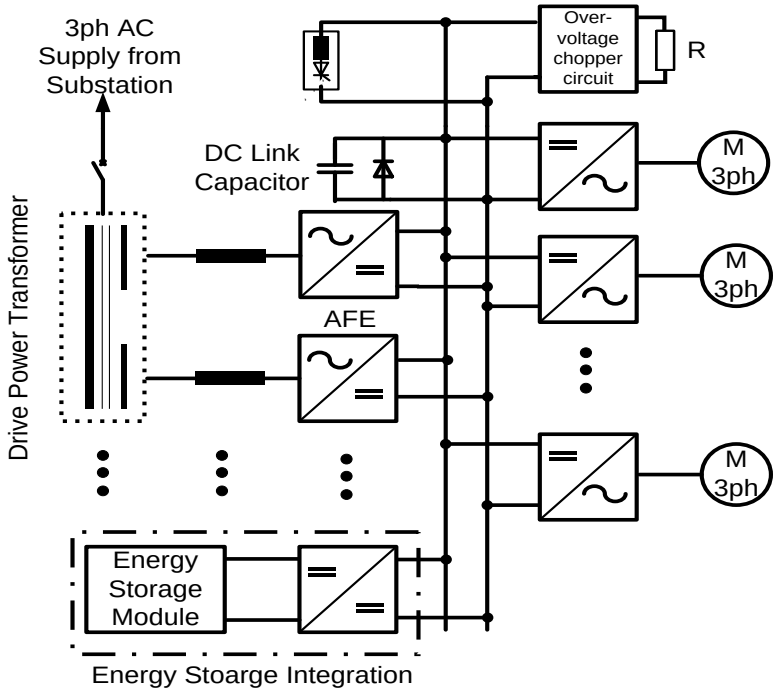

Figure 5-21. Schematic of a multi-motor AC drive system integrated with an ultracapacitor with a separate DC/DC converter.

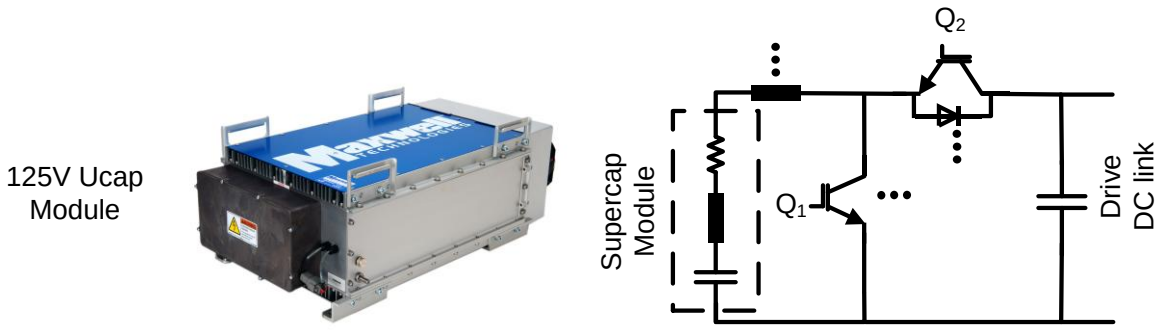

Figure 5-22. Example of an ultracapacitor module and a DC/DC converter suitable for mining applications.

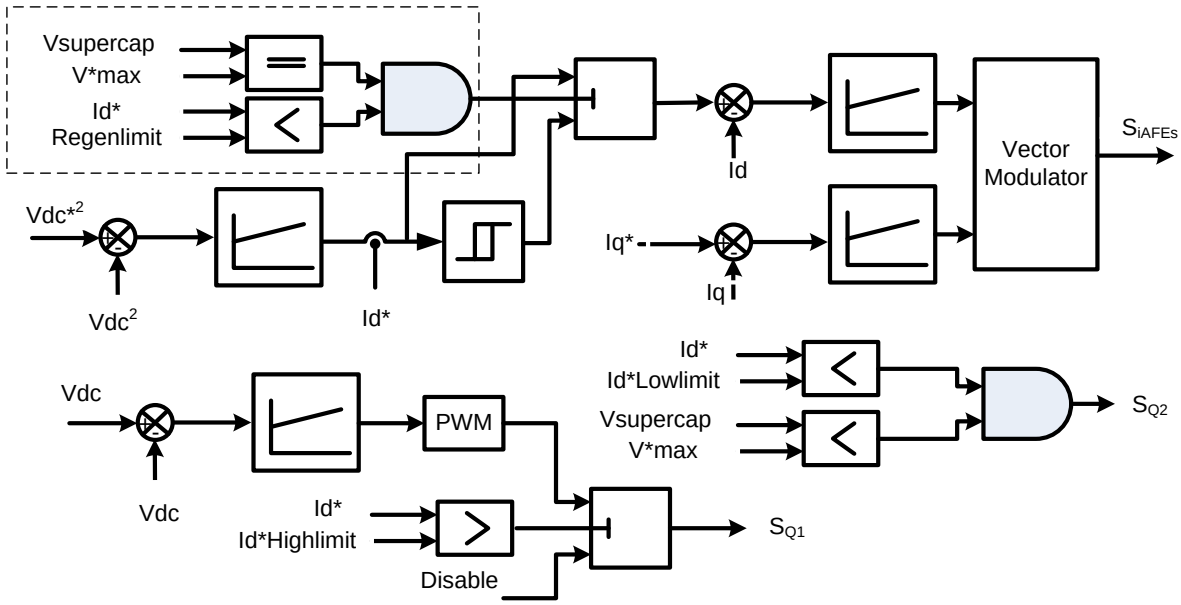

Figure 5-23. Proposed control structure of the shovel converter system when the integrated DC/DC converter as shown in Figure 5-21 contributes to the drive DC link voltage control.

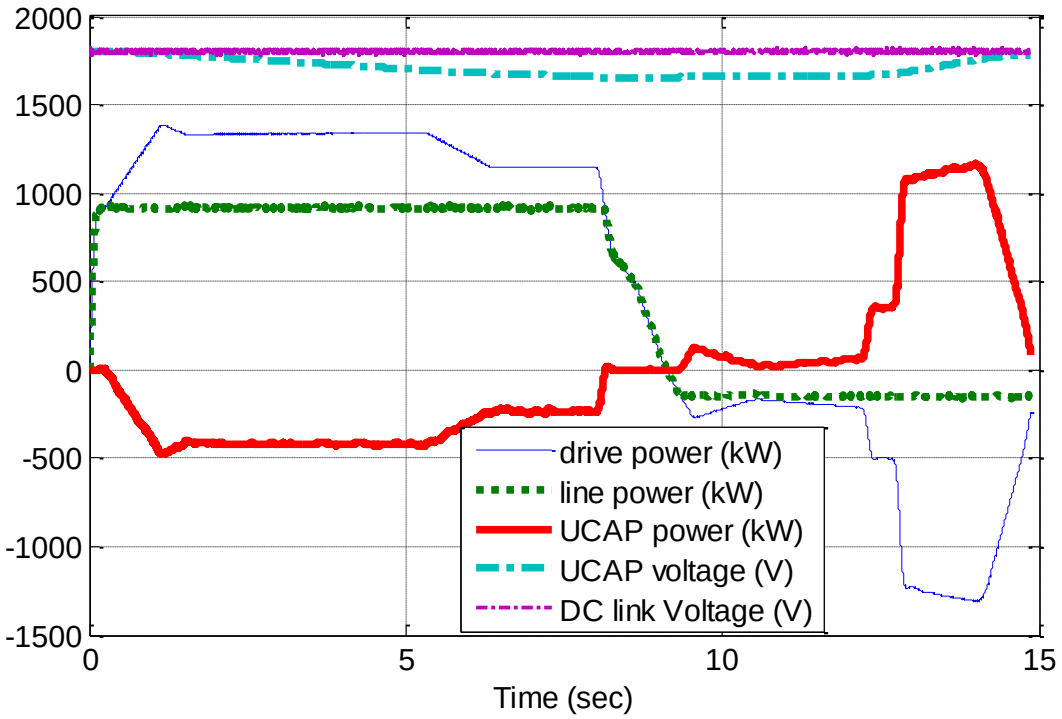

Figure 5-24. Simulated dynamic performance of the 1.5MW shovel integrated with ultracapacitors with a separate DC/DC converter as shown in Figure 5-21.

5.7 Hybrid Front End Configurations for High Power Multi-Motor Applications

5.7.1 Unidirectional Front End Converters

Although the proposed ultracapacitor integrations have clear benefits to the system especially in terms of grid side peak current shaving and energy management of the mine, nevertheless, the ratings of the converter components, either electrical or mechanical, would not change significantly for large mining machines like draglines. It can be shown that the benefits from possible downsizing of the components by ultracapacitor cannot be realized for

a dragline or even for a shovel considering the desired THD, and spare converters. On the other hand, it has been shown in Figure 5-18 that the proposed ultracapacitor suffers from low energy density. This lack can prohibit integrating the ultracapacitor to high power mining equipment since it requires enlarging the volume significantly.

Consequently, this dissertation also proposes two straightforward configurations for development of the next generation of high power AC mining equipment such as shovels and draglines. In these configurations, an ultracapacitor through a separate DC/DC converter is still used to harvest the regenerative energy and harness most of the energy in the motoring mode. Therefore, in these configurations, high power unidirectional rectifiers can be used obviously with higher PCC current THD. To overcome the current THD problem, multi-pulse diode bridge rectifiers or thyristor based converters (such as 12-pulse) are built with multi-winding transformers. These transformers are not necessarily additional equipment in the mines and only the group connections are different. For further PCC current THD improvement, first a hybrid parallel active filter is proposed at the PCC, rated at ~ 3% to 5% of the front end converters, as shown in Figure 5-25. Selected results for this configuration projected for 1.5MW shovel systems are shown in Figure 5-26 and the controller hardware verification - for a six-pulse diode bridge -Figure 5-27, developed at Bhattacharya's research group at FREEDM System Center, 99. A Thyristor-based front end converter may be preferred, as it can better assure control of the DC link voltage than the diode bridge option. Consequently, the proposed configuration has the advantages of currently installed AFEs that are much simpler and potentially lighter, and with higher efficiency and more reliable and robust operation under system fault conditions. This configuration can be applied to larger

mining equipment like dragline system too where the system benefits become more apparent. Unity power factor operation for shovels and a small leading one (~2% p.u. VAR) for draglines can be ensured with the help of the hybrid parallel active filter. It is believed that this approach will enable integration of the energy storage system into mining equipment, since it enjoys greatly improved power density of the front end converters.

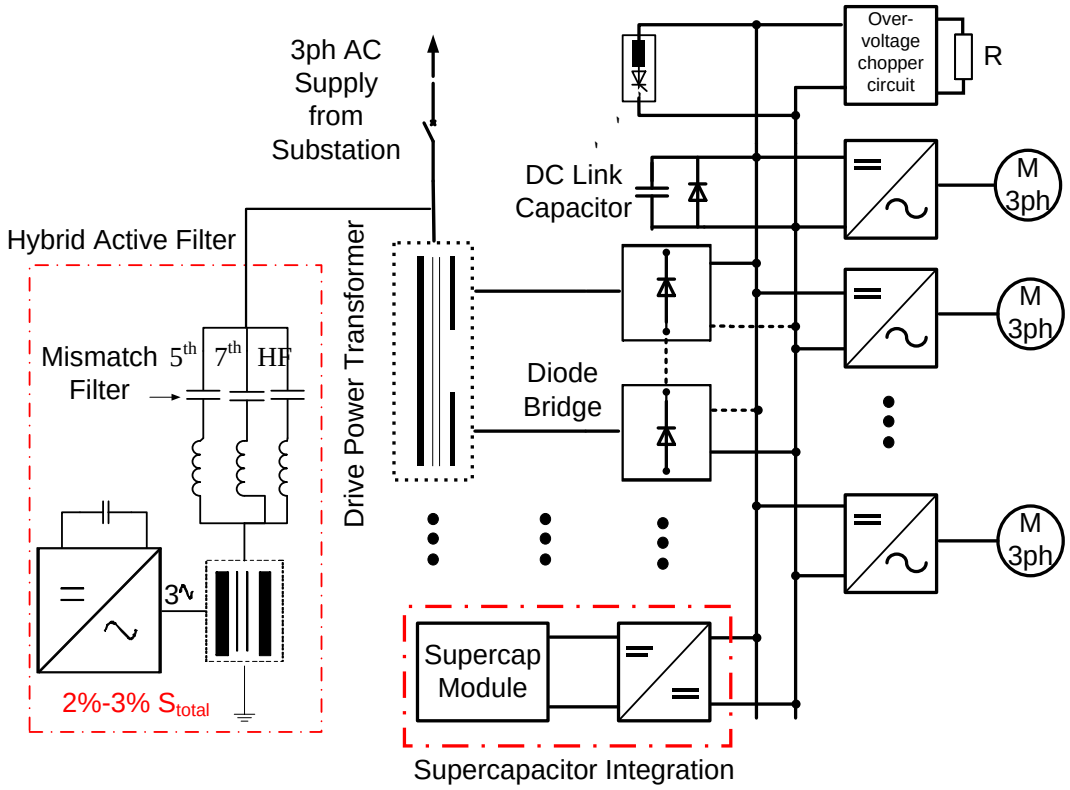

Figure 5-25. Unidirectional front end assisted with fractionally rated hybrid active filter integrated with ultracapacitor.

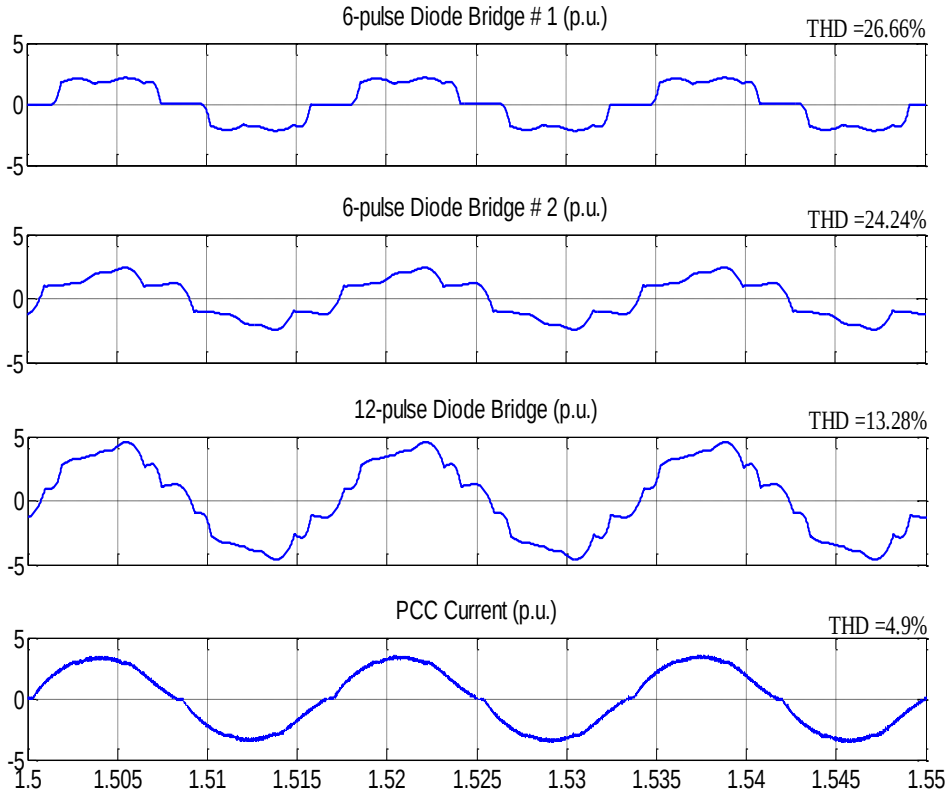

Figure 5-26. Simulated 1.5MW unidirectional front end assisted with hybrid active filter as shown in Figure 5-25.

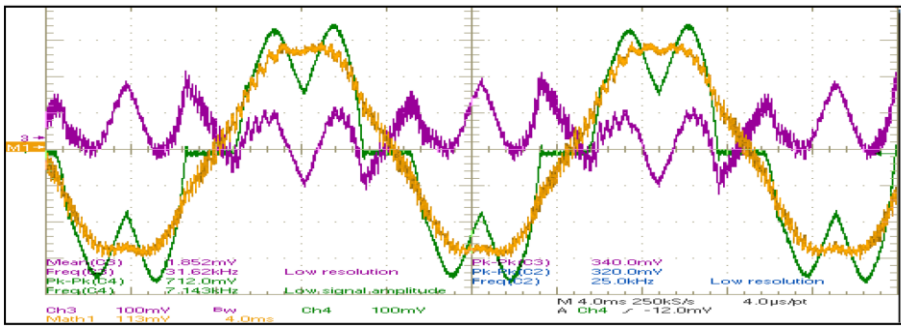

Figure 5-27. Results of active filter controller hardware verification for a six-pulse diode bridge front-end.

5.7.2 **Hybrid Front End Converters**

In the second proposed system presented in Figure 5-28, main front end converters are Thyristor-based as currently implemented. The ultracapacitor modules are connected to the DC link through a separate DC/DC converter for peak-shaving. One (or several for larger systems) bidirectional AFE is connected to the DC link to perform active filtering while providing a partial path for the power to and from the machines. To develop the hybrid configuration, Figure 5-29 presents the proposed control structure for the hybrid architecture with specific attention to the main front ends and AFEs.

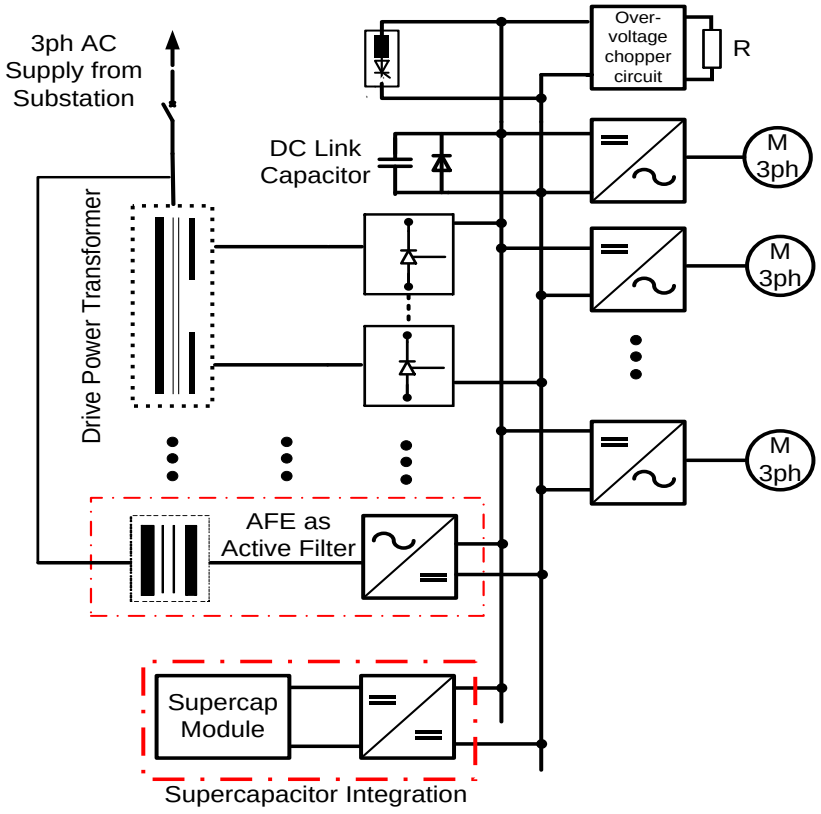

Figure 5-28. Hybrid configuration for large multi-motor applications.

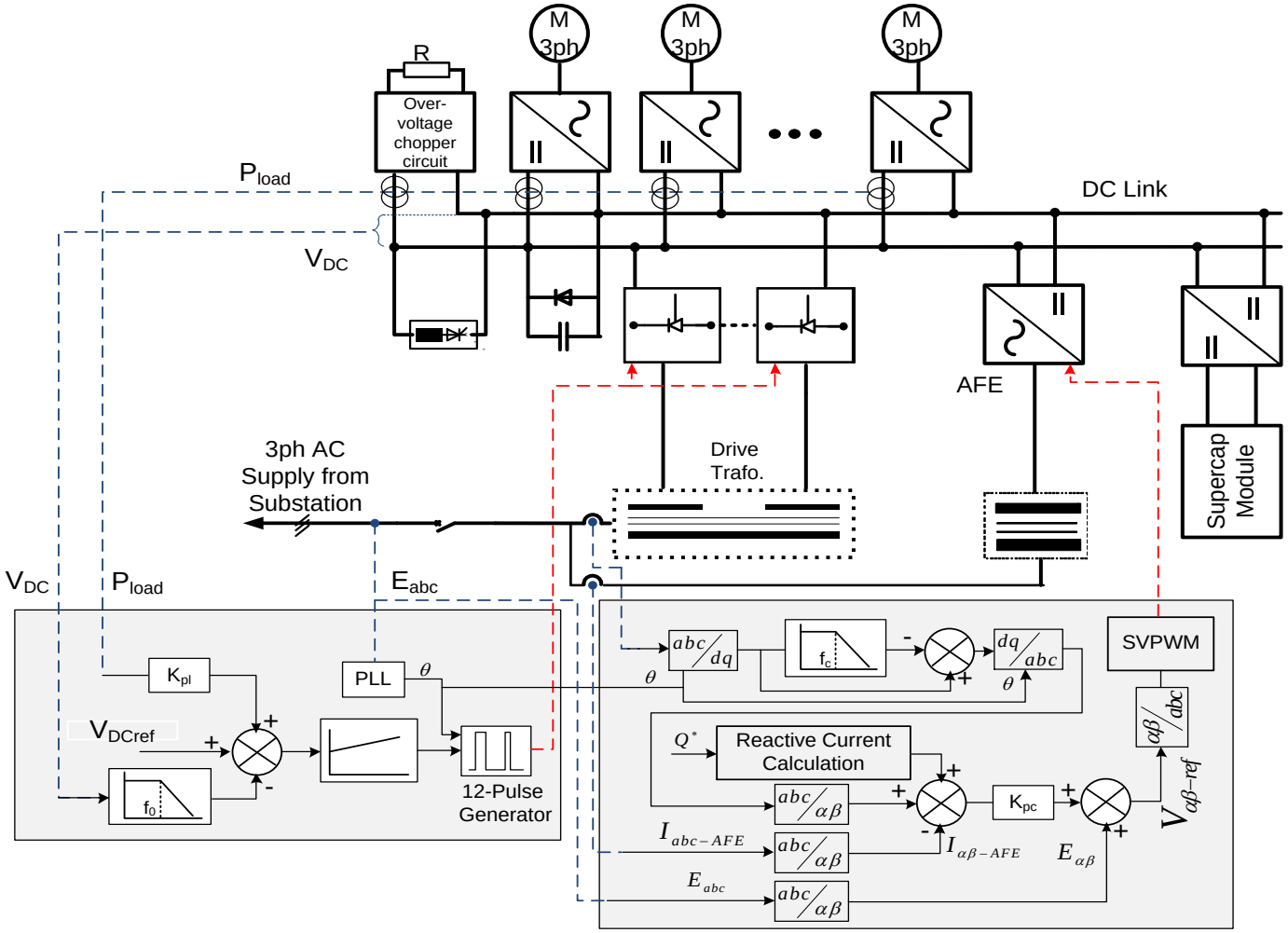

Figure 5-29. Proposed control structure of hybrid front end architecture for large multi-machine systems including mining equipment.

The parallel active filter control is based on the Synchronous Reference Frame (SRF) controller structure using the load current harmonic extraction method, [10]. Figure 5-30 shows the simulated currents for the proposed system at PCC and Figure 5-31 shows the frequency spectrum and total harmonic distortion (THD) of the current at PCC before and after compensation. As can be seen with THD, at the point of common coupling, less than 5% of the stringent IEEE 519 requirements are met. An example of dynamic operation of the proposed configuration is shown in Figure 5-32 and Figure 5-33 for a lab test-bed rated at 12kVA/400VDC. This circuit can also act as the pre-charging circuit if needed. In addition using this AFE ensures the available capacity to provide the Var required in mines. This option appears more advantageous than other configurations in terms of active filter controls, structure, and reliability of the whole system.

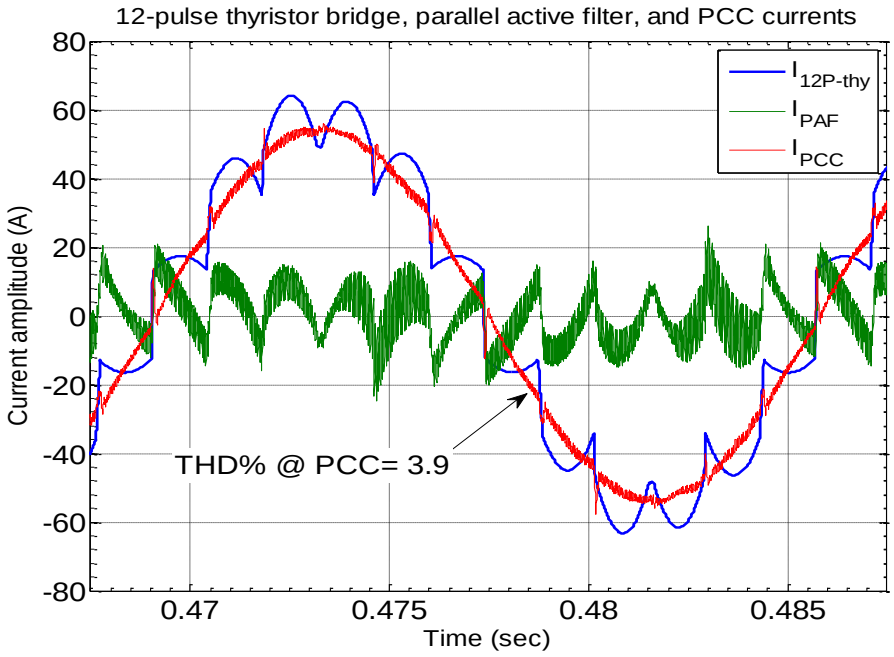

Figure 5-30. Hybrid front end's PCC current as shown in Figure 5-28.

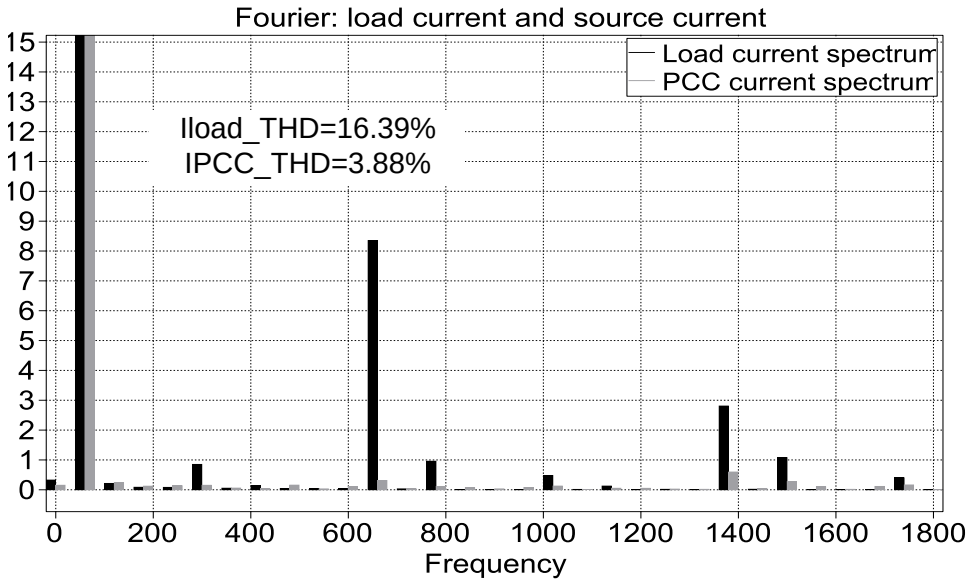

Figure 5-31. Frequency spectrum of load and PCC currents for the proposed hybrid configuration.

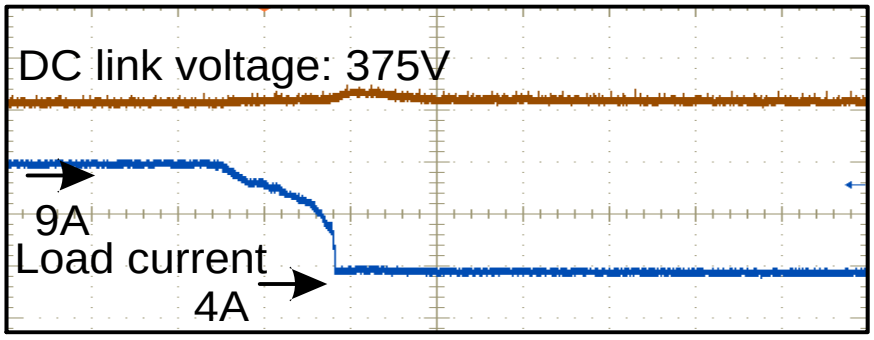

Figure 5-32. DC link dynamics of hybrid configuration- an example.

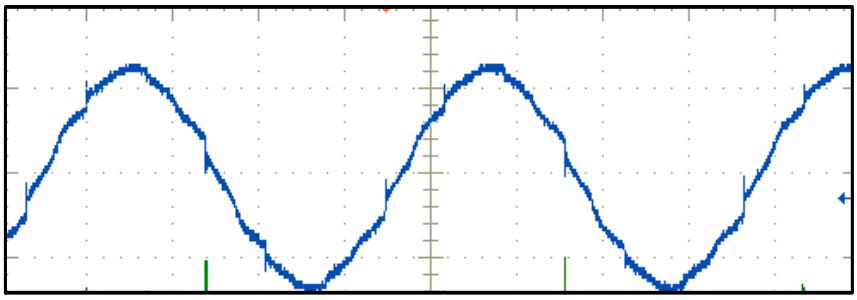

Figure 5-33. Nominal PCC current (ph A) of the hybrid configuration with a two-thyristor bridge and one AFE as shown in Figure 5-28

5.8 **Summary**

To supply the AC high power drive systems several Active Front Ends (AFE) with DC choppers are used to ensure a reliable operation and an acceptable harmonic current spectrum. Recently, integration of the energy storage system with the mining equipment has received industry attention, especially for peak load shaving and smarter energy management of the mine. Currently, the regenerative energy is often burnt into the choppers and is not fed back to the grid. The industry is motivated to capture this regenerative power since it can be as high as 60% of the motoring power and as high as 24 MW. Therefore, there is a possibility of large cost reduction and component downsizing. However, the present status of development seems to be not very promising mainly because energy storage systems are still considered to be add-on parts to existing products.

This research investigated the operation of the current state-of-the-art front end converter systems for multi-motor applications. In particular, two power conversion configurations and a methodology to determine the suitable energy storage technology for development of the multi-motor mobile mining equipment have been introduced.

It has been shown that for relatively slow machines (load cycle ~ 30-60 sec) like draglines NaS battery is the technology of choice in terms of energy price. For relatively faster equipment (load cycle ~10-30 sec) like shovels, the ultracapacitor presents the best economic value in terms of energy price. Several factors besides economy have been identified for energy storage integration including volume, mass, temperature and required number of energy storage systems. It has been shown that despite the economic values of a

particular technology either for either shovels or draglines, each technology has significant drawbacks. For instance, the ultracapacitor is significantly heavier and bulkier than lithium-ion batteries for mining applications. On the other hand, the ultracapacitor exceeds other technologies in terms of required number of replacement units over the life time of the mining equipment. Therefore, this chapter proposes ultracapacitor as the preferred technology for mobile mining equipment despite its very low energy density, which can prohibit its integration at present.

Consequently, this chapter proposed that the enabling technology for energy storage integration for mobile mining equipment is front end converters with higher power density than the current state-of-the-art front end technologies. In particular, the main body of the front end is proposed to become unidirectional. In other words, all the AFEs are replaced with robust and unidirectional rectifiers which use diodes or thyristors. The ultracapacitor modules are connected to the DC link through a separate DC/DC converter for the peak-shaving purpose. To meet the current harmonic content requirements of the mines' power system, the proposed configurations are equipped with active filters. In the first option, a fractionally rated hybrid parallel active filter is integrated in the AC side after the drive transformer. In the second option which is called hybrid configuration the active filter is connected to the main DC link. This configuration can use a pure active filter that has a relatively simpler structure than the hybrid and its rating for mining equipment is expected to be comparable. In addition, this integration provides a partial path for the drive power and can be also used as the pre-charging circuit if needed. With the hybrid configuration we can envision larger mobile equipment.

Chapter 6. CONCLUSIONS AND FUTURE WORK

6.1 Conclusion of Present Work

This dissertation has investigated the potentials and challenges for VSC-based transmission technologies. The technology in this dissertation is characterized in terms of switching frequency operation and switching patterns as either vector- or angle-controlled-based converters.

This dissertation addressed the DC link voltage control issues for vector-controlled VSC-based transmission systems under power system disturbances. Having analyzed the state-of-the-art methods of mitigating the DC link voltage fluctuations under grid faults, a control structure in the commonly used dq-synchronous frame is proposed. The proposed structure obviates the need for sequence extraction block or resonant compensator which is often proposed. Therefore, there is no diminishing bandwidth factor making it suitable for transmission applications for which the switching frequency is limited to a few hundred Hertz. The control scheme; however, utilizes the interaction of the converters, the load, bus voltage and their derivatives to compensate for the phase delay in the current regulator. The RTDS verification of the controller attained less than 1% DC link voltage deviation under most common faults, demonstrating the applicability and effectiveness of the proposed

scheme for different transmission applications denoted as HVDC, drive and hybrid power systems.

This dissertation has introduced the possibility of automatic control of active and reactive power for voltage-sourced converters through an angle-control structure. A new control framework that uses the properties of a SITO feedback system is developed for voltage-sourced converters. Clearly, one actuator, in this case the angle cannot be used to regulate two outputs (active and reactive power) to arbitrary setpoint values. Nevertheless, this dissertation shows that a one-dimensional class of setpoint values is feasible for the VSC technology. Design limitations and tradeoffs imposed by the plant and controller for such a system have been explained. This work is an enhancement in the operational region of the existing shunt family of FACTS devices that can also be extended for transmission level VSC-based HVDC systems.

With the knowledge gained in control methods for VSC technology, this dissertation proposed the concept of Modular Transformer Converter (MTC) based on VSC technology to develop transmission level power electronic systems such as FACTS controllers. The MTC concept has been initially perceived to reduce the cost of transmission level power electronics which can be retrofit into the AC network. Unlike common approaches, the MTC system can be utilized or commercialized by itself and it will be a by-product of this research for various high power and medium-voltage power conversion applications – such as power conversion technology for large rated wind generators (type IV and beyond) [~7MW and higher (10MW) which are being developed now]. In other words, the proposed MTC concept can open a broader market for the 10MW range and MV drives applications but with lighter

weight and more efficient cooling than in the common advanced technologies in the drives field. As a consequence, utility-scale high power electronics may not require detailed custom design and engineering for power converters and therefore, system costs may follow the economies of scale.

Through development of the MTC, this dissertation identified and introduced several applications such as *Recovery Transformer*, *Transformer Life Extender*, *Re-locatable Transmission Controller,* and *Seasonal Renewable Transmission Controller*. In fact, MTC enables a versatile transmission controller, the Convertible Static Transmission Controller (CSTC) with added values compared to state-of-the-art technologies such as the NYPA Convertible Static Compensator (CSC). Existing FACTS solutions enable dynamic control for transmission lines; however, the MTC based CSTC concept provides the flexibility of full or partial utilization for transmission lines and power transformers. This flexibility effectively increases the system's spare capacity and operating margins, and also provides back-up in case of power transformer failure (or forced reduced transformer rating operation) scenarios by providing real-time continuous power flow control and thereby, increased transfer capacity of existing transmission systems. For transformer life extension or partial bypass purposes, the CSTC operates as a substation voltage/phase angle regulator which is different from conventional BTB HVDC applications. The proposed function enables a *locally controlled* CSTC which does not complicate the power system operation and can be utilized and inspired as the active mobile substation or recovery transformer. For power flow control with specific attention to renewable generation transmission in the meshed network, less complex coordinated control can be obtained with the CSTC concept. It has been shown

and concluded that the Dual Series Static Compensator (DSSC) mode or series-series mode available in the CSTCs provides significantly superior performance in terms of operating characteristics compared to conventional power flow controllers. Finally, it is believed that 10 to 100 MVA MTC-based CSTC which can be retrofitted into existing transmission substations and transformers have a strong potential to improve the reliability, controllability and efficiency of the grid.

Energy storage systems are expected to play key roles in future energy management. Current state-of the-art mobile mining equipment such as shovels and draglines are grid-connected high-power multi-machine systems up to 24 MW. A control structure was proposed that ascertains satisfactory operation in both motoring and generating modes of the equipment. The other contribution of the controller is to ensure an insignificant circulating current with split DC links and separate drive transformers, which increases the reliability of the whole system and the availability of the components. This dissertation also proposed the integration of supplementary energy storage to capture and reuse the regenerative power which is currently burnt into the DC choppers. In particular, it has been shown that the ultracapacitor is the technology of choice in terms of energy price, temperature characteristics and engineering efforts. However, this dissertation has identified advanced VSC technology as the enabling technology for this integration. Consequently, the so-called "Hybrid Configuration" is introduced, configuration that has greatly improved efficiency, density, and reliability compared to current state-of-the-art technologies.

6.2 Contributions

In summary, the key contributions of this dissertation are as follows:

1. Proposed control structures for resilient operation of the vector-controlled voltage-sourced converter under power system faults and disturbances.
2. Identified fault cases and proposed a control structure in hybrid power systems where a back-to-back voltage-sourced converter system operates in parallel with a transformer or a short AC transmission line. In this case, both converters see the faults, a factor which had not been addressed in the prior literatures.
3. Introduced and gave operational analysis of complete angle-controlled VSC systems that can be extended for point-to-point HVDC applications.
4. Proposed and developed existing and imminent standard VSC-based AC/AC drive converter systems for utility applications with a broad market compared to existing solutions for FACTS controllers, with reduced engineering effort and reduced custom-designed converters. The approach developed is called Modular Transformer Converter or MTC for utility applications.
5. Proposed the concept of Convertible Static Transmission Controller (CSTC) based on the MTC approach. The MTC-based CSTC concept provides the flexibility of full or partial utilization for the transmission lines and power transformers with different modes as follows:
    a. Shunt-shunt mode for transformer (partial) back up purposes and Var support
    b. Series-shunt mode for power flow control and Var support

c. Series-series mode for power flow control

6. Introduced of Dual Series Static Compensator (DSSC) as a new FACTS controller. DSSC is a back-to-back VSC system that is connected across the power transformer and each converter is inserted in series to the line. This mode is available in the CSTC. The operation characteristic of the DSSC in terms of PQ control is much wider than that of existing power flow controllers such as SSSC or UPFC.
7. Proposed a synchronous frame-based controller that is synchronized and locked with the line current rather than the commonly used voltage for the family of series static compensators including the DSSC. The significance of the proposed control structure is to have inherently decoupled control of active and reactive power.
8. Proposed a control structure and architecture for staggered VSC-based Active Front Ends (AFEs) interfacing with drive transformers for high power multi-machine systems such as advanced large mining equipment.
9. Proposed supplementary energy storage system for high power multi-machine systems and an architecture to capture the regenerative energy which is currently burnt into DC choppers.
10. Presented a methodology to determine and compare energy storage technologies for several applications including peak-shaving in high power mobile mining equipment. The outcome of the study showed that the ultracapacitor is the preferred technology for large mobile mining equipment.

11. Proposed active filter solutions for all AC multi-machine systems such as large mining equipment. The outcome of the proposed solution was to introduce architectures for front end converters as simple as three phase diode bridge converters.
12. Proposed hybrid configuration as a new architecture for high power multi-machine systems. In the hybrid configuration, the main front end is a group of three phase thyristor-based converters and the regenerative power is captured and reused through a separate converter. In addition, a group of AFEs performs active filtering and provides partial paths for regenerative power to increase the reliability.

6.3 **Future Work**

Angle-controlled VSCs have been specifically developed for transmission applications including FACTS controllers. Theoretically, this technology does not require a DC capacitor to control the reactive power making it a different concept compared to other reactive power compensators such as capacitor banks or SVCs. However, the fault analysis of this type of converters is still based on the passive components and not the control. Specifically, one can show that the DC link capacitance plays a critical role under power system disturbances. Large DC capacitance confines the DC link oscillations whereas the negative sequence current increases. On the other hand, smaller capacitors that are yet beyond the capacitance associated with the converter resonant frequency can confine the negative sequence current under unbalanced conditions. It can be concluded that there is still an opportunity for

research into introducing advanced controllers to mitigate the DC link voltage oscillations and overcurrent issues in the angle-controlled converters. This dissertation has identified several areas of research to address the problem. These activities include advanced synchronization signals such as Instantaneous PLL or IPLL, in which the controller is no longer constructed based on a positive sequence voltage. Another possible approach would be to investigate control structures in the stationary reference frame compared to the commonly used dq reference frame. Resonant compensators are inevitable in controllers based on the stationary reference frame, which should be investigated further since there are few reports on the applicability of the method for transmission level applications. The most straightforward control structure would be to use hybrid controllers. In other words, if possible, the VSC operates with vector control principles under unbalance conditions and operates with angle control ones under steady state conditions to meet efficiency and harmonic requirements.

The transformers in the proposed MTC are essential parts of the system. Although many researchers and developers propose transformerless vector-controlled multilevel VSCs, transmission level power electronics are often accompanied by the transformer. In fact, the problem is not using the transformer per se but using unconventional or overrated transformers. Different B-H curves in series-connected transformers can cause cascading saturation of the transformers (especially under power system faults) and shutting down the converter station as a consequence. Therefore, separate research is needed to design the transformer magnetic and the conductor interfacing the MTC power converters with non-sinusoidal waveforms.

This dissertation introduced a hardware-based asset management solution with an MTC approach for transformer life extension purposes. Although several practical papers propose diagnostic protocols to monitor the state of the health of a power transformer, to the best knowledge of the author, no online method is used to control the power flow in the transformer. Therefore, there must be research on developing protocols to monitor and control the main transformer of the CSTC concept for centralized and distributed mode of control. In addition, methods and metrics should be developed to test the resiliency and stability of the interconnected CSTC-based transmission controllers. To achieve the claimed features of the CSTC as the transmission asset that can be retrofit into existing assets, understanding the magnetic and its state of health is a key. Consequently, this dissertation proposes immediately to develop the protocols to monitor the transmission transformer performance in terms of L/R after disturbance signatures and increased harmonics level.

This dissertation has shown that compared to current state-of-the-art technology, the alternative power electronic system is the enabling technology for energy storage integration in high-power mining equipment. Therefore, a hybrid configuration was proposed which increases the power density of the front-end converters in mining equipment. In the course of concept development, this dissertation has identified a transformerless approach which may further increase the power density of the front end converters and facilitate the integration of energy storage systems. Isolation transformers used in the state of the art solution and the proposed hybrid configuration inherently behave like common-mode impedances and consequently very popular in the drive field especially those with high reliability requirements. Recently, it has been shown that for smaller machines tuned passive filter

networks at the AC side can confine the common-mode voltages produced by the power electronics. Therefore, there is the potential for research to evaluate the elimination of transformers in mining equipment as well. This author believes that the key to addressing the issue is identifying system parameters that take into account the capacitance of cable and machines.

Bibliography

1. A. Petersson, and A. Edris, “Dynamic performance of the Eagle Pass back-to back HVDC light tie ,” IEEE 7th Inter. Conf. on AD-DC Power Transmission, 2001.
2. S. Teeuwsen, “Modeling the Trans Bay Cable project as voltage-sourced converter with modular multilevel converter design,” In Proc. IEEE Power and Energy Soci. Annu. Meeting, 2011.
3. N. G. Hingorani and L. Gyugyi, Understanding FACTS, New Jersey: IEEE Press, 1999.
4. M. Callavik, “ABB-HVDC grids for integration of renewable power sources,” EPRI HVDC & FACTS Users Meeting, 2010.
5. V. Hild and J. Vivian, “Siemens HVDC & FACTS innovations and projects,” EPRI HVDC & FACTS Users Meeting, 2010.
6. N. MacLeod, C. Davidson, and N. Kirby, “Alstom-A Multi-level topology for voltage source converter HVDC transmission projects,” EPRI HVDC and FACTS Users Meeting, 2010.
7. C. Schauder and H. Mehta, “Vector analysis and control of advanced static VAR compensators,” Proc. Inst. Elect. Eng.-C, vol. 140, Jul. 1993.
8. S. Bhattacharya, B. Fardenesh, B. Sherpling, “Convertible Static Compensator: Voltage Soucre Converter Based FACTS Application in the New York 345 kV Transmission System”, Proc. of the 5th International Power Electronics Conference (IPEC), Niigata, Japan, April 2005.

9. H. Polinder, D. Bang, R. Rooji, A. McDonald, and M. Mueller, “10-MW wind turbine direct-drive generator design with pitch or active speed stall control,” IEEE IEMDC’07, 2007.
10. B. Parkhideh and S. Bhattacharya, “Towards smart transmission substations with Modular Transformer Converter (MTC) system,” In Proc. IEEE Power and Energy Soci. Annu. Meeting, 2011.
11. H. Akagi, Y. Kanazawa, and A. Nabae, “Instantaneous reactive power compensators comprising switching devices without energy storage components," IEEE Trans. Industry Applications, Apr. 1984.
12. L. Moran, P. D. Ziogas, amd G. Joos, “Design aspects of synchronous PWM rectifier-inverter systems under unbalanced input voltage conditions,” IEEE Trans. Industry Applications, Nov. 1992.
13. P. N. Enjeti and S. A. Choudhury, “A new control strategy to improve the performance of a PWM AC to DC converter under unbalanced operating conditions,” IEEE Trans. Power Electronics, Oct. 1993.
14. P. Rioual, H. Pouliquen, and J. P. Louis, “Regulation of a PWM rectifier in the unbalanced network state using a generalized model,” IEEE Trans. Power Electronics, May 1996.
15. A. V. Stankovic and T. A. Lipo, “A novel control method for input output harmonic elimination of the PWM boost type rectifier under unbalanced operating conditions,” IEEE Trans. Power Electronics, Sep. 2001.

16. Y. S. Suh, V. Tijeras, and T. A. Lipo, “A control method in dq synchronous frame for PWM boost rectifier under generalized unbalanced operating conditions,” in Proc. IEEE Power Electr. Spec. Conference, Cairns, 2002.
17. Y. S. Suh, V. Tijeras, and T. A. Lipo, “A nonlinear control of the instantaneous power in dq synchronous frame for PWM AC/DC converter under generalized unbalanced operating conditions,” in Proc. IEEE Ind. Appl. Soc. Annu. Meeting, Chicago, IL, Oct. 2002.
18. Y. S. Suh and T. A. Lipo,“Control scheme in hybrid synchronous stationary frame for PWM boost rectifier under generalized unbalanced operating conditions” IEEE Trans. Industry Applications, May 2006.
19. Y. Komatsu and T. Kawabata, “A control method of active power filter in unsymmetrical and distorted voltage system,” in Proc. IEEE Power Conversion Conference, Nagaoka 1997.
20. J.G. Hwang, P.W. Lehn, and M. Winkelnkemper, “Control of grid connected AC-DC converters with minimized DC link capacitance under unbalanced grid voltage condition,” In Proc. Conf. EPE, 2007.
21. H. Song and K. Nam, “Dual current control scheme for PWM converter under unbalanced input voltage conditions,” IEEE Trans. Ind. Electr., 1999.
22. A. Yazdani and R. Iravani, “A unified dynamic model and control for the voltage-sourced converter under unbalanced grid conditions,” IEEE Trans. Power Delivery, Jul. 2006.

23. D. Roiu, R. Bojoi, L. R. Limongi, and A. Tenconi, “New stationary frame control scheme for three phase PWM rectifiers under unbalanced voltage dips conditions,” in Proc. IEEE Ind. Appl. Soc. Annu. Meet., Alberta, 2008.
24. Q. Yu, L Norum, T. Undeland, and S. Round, “Investigation of dynamic controllers for a unified power flow controller,” in Proc. IEEE Ind. Electro. Annu. Meeting, 1996.
25. L. Xu, B. R. Andersen, and P. Cartwright, “VSC transmission operating under unbalanced AC conditions - analysis and control design,” IEEE Trans. Power Delivery, Jan. 2005.
26. H. Fujita, Y. Watanabe, and H. Akagi, “Control and analysis of a unified power flow controller,” IEEE Trans. Power Electronics, Nov. 1999.
27. Q. Yu, S. D. Round, L. E. Norum, and T. M. Undeland, “Dynamic control of a unified power flow controller,” in Proc. IEEE ower Electr. Spec. Conference. 1996..
28. C. Du, M. H. J. Bollen, E. Agneholm, and A. Sannino, “A new control strategy of a VSC–HVDC system for high-quality supply of industrial plants,” IEEE Trans. Power Delivery,, Oct. 2007.
29. A. Yazdani and R. Iravani, “Dynamic model and control of the NPC-based back-to-back HVDC system,” IEEE Trans. Power Delivery, Jan. 2006.
30. M. Hagiwara and H. Akagi, “An approach to regulating the DC link voltage of a voltage-source BTB system during power line faults,” IEEE Trans. on Industry Applications, Sep. 2005.

31. M. Winkelnkemper, “Reduzierung von Zwischenkreiskapazitäten in Frequenzumrichtern fur Niederspannungsantribe,” PhD dissertation, Dept. Electrical and Computer Engineering, TU Berlin, Berlin, 2005.
32. B. Parkhideh, S. Bhattacharya, J. Mazumdar, and W. Koellner, “Modeling and control of large shovel converter systems integrated with supercapacitor,” In Proc. IEEE Ind. Appl. Soc. Annu. Meet., Alberta 2008.
33. P. Rodriguez, A. Timbus, R. Teodorescu, M. Liserre, and F. Blaabjerg, “Reactive power control for improving wind turbine system behavior under grid faults,” IEEE Trans. on Power Electronics, July 2009.
34. P. Maibach, A. Faulstich, M. Eichler, and S. Dewar, “Full-scale medium-voltage converters for wind power generators up to 7MVA,” ABB white paper.
35. R. W. Erickson and D. Maksimovic, “Fundamentals of power electronics,” 2nd ed, NY: Springer, 2000.
36. Y. Ye, M. Kazerani, and V. H. Quintana, “Modeling, control, and implementation of three-phase PWM converters,” IEEE Trans. on Power Electronics, May 2003.
37. B. Parkhideh and S. Bhattacharya, “A practical approach to controlling the back-to-back voltage source converter system,” In Proc. IEEE Ind. Electr. Soc. Annu. Meet., Orlnado, 2008.
38. Z. Xi and S. Bhattacharya, “STATCOM control with instantaneous phase-locked loop for performance improvement under single-line to ground fault,” In Proc. IEEE Ind. Electro. Soc. Annu. Meet., 2008.

39. P. W. Lehn and R. Iravani, “Experimental evaluation of STATCOM closed loop dynamics,” IEEE Trans. on Power Delivery, Oct. 1998.B. Parkhideh and S. Bhattacharya, “Resilient operation of voltage-sourced BTB HVDC systems under power system disturbances,” In Proc. IEEE PES General Meet., 2009.
40. M. Hagiwara, H. Fujita, and H. Akagi, “Performance of a self-commutated BTB HVDC link system under a single-line-to-ground fault condition,” IEEE Trans. on Power Electronics, Jan. 2003.
41. A. Yazdani, R. Iravani, “Dynamic model and control of the NPC-based back-to-back VDC system,” IEEE Trans. on Power Delivery, Vol. 21, No. 1, 2006.
42. R. A. Freeman and P.V. Kokotovi,“A New Lyapunov Function for the Backstepping Design of ’Softer’ Robust Nonlinear Control Laws,” Technical Report CCEC-92-0520, Center for Control Engineering and Computation. University of California at Santa Barbara, 1992.
43. B. Parkhideh and S. Bhattacharya, “A unified Modular Transformer Converter (MTC) system with advanced angle control structure” In Proc. IEEE Energy Conver. Exhib. and Cong., 2011.
44. C. Schauder, “DC power regulator incorporating high power ac to dc converter with controllable dc voltage and method of use.” US Patent 6433520, Aug 2002.
45. S. Bhattacharya, and Zhengping Xi., “Control reconfiguration of VSC based STATCOM for De-icer application” In Proc .IEEE Power Eng. Soc. General Meeting, 2008

46. M. Hagiwara, H. Fujita, and H. Akagi,, "Performance of a self-commutated BTB HVDC link system under a single-line-to-ground fault condition," IEEE Trans. On Power Electronics, 2003.
47. H W. Bode, Feedback amplifier Design. Princeton, NJ: Van Nostrand, 1945.
48. J. Freudenberg and R. Middleton, "Properties of single input, two output feedback systems," Int. Jnrl. of Control, 72, 1999.
49. A. R. Woodyatt, J. S. Freudenberg, and R. H. Middleton, "An integral constraint for single input two output feedback systems," Automatica , 37, 2001.
50. A. R. Woodyatt, J. S. Freudenberg, and R. H. Middleton, "Integral constraint for single input two output feedback systems," The University of Newcastle, Australia, Technical Report EE9703.
51. http://www.eia.doe.gov/cneaf/electricity/page/disturb_events_archive.html.
52. K. H. LaCommare, and J. Eto, "Cost of power interruptions to electricity consumers in the United States," LBNL report-58164, 2006.
53. D. Lineweber, and S. Mcnulty. "The cost of power disturbances to industrial and digital economy companies," Report no. TR-1006274, 2001.
54. A. Naderian, R. Piercy, S. Cress, J. Service, and W. Fan, "An approach to power transformer asset managemenr using health index," *IEEE Electrical Insulation Magazine*, 2009.
55. D. Woodcock, "Transformer fleet health and risk management," *IEEE PES Transformer Committee Tutorial*, 2007.
56. http://www.nerc.com/filez/tadswg.html

57. FERC, “transmission planning and cost allocation by transmission owning and operating public utilities,” Doc. No. RM10-23-000, 2010.
58. S. Fink, C. Mudd, K. Porter, and B. Morgenstem, “Wind energy curtailment case studies”, NREL/SR-550-46716, 2009.
59. www.abb.com
60. K. Sen, M. Sen, “Versatile power flow transformer for compensating power flow in a transmission line,” US Patent No: 6,335,613, Jan. 2002.
61. S. Bhattacharya, B. Fardenesh, B. Sherpling, “Convertible Static Compensator: Voltage Source Converter Based FACTS Application in the New York 345 kV Transmission System”, Proc. of the 5th International Power Electronics Conference (IPEC), Niigata, Japan, April 2005.
62. M. Maharsi, L. Tang, and S. Bala , “Hybrid distribution transformer,” US Patent No.: US2010/0220499A1
63. D. Divan, and J. Sastry, “Controllable network transformers,” IEEE Proc. PESC’08.
64. www.abb.com
65. Seunghun Baek and Subhashish Bhattacharya, “Analytical modeling of a medium-voltage and high-frequency inductor-integrated coaxial-type 25kVA power transformer for solid state transformer application”, accepted in IEEE Energy Conversion Congress and Exposition (ECCE) proceedings, 17-22 Sept. 2011.
66. Seunghun Baek, Sumit Dutta and Subhashish Bhattacharya; “Design and characterization of a three-phase dual active bridge dc/dc converter in wye-delta connection for a high frequency and high power applications”, accepted in IEEE

Energy Conversion Congress and Exposition (ECCE) proceedings, 17-22 Sept. 2011.

67. Yu Du; Seunghun Baek; Bhattacharya, S.; Huang, A.Q.; , "High-voltage high-frequency transformer design for a 7.2kV to 120V/240V 20kVA solid state transformer," IECON 2010 - 36th Annual Conference on IEEE Industrial Electronics Society , vol., no., pp.493-498, 7-10 Nov. 2010
68. Chun-kit Leung; Dutta, S.; Seunghun Baek; Bhattacharya, S.; , "Design considerations of high voltage and high frequency three phase transformer for Solid State Transformer application," IEEE Energy Conversion Congress and Exposition (ECCE) , vol., no., pp.1551-1558, 12-16 Sept. 2010
69. Seunghun Baek; Du, Y.; Gangyao Wang; Bhattacharya, S.; , "Design considerations of high voltage and high frequency transformer for solid state transformer application," IECON 2010 - 36th Annual Conference on IEEE Industrial Electronics Society , vol., no., pp.421-426, 7-10 Nov. 2010
70. Bhattacharya, S.; Tiefu Zhao; Gangyao Wang; Dutta, S.; Seunghun Baek; Yu Du; Parkhideh, B.; Xiaohu Zhou; Huang, A.Q.; , "Design and development of Generation-I silicon based Solid State Transformer," IEEE Applied Power Electronics Conference and Exposition (APEC), 2010 , vol., no., pp.1666-1673, 21-25 Feb. 2010
71. Bhattacharya, S.; Tiefu Zhao; Gangyao Wang; Dutta, S.; Seunghun Baek; Yu Du; Parkhideh B.; Xiaohu Zhou; Huang, A.Q.; "Design and development of Generation-I silicon based Solid State Transformer," IEEE Proc. APEC, 2010.

72. E. Muljadi, “New challenges in high penetration wind power generation,” NREL, 2010.
73. C. Schauder, M. Gernhardt, E. Stacey, T. Lemak, L. Gyugyi, T. W. Cease, and A. Edris, “Operation on +/- 100 MVAR TVA STATCON,” IEEE Trans. On Power Delivery, 1997.
74. Babak Parkhideh, and Subhashish Bhattacharya, “Active power transfer capability of shunt family of FACTS devices based on angle control,” IEEE ECCE’09, 2009.
75. Babak Parkhideh, and Subhashish Bhattacharya, “Towards smart transmission substations with Modular Transformer Converter (MTC),” IEEE PES General Meeting 2011.
76. S. Bhattacharya et. al. “ NYPA CSC TNA Studies,” EPRI Internal Report
77. Power Systems Test Case Archive, http://www.ee.washington.edu/research/pstca/.
78. Babak Parkhideh and Subhashish Bhattacharya, “A Unified Modular Transformer Converter (MTC) system with advanced angle control structure,” IEEE Proc. ECCE’11, 2011.
79. Z. Xi, and S. Bhattacharya, “STATCOM operation strategy under power system faults,” IEEE PES General Meeting, 2007.
80. J. Sun, L. Hopkins, B. Shperling, B. Fardanesh, M. Graham, M. Parisi, S. McDonald, S. Bhattacharya, S. Bekowitz, A. Edris, “Operating Characteristics of the Convertible Static Compensator on the 345 kV Network”, IEEE PES Power Systems Conference & Exposition, NY, October 2004.

81. S. Bhattacharya, Z. Xi, B. Fardanesh, E. Uzonovic, “Control Reconfiguration of VSC Based STATCOM for De-icer Application”, IEEE Power Engineering Society General Meeting, 2008.
82. www.wikipedia.com
83. Power Systems Test Case Archive, http://www.ee.washington.edu/research/pstca/.
84. L. Martin, D. Retzmann, and C. Schimpf, “HVDC state-of-the-art technologies-from smart grid to super grid,” *EPRI HVDC and FACTS Users Conference,* 2009.
85. H. Mirzaee, A. De, A. Tripathi, and S. Bhattacharya “Design comparison of high power medium-voltage converters based on 6.5kV Si-IGBT/Si-PiN JBS diode, and 10kV SiC MOSFET/SiC-JBS diode,” In Proc. at IEEE ECCE’11, 2011
86. L. Gyugyi, C. D. Schauder, S. L. Williams, T. R. Rietman, D. R. Torgerson, A. Edris, “The unified power flow controller: a new approach to power transmission control,” *IEEE Trans. on Power Delivery*, 1995.
87. W. Koellner, “A new all AC gearless drive system for large mining dragline” in *IEEE Industry Applications Society Annual Meeting*, IAS’06, 2006.
88. Z. Zhiming, “China’s first AC powered walking dragline in coal mining,” in *MINExpo International*, 2008.
89. Bucyrus 8750 series dragline brochure, http://www.bucyrus.com.
90. J. Rodriguez, L. Moran, J. Pontt, J. Esponoza, R. Diaz, and E. Silva, “Operating experience of shovel drives for mining applications,” in *IEEE Transactions. on Industry Applications*, 2004.

91. B. Parkhideh, S. Bhattacharya, J. Mazumdar, and W. Koellner, "Utilization of supplementary energy storage systems in high power mining converters," in *IEEE Industry Applications Society Annual Meeting*, IAS'08, 2008.
92. L. Casson, "Operating an 8750 dragline on diesel generators," *Western Mining Electrical Association*, 2000.
93. T. Sopko, B. Kuras, and M. Guven, "Electric drive system having DC bus voltage control," US Patent 7,298,102 B2, 2007.
94. Energy Storage Association website : www.electricitystorage.org
95. P. Logan, "Creating a better energy ecosystem," in *20th Energy Storage Association Annual Meeting*, *ESA'10*, 2010.
96. D. Newman and et. al : Engineering Economic Analysis, 10th edition
97. H. Meiwes, and D. Sauer, "Technical and economic assessment of storage technologies for power supply grids," *Sandia-DOE EESAT Conference*, 2009.
98. Maxwell Technologies, BOOSTCAP ultracapacitor BMOD data sheet.
99. M. Kumar, "Control implementations for high bandwidth shunt active filter," M.Sc. thesis, North Carolina State University, 2011.
100. S. Bhattacharya, "High power active filter systems," PhD dissertation, University of Wisconsin-Madison, 2003.